GFZ German Research Centre for Geosciences, Section 'Climate Dynamics and Landscape Evolution'

Und

Universität Potsdam
Institut für Geowissenschaften

Dynamics of the Geomagnetic Field during the last Glacial

Kumulative Dissertation

Zur Erlangung des akademischen Grades

“doctor rerum naturalium”
(Dr. rer. nat.)
in der Wissenschaftsdisziplin Geophysik

eingereicht an der Mathematisch-Naturwissenschaftlichen Fakultät der Universität Potsdam

von

Liu Jiabo

Potsdam, Januar 2019

Supervisors

Priv. Doz. Dr. Norbert Nowaczyk
Universität Potsdam
Helmholtz-Zentrum Potsdam Deutsches GeoForschungsZentrum

Prof. Dr. Helge Wolfgang Arz
Leibniz-Institute for Baltic Sea Research

Published online at the
Institutional Repository of the University of Potsdam:
https://doi.org/10.25932/publishup-42946
https://nbn-resolving.org/urn:nbn:de:kobv:517-opus4-429461

Erklärung

Hiermit erkläre ich gemäß §12 Abs. 1 Nr. 7 der Promotionsordnung der Mathematisch-Naturwissenschaftlichen Fakultät der Universität Potsdam, dass ich die von mir vorge- legte Dissertation mit dem Titel

"Dynamics of the Geomagnetic Field during the last Glacial"

selbstständig angefertigt, benutzte Quellen und Hilfsmittel vollständig angegeben und wörtliche und sinngemäße Zitate als solche gekennzeichnet habe sowie Tabellen, Karten und Abbildungen, die anderen Werken in Wortlaut oder dem Sinn nach entnommen sind, in jedem Einzelfall als Entlehnung kenntlich gemacht habe. Diese Dissertation wurde noch keiner anderen Fakultät oder Hochschule zur Prüfung vorgelegt und ist, abgesehen von unten angegebenen Teilpublikationen, noch nicht veröffentlicht worden. Ich erkläre, dass ich solche Veröffentlichungen vor Abschluss des Promotionsverfahrens nicht vornehmen werde. Die Bestimmungen der Promotionsordnung sind mir bekannt.

Teilveröffentlichungen:

- **Liu, J.**, Nowaczyk, N.R., Wirth, R., Arz, H.W., 2019. Magnetic mineral diagenesis in the Black Sea - from lacustrine to marine. (**in preparation**)
- **Liu, J.**, Nowaczyk, N.R., Frank, U., Arz, H.W., 2018. Full-vector paleosecular variation from 14.5 ka back to 68.9 ka as reconstructed from Black Sea sediments. Quaternary Science Reviews. (**under review**)
- **Liu, J.**, Nowaczyk, N., Frank, U., Arz, H., 2019. Geomagnetic paleosecular variation record spanning from 40 to 20 ka – implications for the Mono Lake excursion from Black Sea sediments. Earth Planet. Sci. Lett. 509, 114–124. doi:10.1016/j.epsl.2018.12.029
- **Liu, J.**, Nowaczyk, N.R., Frank, U., Arz, H.W., 2018. A 20–15 ka high-resolution paleomagnetic secular variation record from Black Sea sediments – no evidence for the 'Hilina Pali excursion'? Earth Planet. Sci. Lett. 492, 174s–185. doi:10.1016/j.epsl.2018.04.014
- Nowaczyk, N.R., **Liu, J.**, Frank, U., Arz, H.W., 2018. A high-resolution paleosecular variation record from Black Sea sediments indicating fast directional changes associated with low field intensities during marine isotope stage (MIS) 4. Earth Planet. Sci. Lett. 484, 15–29. doi:10.1016/j.epsl.2017.12.009

Ort, Datum, Unterschrift (Liu Jiabo)

Abstract

Geomagnetic paleosecular variations (PSVs) are an expression of geodynamo processes inside the Earth's liquid outer core. These paleomagnetic time series provide insights into the properties of the Earth's magnetic field, from normal behavior with a dominating dipolar geometry, over field crises, such as pronounced intensity lows and geomagnetic excursions with a distorted field geometry, to the complete reversal of the dominating dipole contribution. Particularly, long-term high-resolution and high-quality PSV time series are needed for properly reconstructing the higher frequency components in the spectrum of geomagnetic field variations and for a better understanding of the effects of smoothing during the recording of such paleomagnetic records by sedimentary archives.

In this doctorate study, full vector paleomagnetic records were derived from 16 sediment cores recovered from the southeastern Black Sea. Age models are based on radiocarbon dating and correlations of warming/cooling cycles monitored by high-resolution X-ray fluorescence (XRF) elementary ratios as well as ice-rafted debris (IRD) in Black Sea sediments to the sequence of 'Dansgaard-Oeschger' (DO) events defined from Greenland ice core oxygen isotope stratigraphy.

In order to identify the carriers of magnetization in Black Sea sediments, core MSM33-55-1 recovered from the southeast Black Sea was subjected to detailed rock magnetic and electron microscopy investigations. The younger part of core MSM33-55-1 was continuously deposited since 41 ka. Before 17.5 ka, the magnetic minerals were dominated by a mixture of greigite (Fe_3S_4) and titanomagnetite ($Fe_{3-x}Ti_xO_4$) in samples with SIRM/κ_{LF} >10 kAm^{-1}, or exclusively by titanomagnetite in samples with SIRM/κ_{LF} ≤10 kAm^{-1}. It was found that greigite is generally present as crustal aggregates in locally reducing micro-environments. From 17.5 ka to 8.3 ka, the dominant magnetic mineral in this transition phase was changing from greigite (17.5 – ~10.0 ka) to probably silicate-hosted titanomagnetite (~10.0 – 8.3 ka). After 8.3 ka, the anoxic Black Sea was a favorable environment for the formation of non-magnetic pyrite (FeS_2) framboids.

Aiming to avoid compromising of paleomagnetic data by erroneous directions carried by greigite, paleomagnetic data from samples with SIRM/κ_{LF} >10 kAm^{-1}, shown to contain greigite by various methods, were removed from obtained records. Consequently, full vector paleomagnetic records, comprising directional data and relative paleointensity (rPI), were derived only from samples with SIRM/κ_{LF} ≤10 kAm^{-1} from 16 Black Sea sediment cores. The obtained data sets were used to create a stack covering the time window between 68.9 and 14.5 ka with temporal resolution between 40 and 100 years, depending on sedimentation rates.

At 64.5 ka, according to obtained results from Black Sea sediments, the second deepest minimum in relative paleointensity during the past 69 ka occurred. The field minimum during MIS 4 is associated with large declination swings beginning about 3 ka before the minimum. While a swing to 50°E is associated with steep inclinations (50-60°) according to the coring site at 42°N, the subsequent declination swing to 30°W is associated with shallow inclinations of down to 40°. Nevertheless, these large deviations from the direction of a geocentric axial dipole field (I=61°, D=0°) still can not yet be termed as 'excursional', since latitudes of corresponding VGPs only reach down to 51.5°N (120°E) and 61.5°N (75°W), respectively. However, these VGP positions at opposite sides of the globe are linked with VGP drift rates of up to 0.2° per year in between. These extreme secular variations might be the mid-latitude expression of the Norwegian–Greenland Sea excursion found at several sites much further North in Arctic marine sediments between 69°N and 81°N.

At about 34.5 ka, the Mono Lake excursion is evidenced in the stacked Black Sea PSV record by both a rPI minimum and directional shifts. Associated VGPs from stacked Black Sea data migrated from Alaska, via central Asia and the Tibetan Plateau, to Greenland, performing a clockwise loop. This agrees with data recorded in the Wilson Creek Formation, USA., and Arctic sediment core PS2644-5 from the Iceland Sea, suggesting a dominant dipole field. On the other hand, the Auckland lava flows, New Zealand, the Summer Lake, USA., and Arctic sediment core from ODP Site-919 yield distinct VGPs located in the central Pacific Ocean due to a presumably non-dipole (multi-pole) field configuration.

A directional anomaly at 18.5 ka, associated with pronounced swings in inclination and declination, as well as a low in rPI, is probably contemporaneous with the Hilina Pali excursion, originally reported from Hawaiian lava flows. However, virtual geomagnetic poles (VGPs) calculated from Black Sea sediments are not located at latitudes lower than 60° N, which denotes normal, though pronounced secular variations. During the postulated Hilina Pali excursion, the VGPs calculated from Black Sea data migrated clockwise only along the coasts of the Arctic Ocean from NE Canada (20.0 ka), via Alaska (18.6 ka) and NE Siberia (18.0 ka) to Svalbard (17.0 ka), then looping clockwise through the Eastern Arctic Ocean.

In addition to the Mono Lake and the Norwegian–Greenland Sea excursions, the Laschamp excursion was evidenced in the Black Sea PSV record with the lowest paleointensities at about 41.6 ka and a short-term (~500 years) full reversal centered at 41 ka. These excursions are further evidenced by an abnormal PSV index, though only the Laschamp and the Mono Lake excursions exhibit excursional VGP positions. The stacked Black Sea paleomagnetic record was also converted into one component parallel to the direction expected from a geocentric

axial dipole (GAD) and two components perpendicular to it, representing only non-GAD components of the geomagnetic field. The Laschamp and the Norwegian–Greenland Sea excursions are characterized by extremely low GAD components, while the Mono Lake excursion is marked by large non-GAD contributions. Notably, negative values of the GAD component, indicating a fully reversed geomagnetic field, are observed only during the Laschamp excursion.

In summary, this doctoral thesis reconstructed high-resolution and high-fidelity PSV records from SE Black Sea sediments. The obtained record comprises three geomagnetic excursions, the Norwegian–Greenland Sea excursion, the Laschamp excursion, and the Mono Lake excursion. They are characterized by abnormal secular variations of different amplitudes centered at about 64.5 ka, 41.0 ka and 34.5 ka, respectively. In addition, the obtained PSV record from the Black Sea do not provide evidence for the postulated 'Hilina Pali excursion' at about 18.5 ka. Anyway, the obtained Black Sea paleomagnetic record, covering field fluctuations from normal secular variations, over excursions, to a short but full reversal, points to a geomagnetic field characterized by a large dynamic range in intensity and a highly variable superposition of dipole and non-dipole contributions from the geodynamo during the past 68.9 to 14.5 ka.

Kurzfassung

Die geomagnetischen Paläosäkularvarionen sind ein Ausdruck dynamischer Konvektionsprozesse im flüssigen äußeren Erdkern als Quelle des Erdmagnetfeldes, dem Geodynamo. Paläomagnetische Zeitserien erlauben daher Rückschlüsse auf die veränderlichen Eigenschaften des Erdmagnetfeldes in Raum und Zeit, von stabilen Zuständen mit relativ hoher Feldstärke und dominierender Dipolgeometrie, bei der die magnetischen Pole nur in hohen Breiten migireren, über Feldkrisen wie Intensitätsminima und geomagnetischen Exkursionen mit komplexeren Geometrien, bishin zur vollständigen und dauerhaften Umpolung des Dipolhauptfeldes. Eine geomagnetische Exkursion, als Extremfall der Paläosekularvariationen, ist charakterisiert durch kurzfristige ($<10^4$ Jahre) Abweichungen der paläomagnetischen Richtungen von der Richtung, die ein geozentrischer axialer Dipol produziert. Die aus paläomagnetisch bestimmten Richtungen abgeleiteten Positionen des virtuellen geomagnetischen (Nord-) Pols (VGP) liegen dabei per Definition südlich von 45°N.

Für diese Doktoarbeit wurden sechzehn Sedimentkerne aus dem Schwarzen Meer herangezogen, um das Verhalten des Erdmagnetfeldes der letzten ca. 70 ka zu untersuchen. Die dabei rekonstruierten Feldvariationen umfassen drei geomagnetische Exkursionen: die 'Norwegian-Greenland Sea excursion' (64.5 ka), die 'Laschamps excursion' (41.0 ka), sowie die 'Mono Lake excursion' (34.5 ka). Alle drei Ereignisse sind mit ausgeprägten Minima in der Feldintensität verbunden. Insbesondere während der 'Laschamps excursion', kam es zu einer kurzfristigen (0.5 ka) aber vollständigen Umpolung, während für die 'Mono Lake excursion' nur ein stark verzerrtes Dipolfeld anzunehmen ist. Die in der Literatur postulierte 'Hilina Pali excursion' (18.5 ka) konnte trotz in diesem Zeitraum zeitlich hochaufgelöster Datenreihen aus dem Schwarzen Meer nicht verifiziert werden. Für sie konnte, ähnlich wie für die 'Norwegian Greenland Sea excursion', lediglich stärker ausgeprägte, zum Teil zeitlich beschleunigte Änderungen in Inklination und Deklination der Magnetfeldrichtung nachgewiesen werden.

Acknowledgments

My first thanks go to my supervisor Norbert Nowaczyk for his constant support during my studies at the GFZ Potsdam. He has a wide range of knowledges on paleomagnetism, instruments and programing. It was a pleasure to work with him during my PhD studies. Special thanks go to Helge Arz for inspiring scientific discussions, and for providing the opportunities to work on the Black Sea sediments. Further thanks also go to Achim Brauer for supporting my study at the GFZ.

Many thanks go to Ute Frank for her help on magnetic measurements and for discussions on measured results. I also would like to thank Martina Duwe for her IT support and friendly help. My thanks also go to Monika Korte for training me in magnetic field modelling and providing me the source code.

A lot of thanks go to everyone from GFZ section 4.3 (formerly section 5.2) for their help and discussions. Particularly, my thanks go to Christine Gerschke for her helps on administrative issues. I would also like to thank the China Scholarship Council for funding my PhD studies at the GFZ Potsdam.

Many thanks go to S. Plewe, M. Duwe, T. Moldenhawer, and F. Brendel for their technical and logistical help during processing and sub-sampling of the cores. And thanks also go to the captains and crews of *RV Meteor*, cruise M72/5 and *RV Maria S. Merian*, cruise MSM33, for their efforts in providing optimal working conditions for producing best scientific results.

Finally, I want to thank my family for their support in the past years, so that I could have a very enjoyable life during my studies. I also thank my friends for all the colorful time we have spent together.

Table of contents

List of figures

List of tables

1 Introduction

1.1 Geomagnetic paleosecular variations and field excursions

Nowadays, the Earth's magnetic field can be directly measured at the Earth's surface, including ground and satellite observations. Continuous and systematic recording of both field directions and intensities has a history of about two centuries (since 1830, reviewed by Kono, 2007). On the other hand, over geological timescales, the information about the Earth magnetic field can be only derived indirectly from the remanent magnetization in crustal rocks. Theoretically, the relation between the magnetic field (B) and the remanent magnetization (M) acquired in that field is very straightforward (Kono, 2007). Their directions are generally parallel, and their intensities are approximately proportional to each other with the proportionality constant being determined by the magnetic properties of rocks (e.g., Dunlop and Ozdemir, 2000; Dunlop and Waddington, 1975; Tauxe et al., 2006).

The thermoremanent magnetization (TRM) of burnt brigs or pottery, and lava flows, that cooled down within the Earth's magnetic field, can provide full-vector information on geomagnetic field variations, that is, absolute paleointensity data and directional information on inclination and declination as well (e.g., Ben-yosef et al., 2017; Cassata et al., 2008). However, archaeomagnetic data, often with a fairly precise dating, extends only a few thousand years back in time and are often available only from restricted areas (e.g., Ben-yosef et al., 2017; Bowles et al., 2002; Cai et al., 2016; Shaar et al., 2016). Lava flows can be found from almost every time interval and from all over the globe (e.g., Cassata et al., 2008; Kissel et al., 2011; Laj et al., 2014, 2002; Teanby et al., 2002). But, obtained data sets, like the ones derived from archaeological artifacts, represent only spot-readings of geomagnetic field variations (e.g., Cassata et al., 2008; Kissel et al., 2011). In addition, a precise dating is often a problem, especially for younger lava flows (e.g., Singer et al., 2014; Zhu et al., 2000), so that it is rarely possible to reconstruct long and continuous high-resolution records for absolute intensity and directional variations from these paleomagnetic archives. Lacustrine and marine sediments can help to overcome this problem to some degrees. Magnetic particles get easily aligned with the geomagnetic field within the water body and get fixed in orientation during settlement of the sediments (Tauxe et al., 2006). This detrital remanent magnetization (DRM) can continuously record directional changes of the geomagnetic field (Tauxe and Yamazaki, 2007). The DRM intensity is mostly proportional to the concentration of magnetic particles being present in the sediments but also to the intensity of the ambient geomagnetic field during deposition of the

sediments (Tauxe, 1993). By normalizing with a concentration related parameter, it is then possible to estimate at least relative variations of the geomagnetic field intensity at high-resolution and for long time series (e.g., Channell et al., 2018, 2009; Guyodo and Valet, 1996; Laj et al., 2004, 2000; Lund et al., 2006). Nevertheless, Tauxe et al. (2006) suggested that DRM intensity is not linearly related to field strength under many natural conditions.

Geomagnetic paleosecular variations (PSVs) are an expression of geodynamo processes inside the Earth's liquid outer core (Merrill and McFadden, 1999). These paleomagnetic time series provide insights into the properties of the Earth's magnetic field, from normal behavior with a dominating dipolar geometry, over field crises, such as pronounced intensity lows and geomagnetic excursions with a distorted field geometry, to the complete reversal of the dominating dipole contribution (e.g., Laj and Channell, 2015; Roberts, 2008; Valet et al., 2005). In the past decades, PSV records obtained from long marine sediment cores, have rapidly extended our understanding of the geomagnetic field and its temporal variability over the past few million years (e.g., Channell et al., 2012; Lund et al., 2006; Valet et al., 2008). The relative paleointensity (rPI, Tauxe, 1993), obtained from sediments in the past decades have yielded a lot of new information about the dynamics in geomagnetic field behavior (Roberts et al., 2013) and can serve as a reference signal that has become widely used for dating purposes of sedimentary sequences (e.g., Channell et al., 2009; Laj et al., 2004, 2000; Stoner et al., 2002). With greater global coverage and further back in time, PSV records are able to assess the signals of dipolar versus non-dipolar geomagnetic field contributions (Roberts et al., 2013).

A geomagnetic field excursion is a 'brief' ($<10^4$ years) but significant deviation of paleomagnetic directions from the direction of a geocentric axial dipole (GAD). Associated virtual geomagnetic poles (VGPs) then move out of the area of normal secular variation (reveiwed by Laj and Channell, 2015), i.e., to latitudes below 45°. With increasing numbers of high-fidelity paleomagnetic records, numerous geomagnetic excursions have been discovered in the last few decades. Some well-validated excursions, such as the Laschamp excursion (e.g., Bonhommet, 1967; Gillot et al., 1979; Guillou et al., 2004; Nowaczyk et al., 2012; Plenier et al., 2007; Roperch et al., 1988) and the Iceland Basin excursion (e.g., Channell, 2014, 2006; Channell et al., 1997; Knudsen et al., 2006; Weeks et al., 1995), have been demonstrated to have a global appearance with their VGPs reaching high southern latitudes (Laj et al., 2006), whereas some postulated excursions, associated with less pronounced paleointensity lows, are sporadically reported due to inadequate paleomagnetic recordings (Roberts, 2008). In addition, high resolution and high-fidelity records of sedimentary PSV records allowed the estimation

of durations and field geometries of geomagnetic field excursions (e.g., Bourne et al., 2012; Channell, 2014, 2006; Channell et al., 2017; Laj et al., 2006; Nowaczyk et al., 2012).

Nevertheless, one of the major difficulties in understanding the temporal and spatial scales of PSV is the limited and uneven distribution of paleomagnetic data (Johnson and McFadden, 2015, e.g., PSV records for the past 100 ka reviewd by S. Panovska et al., 2018). Besides, obtained stacks of PSV records often represent only smoothed time series due to large areal stacking and/or low sedimentation rates (e.g., Channell et al., 2018; Laj et al., 2004; Panovska et al., 2018). Accordingly, high resolution PSV records, with global coverage and further back in time, are in needed for a better understanding of the effects of smoothing on paleomagnetic records and reconstructing the higher frequency components in the spectrum of geomagnetic field variations. And, to a certain degree, geomagnetic excursions, are not yet satisfactorily understood in terms of their occurring frequency, individual duration, and pattern of field behavior and geometry (e.g., Channell et al., 2017; C. Kissel et al., 2011; Laj et al., 2014; Roberts, 2008). In order to answer these questions, obtaining high-resolution sedimentary excursion records with good age control from sites with sedimentation rates >10 cm/kyr and estimating excursion duration with high chronological precision are urgently required (reviewed by Roberts, 2008).

1.2 Scientific objects of the doctoral project

This doctorate thesis is aiming to create high resolution paleomagnetic records with both directions and intensities from sixteen Black Sea sediment cores recovered during two ship expeditions of M72/5 and MSM33. To achieve this aim, five main objects have been investigated in the doctorate project:

I. Performing detailed rock magnetic and electron microscopy analyses to identify and characterize magnetic minerals in the studied Black Sea sediments.

II. To study how the mid-latitude geomagnetic field behaviour in the Black Sea area refers to a probable reversal of the geomagnetic field restricted to high latitudes, during the postulated Norwegian-Greenland Sea excursion (64.5 ka BP).

III. Understanding the Earth's magnetic field behavior during the Mono Lake excursion (34.5 ka BP).

IV. To test whether the postulated 'Hilina Pali' excursion (18.5 ka BP) finds an expression in the paleomagnetic record from the Black Sea area.

V. Reconstructing full vector paleosecular variation records from the whole collection of cores recovered from the southeastern Black Sea and providing general insights into the geomagnetic field behavior across geomagnetic excursions and phases of normal secular variations.

1.3 Study site and material

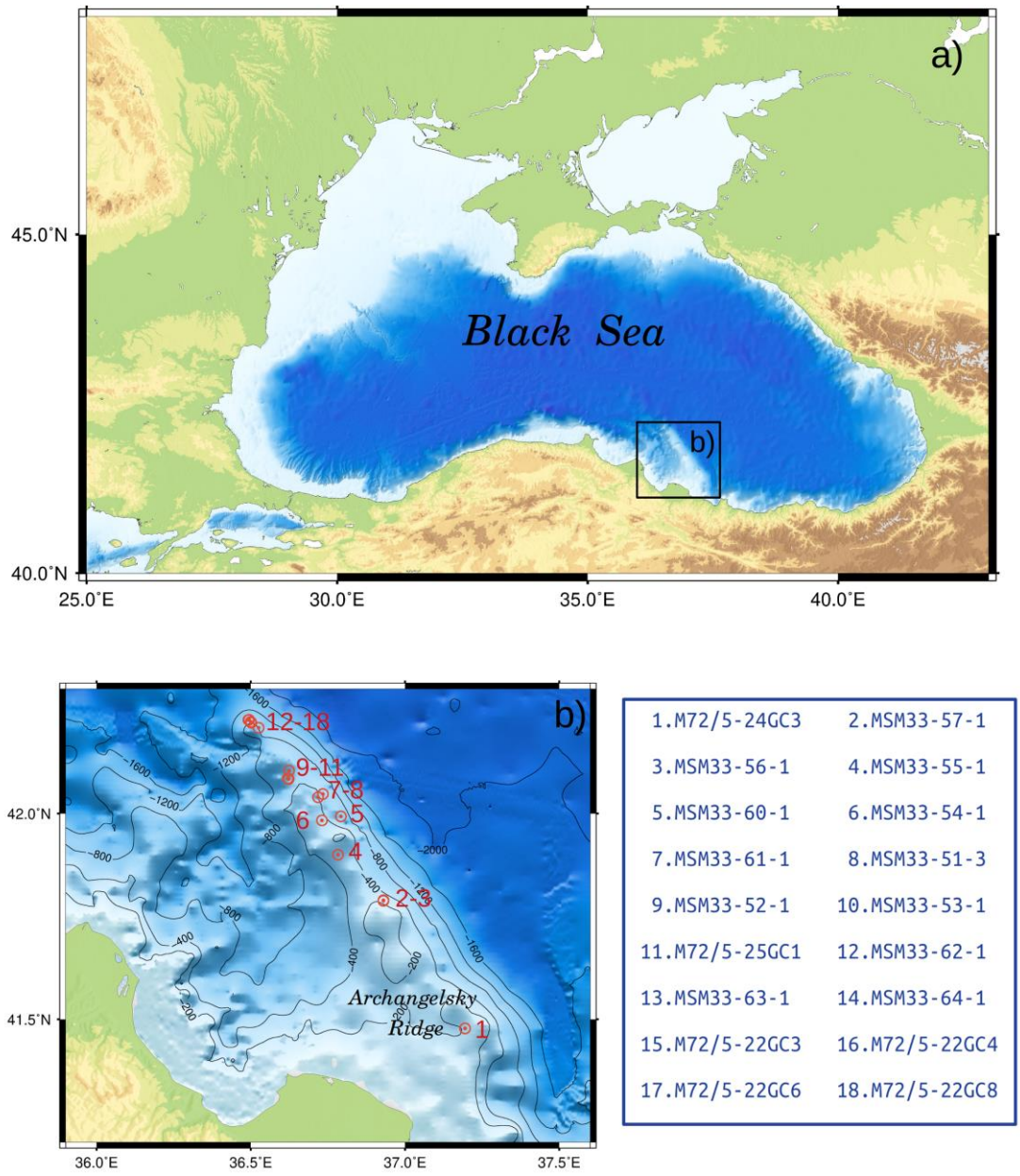

Figure 1.1 a) Overview map of the Black Sea. Location of the study area is marked by the black rectangle in the south-eastern Black Sea. b) Close-up view of the study area. Investigated cores were recovered along the Archangelsky Ridge. Core labels are listed in the table at right.

For this study, a total of eighteen sediment cores recovered during two ship expeditions from the Archangelsky Ridge in the SE Black Sea were investigated (Fig. 1.1). The expedition M72/5 of German research vessel *RV METEOR* in 2007 provided six cores, and the expedition MSM33 of German research vessel *RV Maria S. Merian* in 2013 provided a total of fifteen

cores from the SE Black Sea. The sediment cores were taken from water depths between 208 and 848 m, with core lengths ranging from 682 to 1027 cm (Table 1.1). All six M72/5 cores and twelve MSM33 cores (Table 1.1) have been investigated up to now.

Sediments investigated for this study cover mostly the last glacial, marine isotope stage (MIS) 4 to 2, and the Holocene (MIS 1). During the last glacial to the early Holocene, the Black Sea was disconnected from the Mediterranean Sea, with its lake level temporarily lying at around -100 m below modern sea level (e.g., Major et al., 2006; Shumilovskikh et al., 2012). Thus, fine-grained siliciclastic sediments with variable carbonate content (25 – 40%, Nowaczyk et al., 2012) were deposited under limnic and oxic water conditions for this time window at the study site. Due to global sea-level rise during the last deglaciation and a subsequent ingression of marine seawater through the sill of the Bosporus (modern water depth 36 m) at around 8.3 ka (e.g., Kwiecien et al., 2008; Major et al., 2006), the Black Sea was turned into the World's largest anoxic basin. Since then finely laminated organic-rich sapropelitic sediments and coccolith oozes were deposited (e.g., Bahr et al., 2005; Shumilovskikh et al., 2013).

Table 1.1: Coring locations, sampling and analysis statistics for investigated cores from RV Meteor expedition M72/5 (2007) and RV Maria S. Merian expedition MSM33 (2013).

						Age intervals for stacking inclination, declination, and relative paleointensity				
Core number	Site latitude	Site longitude	Water depth [m]	Core length [cm]	Collected samples	*14.5 – 20.0 ka*	*20.1 – 39.40 ka*	*39.44 – 42.6 ka*	*42.7 – 59.0 ka*	*59.1 – 68.9 ka*
						Stack resolution (Ref.):				
						50 a (1)	*100 a (2)*	*40 a (3)*	*100 a (4)*	*100 a (5)*
M72/5-24GC3	41° 28.66' N	37° 11.68' E	208.0	885	449	#	#			
MSM33-55-1 PC	41° 54.01' N	36° 46.98' E	362.4	948	403	#	#			#
MSM33-56-1	41° 47.33' N	36° 55.81' E	373.9	736	302					
MSM33-57-1	41° 47.38' N	36° 55.95' E	374.0	778	323	#	#			
MSM33-54-3 PC	41° 58.99' N	36° 43.85' E	382.2	953	413	#	#			#
M72/5-25GC1	42° 06.21' N	36° 37.43' E	418.0	952	412	#	#			
MSM33-51-3 PC	42° 02.38' N	36° 43.08' E	428.4	1027	375	#	#			#
MSM33-53-1	42° 05.01' N	36° 37.37' E	443.4	797	370	*too much samples contaminated by greigite*				
MSM33-52-1	42° 05.08' N	36° 37.19' E	467.3	682	288	*long hiatusses - no useful data*				
MSM33-61-1	42° 02.85' N	36° 44.02' E	479.3	746	314	#	#			
MSM33-60-1	41° 58.62' N	36° 47.53' E	498.8	739	395	#				
MSM33-64-1	42° 12.46' N	36° 31.52' E	660.5	721	392	#			#	#
MSM33-62-1	42° 13.15' N	36° 30.11' E	767.3	747	331	#				#
MSM33-63-1	42° 13.27' N	36° 30.00' E	785.5	704	348	#				#
M72/5-22GC3	42° 13.53' N	36° 29.55' E	838.0	839	318	#		#	#	
M72/5-22GC4	42° 13.54' N	36° 29.53' E	842.0	866	393	#		#	#	#
M72/5-22GC6	42° 13.57' N	36° 29.65' E	843.0	800	343	#		#	#	#
M72/5-22GC8	42° 13.53' N	36° 29.59' E	847.0	945	372	#		#	#	#

1) Liu et al. (2018), **2)** Liu et al. (2018 accepted.), **3)** Nowaczyk et al. (2012, 2013), **4)** this study, **5)** Nowaczyk et al. (2018)

1.4 Methods

1.4.1 Rock magnetism and paleomagnetism

For correlation purposes all cores were logged for magnetic susceptibility at 1 mm intervals applying fully automated split-core logging systems. Measurements were performed on the split-surface of the core segments using a Bartington MS2E-1 spot-reading sensor. For paleo- and rock magnetic purposes clear rectangular plastic boxes (inner dimension 20×20×15 mm) with a volume of 6 cm^3 were used. In most cases boxes were pressed into one half of the core sections side-by-side with a spacing of 24 to 30 mm. Intervals that were identified from the logging results to be promising in advance, e.g., having recorded an excursion, were sampled at high-resolution in two parallel rows with the square-shaped boxes being rotated by 45°, yielding an effective resolution of 16 to 17 mm (Nowaczyk et al., 2012). An AGICO Multi-function Kappabridge MFK1-A was then used to determine the low-field magnetic susceptibility κ_{LF}, and its anisotropy (AMS), of these samples.

The natural remanent magnetization (NRM) and the anhysteretic remanent magnetization (ARM) were measured with a 2G Enterprises 755 SRM (cryogenic) long-core magnetometer equipped with a sample holder for eight discrete samples at a separation of 20 cm. In order to clean the primary magnetization from subsequently acquired viscous components and for testing the stability of the magnetization, the magnetometer's in-line tri-axial alternating field (AF) demagnetizer was used to stepwise demagnetize the NRM and ARM of the samples. The NRM was measured after application of AF peak amplitudes of 0, 5, 10, 15, 20, 30, 40, 50, 65, 80, and 100 mT. Directions of the characteristic remanent magnetization (ChRM) were determined by principle component analysis (PCA) according to Kirschvink (1980). The error range of the ChRM, assumed to represent the samples' primary magnetization, is given as the maximum angular deviation (MAD). The ARM was imparted along the samples' z-axis with a static field of 0.05 mT and an AF field of 100 mT. Demagnetization then was performed in steps of 0, 10, 20, 30, 40, 50, 65, and 80 mT. The median destructive field of the ARM (MDF_{ARM}), defined as the calculated field level where the ARM is reduced to 50%, was determined to estimate the coercivity of the sediments. The slope of NRM intensity versus ARM intensity of common demagnetization steps was used to determine the relative paleointensity (rPI). In most cases, demagnetization steps from 20 to 65 mT were used to determine the rPI.

A 2G Enterprises 660 pulse magnetizer was used to impart an isothermal remanent magnetization (IRM) along the samples' z-axes. Since IRM intensities often exceed the measuring range of cryogenic magnetometers, the samples' IRMs were measured with a Molyneux spinner magnetometer. A peak field of 1.5 T was used to saturate the samples. The acquired magnetization is defined as the saturated IRM (SIRM). A backfield of -0.2 T was applied in order to determine the S-ratio, defined as $0.5\times(1-(\mathrm{IRM}(-0.2\ \mathrm{T})/\mathrm{SIRM}))$, with $0 \leq S \leq 1$. Detailed IRM acquisition curves and first order reversal curves (FORC) measurements were performed using a 4" Princeton Measurements Corporation 'MicroMag' alternating gradient magnetometer (AGM). IRM acquisitions curves were obtained by applying 61 logarithmically spaced field steps from 2 mT to 1 T. The IRM component analyses were calculated using the software "pyIRM", based on a Gaussian mixture model, available on https://github.com/botaoxiongyong/pyIRM. The protocol and calculation of irregular FORC (irFORC) and transient hysteresis FORC (tFORC) diagrams were performed following Zhao et al. (2017, 2015). All paleo- and rock magnetic investigations on discrete samples were performed at the Helmholtz Centre Potsdam, GFZ German Research Centre for Geosciences, Potsdam, Germany.

1.4.2 XRF-logging

In general, the archive halves of split cores were used for down-core X-ray fluorescence (XRF) scanning. The M72/5 cores were processed at the MARUM lab of Bremen University, Germany, using an Avaatech XRF core scanner configured with an Amptek detector. Counts of major elements were obtained every 1 to 2 cm with an integration time of 15 seconds and a X-ray current of 0.15 mA (Röhl and Abrams, 2000). The MSM33 cores were processed at the Leibnitz Institute for Baltic Sea Research Warnemünde, Rostock, Germany, using an ITRAX XRF Core Scanner (COX Analytics; e.g., Croudace et al., 2006). The XRF core logger was operated with a Cr-tube at 30 kV and 30 mA and a SDD Si drift detector, with an exposure time of 15 seconds and a step size of 1 mm. Data obtained from this method was mainly used for correlation purposes.

1.4.3 Electron microscopy

Scanning Electron Microscope (SEM) investigations, together with energy dispersive X-ray spectroscopy (EDS), were performed for both standard SEM stubs and polished sections. All SEM samples were prepared using intact sub-samples from sediments, that is, without extraction of the magnetic minerals. The electron backscatter mode was used for all SEM observations. The intensity of backscattered electrons is proportional to the atomic number of

the elements in an analyzed particle. Thus, the iron oxides and sulphides, with relatively heavy ions, appear much brighter than silicates and carbonates in the backscatter mode (Nowaczyk, 2011). For SEM imaging, all samples of this study were sputtered with carbon (C). The SEM measurements for standard SEM stubs were performed using a Carl Zeiss SMT Ultra 55 Plus, generally with an acceleration voltage of 20 kV, an aperture of 120 μm and a working distance of ~12 mm. The investigations were performed at the Helmholtz Centre Potsdam, GFZ German Research Centre for Geosciences, Potsdam, Germany. With the similar settings, some investigations were also performed using a Carl Zeiss MERLIN VP compact at the Leibniz Institute for Baltic Sea Research Warnemünde (IOW), Rostock, Germany.

Transmission Electron Microscope (TEM) analyses were performed for magnetic extracts obtained from the top part (late Holocene) of core MSM33-55-1. The procedures of extracting magnetic minerals was following Nowaczyk (2011) with the probe of 'type B', a 2 cm diameter magnet placed completely inside a plastic probe submerged into the diluted sediment slurry. The preparing process of TEM samples have been discussed in details by Wirth (2004, 2009). The TEM-ready foils were placed on a perforated carbon film on a copper grid. The TEM observations were performed using a FEI Tecnai G2 F20 X-Twin TEM with a Schottky field emitter as an electron source. The TEM was equipped with a Fishione high-angle annular dark-field detector (HAADF), an EDAX X-ray analyzer. High-resolution lattice fringe images were used to calculate the diffraction pattern (fast Fourier transform, FFT) of minerals. The observed d-spacings and angles between adjacent planes were compared with the d-spacings and angles calculated from literature data. The TEM analyses were performed at the Helmholtz Centre Potsdam, GFZ German Research Centre for Geosciences, Potsdam, Germany.

1.5 Thesis structure

This thesis is organized as a "cumulative dissertation" based on five manuscripts. A general introduction is given in the preceding chapter (chapter 1) and followed by five chapters of manuscripts (chapter 2-6). The doctoral candidate is leading author of four manuscripts (chapters 2,4,5,6). Three manuscripts (chapters 3,4,5) have been published and another manuscript (chapter 6) is under review. One further manuscript (chapter 2) is in preparation. The last chapter (chapter 7) summarizes and discusses the main results of this thesis with respect to the main aims as well as future perspectives. The following sections present a summary of the five manuscripts and the contributions from the doctoral candidate.

Chapter 2 manuscript #1 (manuscript in preparation)

Magnetic mineral diagenesis in the Black Sea - from lacustrine to marine

By

Liu Jiabo, Norbert Nowaczyk, Richard Wirth, Helge Arz

This manuscript analyzes the diagenesis of magnetic minerals in the Black Sea sediments since about 41 ka. For this, core MSM33-55-1 was subjected to detailed rock magnetic and electron microscopy investigations. The younger part of core MSM33-55-1 was continuously deposited since 41 ka. Before 17.5 ka, the magnetic minerals are dominated by a mixture of greigite (Fe_3S_4) and titanomagnetite ($Fe_{3-x}Ti_xO_4$), or exclusively by titanomagnetite. From 17.5 ka to 8.3 ka, the dominant magnetic mineral in this transition phase was changing from greigite (17.5 – 10ka) to probably silicate-hosted titanomagnetite (10 – 8.3 ka). Between 8.3 ka and the present, the anoxic Black Sea was a favorable environment for the formation of non-magnetic pyrite (FeS_2) framboids.

The doctoral candidate is the leading author and contributed about 90% to this paper. He conducted rock magnetic analysis, SEM and TEM observations and wrote this manuscript. N. Nowaczyk contributed to the SEM observations and helped to create the age model. R. Wirth contributed to the TEM analyses. H. Arz provided the XRF-logging data and helped to create the age model. All co-authors contributed to the manuscript by proofreading and discussions.

Chapter 3 manuscript 4 (Nowaczyk et al., 2018)

A high-resolution paleosecular variation record from Black Sea sediments indicating fast directional changes associated with low field intensities during marine isotope stage (MIS) 4

Published in Earth and Planetary Science Letters 484 (2018), 15-29

By

Norbert Nowaczyk, **Liu Jiabo**, Ute Frank, Helge Arz

This paper presents high-resolution paleosecular variation (PSV) records between 58 ka and 69 ka (MIS4) reconstructed from nine Black Sea sediment cores. At 64.5 ka, the second deepest minimum in relative paleointensity during the past 69 ka occurred, with the Laschamp geomagnetic excursion at 41 ka being associated with the lowest field intensities. The field minimum during MIS 4 is associated with large declination swings beginning about 3 ka before the minimum. While a swing to 50°E is associated with steep inclinations (50-60°) according to the coring site at 42°N, the subsequent declination swing to 30°W is associated with shallow inclinations of down to 40°. Latitudes of corresponding virtual geomagnetic poles (VGP) only reach down to 51.5°N (120°E) and 61.5°N (75°W), respectively, which denotes no excursion. Nevertheless, these extreme secular variations might be the mid-latitude expression of the Norwegian–Greenland Sea excursion with partly reversed inclinations found at several sites much further North in Arctic marine sediments between 69°N and 81°N.

The doctoral candidate contributed about 30% to this manuscript. He was attending the paleomagnetic sampling, conducted paleomagnetic and rock magnetic measuring for MSM33 cores. He provided the rock magnetic analysis shown in Fig. 5.7 of the manuscript and wrote the paragraphs about first order reversal curve (FORC) diagrams.

Chapter 4 manuscript 3 (Liu et al., 2019)

Geomagnetic paleosecular variation record spanning from 40 to 20 ka - implications for the Mono Lake excursion from Black Sea sediments

Published in Earth and Planetary Science Letters 509 (2019), 114–124.

By

Liu Jiabo, Norbert Nowaczyk, Ute Frank, Helge Arz

This paper describes the full-vector paleosecular variation (PSV) record between 20 and 40 ka reconstructed from seven Black Sea sediment cores. At about 34.5 cal. ka BP, the Mono Lake excursion is evidenced in the stacked Black Sea PSV record by both a relative paleointensity (rPI) minimum and directional shifts. Associated virtual geomagnetic poles from stacked Black Sea data migrated from Alaska, via central Asia and the Tibetan Plateau, to Greenland, performing a clockwise loop. This agrees with data recorded in the Wilson Creek Formation, USA., and Arctic core PS2644-5 from the Iceland Sea, suggesting a dominant dipole field. On the other hand, the Auckland lava flows, New Zealand, the Summer Lake, USA., and Arctic core ODP-919 yielded distinct VGPs located in the central Pacific Ocean presumably due to a non-dipole field configuration.

The doctoral candidate was the leading author and contributed about 80% to this paper. He was attending the paleomagnetic sampling, conducted paleomagnetic and rock magnetic measuring for MSM33 cores, and wrote this manuscript. N. Nowaczyk and U. Frank conducted the paleomagnetic measurements for M72 cores. H. Arz provided XRF-logging data and accelerator mass spectrometry (AMS) ^{14}C ages for constructing age models of all Black Sea cores. All co-authors contributed to the manuscript by proofreading and discussions.

Chapter 5 manuscript 2 (Liu et al., 2018)

A 20–15 ka high-resolution paleomagnetic secular variation record from Black Sea sediments – no evidence for the 'Hilina Pali excursion' ?

Published in Earth and Planetary Science Letters 492 (2018), 174-185

By

Liu Jiabo, Norbert Nowaczyk, Ute Frank, Helge Arz

This paper introduces a very detailed high-quality paleosecular variation (PSV) record spanning from 20 to 15 ka obtained from sixteen Black Sea cores. Since the sedimentation rates in the investigated time window are up to 50 cm ka^{-1}, the obtained PSVs records enabled a stacking using 50-year bins. A directional anomaly at 18.5 ka, associated with pronounced swings in inclination and declination, as well as a low in relative paleointensity (rPI), is probably contemporaneous with the Hilina Pali excursion, originally reported from Hawaiian lava flows (Coe et al., 1978). However, virtual geomagnetic poles (VGPs) calculated from Black Sea sediments are not located at latitudes lower than 60° N, which denotes normal, though pronounced secular variations. Together with other global records, the obtained PSV record from the Black Sea does not support the occurrence of the postulated 'Hilina Pali excursion' at about 18.5 ka.

The doctoral candidate is the leading author and contributed about 80% to this paper. He was attending the paleomagnetic sampling, conducted paleomagnetic and rock magnetic measurements on seven MSM33 cores, and wrote this manuscript. N. Nowaczyk and U. Frank provided the paleomagnetic datasets from six M72 cores and three MSM33 cores. H. Arz provided XRF-logging data for constructing age models of all Black Sea cores. All co-authors contributed to the manuscript by proofreading and discussions.

Chapter 6 manuscript 5 (under review)

Full-vector paleosecular variation from 14.5 ka back to 68.9 ka as reconstructed from Black Sea sediments

Currently under review by Quaternary Science Reviews

By

Liu Jiabo, Norbert Nowaczyk, Ute Frank, Helge Arz

This paper summarizes the full vector paleomagnetic records between 14.5 ka and 68.9 ka obtained from 16 sediment cores recovered from the southeastern Black Sea. Reconstructed prominent lows of paleointensity at about 64.5 ka, 41.6 ka and 34.5 ka are coeval with the Norwegian–Greenland Sea excursion, the Laschamp excursion, and the Mono Lake excursion, respectively. The excursions are further evidenced by an abnormal PSV index, though only the Laschamp and the Mono Lake excursions exhibit excursional virtual geomagnetic pole (VGP) positions. The stacked Black Sea paleomagnetic record was converted into one component parallel to the direction expected from a geocentric axial dipole (GAD) and two components perpendicular to it, representing only non-GAD components of the geomagnetic field. The Laschamp and the Norwegian–Greenland Sea excursions are characterized by extremely low GAD components, while the Mono Lake excursion is marked by large non-GAD contributions.

The doctoral candidate was the leading author and contributed about 70% to this paper. He was attending the paleomagnetic sampling, conducted paleomagnetic and rock magnetic measurements on seven MSM33 cores, and wrote this manuscript. N. Nowaczyk and U. Frank conducted the paleomagnetic measurements for six M72 cores and three MSM33 cores. H. Arz provided XRF-logging data and AMS ^{14}C datings for constructing age models of all Black Sea cores. All co-authors contributed to the manuscript by proofreading and discussions.

2 Magnetic mineral diagenesis in the Black Sea - from lacustrine to marine

manuscript in preparation

Liu Jiabo [1,*], Norbert Nowaczyk [1], Richard Wirth [2], Helge Arz [3]

[1]GFZ German Research Centre for Geosciences, Section 'Climate Dynamics and Landscape Evolution', 14473 Potsdam, Germany.

*(jiabo@gfz-potsdam.de)

[2]GFZ German Research Centre for Geosciences, Section 4.4 – Interface Geochemistry, 14473 Potsdam, Germany

[3]Leibniz Institute for Baltic Sea Research Warnemünde, 18119 Rostock, Germany

Abstract:

Magnetic minerals are sensitive indicators of sedimentary redox conditions and of changes in those conditions throughout time. Knowing the diagenetic alteration of magnetic minerals in sediments is crucial for the interpretation of their environmental magnetic as well as paleomagnetic records. The Black Sea was an isolated fresh water lake during the last glacial and turned into a marginal sea after getting connected to the Mediterranean Sea at about 8.3 ka. In order to investigate the diagenesis of magnetic minerals in the associated changing hydrological conditions, core MSM33-55-1 recovered from the southeast Black Sea was subjected to detailed rock magnetic and electron microscopy investigations. The younger part of core MSM33-55-1 was continuously deposited since 41 ka. In the Black Sea, three hydrological phases, the lacustrine (40.5-17.5 ka), the transitional (17.5-8.3 ka) and the marine (8.3-0 ka) phases can be recognized for the past 41 ka. Before 17.5 ka, magnetic minerals are dominantly mixtures of greigite and titanomagnetite in samples with SIRM/κ_{LF} larger than10 kAm^{-1}, or exclusively titanomagnetite in samples with SIRM/κ_{LF} less than 10 kAm^{-1}. Specifically, greigite was generally found together with pyrite in crustal aggregates with apparent Liesegang ring. Between 17.5 ka and 8.3 ka, magnetic minerals were changing from dominantly greigite (17.5 – ~10.0 ka) to probably silicate-hosted titanomagnetite (~10.0 – 8.3 ka). Additionally, abrupt increasing amount of pyrite was indicated after about 14.5 ka. After 8.3 ka, the anoxic Black Sea was a favorable environment for the formation of pyrite framboids. Nevertheless, some silicate-hosted titanomagnetite/magnetite particles are evidenced in the anoxic marine sediments. Thus, the varying occurrences of different varieties of iron oxides

and iron sulphides, revealed by this study, demonstrates the complexities of diagenetic processes in changing environments like in the waterbody of the Black sea basin.

Keywords:

Magnetic mineral diagenesis; Black Sea; rock magnetism; SEM; TEM; greigite

2.1 INTRODUCTION

Magnetic minerals are sensitive indicators of sedimentary redox conditions and of changes in these conditions through time (Roberts, 2015). Iron oxides (e.g., titanomagnetite) are generally preserved in oxic environments and can record a stable depositional (primary) magnetization (Tauxe, 1993). On the other hand, iron sulphides (e.g., greigite) are generally formed due to diagenesis in anoxic environments and lead to a chemical (secondary) remanent magnetization (e.g., Roberts & Turner, 1993; Roberts & Weaver, 2005; Rowan et al., 2009; Snowball, 1993, 1997). Therefore, knowing the type of magnetic minerals present in marine or lacustrine sediments is important for environmental magnetic and paleomagnetic interpretations.

During the last glacial until the early Holocene, the Black Sea basin was hosting a freshwater body disconnected from the Mediterranean Sea, with its lake level temporarily lying at around -100 m below modern sea level (e.g., Constantinescu et al., 2015; Major et al., 2006). In this phase, fine-grained siliciclastic sediments, deposited under limnic and oxic bottom water conditions, have provided high-quality paleomagnetic records with high-resolution that are comparable with global records (e.g., Nowaczyk et al., 2018, 2013, 2012; Liu et al., 2018, 2019, 2018subm). Nevertheless, the sporadic occurrence of greigite in sediments of the freshwater phase of the Black Sea basin is not yet satisfactorily understood.

Due to the global sea-level rise during the last deglaciation and a subsequent ingression of marine seawater through the sill of the Bosporus (modern water depth 36 m) after about 8.3 ka (e.g., Kwiecien et al., 2008; Major et al., 2006), the Black Sea was turned into the World's largest anoxic basin. Since then, finely laminated organic-rich sapropelitic sediments and coccolith oozes were deposited (e.g., Bahr et al., 2005; Shumilovskikh et al., 2013). From these anoxic Black Sea sediments, pyrite framboids were commonly reported (e.g., Wilkin et al., 1996), but no greigite was found. The paleo- and rock magnetic results from the Holocene Black Sea sediments indicate a stable magnetization, but with a low intensity (e.g., Nowaczyk et al., 2013, 2012; Liu et al., 2019, 2018subm). However, it is not yet known which type of magnetic minerals could survive in the anoxic Black Sea.

Here we discuss results from a sediment core from the Southeastern Black Sea, continuously deposited since the last glacial, that was subjected to detailed rock magnetic and electron

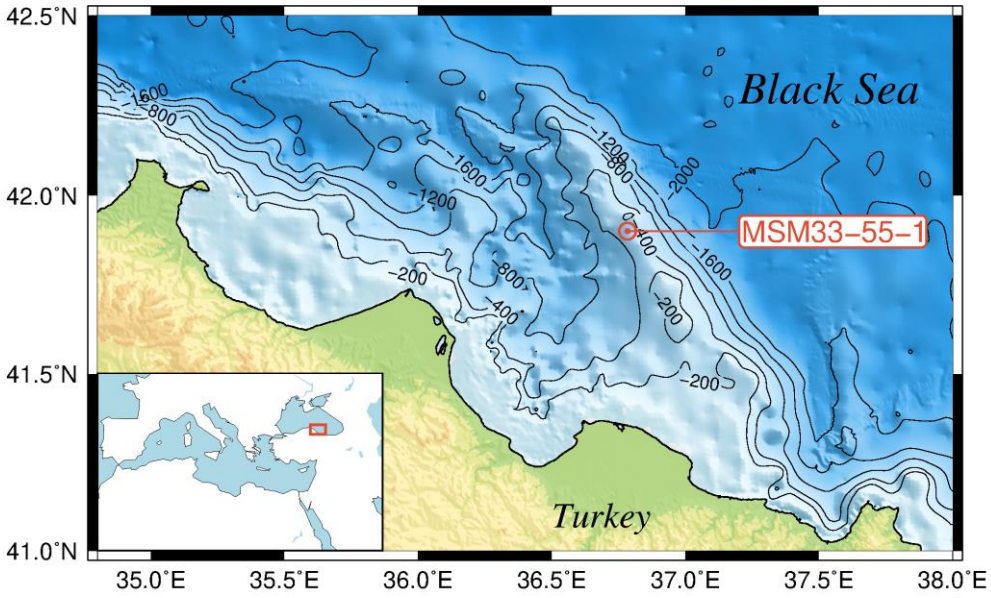

Figure 2.1 Bathymetric map of the southeastern Black Sea. Core MSM33-55-1 was taken from the Archangelsky Ridge in a water depth of 362 m.

microscopy analyses. Different types of magnetic minerals preserved in the Black Sea sediments are identified for three hydrological intervals. Additionally, the processes related to the diagenesis of magnetic minerals in the Black Sea are also discussed.

2.2 MATERIAL AND METHODS

2.2.1 Sediments under investigation

Piston core MSM33-55-1 was recovered from 362 m water depth from the central axis of the Archangelsky Ridge in the southeastern Black Sea by the German *RV Maria S. Merian* in 2013 (cruise MSM33, Fig. 2.1). The 953 cm long core was cut on board into 1 m segments. Splitting of the core segments into working and archive halves was performed onshore at the Leibnitz Institute für Ostseeforschung Warnemünde (IOW; Leibnitz Institute for Baltic Sea Research) in Rostock, Germany.

2.2.2 Methods

Rock magnetism

Core MSM33-55-1 was logged for magnetic susceptibility at 1 mm intervals applying a fully automated split-core logging system. Measurements were performed on the split-surface of the core segments using a Bartington MS2E-1 spot-reading sensor. The obtained log of magnetic susceptibility was used for correlation to other parallel sediment cores from the southeastern Black Sea. Discrete samples from core MSM33-55-1 were taken by using rectangular plastic boxes (inner dimension 20×20×15 mm) with a volume of 6 cm^3. Results from their paleomagnetic analyses are presented in Lie et al. (2019). The low-field magnetic susceptibility

κ_{LF}, and its anisotropy (AMS) of discrete samples were determined by using an AGICO Multi-function Kappabridge MFK1-A.

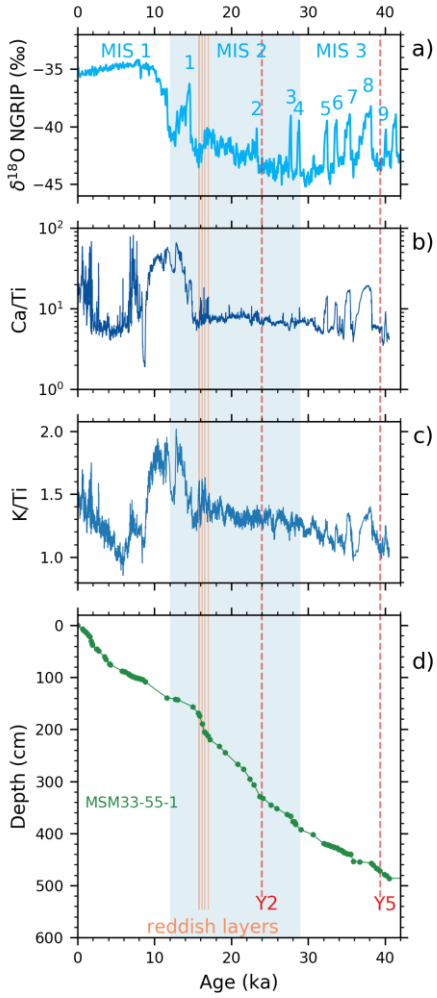

Figure 2.2 Age model of core MSM33-55-1. a) the oxygen isotope ($\delta^{18}O$) record from Greenland ice-cores (NGRIP) according to the GICC05 age model (Svensson et al., 2008). b) XRF Ca/Ti ratios and c) K/Ti ratios from core MSM33-55-1. d) Age depth model of core MSM33-55-1. Vertical red dashed lines indicate identified tephra layers: Y2-tephra layer from the Cape Riva eruption, Santorini, Greece (e.g., Fabbro et al., 2013), Y5-tephra from Campanian Ignimbrite eruption, Phlegraean Fields, Italy (e.g., De Vivo et al., 2001). The vertical orange lines between 15 and 17 ka mark the reddish layers found in Black Sea sediments (Liu et al., 2018) correlated to the meltwater events investigated by Bahr et al. (2006) and Soulet et al. (2013) in the western Black Sea. Numbers in the NGRIP $\delta^{18}O$ record from 1 through 10 denote the so-called Dansgaard-Oeschger events (Dansgaard et al., 1993). MIS – marine isotope stage.

The anhysteretic remanent magnetization (ARM) was imparted along the samples' z-axes with a static field of 0.05 mT and an alternating field (AF) of 100 mT. The ARM was measured on a cryogenic 2G Enterprises 755 SRM long-core magnetometer. The susceptibility of ARM (κ_{ARM}) is the ratio of the acquired ARM to the static field applied (κ_{ARM} = ARM/static field). A 2G Enterprises 660 pulse magnetizer was used to impart an isothermal remanent

magnetization (IRM), with the IRM acquired in a field of 1.5 T defined as the saturation IRM (SIRM). The samples' IRMs were measured with a Molyneux spinner magnetometer. A backfield of -0.2 T was applied in order to determine the S-ratio, defined as 0.5×(1-(IRM(-0.2 T)/SIRM)), with $0 \leq S \leq 1$.

Detailed IRM acquisition curves and first order reversal curves (FORC) measurements were performed using a 4" Princeton Measurements Corporation 'MicroMag' alternating gradient magnetometer (AGM). Complete IRM acquisitions curves were obtained by applying 61 logarithmically spaced field steps from 2 mT to 1 T. The IRM component analyses were calculated using the software "pyIRM", based on a Gaussian mixture model, available on https://github.com/botaoxiongyong/pyIRM. The protocol and calculation of irregular FORC (irFORC) were performed following Zhao et al. (2017, 2015). The irFORC diagrams were calculated with a smooth factor (SF) of 3 for all studied samples (following Zhao et al., 2017, 2015). All paleo- and rock magnetic investigations on discrete samples were performed at the Helmholtz Centre Potsdam, GFZ German Research Centre for Geosciences, Potsdam, Germany.

XRF-logging

In general, the archive halves of split cores were used for down-core X-ray fluorescence (XRF) scanning. Core MSM33-55-1 was processed at the Leibnitz Institute for Baltic Sea Research Warnemünde (IOW), Rostock, Germany, using an ITRAX XRF Core Scanner (COX Analytics; e.g., Croudace et al., 2006). The XRF core logger was operated with a Cr-tube at 30 kV and 30 mA and an SDD Si drift detector, with an exposure time of 15 seconds and a step size of 1 mm. Data obtained from this method was mainly used for correlation purposes.

Electron microscopy

Scanning Electron Microscope (SEM) investigations, together with energy dispersive X-ray spectroscopy (EDS), were performed for both standard SEM stubs and polished sections. All the SEM samples were prepared using intact sub-samples from sediments, that is, without extraction of the magnetic minerals. The electron backscatter mode was used for all SEM observations. The intensity of backscattered electrons is proportional to the atomic number of the elements in an analyzed particle. Thus, the iron oxides and sulphides, with relatively heavy ions, appear much brighter than silicates and carbonates in the backscatter mode (Nowaczyk, 2011). For SEM imaging, all samples of this study were sputtered with carbon (C). The SEM measurements for standard SEM stubs were performed using a Carl Zeiss SMT Ultra 55 Plus, generally with a voltage of 20 kV, an aperture of 120 μm and a working distance of ~12 mm.

The investigations were performed at the Helmholtz Centre Potsdam, GFZ German Research Centre for Geosciences, Potsdam, Germany. With the similar settings, the polished sections were observed using a Carl Zeiss MERLIN VP compact at the Leibniz Institute for Baltic Sea Research Warnemünde (IOW), Rostock, Germany.

Transmission Electron Microscope (TEM) analyses were performed for magnetic extracts obtained from the top part (late Holocene) of core MSM33-55-1. The procedures of extracting magnetic minerals was following Nowaczyk (2011) with the probe of type B, a complete 2 cm diameter magnet inside a plastic probe submerged into the diluted sediment slurry. The preparing process of TEM samples have been discussed in details by Wirth (2004, 2009). The TEM-ready foils were placed on a perforated carbon film on a copper grid. The TEM observations were performed using a FEI Tecnai G2 F20 X-Twin TEM with a Schottky field emitter as an electron source. The TEM was equipped with a Fischione high-angle annular dark-field detector (HAADF), an EDAX X-ray analyzer. High-resolution lattice fringe images were used to calculate the diffraction pattern (fast Fourier transform, FFT) of minerals. The observed d-spacings and angles between adjacent planes were compared with the d-spacings and angles calculated from literature data. The TEM analyses were performed at the Helmholtz Centre Potsdam, GFZ German Research Centre for Geosciences, Potsdam, Germany.

2.3 AGE MODEL AND HYDROLOGICAL VARIATIONS

2.3.1 Age model

Investigated core MSM33-55-1 belongs to a set of eighteen sediment cores, including six cores taken during cruise M72 of German research vessel *R.V. Meteor,* all recovered from the Archangelsky Ridge in the Southeastern Black Sea. These cores have been subjected to comprehensive paleomagnetic analyses (Liu et al., 2018, 2019, 2018subm; Nowaczyk et al., 2018). Their age models are mainly based on radiocarbon dating of one of these cores (Nowaczyk et al., 2012) and tephrochronology (Cullen et al., 2014). Further age constrains were achieved by tuning IRD (ice rafted debris) counts (Nowaczyk et al., 2013, 2012) and XRF logs (mainly Ca/Ti and K/Ti ratios) (Liu et al., 2018, 2019, 2018subm; Nowaczyk et al., 2018, 2013, 2012) as proxies for Dansgaard-Oeschger warming events, to the oxygen isotope ($\delta^{18}O$) record from Greenland ice cores (NGRIP, Svensson et al., 2008). The correlation between core MSM33-55-1 and other M72 and MSM33 cores were presented by Liu et al. (2018, subm1, subm).

After a hiatus at about 40.5 ka, sediments recovered in core MSM33-55-1 were continuously deposited between 40.5 ka and the present. These sediments from upper (younger) part of core MSM33-55-1were investigated for this study. In Fig. 2.2, the correlation of XRF Ca/Ti (Fig.

2.2b) and K/Ti ratios (Fig. 2.2c) from core MSM33-55-1 to the NGRIP $\delta^{18}O$ (Fig. 2.2a) is shown for the time window from 0 ka back to 40.5 ka. In addition, four reddish layers between 15 ka and 18 ka (Fig. 2.2), representing meltwater events (e.g., Bahr et al., 2006; Soulet et al., 2013), were also evidenced in core MSM33-55-1 (Liu et al., 2018). Further tie points were provided by Cullen et al. (2014) by identification of the Y2 and Y5 tephra layers (Fig. 2.2), related to the Cape Riva eruption of Santorini at about 21.8 ka (e.g., Fabbro et al., 2013) and the Campanian Ignimbrite (C.I.) eruption at 39.3 ka (e.g., De Vivo et al., 2001), respectively.

2.3.2 Hydrological and lithological variations

Nowadays, the Black Sea is a semi-closed basin that is connected to the Marmara and Mediterranean Seas through the rather shallow Bosporus sill (37 m below present sea-level, mbpsl) and the deeper Dardanelles sill (87 mbpsl), respectively. During the last glacial, when global (and also Mediterranean) sea-level was below the depth of the Bosporus sill, the Black Sea was cut off from the Mediterranean Sea and turned into a giant freshwater/ brackish lake (e.g., Badertscher et al., 2011; Soulet et al., 2010; Wegwerth et al., 2016). The freshwater level in the Black Sea basin was temporarily lying at around -100 m below modern sea level (e.g., Major et al., 2006; Shumilovskikh et al., 2012). Until about 17.5 ka, fine-grained siliciclastic sediments with variable carbonate content (25 – 40%, Nowaczyk et al., 2012) were deposited at the study site.

After 17.5 ka, the hydrology of the Black Sea was strongly affected by large meltwater discharges originating from the stepwise decay of the Fennoscandian ice sheet (Bahr et al., 2006; Soulet et al., 2013). Between 17.5 and 14.5 ka, the repeated seasonal floods over four successive periods of ~220 y raised the Black Sea water level by around 100 m, until the sill of the Bosporus Strait was reached, leading to the flooding of the wide northwestern shelf of the Black Sea basin and an associated drastic retreat of the coastline (Soulet et al., 2013). The meltwater floods would thus have led to the erosion of the uppermost glacial sedimentary deposits in drainages of Lake Disna, and a subsequent transport of the reddish clays into the Black Sea (Soulet et al., 2013).

Due to global sea-level rise during the last deglaciation and a subsequent ingression of marine seawater through the sill of the Bosporus at around 8.3 ka (e.g., Kwiecien et al., 2008; Major et al., 2006), the Black Sea was turned into the World's largest anoxic basin. Since then finely laminated organic-rich sapropelitic sediments and coccolith oozes were deposited (e.g., Bahr et al., 2005; Shumilovskikh et al., 2013).

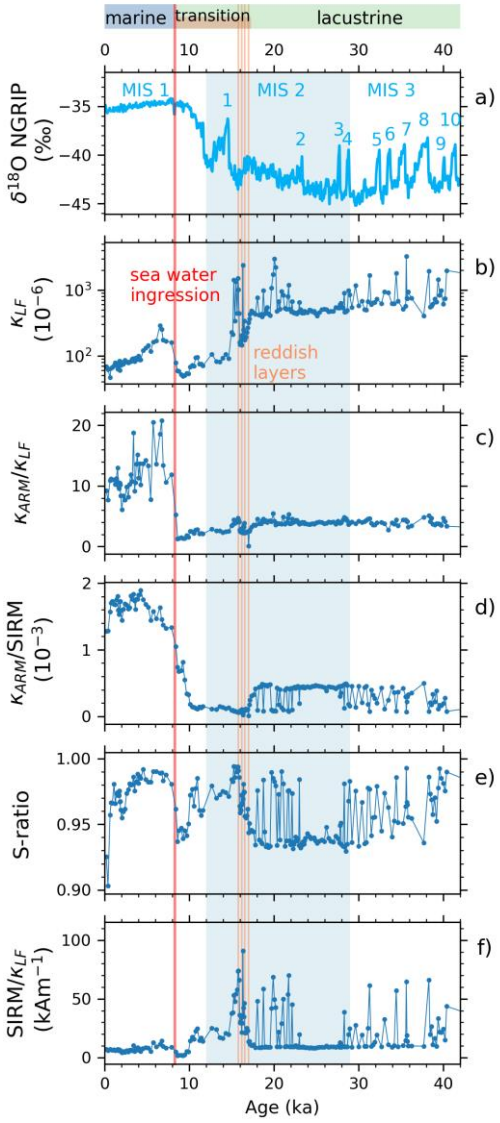

Figure 2.3 a) NGRIP $\delta^{18}O$ record (Svensson et al., 2008) with Dansgaard-Oeschger events indicated by numbers (Dansgaard et al., 1993). b-f) Rock magnetic results from core MSM33-55-1 for the past 41 ka. κ_{LF} – low-field magnetic susceptibility. κ_{ARM} – the susceptibility of anhysteretic remanent magnetization (ARM). SIRM – saturated isothermal remanent magnetization. MIS - marine isotope stages. The vertical red line indicates Mediterranean Sea water ingression through the Bosporus strait into the Black Sea at about 8.3 ka (e.g., Kwiecien et al., 2008; Major et al., 2006). Reddish layers, representing meltwater events identified in Black Sea sediments (Soulet et al., 2013; Bahr el al. 2006), are indicated by four vertical orange bars. Three hydrological phases, the lacustrine, the transition and the marine are indicated on the top (detailed discussions in chapter2.3.2).

In Fig. 2.3, the Mediterranean Sea water ingression at about 8.3 ka is indicated by the vertical red solid line and four meltwater events between 15 and 18 ka are indicated by vertical orange bars. Based on the two major hydrological events that occurred in the Black Sea, the studied sediments are discussed in three hydrological phases. The lacustrine phase (40.5 - 17.5 ka) represents the oxic Black Sea waterbody. The transition phase (17.5 - 8.3 ka) represents the

Black Sea with relative high water level after meltwater events, whereas the marine phase represents the anoxic Black Sea between 8.3 ka and present.

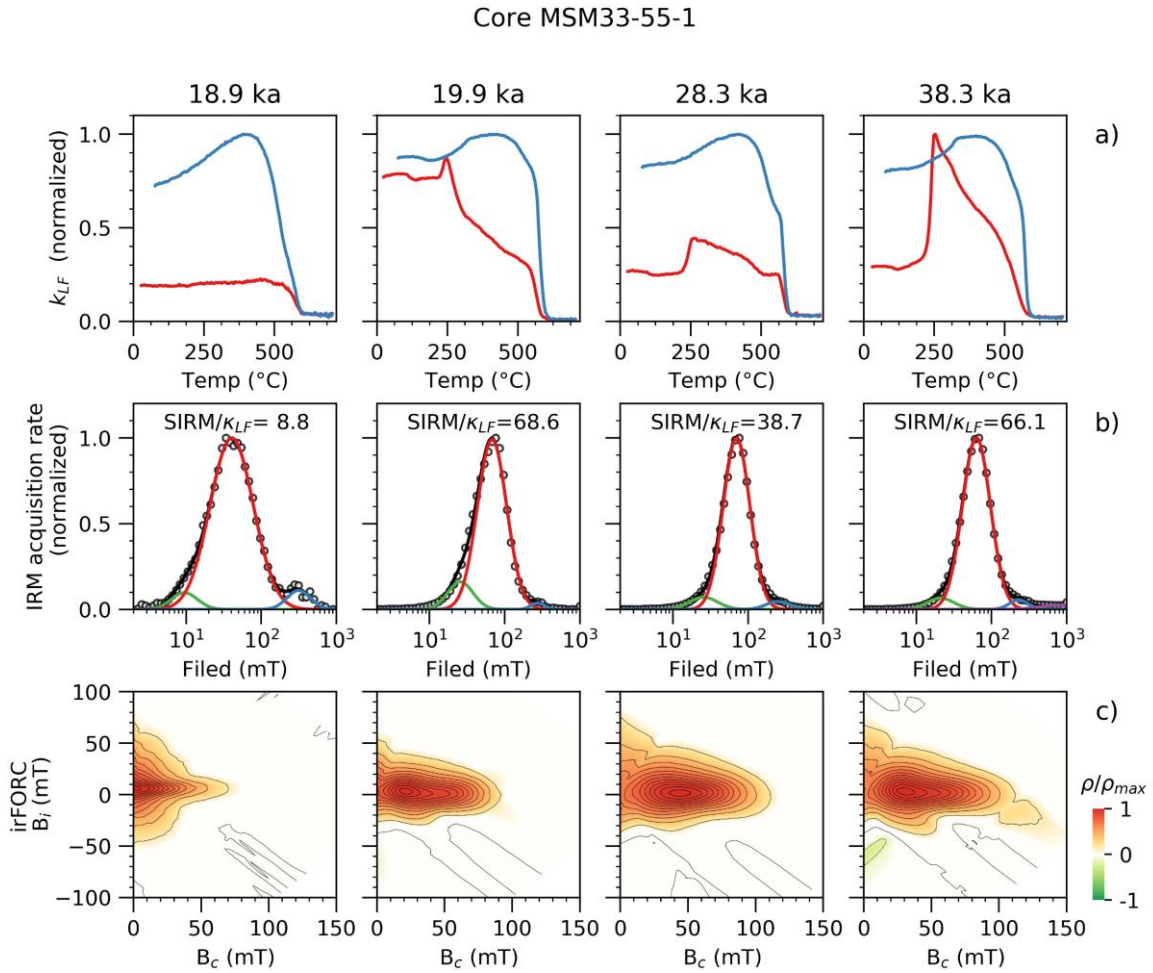

Figure 2.4 Rock magnetic results from samples selected from the lacustrine phase (41.0-17.5 ka, see Fig. 2.3). a) high-temperature magnetic susceptibility curves, b) IRM decomposition curves, c) irregular FORC (irFORC) diagrams. In the high-temperature magnetic susceptibility graphs, red (blue) lines denote heating (cooling) curves. In b) the IRM decomposition graphs, circles indicate IRM acquisition rates determined from measured data. The green, red and blue lines represent three different components fitted to these data, whereas the black line is the fitted total coercivity spectrum. SIRM/κ_{LF} ratios are given in kAm^{-1}. The irFORC for all samples were calculated with a smooth factor (SF) of 3, and the FORC distributions ρ were normalized by their respective maximum ρ_{max}. A detailed discussion is given in section 2.4.2 in the text.

2.4 RESULTS

2.4.1 Rock magnetic variations during the past 40.5 ka

The complete paleomagnetic and some rock magnetic data from core MSM33-55-1 have been presented with depth by Liu et al., (2019). In Fig. 2.3, rock magnetic parameters of core MSM33-55-1, together with the NGRIP $\delta^{18}O$ (Svensson et al., 2008), are shown for the time window between 0 and 40.5 ka. Hydrological variations in the Black Sea was discussed for the

past 40.5 ka in chapter 2.3.2. Three hydrological phases, the lacustrine (40.5 - 17.5 ka), the transitional (17.5 - 8.3 ka) and the marine (8.3 - 0 ka) phases can be recognized for the studied time interval. The three hydrological phases are indicated in the top of Fig. 2.3.

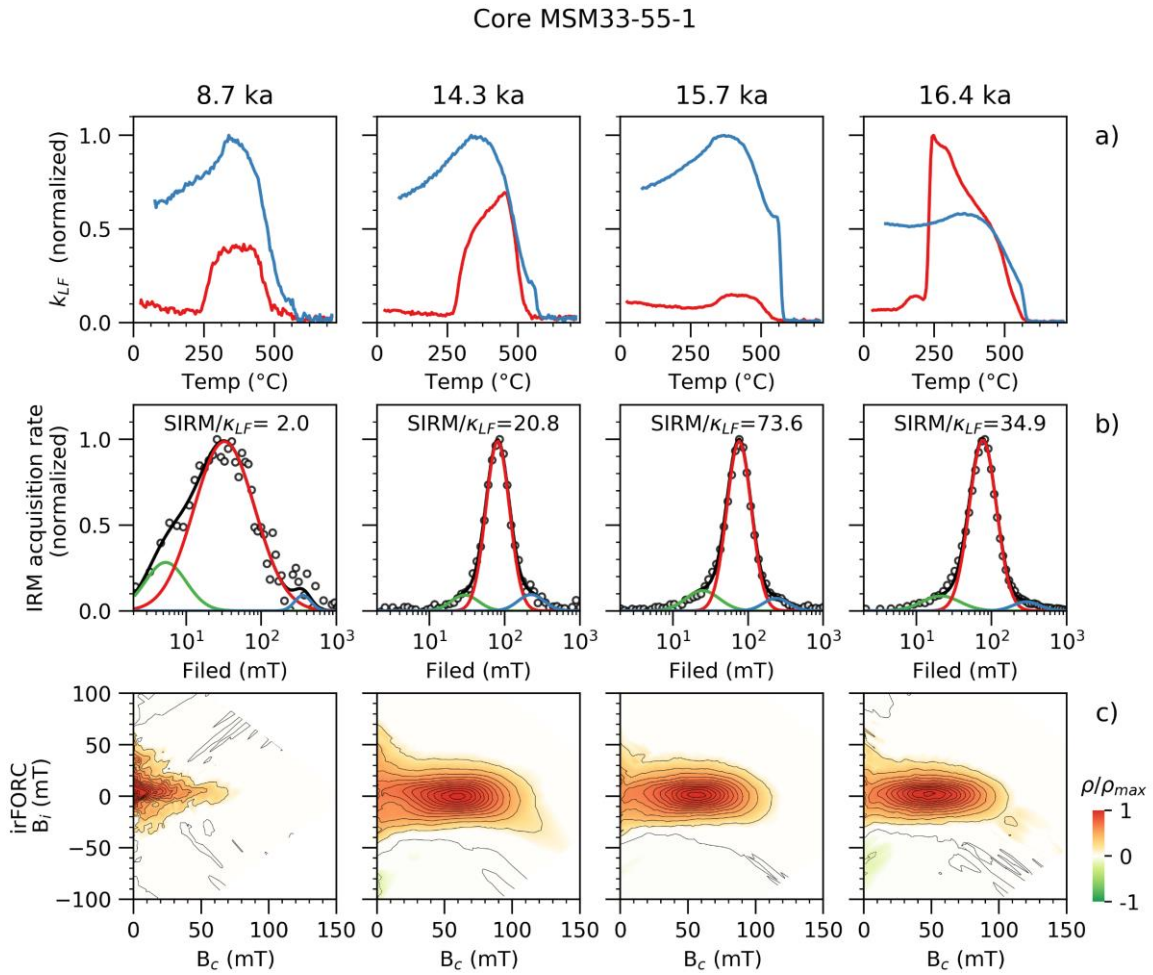

Figure 2.5 Rock magnetic results from samples selected from the transition phase (17.5-8.3 ka, see Fig. 2.3). a) high-temperature magnetic susceptibility curves, b) IRM decomposition curves, c) irregular FORC (irFORC) diagrams. For a more detailed figure caption please refer to Fig. 2.4 and discussion refer to chapter 2.4.3 in the text.

For the lacustrine phase, the magnetic concentration parameter of κ_{LF} exhibit fairly constant low values ($400 \times 10^{-6} < \kappa_{LF} < 700 \times 10^{-6}$) with sporadically deviations to high values ($>700 \times 10^{-6}$, Fig. 2.3b). Specifically, the samples with high magnetic concentrations (high κ_{LF} values) are characterized by fine magnetic grain sizes (κ_{ARM}/SIRM <0.4 and SIRM/κ_{LF} >10 kAm^{-1}) and low magnetic coercivities (S-ratio >0.95). In addition, high SIRM/κ_{LF} ratios were frequently used to indicate the presence of single domain (SD) greigite particles in sedimentary environments (e.g., Roberts et al., 2011; Snowball, 1991), where enhanced SIRM values compared to κ_{LF} denote the superior magnetic recording capability of SD particles (reviewed by Liu et al., 2012). From the transition phase (after 17.5 ka), samples from before about 10.0

ka are characterized by similar magnetic properties like the samples with high κ_{LF} values from the lacustrine phase (e.g., comparable κ_{ARM}/κ_{LF}, κ_{ARM}/SIRM, S-ratio and SIRM/κ_{LF} shown in Fig. 2.3c-f). Between about 10.0 ka and 8.3 ka, values of κ_{LF} (<70 $\times10^{-6}$), S-ratio (<0.95) and SIRM/κ_{LF} (<5 kAm^{-1}) are the lowest for the past 40.5 ka. Samples from the marine phase are characterized by highest values of κ_{ARM}/κ_{LF} (>6) and κ_{ARM}/SIRM (>1.2 $\times10^{-3}$) ratios. Peters & Dekkers (2003) suggested that κ_{ARM}/κ_{LF} greater than 5 and κ_{ARM}/SIRM greater than 1 $\times10^{-3}$ are indicative of the presence of very small magnetite grains. Specifically, the κ_{ARM}/SIRM ratio was interpreted to reflect the relative abundance of the non-interacting biogenic magnetite component and interacting terrigenous magnetite component by Yamazaki & Ikehara (2012). In addition, larger κ_{ARM}/SIRM ratios (>~1 $\times10^{-3}$) represent higher proportion of non-interacting components in sediments from the North Pacific Ocean (Yamazaki, 2008), the West Pacific Ocean (Ontong-Java Plateau, Yamazaki, 2009), the eastern equatorial Pacific Ocean (Yamazaki, 2012), and the Southern Ocean (Yamazaki and Ikehara, 2012).

2.4.2 high-temperature κ_{LF}, IRM decomposition and FORC diagrams

Results of detailed rock magnetic analyses performed on samples from 18.9 ka, 19.9 ka, 28.3 ka, and 38.3 ka from the lacustrine phase are shown in Fig. 2.4. The sample from 18.9 ka, with a SIRM/κ_{LF} ratio of 8.8 kAm^{-1}, exhibits a rock magnetic behavior differing clearly from the other samples, with SIRM/κ_{LF} ratios >30 kAm^{-1}. The high-temperature κ_{LF} curve from sample at 18.9 ka has more or less constant values until 500°C with a subsequent drop at about 580°C, indicative for the Curie-temperature of magnetite at (Fig. 2.4a). In contrast, the heating curves of samples from 19.9 ka, 28.3 ka and 38.3 ka are identically peaking at about 250°C and then decreasing from 250°C to 500°C (Fig. 2.4a). This pattern, together with fairly high SIRM/κ_{LF} ratios (>10 kAm^{-1}), is generally observed in greigite bearing samples (e.g., Roberts et al., 2011). Although the three samples also exhibit Curie-temperatures of magnetite at about 580°C, it is not evident whether the magnetite was of detrital origin or formed during heating. The IRM acquisition curves of all samples from the lacustrine phase can be decomposed into three components (Fig. 2.4b). Specifically, the dominant component, indicated by red lines, contribute to more than 86% of the total IRM. The dominant component of sample from 18.9 ka has a median field of 41 mT and a dispersion parameter (DP) value of 0.29. The dominant components in samples from 19.9 ka, 28.3 ka and 38.3 ka, by comparison, have much higher median fields (62-71 mT) and narrower distributions (DP = 0.18-0.19). The irFORC diagram of sample from 18.9 ka exhibit distributions spreading along the Bi (interaction field) axis up to 50 mT, with coercivity peaking at Bc (coercivity) ~10 mT. This pattern has been interpreted as typical behavior of geological pseudo-single domain (PSD) materials (e.g., Zhao et al., 2015),

or further evidenced as vortex state materials (e.g., Zhao et al., 2017). In contrast, samples from 19.9 ka, 28.3 ka, and 38.3 ka demonstrate apparent concentric contours, indicating strong magnetostatic interactions of single domain (SD) particles (e.g., Roberts et al., 2014).

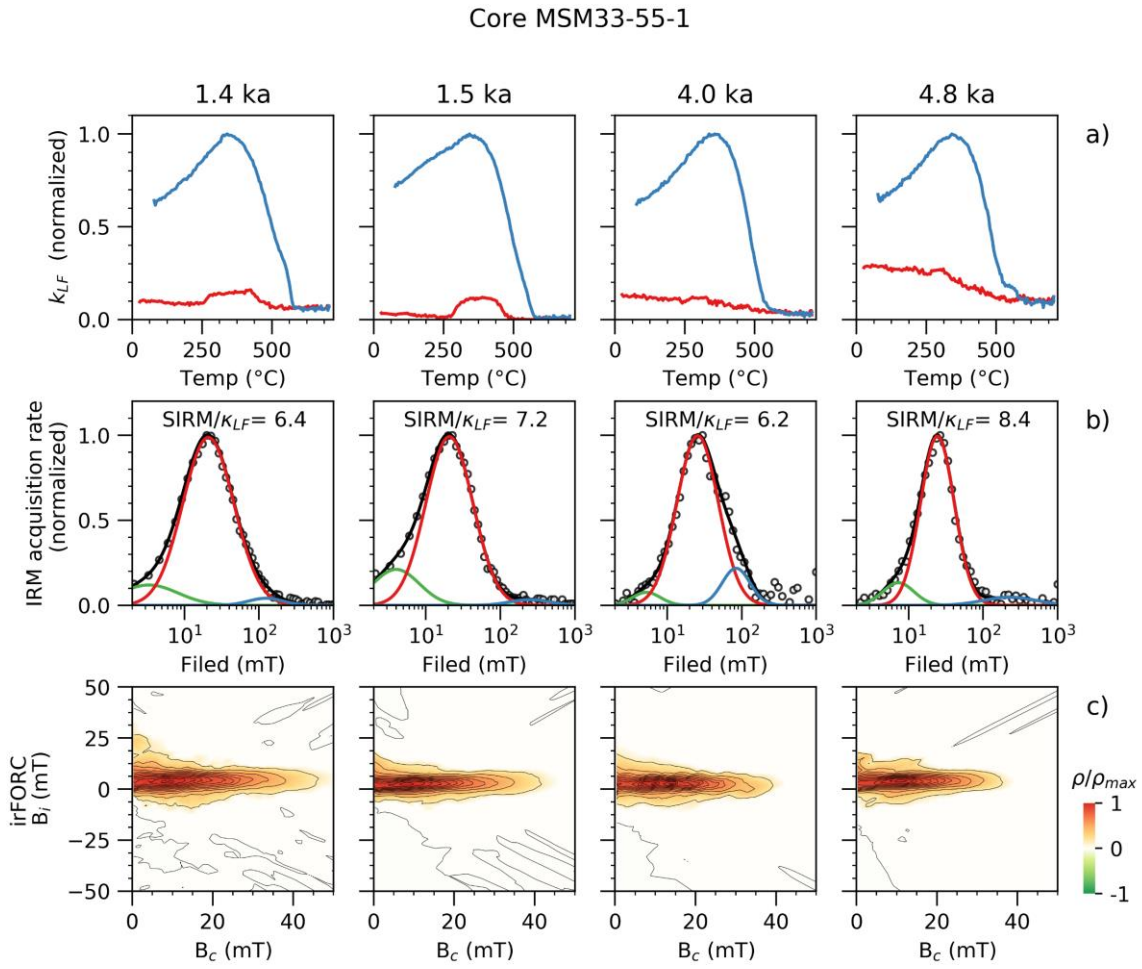

Figure 2.6 Rock magnetic results from samples selected from the marine phase (8.3-0 ka) from core MSM33-55-1. a) high-temperature magnetic susceptibility curves, b) IRM decomposition curves, c) irregular FORC (irFORC) diagrams. For more detailed figure captions please refer to Fig. 2.4 and discussion refer to chapter 2.4.4 in the text.

In Fig. 2.5, rock magnetic results are shown for samples from 8.7 ka, 14.3 ka, 15.7 ka, and 16.4 ka from the transition phase. In high-temperature κ_{LF} experiments, although the heating curves are fairly different, their cooling curves exhibit a consistent increase below about 580°C. The pattern of cooling curves likely indicates the forming of magnetite during the heating experiment. The samples from 14.3 ka, 15.7 ka, and 16.4 ka, with SIRM/κ_{LF} ratios larger than 20 kAm^{-1} have comparable IRM components and FORC diagrams. In addition, their IRM components and FORC diagrams are identical with that of samples from 19.9 ka, 28.3 ka and 38.3 ka from the lacustrine phase (Fig. 2.4). On the other hand, the sample from 8.7 ka, with

the lowest SIRM/κ_{LF} ratio of 2 kAm^{-1}, exhibits apparently different IRM components and FORC diagrams. Its dominant IRM component has a median field of about 32 mT and a DP value of about 0.4. And its irFORC diagram is similar to that of sample from 18.9 ka from the lacustrine phase, though with apparently weak distributions.

In Fig. 2.6, detailed rock magnetic analyses are shown for samples from 1.4 ka, 1.5 ka, 4.0 ka and 4.8 ka from the marine phase. Their high-temperature κ_{LF} curves exhibit no clear expression of a Curie-temperature during heating (Fig. 2.6a). Nevertheless, the rise in κ_{LF} below 580°C in the cooling curves, indicating the presence/forming of magnetite, is ubiquitously observed in all samples selected from the marine phase. Their IRM acquisition curves are generally fitted with three components (Fig. 2.3b), with the dominant IRM component (red lines) occupying more than 80% of total IRM. And the dominant IRM component has a median field between 20 and 25 mT and a fitted dispersion parameter (DP) in the range of 0.23 – 0.34. Similar patterns of irFORC were observed for all samples from the marine phase. Their irFORC diagrams exhibit coercivities peaks at about B_c ~10 mT and distributions spreading along the B_i axis between -10 and 25 mT (Fig. 2.3c). Though with fairly narrow vertical distribution, this pattern of irFORC is in contrast with the "central ridge" of biogenetic magnetite (e.g., Zhao et al., 2015) with broader spreading along B_i axis. On the other hand, the irFORC diagrams from samples from the marine phase demonstrate a comparable pattern with that of silicate hosted magnetite inclusions (e.g., Chang, Roberts, et al., 2016).

2.4.3 Scanning Electron Microscope of bulk samples

The samples from all hydrological phases (shown in Fig. 2.4-2.6) were further subjected to SEM observations. In Fig. 2.7, backscattered SEM images and EDS (energy dispersive X-ray spectroscopy) analyses on bulk material are shown for samples (from 18.9 ka, 19.9 ka, 28.3 ka, and 38.3 ka) from the lacustrine phase. In terms of EDS analyses, the ratios of Fe/S based on their weight percentages are given for all iron sulphides (Fig. 2.7g-h). Theoretically, greigite has a Fe/S ratio of 1.306, according to its molecular formula. Greigite, indicated by rock magnetic results (Fig. 2.4) and EDS analyses (Fig. 2.7g-h), is ubiquitously found in the samples from 19.9 ka, 28.3 ka and 38.3 ka (Fig. 2.7b-f). In Fig. 2.7b, greigite particles are generally aggregated in big patches (>1 mm) in the lacustrine sediments. Note, the greigite patch shown in Fig. 2.7b was expanded due to flattening on the SEM sample holder. And those greigite patches are comprised of very fine particles (Fig. 2.7b-e). In addition to greigite, titanomagnetite particles are also commonly found in the samples from 19.9 ka, 28.3 ka, and

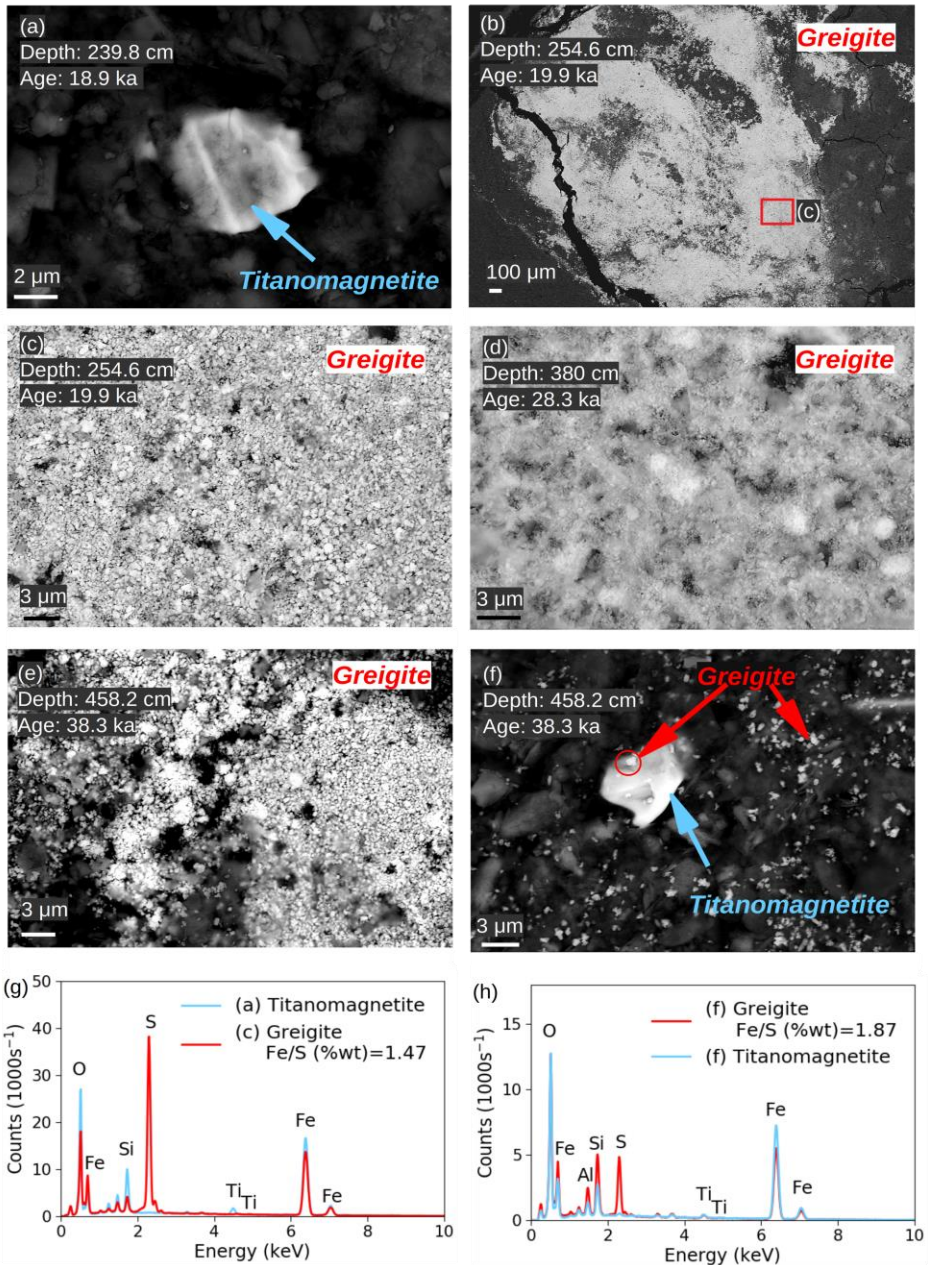

Figure 2.7 a-d) Backscattered Scanning Electron Microscope (SEM) images of selected samples from the lacustrine phase (17.5-41 ka, see Fig. 2.3). a) A titanomagnetite particle. b) Overview of a large greigite patch. c) A close-up view of b) shows an enormous amount of fine-grained greigite particles. d) and e) exhibit the common existence of fine-grained greigite. f) A particle of titanomagnetite with fine-grained greigite particles around. e-f) Selected Energy dispersive spectroscopy (EDS) analyses of particles shown in corresponding SEM images.The Fe/S (%wt) is the ratio of Fe/S based on the Mol-weight percentage given by EDS analyses. Greigite has a theoretical Fe/S ratio of 1.306.

38.3 ka. In Fig. 2.7f, a large piece of titanomagnetite with fine greigite particles in the sample from 38.3 ka is shown as an example. On the other hand, only titanomagnetite was observed in the sample from 18.9 ka (Fig. 2.7a).

The backscattered SEM images and EDS results of samples (from 8.7 ka, 14.3 ka, 15.7 ka and 16.4 ka) from the transition phase are shown in Fig. 2.8. The iron sulphides evidenced by peaks

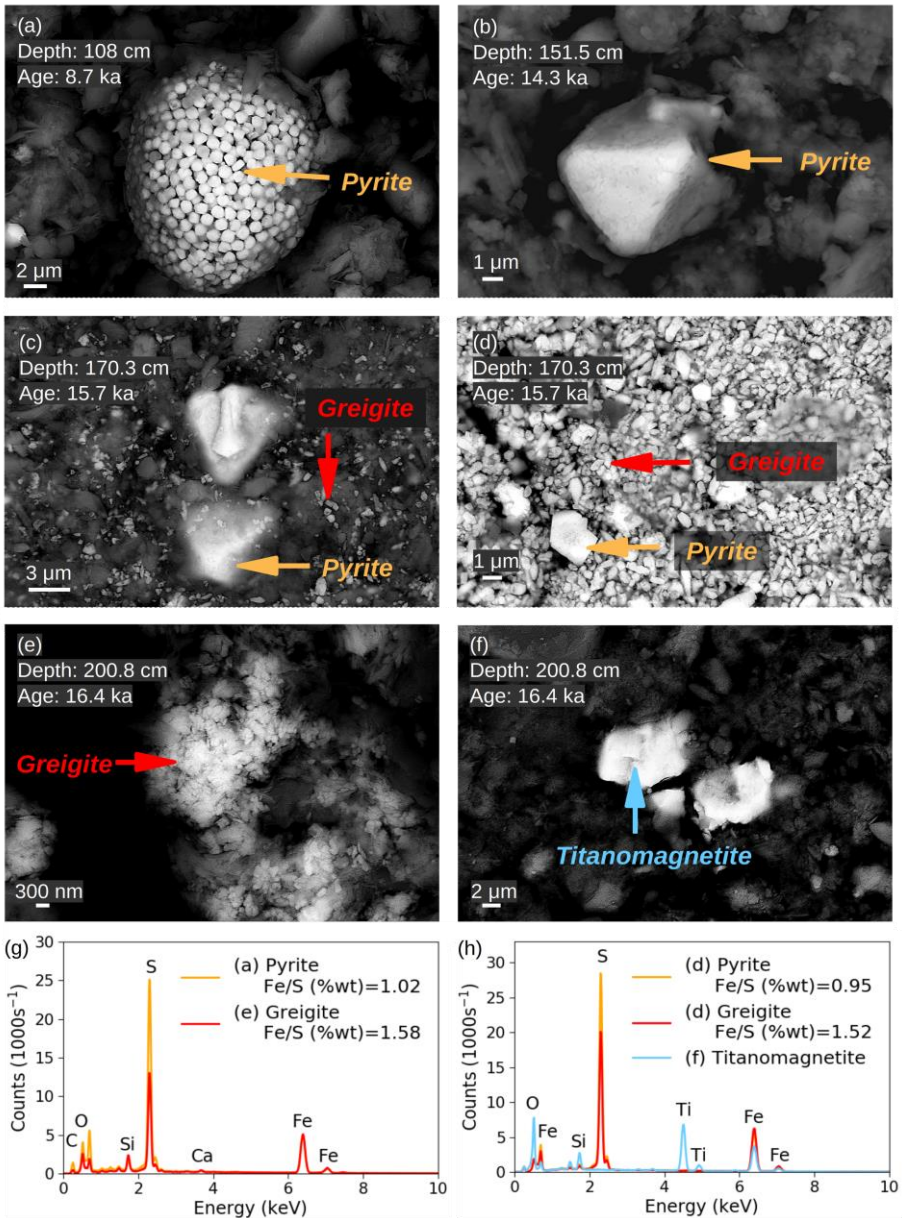

Figure 2.8 a-d) Backscattered SEM images for selected samples from transition phase (8.3-17.5 ka). a) A pyrite framboid. b) A euhedral pyrite particle. c) Coarse-grained euhedral pyrite particles together with fine-grained greigite particles. d) Coarse-grained pyrite and fine-grained greigite particles. e) Irregular greigite particles. f) Titanomagnetite particles. e-f) Selected EDS analyses of crystals shown in corresponding SEM images. Pyrite and greigite have theoretical Mol-weight Fe/S ratios of 0.871 and 1.306, respectively.

of sulphur (S) in EDS results are prevailing in all samples from the transition phase (Fig. 2.8e-f). For the iron sulphides in samples from the transition phase, their Fe/S ratios are indicated in the EDS figures (Fig. 2.8g-h). Note, pyrite and greigite have theoretical Fe/S ratios of 0.871 and 1.306 (Mol-weight), respectively. In the sample from 16.4 ka, greigite was often observed with irregular shapes (Fig. 2.8e). Besides, titanomagnetite particles were also found in this sample. In the sample from 15.7 ka (Fig. 2.8c-d), both greigite and pyrite particles were evidenced by EDS analyses (Fig. 2.8h). Notably, pyrite is generally observed as large

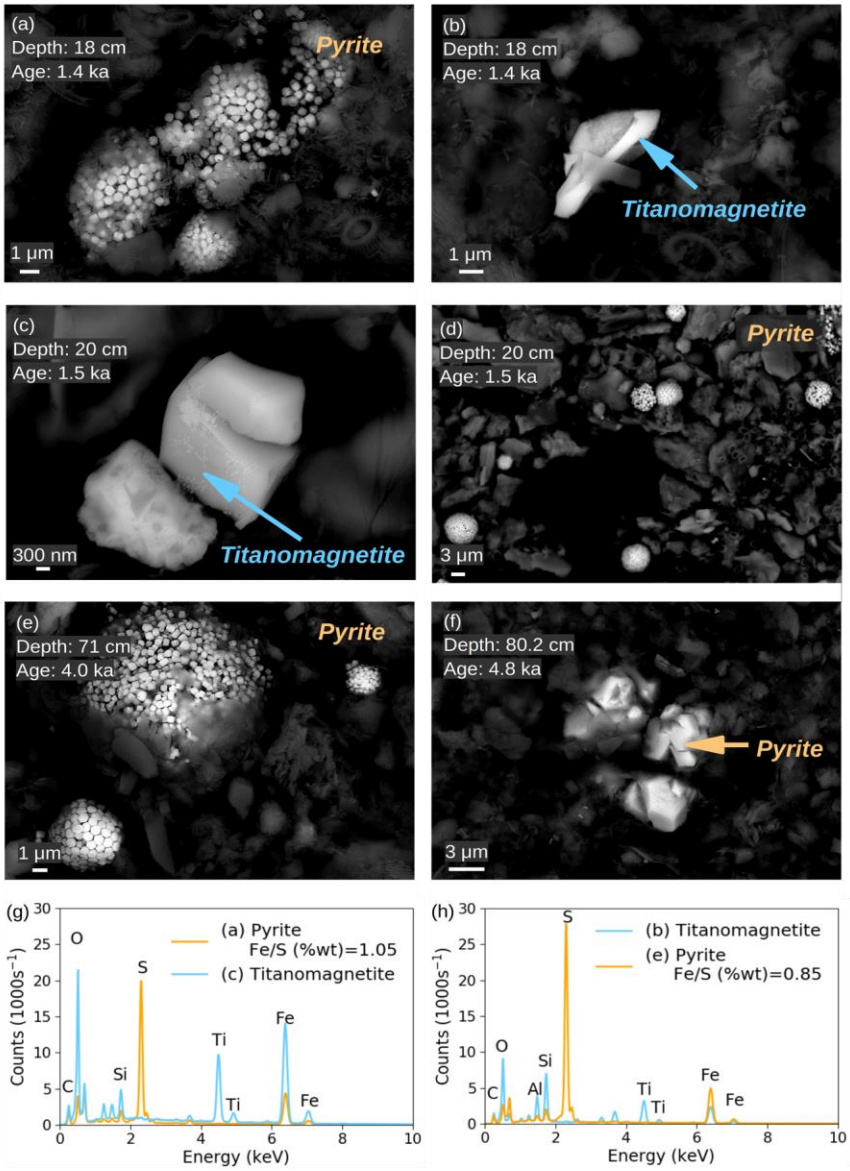

Figure 2.9 a-f) Backscattered SEM images of selected samples from marine phase (0-8.3 ka). a) Collapsed pyrite framboids. b) and c) fine-grainsized titanomagnetite particles. c) and e) Pyrite framboids with a variety of grainsizes. f) Irregular shaped pyrite particles. g-h) EDS analyses of minerals indicated in the SEM images. Pyrite has a theoretical Mol-weight Fe/S ratio of 0.871.

grainsized euhedral and irregular particles, while greigite is present as much finer grainsized irregular shapes (Fig. 2.8c-d). In the sample from 14.3 ka, euhedral pyrite particles were prevalently observed (Fig. 2.8b). Pyrite framboids are in dominant in the sample from 8.7 ka (Fig 8a).

In Fig. 2.9, backscattered SEM images and EDS analyses are shown for samples (from 1.4 ka, 1.5 ka, 4.0 ka and 4.8 ka) from the marine phase. Note, pyrite has a theoretical Fe/S ratio of 0.87. Ubiquitous forming of pyrite framboids were evidenced in all samples from the marine phase. These results are coinciding with previous studies from the Holocene Black Sea

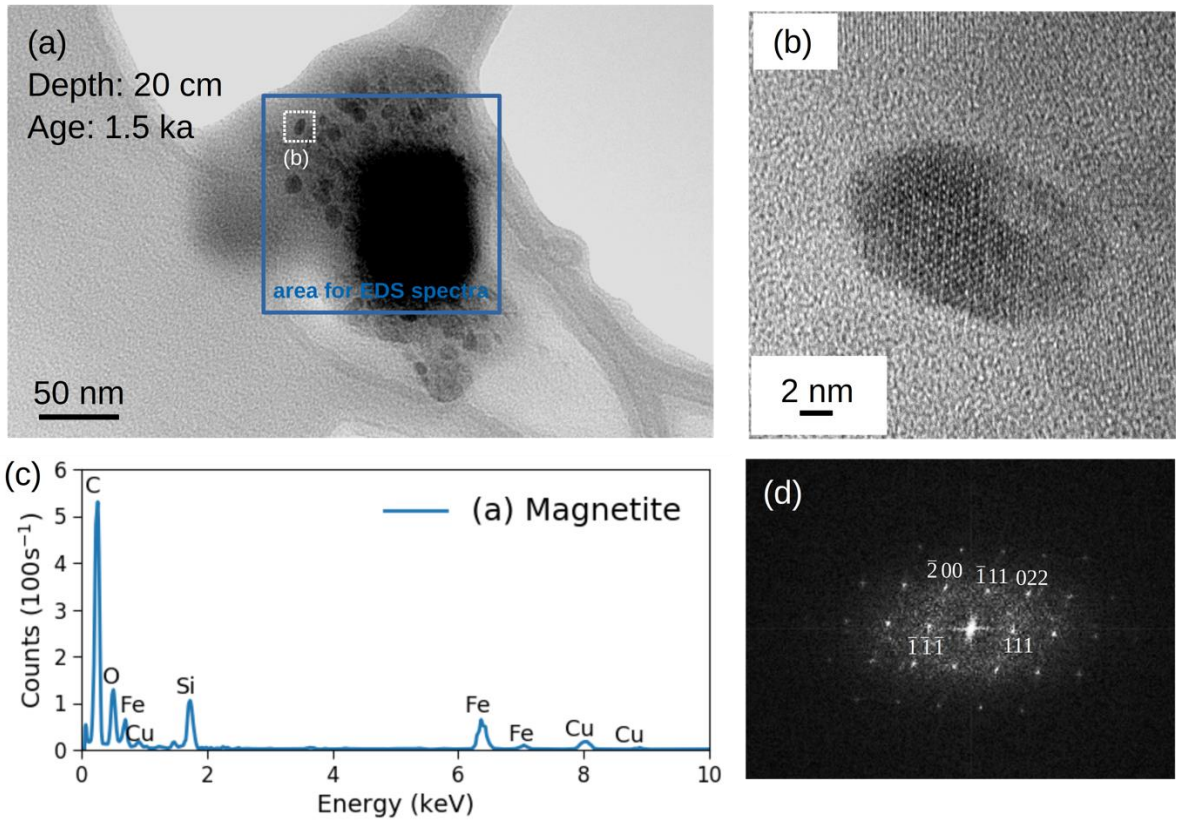

Figure 2.10 a) Bright-field transmission electron microscope (TEM) image of magnetic extracts from the sample from 1.5 ka. b) lattice fringe image from a single crystal in a). c) EDS analyses of the area in a) indicate the magnetite and silicate. Note the peaks of copper (Cu) and carbon (C) are due to the copper grid and carbon film of sample holder, respectively. d) Indexed diffraction pattern (FFT) taken from the area in b). The diffraction pattern (FFT) yields values of 36.0°, 35.0°, 54.5°, and 54.5° between adjacent lattice planes, indicating magnetite.

sediments (e.g., Wilkin et al., 1996; Wilkin & Arthur, 2001). In addition to pyrite framboids, some irregular pyrite particles (Fig. 2.9f) and titanomagnetite particles (Fig. 2.9b-c) were also found, though infrequently. Interestingly, besides Oxygen (O), Titanium (Ti) and Iron (Fe), the EDS analyses of titanomagnetite particles also indicate apparent peaks of silica (Si) and aluminum (Al) (Fig. 2.9g-h). This pattern of EDS results indicates those titanomagnetite particles are rich in silicates, or, probably silicate-hosted. Presumably, those titanomagnetite particles were preserved in the anoxic Black Sea due to protection by surrounding silicates (e.g., Chang, Heslop, et al., 2016).

2.4.4 Transmission Electron Microscope of magnetic extractions from the Marine phase

TEM and EDS analyses of magnetic extracts from the sample from 1.5 ka from the marine phase revealed the existence of extremely fine grainsized magnetic particles (Fig. 2.10). In Fig. 2.10a, a bright-field TEM image is shown for one magnetic particle. Obviously, this magnetic particle exhibits nanosized magnetic mineral grains embedded in host minerals (Fig. 2.10a). In

addition, the EDS analyses from this magnetic particle demonstrates peaks of Iron (Fe), Oxygen (O) and Silica (Si) (Fig. 2.10c), which denotes magnetite and silicate. Note the peaks of Copper (Cu) and Carbon (C) in the EDS analyses are due to the TEM sample holder's copper grid and the carbon film, respectively. For one magnetic mineral grain from Fig. 2.10a, its lattice fringe image is shown in Fig. 2.10b. The diffraction pattern (FFT) of the lattice fringe from Fig. 2.10b yields values of 36.0°, 35.0°, 54.5°, and 54.5° between adjacent lattice planes (Fig. 2.10d). This pattern is indicative for magnetite. Thus, the TEM and EDS analyses revealed that the particle shown in Fig. 2.10a is likely a silicate-hosted magnetite inclusion (e.g., Chang, Roberts, et al., 2016).

2.4.5 Scanning Electron Microscope of polished sections

In Fig. 2.11, backscatter SEM images are shown from polished sections of four samples from the marine, the transition and the lacustrine phases. The two samples (from 31.2 ka and 35.6 ka) are from the lacustrine phase, with SIRM/κ_{LF} ratios of 58.6 kAm^{-1} and 65.8 kAm^{-1}, respectively. Their backscattered SEM images are shown in Fig. 2.11a-f. Large crusts of iron sulphides in size of a few millimeters are sporadically observed in the two samples (Fig. 2.11a and d). An assemble of crusts of iron sulphides from sample from 31.2 ka is shown in Fig. 2.11a. A close-up view of one single crust from Fig. 2.11a clearly shows a white rim and a grey core in backscattered SEM images (Fig. 2.11b and c). The pattern of the white rim is comparable to so-called Liesegang ring structures that often observed in sedimentary rocks (Leveson, 1966). Corresponding EDS analyses for the crust indicate the Liesegang ring structure and the grey core are composed of greigite and pyrite, respectively (Fig. 2.12a). The crusts structure in Fig. 2.11a was further confirmed by EDS elementary mapping (Fig. 2.13). Another huge crust of iron sulphides from sample from 35.6 ka is presented in Fig. 2.11d. In addition to crusts of iron sulphides, titanomagnetite is commonly found in polished sections of samples from the lacustrine phase (see Fig. 2.14). In Fig. 2.11e, a large particle of titanomagnetite from 35.6 ka is shown with an apparent ilmenite skeleton. A close-up view illustrates that the large titanomagnetite particle is surrounded by fine-grained titanomagnetite grains (Fig. 2.11f, EDS analyses in Fig. 2.12b).

In Fig. 2.11g-i, backscatter SEM images of the polished section from 13.9 ka from the transition phase are shown. In this sample, pyrite was ubiquitously found in euhedral shapes with grainsizes in the ranges of a few micrometers (Fig. 2.11g). On the other hand, large irregular shaped pyrite particles were rarely observed (Fig. 2.11h). The close-up view of the pyrite cross section in Fig. 2.11h exhibits patches and cracks of iron sulphates inside the pyrite particle (Fig. 2.11i, EDS analyses shown in Fig. 2.12c).

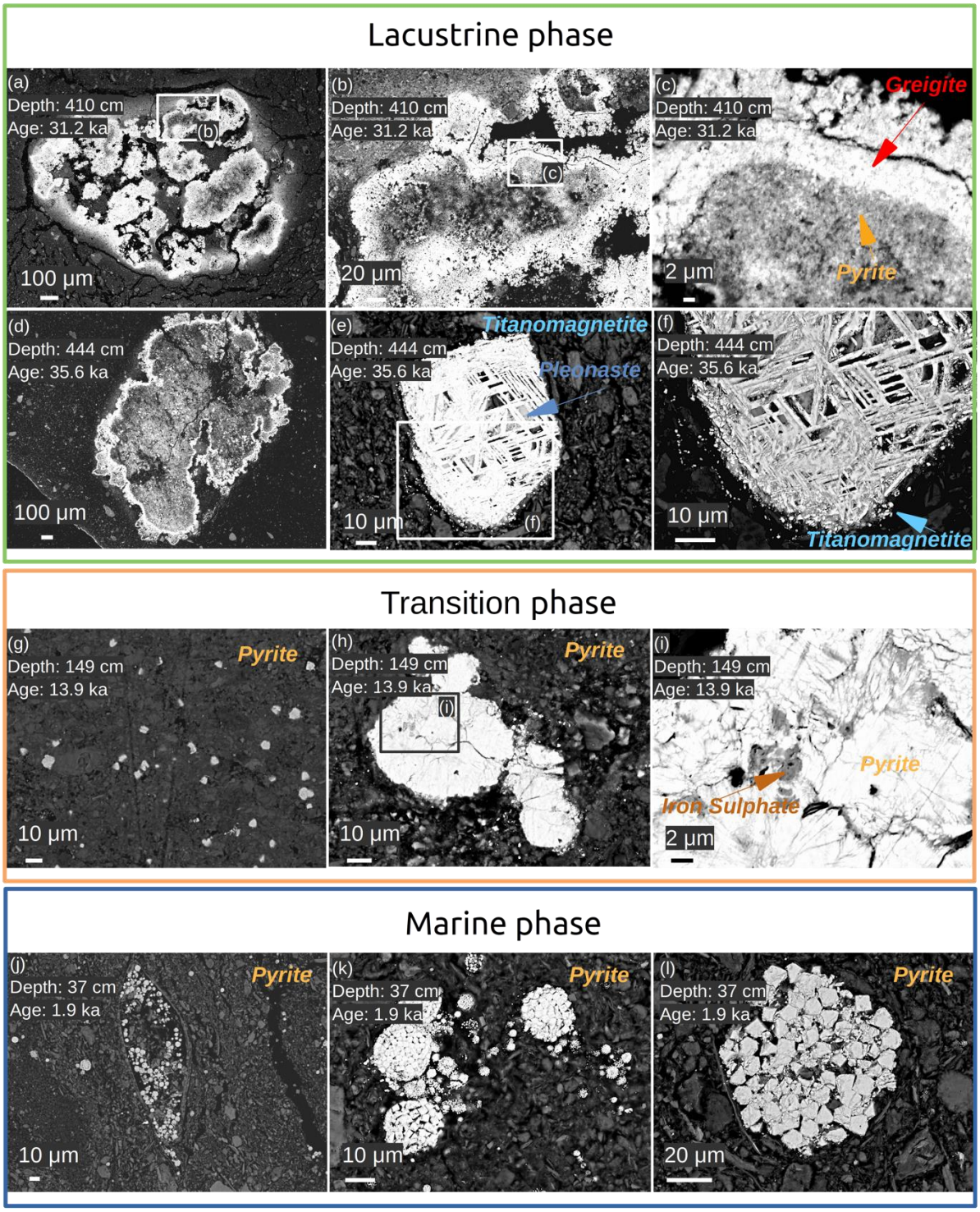

Figure 2.11 Backscattered SEM images of polished sections of samples from a-f) the lacustrine phase, g-i) the transition phase and j-l) the marine phase. a) An assemble of crusts of iron sulphides. b) A close-up view of a) exhibit one crust with a white rim and a grey core. c) Further close-up view of b) reveals greigite in the rim and pyrite in the core. d) A large crust of iron sulphides. e) Titanomagnetite with ilmenite skeleton and some pleonaste inside. f) Close-up view of the titanomagnetite in e) exhibits fine-grainsized titanomagnetite particles surrounding. g) Overview of euhedral pyrite particles dispersed in sediment. h) Cross section of a large pyrite particle. i) Close-up view of h) reveals cracks and patches of iron sulphates. j) A cluster of fine-grainsized pyrite framboids. k) Pyrite framboids with various grainsizes and shapes. l) A large pyrite framboid composed of euhedral pyrite particles.

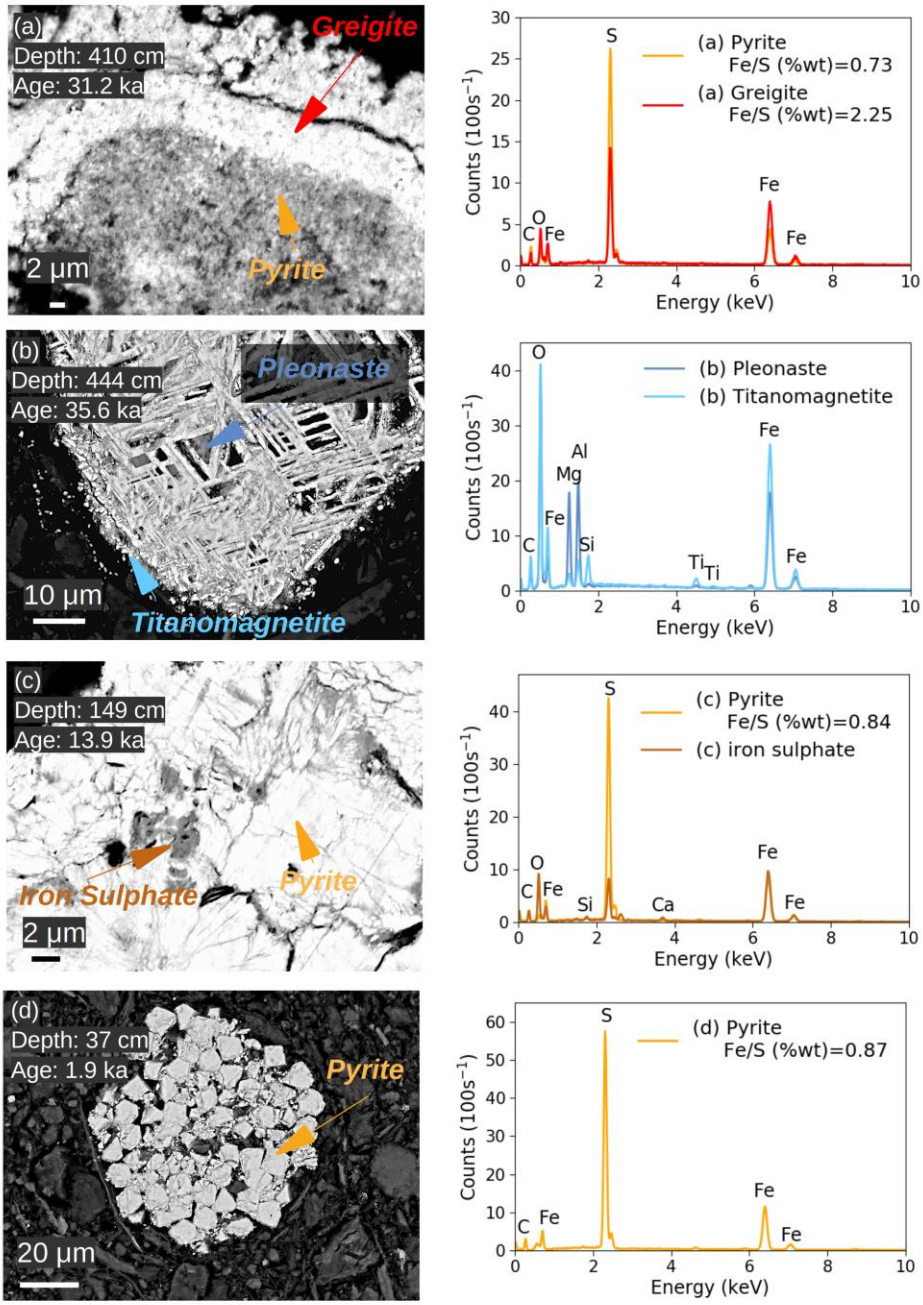

Figure 2.12 Selected SEM images of polished section (left column) from Fig. 2.11, shown together with corresponding EDS analyses (right column). a) The rim of one sulphide crust. Its EDS analyses indicate that the bright rim is greigite and the grey core is pyrite. b) Titanomagnetite with ilmenite skeleton. Its EDS analyses indicate that probably pleonaste ($(Mg,Fe)Al_2O_4$) inside and fine-grainsized titanomagnetite particles surrounding. c) Close-up view of pyrite cross-section. In addition to pyrite, some iron sulphates were also evidenced by the peaks of iron (Fe), sulphur (S), and oxygen (O) in the EDS results. However, it is not possible to determine the specific type of the iron sulphates. d) A cross-section of pyrite framboid. Pyrite and greigite have theoretical Mol-weight Fe/S ratios of 0.871 and 1.306, respectively.

For the polished section of sample from 1.9 ka from the marine phase, SEM and EDS analyses indicate ubiquitous pyrite framboids (Fig. 2.11j-l, EDS analyses shown in Fig. 2.12d).

Backscatter SEM images of this sample demonstrate that pyrite framboids have diameters ranging from a few hundred nanometers (Fig. 2.11j,k) to about dozens of micrometers (Fig. 2.11k,l). In contrast to the size of pyrite framboids (with a narrow size distribution and maximum size <18 μm) reported by Wilkin et al. (1997) and Wilkin & Arthur (2001), the pyrite framboids found in this study show larger size distributions (Fig. 2.11j-l). Additionally, nanosized pyrite particles were commonly observed inside cross-sections of all pyrite framboids (Fig. 2.11k,l).

2.5 DISCUSSION

Lacustrine phase (41 – 17.5 ka B.P)

Between 41 ka and 17.5 ka, the Black sea experienced several variations in lake level, primary productivity and salinity due to stadial/interstadial oscillations (Wegwerth et al., 2016, 2015). Nevertheless, the Black Sea was an isolated freshwater lake for this time interval (e.g., Constantinescu et al., 2015; Major et al., 2006; Soulet et al., 2010; Wegwerth et al., 2016). In sediments from this lacustrine phase, detailed rock magnetic and SEM-EDS analyses indicate magnetic minerals in samples with SIRM/κ_{LF} ratios lower than 10 kAm^{-1} are exclusively titanomagnetite. On the other hand, samples with SIRM/κ_{LF} ratios larger than 10 kAm^{-1} have both greigite and titanomagnetite. Specifically, greigite was generally found together with pyrite in crustal aggregates (Fig. 2.11.a-d). Since titanomagnetite was also common in these greigite bearing samples (Fig. 2.11e-f, sell also Fig. 2.14), the crusts of iron sulphides were highly likely formed in localized reducing micro-environments. The localized formation of pyrite/greigite, together with preservation of iron oxides in unaffected parts of the sediments, was previously reported in local sulphate-rich sediments from the Lake Baikal, Russia (e.g., Demory et al., 2005). Roberts (2015) also presented iron sulphide (euhedral pyrite) aggregates that formed in sulphidic microenvironments within otherwise oxic sediments, though from unknow provenance. Roberts (2015) suggested such sulphidisation occurred around isolated pieces of decaying organic matter in environments where the overall supply of organic matter was insufficient to drive sulphidisation of the entire sediment volume. Additionally, the so-called Liesegang ring (white rim in backscatter SEM images) was observed in all crusts of iron sulphides from samples from the lacustrine phase (Fig. 2.11a-d). Their corresponding EDS analyses (Fig. 2.12, Fig. 2.13) revealed that the Liesegang rings and grey cores are composed of greigite and pyrite, respectively. Allen (2002) suggested that, in iron-rich environments, pyrite formation is confined to the decaying organism, and the Liesegang effect is limited due to the restricted diffusion of dissolved sulphide. Thus, the crusts of iron sulphides in the

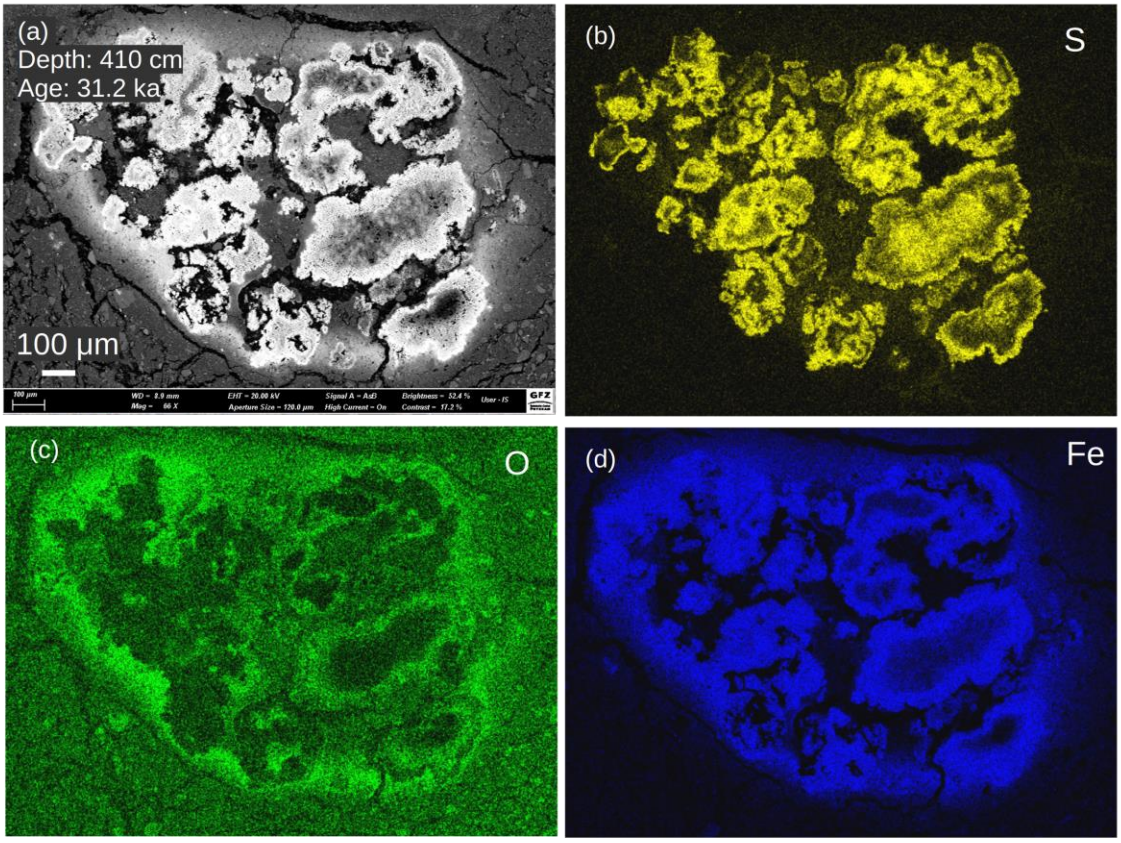

Figure 2.13 Backscattered SEM images of polished sections of samples from 31.2 ka. And EDS digital images of elements b) S, c) O and d) Fe.

lacustrine Black Sea sediments were likely formed in sulphide restricted micro environment due to decaying of organic matters.

Transition phase (17.5 – 8.3 ka B.P)

From 17.5 ka to 8.3 ka, the Black Sea had experienced a series of changes in input sources and hydrological conditions. Between 17.5 ka and 14.5 ka, the water level of the Black Sea was rising due to melt water pulses, presumably from a northern source (Bahr et al., 2006; Soulet et al., 2013). At about 14.5 ka, with the onset of the Allerød/Bølling warm period, a drastic shift of water chemistry in the Black Sea was evidenced by $\delta^{18}O$ and XRF-data records (Bahr et al., 2008, 2006; Shumilovskikh et al., 2012). After about 14.5 ka, due to the cessation of the water inflow, an evaporation-driven drop of the water level in the Black Sea was inferred by Bahr et al. (2006). Specifically, the water level of Black Sea was relatively low during the warm periods of the Allerød/Bølling and the Preboreal, and was rising again during the intervening cold period of the Younger Dryas until 8.3 ka (Major et al., 2006).

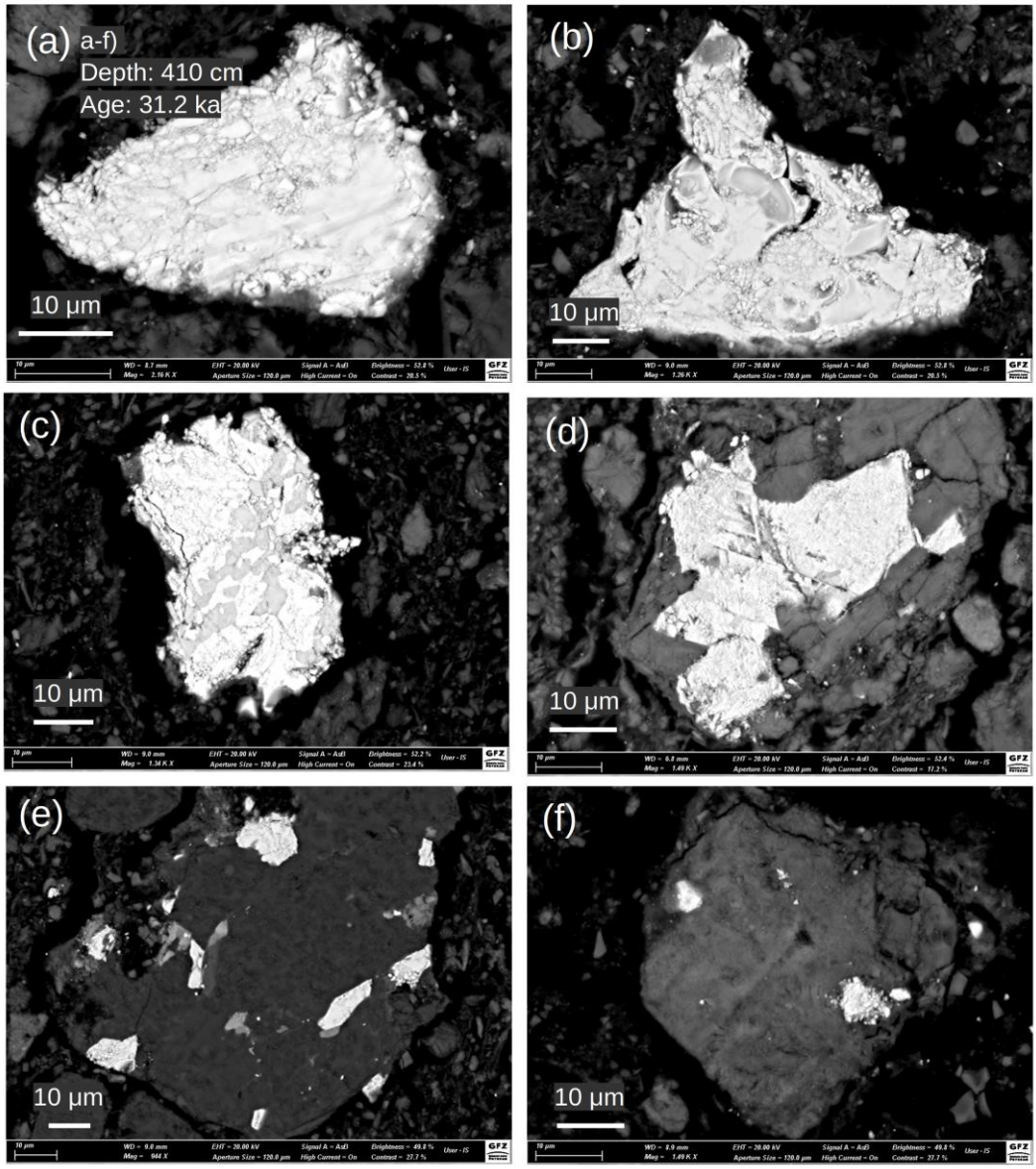

Figure 2.14 a-f) Backscattered SEM images of the polished section from 31.2 ka from the lacustrine phase. Titanomagnetite particles in various grainsizes and shapes are commonly observed.

The rock magnetic and SEM results indicate iron sulphides are commonly existing in samples from the transition phase (Fig. 2.5-7). The SEM-EDS analyses exhibit the dominance by greigite in samples before about 14.5 ka (Fig. 2.8d-e), and by pyrite in samples after 14.5 ka (Fig. 2.8a-c). The dominant iron sulphides changing from greigite to pyrite after about 14.5 ka is also imaged by the bulk rock magnetic results from the transition phase (Fig. 2.3). In addition, the obtained detailed rock magnetic results indicate comparable magnetic properties of samples from between 10.0 ka and 17.5 ka (Fig. 2.5), though with distinct variations in abundance of magnetic particles (Fig. 2.3). In contrast, rock magnetic properties of the sample between 8.3 ka and 10.0 ka are remarkably different (Fig. 2.3, 2.6). Although no magnetic minerals were observed by SEM, the irFORC diagram of sample from 8.7 ka (Fig. 2.5) demonstrate a similar

pattern with that of the titanomagnetite sample from 18.9 ka from the lacustrine phase (Fig. 2.4). However, this interval (~10.0-8.3 ka), shortly before the Mediterranean Sea water ingression, is likely representing the sulfurization front due to sulphide diffusion after the forming of anoxia in the Black Sea (Neretin et al., 2004). Since pyrite framboids were ubiquitously observed in the sample from 8.7 ka (Fig. 2.8a), the magnetic minerals preserved in this interval are probably similar to the silicate-hosted magnetite/titanomagnetite particles in the sediments from the marine phase (see discussion for the Marine phase below). Nevertheless, magnetic properties (e.g., FORC diagrams, κ_{ARM}/κ_{LF}) from samples from this interval (Fig. 2.3,6) and from the marine phase (8.3-0 ka, Fig. 2.3,8) indicate distinct grainsizes. This is likely due to changes in input source after the ingression of Mediterranean Sea water at about 8.3 ka.

Marine phase (8.3 – 0 ka B.P)

After the Mediterranean Sea water ingression at about 8.3 ka, the anoxia in the Black Sea was gradually established (e.g., Eckert et al., 2013), and was favorable for the syngenetic formation of pyrite framboids (e.g., Wilkin & Arthur, 2001). Although biogenetic greigite chains were reported in concretionary methane-seep carbonates in the modern Northwest Black Sea (Reitner et al., 2005), no biogenetic particles were observed in this study. In addition, the studied cross-sections of pyrite framboids shown in Fig. 2.11k,l further revealed that only pyrite particles within these framboids (Fig. 2.12d). On the other hand, titanomagnetite (Fig. 2.9b,d) and silicate-hosted magnetite inclusions (Fig. 2.10) were evidenced in samples from the marine phase by SEM and TEM analyses, respectively.

Particularly, the titanomagnetite is generally characterized by the presence of the silica (Si) peak in the EDS analyses (Fig. 2.9g-h). The pattern probably indicates those titanomagnetite/magnetite are hosted by silicates, which in turn favored their survival in sulphate-rich water conditions (e.g., Chang, Heslop, et al., 2016). In Addition, rock magnetic results (e.g., irFORC diagrams, Fig. 2.6d) of samples from the marine phase exhibit comparable patterns with that of silicate-hosted magnetite inclusions in marine sediments from global sites (e.g., Chang, Roberts, et al., 2016).

2.6 CONCLUSIONS

In the studied Black Sea sediments, the preserved magnetic minerals reflect the changing water conditions throughout the past 41 ka, as well as the variations in the habitus of pyrite after about 17.5 ka. For the lacustrine phase (41.5-17.5 ka), magnetic minerals are dominated by mixtures of greigite and titanomagnetite in samples with $SIRM/\kappa_{LF}$ larger than10 kAm^{-1}, or

exclusively by titanomagnetite in samples with SIRM/κ_{LF} less than 10 kAm^{-1}. Specifically, greigite was generally observed together with pyrite in crustal aggregates with so-called Liesegang ring. In addition, SEM-EDS analyses revealed the Liesegang ring and its core are composed of greigite and pyrite, respectively. These crust structure of iron sulphides likely indicates sulphide restricted pyritization in localized reducing environments due to the decaying of organic matters in the lacustrine Black Sea sediments.In sediments from the transition phase (17.5 -8.3 ka), magnetic minerals were significantly changing from greigite to probably silicates-hosted titanomagnetite at about 10.0 ka. In addition to magnetic minerals, SEM-EDS results illustrate abrupt increasing of euhedral pyrite after about 14.5 ka and ubiquitous pyrite framboids after about ~10.0 ka.For the marine phase (8.3-0 ka), the anoxic Black Sea was favorable for the formation of pyrite framboids. Nevertheless, some silicate-hosted titanomagnetite/magnetite particles were evidenced by SEM and TEM analyses.

Thus, the varying occurrences of different varieties of iron oxides and iron sulphides, revealed by this study, demonstrates the complexities of diagenetic processes in changing environments like in the waterbody of the Black sea basin. In addition, the SIRM/κ_{LF} ratio $\leq$10 kAm^{-1} was proved to be a useful criterion to exclude greigite bearing samples from paleomagnetic studies in the lacustrine Black Sea sediments.

ACKNOWLEGEMENTS

We thank Anja Schreiber and Sacha Plewe for preparing TEM and SEM samples respectively. And we thank S. Plewe, M. Duwe, T. Moldenhawer, and F. Brendel for their technical and logistical help during processing and sub-sampling of the cores. We also thank the captain and crew of *RV Maria S. Merian*, cruise MSM33, for their efforts in providing optimal scientific working conditions. This work was partly funded by the German Research Foundation (Deutsche Forschungsgemeinschaft, DFG SPP 1266 “INTERDYNAMIC” grants AR 367/9-1 and AR 367/9-2), the Gary Comer Science and Education Foundation, U.S.A., and the Chinese Scholarship Council (CSC grant No. 201506180060).

3 A high-resolution paleosecular variation record from Black Sea sediments indicating fast directional changes associated with low field intensities during marine isotope stage (MIS) 4

Published in Earth and Planetary Science Letters 484 (2018), 15-29

Norbert Nowaczyk [1], Liu Jiabo [1], Ute Frank [1], Helge W. Arz [2]

[1] GFZ German Research Centre for Geosciences, Section 'Climate Dynamics and Landscape Evolution', 14473 Potsdam, Germany.

[2] Leibnitz Institute for Baltic Sea Research Warnemünde, 18119 Rostock, Germany.

ABSTRACT

A total of nine sediment cores recovered from the Archangelsky Ridge in the SE Black Sea were systematically subjected to intense paleo- and mineral magnetic analyses. Besides 16 accelerator mass spectrometry (AMS) ^{14}C ages available for another core from this area, dating was accomplished by correlation of short-term warming events during the last glacial monitored by high-resolution X-ray fluorescence (XRF) scanning as maxima in both Ca/Ti and K/Ti ratios in Black Sea sediments to the so-called 'Dansgaard-Oeschger events' recognized from Greenland ice cores. Thus, several hiatuses could be identified in the various cores during the last glacial/interglacial cycle. Finally, core sections documenting marine isotope stage (MIS) 4 at high resolution back to 69 ka were selected for detailed analyses. At 64.5 ka, according to obtained results from Black Sea sediments, the second deepest minimum in relative paleointensity during the past 69 ka occurred, with the Laschamp geomagnetic excursion at 41 ka being associated with the lowest field intensities. The field minimum during MIS 4 is associated with large declination swings beginning about 3 ka before the minimum. While a swing to 50°E is associated with steep inclinations (50-60°) according to the coring site at 42°N, the subsequent declination swing to 30°W is associated with shallow inclinations of down to 40°. Nevertheless, these large deviations from the direction of a geocentric axial dipole field (I=61°, D=0°) still can not yet be termed as 'excursional', since latitudes of corresponding virtual geomagnetic poles (VGP) only reach down to 51.5°N (120°E) and 61.5°N (75°W), respectively. However, these VGP positions at opposite sides of the globe are linked with VGP drift rates of up to 0.2° per year in between. These extreme secular variations might be the mid-latitude expression of a geomagnetic excursion with partly reversed inclinations found at several sites much further North in Arctic marine sediments between 69°N and 81°N. Thus,

the pronounced intensity minimum at 64.5 ka and described directional variations might be the effect of a weak geomagnetic field with a multi-polar geometry in the middle of MIS 4.

KEYWORDS

paleosecular variation, geomagnetic excursion, magnetostratigraphy, Black Sea, XRF-scanning

3.1 INTRODUCTION

Geomagnetic field variations on a geological time scale show a wide range of directional and intensity variations comprising secular variation, excursions, and reversals (e.g., Gubbins, 2008; Roberts, 2008), mathematically often described by time-dependent spherical harmonics (e.g., Shao et al., 1999). This set of functions is a powerful tool to mathematically describe any kind of geomagnetic field variations at the Earth's surface, and even at the core-mantle boundary, per definition, by multipole sources in the centre of the Earth. However, the geophysical process of field generation, the so-called geodynamo, convection of conducting metallic material is occurring eccentrically only within the Earth's liquid outer core. Moreover, these physical processes cannot be separated into pure dipole-related and pure non-dipole-(multipole-) related convection processes. The radial decay of multipoles (including dipoles) is given by $r^{-(n+2)}$, with n being the degree of the multipole (n=1: dipoles, n=2: quadrupoles, n=3: octupoles, etc.). Thus, with increasing distance from the geodynamo sources the (mathematical) dipole term dominates more and more relative to the multipole contributions. On the other hand, with decreasing distance, the contributions of multipole terms (mathematically) dominate the field geometry. The downward continuation of spherical harmonics can be used to quantify the geomagnetic field at the core mantle boundary, that is, at the very top of the geodynamo. The temporal development of spherical harmonics at the core mantle boundary then can be used to derive a description of the real physical processes of the geodynamo (e.g., Gubins & Bloxham, 1987; Maus et al., 2008). Thus, in order to understand the physics of the geodynamo and its expressions at the Earth's surface in form of secular variation, excursions, and reversals, high-quality paleomagnetic data is required from sites all over the globe on long timescales. The Holocene period is one of the best studied time interval of past geomagnetic field variation (e.g., Lund, 1996; Snowball et al., 2007; Zheng et al., 2014), whereas older time windows are rarely covered at a temporal resolution that is high enough to resolve secular variation features of the geomagnetic field.

In this paper we report about a paleosecular variation record from 69 to 58 ka, approximately coeval with marine isotope stage (MIS) 4. Exceptional high sedimentation rates at the continental slope off Turkey in the SE Black Sea during the last glacial favoured a high-

resolution recording of both paleoclimatic and geomagnetic field variations. One outstanding finding from six cores taken in 2007 is the record of the Laschamp geomagnetic excursion (Bonhommet & Babkine, 1967; Gillot et al., 1979; Guillou et al., 2004, Plenier et al., 2007, Laj et al., 2013). It was reproducibly found in four parallel cores from the Archangelsky Ridge (Fig. 3.1), enabling a detailed and well-dated reconstruction of extreme geomagnetic field behaviour in direction and intensity in the Black Sea area between about 43 and 39 ka, including a full but short-term reversal of the field (Nowaczyk et al., 2012, 2013). Together with other data from various locations on Earth it could be concluded that this short reversal

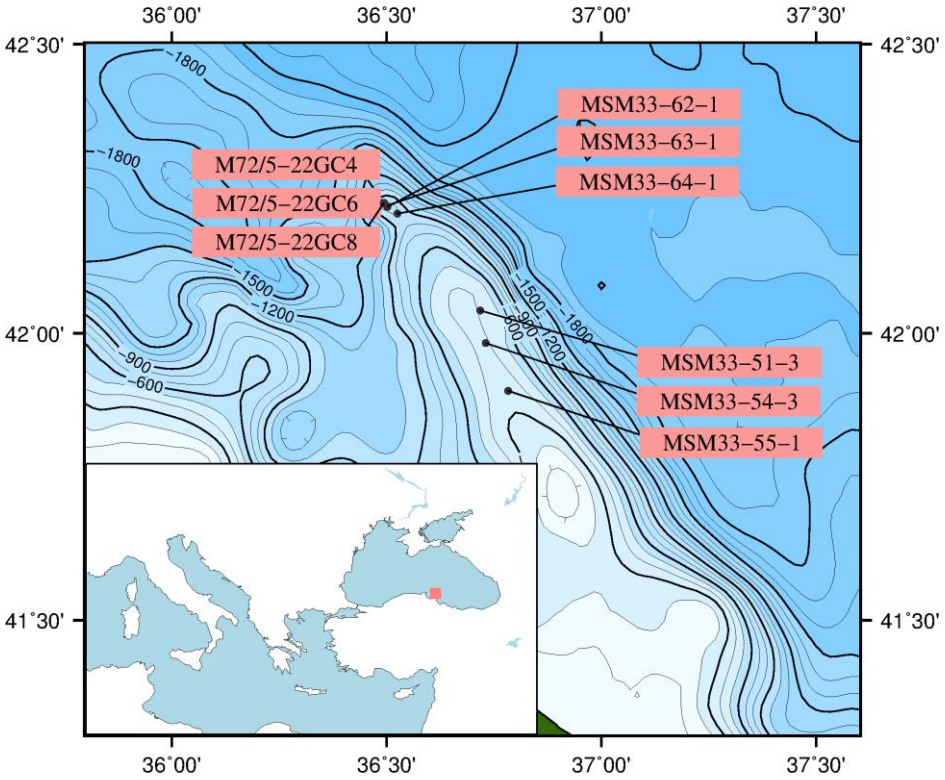

Figure 3.1 Positions of coring sites along the Archangelsky Ridge in the SE Black Sea (see inset) during cruises of *RV Meteor* (M72/5, 2007) and *RV Maria S. Merian* (MSM33, 2013).

was a global phenomenon with a reversed dipolar field configuration for a few hundred years but with a multipole geometry in the transitional phases.

With fifteen new cores recovered in 2013 much more sediment material became available. However, since the study area is tectonically very active, seismically triggered slumping down of sediment packages along the NW dipping Archangelsky Ridge caused a fairly fragmentary sedimentary record in the cores. But, due to the large number of cores covering different intervals in time, complete high-resolution composites could be created for MIS 1 to 4, and MIS 6. The Black Sea is also the world's largest anoxic basin with the consequence that certain

sedimentary sequences are impregnated with diagenetically formed ferrimagnetic greigite (Fe_3S_4; Roberts et al., 2011; Skinner, 1964), partly depending on water depth and/or time interval. Thus, not all time intervals in the Black Sea sedimentary composite are suitable for paleomagnetic studies. Almost no 'greigite contamination' was found in sediments covering most of MIS 4 which is also characterized by high sedimentation rates in the range of 20 to 35 cm ka^{-1}. Therefore, this time interval was chosen for this study in order to create a high-resolution paleosecular variation record. Another reason is that during MIS 4 a pronounced low in geomagnetic field intensity was not only observed in Black Sea sediments (Nowaczyk et al., 2013) but also worldwide (e.g., Channell et al., 2009; Laj et al., 2004). This global minimum in field intensity is coinciding with shallow to steep negative inclinations reported from northern high-latitudes, the so-called 'Norwegian-Greenland Sea excursion' (Løvlie, 1989), after the area where it was found first by Bleil & Gard (1989). It was later confirmed by Nowaczyk & Baumann (1992), Channell et al. (1997), Nowaczyk & Frederichs (1999), Nowaczyk et al. (2003), Simon et al. (2012), and Xuan & Channell (2012). It is therefore quite interesting to study how the mid-latitude geomagnetic field behaviour in the Black Sea area refers to a probable reversal of the geomagnetic field restricted to high latitudes. The analysis of such a non-dipolar (multipole) configuration of the geomagnetic field is important in understanding the general behaviour of the geodynamo throughout time and its expression at various latitudes and longitudes.

3.2 MATERIAL AND METHODS

3.2.1 Sediment coring

The Archangelsky ridge in the south-eastern Black Sea has been in the focus of scientific drilling several times. During two cruises, of German research vessels *RV METEOR* in 2007 (M72/5) and *RV Maria S. Merian* in 2013 (MSM33), respectively, a total of 21 gravity and piston cores, each with 12 cm diameter and lengths between 6.8 and 10.3 m were recovered from various water depths between 362 m and 847 m. The obtained sediments were studied first for their sedimentologic and paleoclimatic records. In this paper, paleo- and rock magnetic records from nine of these cores (Fig. 3.1 and Table 1.1) are discussed in some detail.

3.2.2 X-ray fluorescence (XRF) scanning

X-ray fluorescence (XRF) scanning were performed on split archive core halves. M72/5 cores were processed at the MARUM lab of Bremen University, Germany, using an Avaatech XRF core scanner configured with an Amptek detector. Counts of major elements were obtained every 1 to 2 cm with an integration time of 15 s and a X-ray current of 0.15 mA (Röhl and Abrams, 2000). MSM33 cores were processed at the Leibnitz Institute for Baltic Sea Research

Warnemünde, Rostock, Germany, using an ITRAX XRF Core Scanner (COX Analytics; e.g., Croudace et al., 2006). The core scanner was operated with a Cr-tube at 30 kV and 30 mA and a SDD Si drift detector. Exposure time was 15 seconds and downcore step size was 1 mm.

3.2.3 Paleo- and rock magnetism

All paleo- and rock magnetic investigations were performed at the Helmholtz Centre Potsdam, GFZ German Research Centre for Geosciences, Potsdam, Germany. High-resolution logs of magnetic volume susceptibility were obtained in steps of 1 mm with an automated core logger operating a Bartington MS2E sensor. For measurements the sensor is touching the split surface of the sediment cores which were covered with thin plastic foil. Every 10^{th} measurement a reference reading was obtained in air in order to monitor the sensor's drift which was then subtracted from readings on sediment. The obtained results were mainly used for correlation purposes.

Small cubic plastic boxes of 6 cm^3 were used for magnetostratigraphic investigations. In general, the boxes were pushed side by side into the sediment without a gap along the core's central axis. Partly, core segments were sub-sampled in two parallel rows of sample boxes rotated by 45° in order to achieve a higher spatial resolution (Table 1.1). In order to check the integrity of the magnetic fabric the anisotropy of magnetic susceptibility (AMS) and its bulk value, termed low-field susceptibility κ_{LF}, were determined with an AGICO Multi-function Kappabridge MFK1-A.

Measurements of the natural remanent magnetization (NRM) and the anhysteretic remanent magnetization (ARM) were performed with a cryogenic 2G Enterprises 755 SRM long-core magnetometer equipped with a sample holder for eight discrete samples. The magnetometer's in-line tri-axial alternating field (AF) demagnetizer was used to demagnetize the NRM and ARM of the samples. The NRM was determined after application of AF amplitudes of 0, 5, 10, 15, 20, 30, 40, 50, 65, 80, and 100 mT. Directions of the characteristic remanent magnetization (ChRM) were determined by principle component analysis (PCA) according to Kirschvink (1980). The error range of the ChRM is given as the maximum angular deviation (MAD). The ARM was imparted along the samples' z-axis with a static field of 0.05 mT and an AF field of 100 mT. Demagnetization then was performed in steps of 0, 10, 20, 30, 40, 50, 65, and 80 mT. The median destructive field of the ARM (MDF_{ARM}) was determined to estimate the coercivity of the sediments. The slope of NRM versus ARM of common demagnetization steps was used to determine the relative paleointensity (rPI). In general, demagnetization steps from 20 to 65 mT were used to determine the rPI.

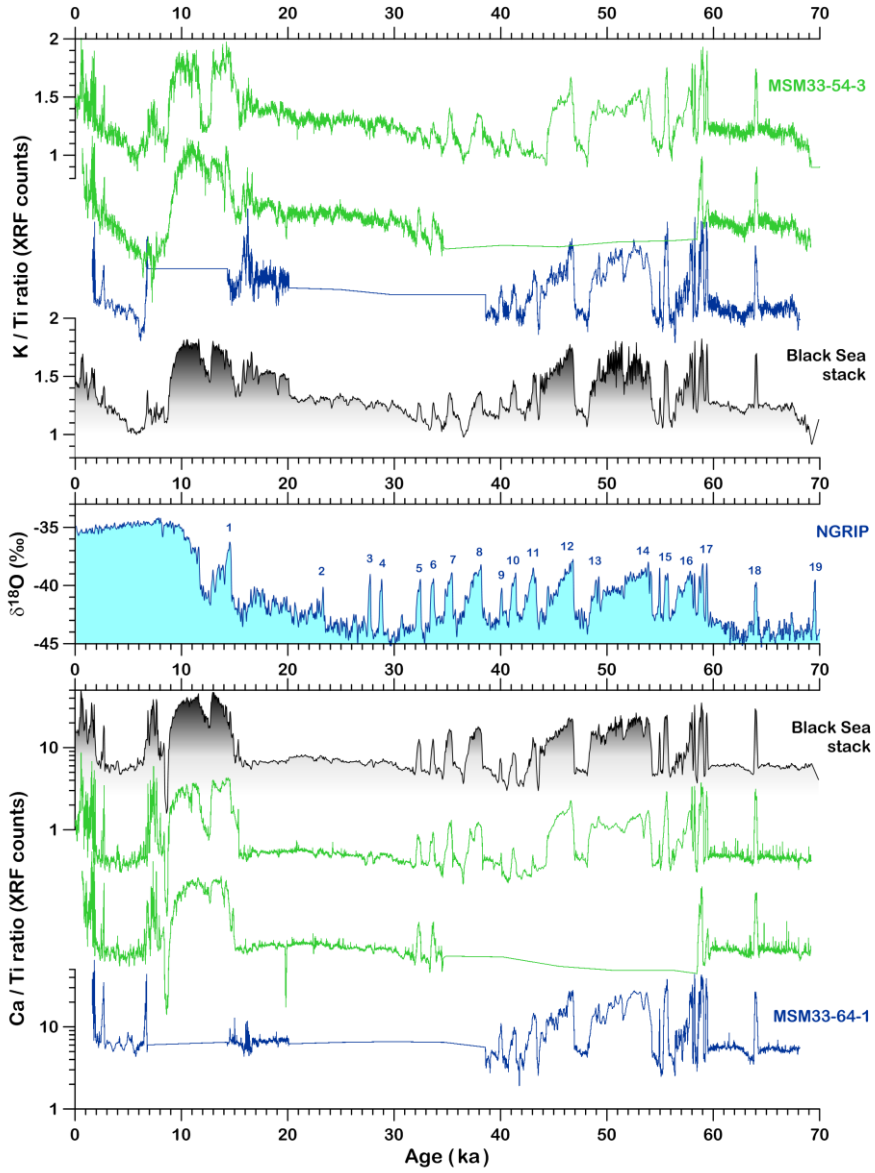

Figure 3.2 K/Ti (top, linear) and Ca/Ti (bottom, logarithmic) elemental ratios from XRF scanning, exemplarily shown from three MSM33 cores (green and blue) for the time window 0 to 70 ka, illustrating the difficulties arising from hiatuses in Black Sea sediments. Nevertheless, stacks (composites) based on all six MSM33 cores used (black), resemble major climatic variations during the last glacial, enabling a detailed correlation to the oxygen isotope record from Greenland ice cores (NGRIP; Svensson et al. 2006, 2008; blue, middle). Numbers in the NGRIP $\delta^{18}O$ plot denote Dansgaard-Oescher events (Dansgaard et al., 1993). Curves of K/Ti (Ca/Ti) ratios are all plotted with the same linear (logarithmic) axis scaling, with some axes not shown, for reasons of clarity. XRF – X-ray fluorescence.

A 2G Enterprises 660 pulse magnetizer was used to impart an isothermal remanent magnetization (IRM) along the samples' z-axes. IRMs were measured with a Molyneux spinner magnetometer, since IRM intensities often exceed the measuring range of cryogenic magnetometers. A total field of 1.5 T was used to saturate the samples. The acquired magnetization is defined as the saturated IRM (SIRM). A backfield of -0.2 T was applied in

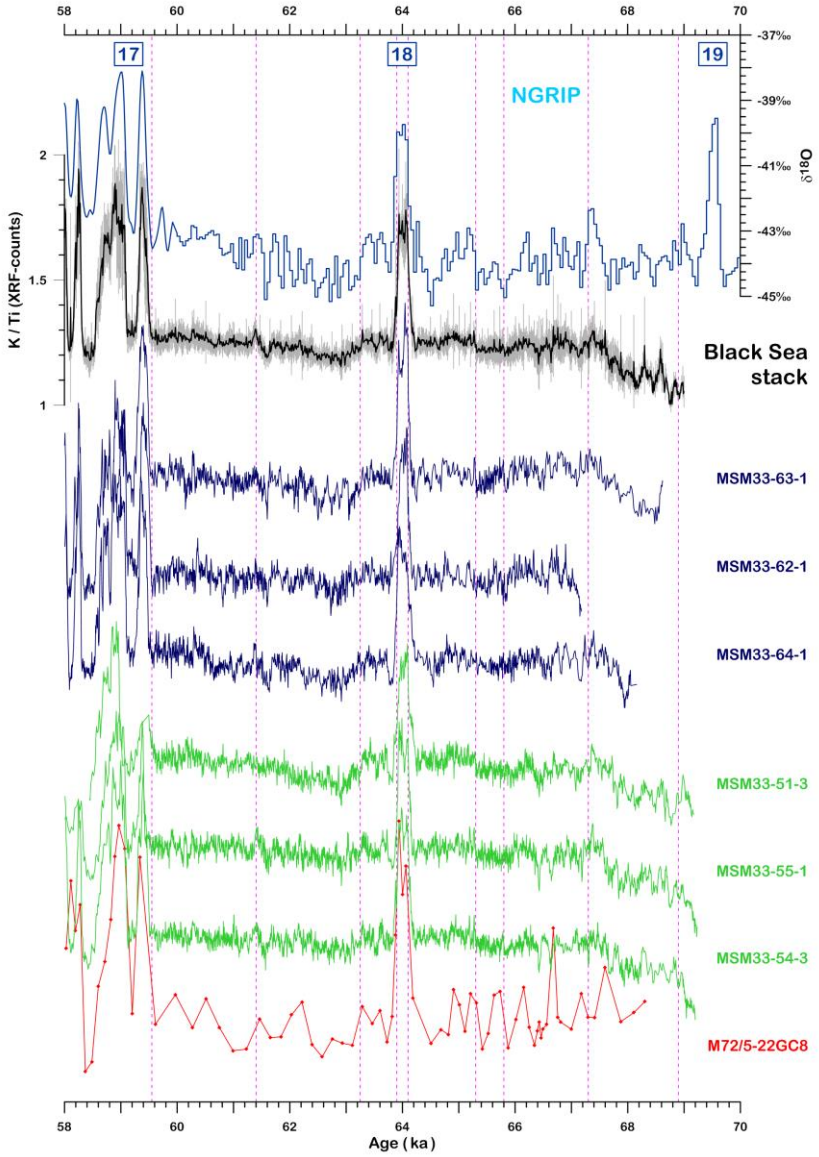

Figure 3.3 Oxygen isotope variations in Greenland ice cores (NGRIP, top; comp. Fig. 2) and K/Ti elemental ratios from XRF scanning of core M72/5-22GC8 (low-resolution, red) and six MSM33 cores (high resolution, blue and green), together with a stack (10 year bins) obtained from all cores (black) for the time window from 58 to 70 ka, roughly equivalent to MIS 4. K/Ti elemental ratios for the individual cores and the stack are plotted all with the same scaling as indicated by the axis to the left of the K/Ti stack. Vertical gray bars in the K/Ti stack denote the 1 σ standard deviation. Framed numbers in the top indicate Dansgaard-Oescher events (Dansgaard et al., 1993). Pink vertical dashed lines mark some major features used for correlation. XRF – X-ray fluorescence.

order to determine the S-ratio, defined as 0.5×(1-(IRM(-0.2 T/SIRM)). The S-ratio is close to 0 for pure haematite (Fe_2O_3) and close to 1 for both magnetite (Fe_3O_4) and greigite (Fe_3S_4). However, due to the large different coercivities of ferrimagnetic magnetite and greigite, on the one hand, and anti-ferromagnetic hematite on the other hand, the S-ratio is not linear. In order to discriminate between magnetite and greigite the ratio of saturation magnetization over magnetic susceptibility SIRM/κ_{LF} was determined. Magnetite and greigite have similar SIRMs

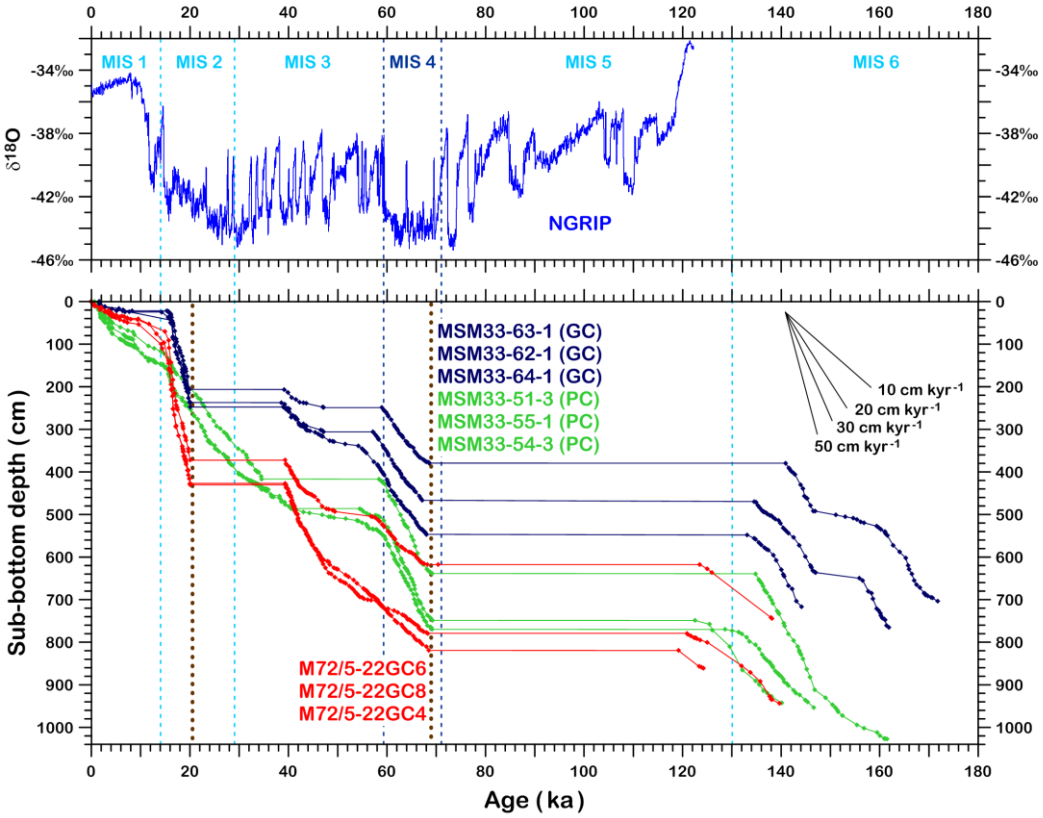

Figure 3.4 Oxygen isotope variations in Greenland ice cores (NGRIP) as the main reference record (top; comp. Fig. 2) and age models (bottom) derived so far for three cores from cruise M72/5 (red) and six cores from cruise MSM33 (green and blue). Note that age models for all cores for ages beyond 69 ka (MIS 5 and 6) are still subject of ongoing research and are thus preliminary. Brown vertical dotted lines indicate major hiatuses from about 21 to 39 ka and 69 ka to the Eemian (early MIS 5). The fan of lines in the upper right indicates the range of sedimentation rates for the studied sediment cores. GC – gravity core, PC – piston core.

but the κ_{LF} of greigite is significantly lower than that of magnetite. Thus the presence of greigite can be indicated by high SIRM/κ_{LF} ratios.

In order to further quantify the different magnetic properties of greigite and magnetite found in Black Sea sediments a few samples were subjected to detailed IRM acquisition and first oder reversal curve (FORC) experiments. Measurements were performed with a Princeton Measurements Corporation "MicroMag" alternating gradient magnetometer (AGM). IRM acquisitions curves were obtained by applying 61 logarithmically spaced field steps from 2 mT to 1 T. The IRM component analyses were calculated using the software "pyIRM", based on a gaussian mixture model, available on https://github.com/botaoxiongyong/pyIRM. The protocol and calculation of irregular FORC diagrams are following Zhao et al. (2015). The FORC diagrams were measured on an irregularly spaced field grid and calculated with a smoothing factor (SF) of 2.

3.3 RESULTS

3.3.1 Age models

For M72/5 cores it could be shown by Nowaczyk et al. (2012) that short-term warming and cooling events during the last glacial, the so-called Dansgaard-Oeschger (DO) events (Dansgaard et al., 1993), are very well reflected by various sedimentological properties of Black Sea sediments. This observation was constrained by 16 accelerator mass spectrometry (AMS) ^{14}C dating and the documentation of the Laschamp geomagnetic excursion (Bonhommet & Babkine, 1967; Laj et al., 2014; Plenier et al., 2007; Roperch et al., 1988) centred at 41 ka. Thus, dating also of MSM33 cores was achieved by tuning their high-resolution XRF logs, mainly Ca/Ti and K/Ti ratios as proxies for DO warming events, to the oxygen isotope record from Greenland ice cores using the GICC05 age model (Andersen et al., 2006; Svensson et al. 2006, 2008) and the extended intimate event stratigraphy (Blockley et al., 2014).

Similar to M72/5 cores, the sedimentary records of MSM33 cores are not complete, exemplarily shown by XRF results from three cores in Fig. 3.2 for the past 69 ka. However, taking all available data (also from M72/5 cores) into account it was possible to precisely locate several hiatuses in the individual records. Finally, a total of nine cores, three M72/5 cores and six MSM33 cores, could be selected that cover marine isotope stage (MIS) 4 completely and at high resolution with sedimentation rates in the order of 15 to 35 cm ka^{-1} (Figs. 3, 4). In the NGRIP oxygen isotope record, MIS 4 is characterized by only the single short DO event 18 in its middle part. Obviously, DO event 19 is not documented in the studied Black Sea sediments. Thus, the only subtle fluctuations throughout the major course of MIS 4 had to serve as reference. Nevertheless, it was possible to achieve detailed age models for MIS 4 in the studied cores. The correlations are strongly supported by the pronounced paleomagnetic variations in direction as well as relative paleointensity, discussed later in this paper. Fig. 3.3 shows K/Ti ratios, one low-resolution record from M72/5-22GC8, the high-resolution records from the six MSM33 cores selected for this study, and a stack into 10 year bins obtained from all cores shown in Fig 3., together with the climatic reference record from NGRIP. Obtained age models for the cores are shown in Fig. 3.4. All coring sites show a major hiatus from 69 ka back to the beginning of the Eemian (early MIS 5) or even late MIS 6. Note that the age models for ages older than 120 ka are preliminary and are still subject of ongoing work. Highest sedimentation rates of up to 50 cm ka^{-1} were determined for the time interval between about 15 and 20 ka at all sites. Paleomagnetic data from this interval will be published elsewhere. Data from around 40 ka with high sedimentation rates around 30 $cmka^{-1}$at site M72/5-22 were published in

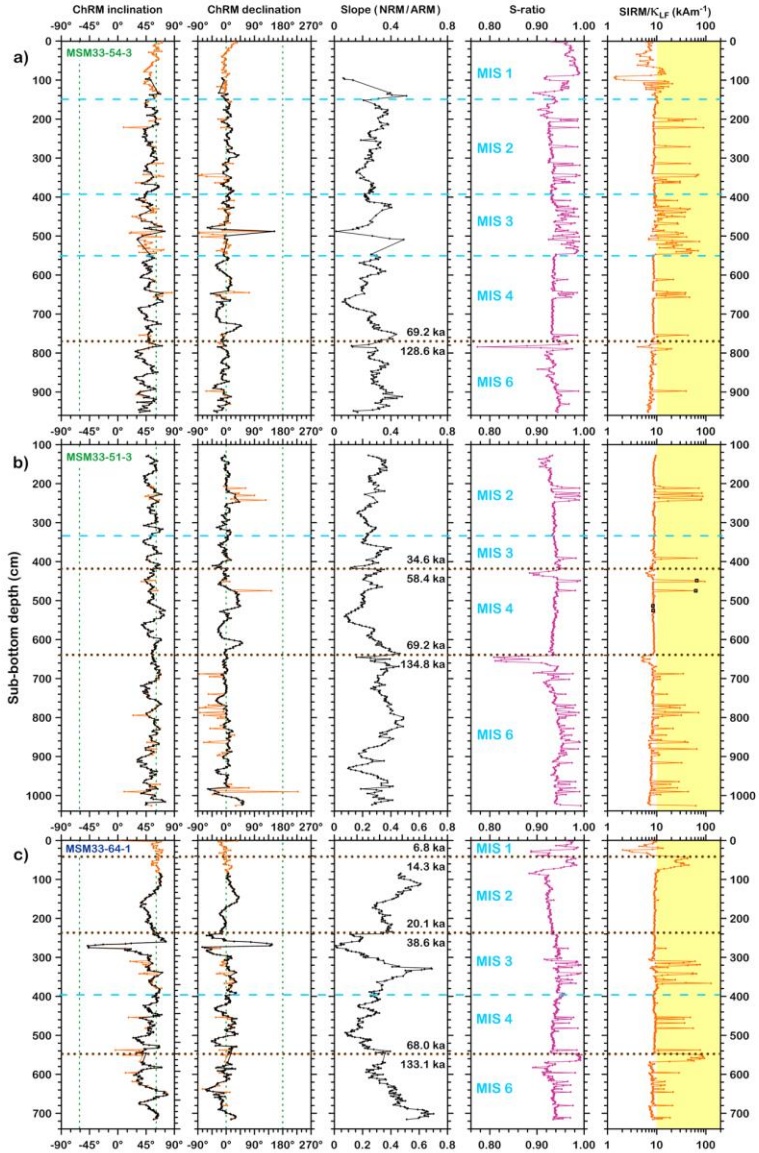

Figure 3.5 Down-core variations of paleo- and rock magnetic data from cores MSM33-54-3, MSM33-61-3, and MSM33–64-1. Black (orange) lines in the ChRM inclination and declination plots (left) represent directional data (not) filtered for greigite (see text for details). Green vertical dashed lines in the directional plots indicate the dipole inclination (±61°) and declination (0, 180°) for normal and reversed polarity, respectively. The slope of NRM versus ARM (middle), taken as proxy for relative paleointensity, was only determined for greigite-free samples. The S-ratio (pink) and the SIRM/κ_{LF} ratio (orange) in the right columns reflect magneto-mineralogic variations mainly caused by hematite (S-ratio < 0.94) and greigite (yellow areas, SIRM/κ_{LF} ratio > 10 Am^{-1}, S-ratio > 0.95) against a background of (titano-) magnetite. Blue labels and blue horizontal dashed lines indicate positions and boundaries of marine isotope stages (MIS), respectively. Brown horizontal dotted lines indicate hiatuses with black labels indicating estimated time missing in the records. Black squares in the SIRM/κ_{LF} graph in b) mark samples subjected to detailed IRM acquisition and FORC experiments (see Fig. 7). NRM – natural remanent magnetization, ARM – anhysteretic remanent magnetization, ChRM – characteristic remanent magnetization, SIRM – saturated isothermal remanent magnetization, κ_{LF} - low field magnetic volume susceptibility.

Nowaczyk et al. (2012, 2013). Paleomagnetic data from MIS 4 available from all nine cores

will be discussed here in detail.

3.3.2 Paleo- and rock magnetism

Complete magnetostratigraphic data from M72/5 cores were already presented in detail by Nowaczyk et al. (2012, 2013). Fig. 3.5 shows paleomagnetic data, ChRM directions and relative paleointensity, and selected rock magnetic data, S-ratio and the SIRM/κ_{LF} ratio, for three of the new MSM33 cores. The Laschamp excursion at 41 ka could be found only in core MSM33-64-1 with a fairly low resolution (Fig. 3.5c). In the other cores this time interval is documented only by very low sedimentation rates, is even missing as in core MSM33-51-3 (Fig. 3.5b), or is massively contaminated by greigite, as in core MSM33-54-3 (Fig. 3.5a), recognizable from high SIRM/κ_{LF} ratios. Since greigite-bearing samples often show erratic directions, consequently, paleomagnetic data was filtered using the same criteria as applied by Nowaczyk et al (2012), that is, omitting samples with SIRM/κ_{LF} ratios >10 kAm^{-1} and S-ratios >0.95. The unfiltered directional data in Fig 5 is shown by orange curves and the filtered data in black. Further on, relative paleointensity was only determined on filtered data, shown in the middle columns of Fig. 3.5. From these records, and from M72/5 data published by Nowaczyk et al. (2013) it is obvious that the middle of MIS 4 is characterized by the second lowest paleointensity of the past 69 ka, at least in Black Sea sediments. But, also other paleointensity records/stacks point to a pronounced global field low at around 65 ka (e.g., Channell et al., 2009; Laj et al., 2004).

Detailed AF demagnetization results from individual samples from this time interval from core MSM33-51-3 are shown in Fig. 3.6, with declinations after correction to a mean value of 0° for the whole core. Directional data show almost no viscous overprint and all vector endpoints migrate straight towards the origins of the diagrams. ChRM directions were generally defined from successive demagnetization steps from 20 to 65 or even to 80 mT (sample 576.1 cm in Fig. 3.6), with MAD values between 0.2° and 2.0°, sometimes 5°, reflecting very stable directions. In general, the highest MAD values were obtained for samples associated with the lowest relative paleointensity. Samples shown in Fig. 3.6 cover an interval with pronounced directional variations, especially in declination, reaching values of around 45°E (samples 576.1 cm and 513.9 cm). Inclination variations are less pronounced as indicated by the red dotted line representing the inclination of 61° for a geocentric axial dipole field (Fig. 3.6, middle). However, shallowest and steepest inclinations can be observed around the interval of lowest relative paleointensity (samples 535.7 cm and 561.9 cm, Fig. 3.6).

The IRM component analysis and irregular FORC diagrams of four selected samples from core MSM33-51-3 are shown in Fig. 3.7. Samples from 448.5 and 474.4 cm have high SIRM/κ_{LF}

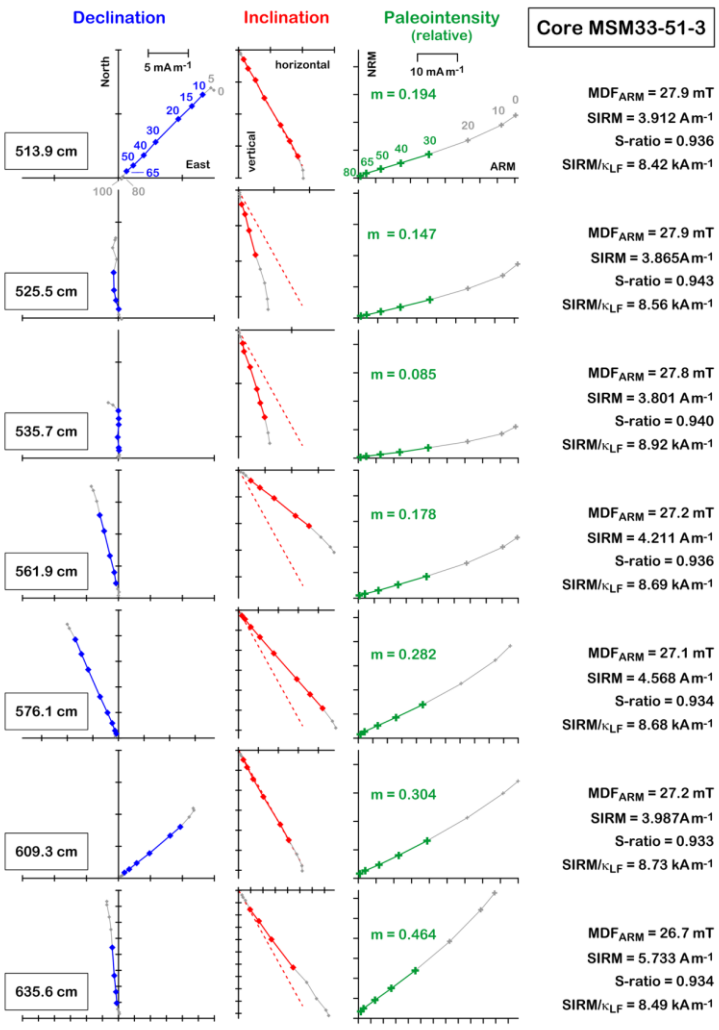

Figure 3.6 AF demagnetization results from seven samples from marine isotope stage (MIS) 4 in core MSM33-51-3, with sampling depths given at the outer left. Vector endpoint diagrams of North versus East (left, blue), illustrate variations in declination, diagrams of horizontal versus vertical component (middle, red), illustrate variations in inclination, whereas the slope (m) in diagrams of common AF steps of NRM intensity versus ARM intensity (right, green) reflects variations in relative paleointensity. Directional data is shown after adjustment of declinations from the whole core to a mean value of 0°. As shown exemplarily for (topmost) sample 513.9 cm, NRM demagnetization steps of 0, 5, 10, 15, 20, 30, 40, 50, 65, 80, 100 mT were used, whereas for the ARM demagnetization a reduced set of AF steps of 0, 10, 20, 30, 40, 50, 65, 80 mT were used. While coloured symbols (numbers) indicate data used for ChRM determination (blue, red) and paleointensity determination (green), respectively, gray small symbols (numbers) indicate raw data. The red dotted line in the inclination plots represent the inclination of 61° of a geocentric axial dipole field. Some basic rock magnetic properties are listed on the outer right. Distance of axis ticks in directional (intensity) plots is 5 (10) mAm^{-1}. Note that for reasons of clarity axes for NRM and ARM in the intensity plots (right) have different scaling, but with an identical ratio in all diagrams. NRM – natural remanent magnetization, ARM – anhysteretic remanent magnetization, MDF – median destructive field, SIRM – saturated isothermal remanent magnetization, κ_{LF} - low field magnetic volume susceptibility.

ratios of 65.5 and 62.5 kAm^{-1}, respectively, indicating single domain greigite (see also Fig. 3.5b). Samples from 513.9 and 525.5 cm have common SIRM/κ_{LF} ratios of 8.4 and 8.5 kAm^{-1},

respectively, interpreted as representing magnetite. The IRM acquisition rates of all samples can be fitted with three components. Note that all samples exhibit one dominant component (red line, Fig. 3.7). For the samples from 448.5 and 474.4 cm, the dominant IRM components occupy 76% and 87% of total IRM with a median field of 72 and 66 mT, respectively. The components have a small dispersion parameter (DP) of 0.13 and 0.17. For the samples from 513.9 and 525.5 cm, the dominant components contribute to 76% and 82% of total IRM with a median field of both 37 mT. Their distributions are broader than the ones from high SIRM/κ_{LF} ratio (greigite) samples, with DP values of 0.28 and 0.29. For all investigated samples, the secondary components indicated by green lines contribute to less than 20%, and the third component (blue lines) account for less than 5% of total the IRM. The irregular FORC diagrams demonstrate concentric contours for the samples with high SIRM/κ_{LF} ratios (448.5 and 474.4 cm), indicating strong magnetostatic interactions of single-domain particles (Roberts et al., 2014). For the samples from 513.9 and 525.5 cm, FORC distributions spreading along the B_i axis up to 50 mT denote typical "pseudo-single domain" or vortex state dominant materials (eg., Zhao et al., 2017) for magnetite samples.

In all samples from MIS 4, with SIRM/κ_{LF} ratios clearly below 10 kAm^{-1}, no acquisition of a gyro-remanent magnetization (GRM) could be observed which would be another indication for the presence of greigite. Rock magnetic parameters from MSM33 cores are similar to data published for M72/5 from the Archangelsky Ridge (Nowaczyk et al., 2012, 2013). Especially sediments deposited during MIS 4 are very homogeneous concerning composition, grain size, and concentration of magnetic minerals as shown in Fig. 3.5 and data listed in Fig. 3.6. Thus, these sediments turned out to be an ideal material to reconstruct geomagnetic field variations in the studied time interval from 69 to 58 ka (~MIS 4). Variations in direction and relative paleointensity from all investigated cores are plotted versus time in Fig. 3.8. The individual records are shown in different colours with the same scaling but with a constant offset. Although a lower temporal resolution (sedimentation rate) is partly also associated with a lower dynamic range in amplitude all cores show typical secular variation patterns in inclination and declination which can be traced from core to core quite easily. The superposition of individual data is shown in the top of Fig. 3.8, with individual data as coloured dots and Fisherian means of directions (Fisher, 1953) and arithmetic means of relative paleotintensity all shown as black curves. Mean directions and intensities were calculated for 100 year bins from 69 to 58 ka, summing up the data from a total of 586 samples. This is almost three times the amount of samples of Nowaczyk et al. (2013), providing a paleointensity stack based on 201 samples for the same time interval, but without stacking directional data.

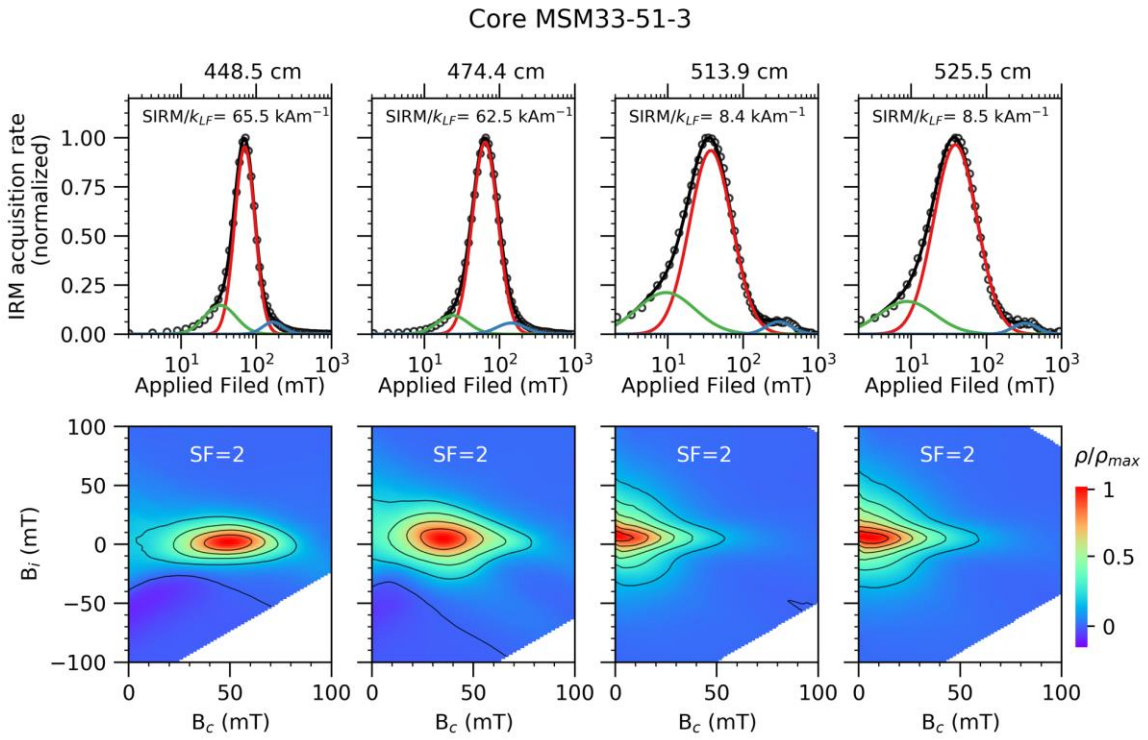

Figure 3.7 Compilation of IRM acquisition component analyses (top) and FORC diagrams (bottom) from four selected MIS 4 samples from core MSM33-51-3, representing greigite (448.5 and 474.4 cm) and magnetite (513.9 and 525.5), respectively (for stratigraphic context, see Fig. 3.5b). In the top graphs circles indicate IRM acquisition rates determined from measured data. The green, red and blue lines represent three different components fitted to these data whereas the black line is the fitted total spectrum (for details, see text). The FORC diagrams were measured on irregularly spaced field grids according to Zhao et al. (2015) and then were calculated with a smoothing factor (SF) of 2. The individual FORC distributions ρ were normalized by their respective maximum ρ_{max}.

Fig. 3.9 shows the stacked paleomagnetic data with α_{95} for the directional data and the 1 σ error for the virtual axial dipole moment (VADM) together with their paleoclimatic context, represented by the 10 year stack of the K/Ti ratio determined from XRF scanning (see. Fig. 3.3). In Fig. 3.9c the angle between the calculated mean direction and the direction of a geocentric axial dipole field along a great circle is also shown. The angle between these two vectors is calculated by the arccosine of their vector product (Nowaczyk & Frederichs, 1999). VADM values were obtained analogously to Nowaczyk et al. (2013) by applying a scaling factor of 14.52 to the relative paleointensity data (slope NRM/ARM). It is interesting to note that the largest deviations from a pure dipole direction are not strictly occurring during to the lowest field values. Pronounced variations in declination start already at about 3000 years before the minimum at a fairly high VADM level of 6×10^{22} A m^2, about 75% of the present day value of 7.628×10^{22} Am^2 (according to the 11th generation International Geomagnetic Reference Field, IGRF-11, Finlay et al., 2011). When reaching the field minimum at 64.5 ka, also the largest inclination changes have occurred. After the intensity minimum directional

variations are less pronounced than before. A similar field behaviour could be observed in Black Sea sediment data also for a few younger pronounced field deviations (Nowaczyk et al., 2012). The absolute rate of change in field intensity in MIS 4 is about twice as large before the minimum as it is after the minimum (Fig. 3.9b), that is, the field decay before the minimum was much faster than the recovery afterwards.

The migration of the virtual geomagnetic poles (VGPs) associated with the reconstructed directional variations are shown in Fig. 3.10. The VGP positions show an elongated distribution, mainly caused by the more pronounced variations in declination before the field minimum, shown in detail in Fig. 3.10b, with ages of certain VGPs indicated. The time interval between individual VGP positions is 100 years. At 66.8 ka and 65.6 ka, VGP latitudes of only 51.5°N (at ~120°E) and 61.5°N (at ~75°W), respectively, were reached (Fig. 3.10b), at roughly opposite sides of the globe. This is not yet the range normally taken as excursional VGP positions (<45°N), but it reflects a case of extreme paleosecular variation. The fastest movement of the VGP occurred between 67.4 and 67.3 ka with a mean drift rate of about 20° in 100 years (0.2°a^{-1}) when crossing the geographic North pole.

3.4 DISCUSSION

Geomagnetic field intensities during MIS 4 as reconstructed from Black Sea sediments in terms of VADM values were generally lower than the present day field with an axial dipole moment of 7.628×10^{22} Am^2, as indicated by the red dotted line in Fig. 3.9b. Lowest values are around 1.2×10^{22} Am^2, only about 16% of the present day value. In sediments deposited at high northern latitudes shortly after the MIS 5/4 transition several data sets probably indicate a major deviation from directions expected for a geocentric axial dipole of normal polarity. Samples in cores from the Kolbeinsey Ridge (Bleil & Gard, 1989; Nowaczyk & Frederichs, 1999), the Fram Strait (Nowaczyk et al., 2003), and the Yermak Plateau (Nowaczyk & Baumann, 1992) show shallow to steep negative inclinations after demagnetization with 65 to 100 mT. Thus, these features were assigned the name 'Norwegian-Greenland Sea excursion' (Løvlie, 1989). For these old cores, besides detailed NRM demagnetization, often no rock magnetic data was obtained so that paleomagnetic results might be treated with caution. However, also Simon et al. (2012) and Xuan & Channell (2012) published data from the Baffin Bay and the Yermak Plateau, respectively, with shallow to steep negative inclinations for MIS 4 sediments. These findings indicates that the geomagnetic field at high latitudes have experienced a short-term but only regional reversal excursion during MIS 4. At the same time in the Black Sea area, about 5000 km further South, where the Laschamp excursion at 41 ka was found in the very detail as a full reversal, only pronounced declination and inclination swings, partly with a high

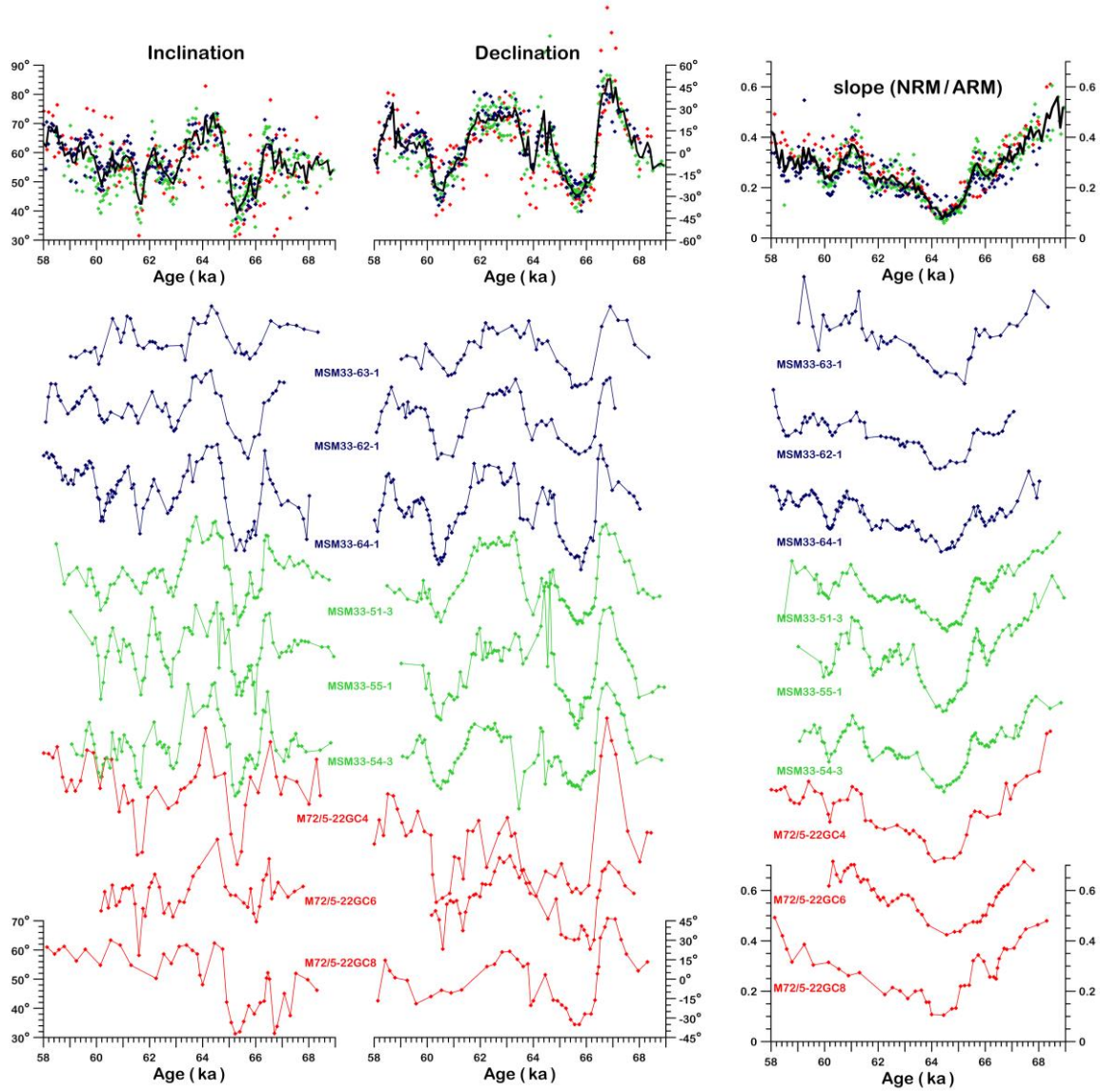

Figure 3.8 ChRM inclinations (left) and declinations (middle) between 58 and 70 ka from the three M72/5 cores (red) and the six MSM33 cores (green and blue) shown as individual records with a constant offset from bottom to top, and all nine records together with common axes in the topmost part (coloured dots). Here black lines represent the Fisherian mean (Fisher, 1953) of inclination and declination, respectively. Relative paleointensities (right) approximated by the slope of NRM versus ARM during AF demagnetization from the three M72/5 cores (red) and the six MSM33 cores (green and blue) shown as individual records with a constant offset from bottom to top, and all nine records together with a common axis in the topmost part (coloured dots). The black line represents the arithmetic mean of all nine records. NRM – natural remanent magnetization, ARM – anhysteretic remanent magnetization.

rate of change, could be found. Judging from obtained rock magnetic parameters and XRF results, sediments in the Black Sea that recorded the Laschamp excursion (Nowaczyk et al., 2012) are not significantly different in composition, (magnetic) grain-size, and concentration from the MIS 4 sediments. Also sedimentation rates are in the same range (20-35 cm ka^{-1}). Thus, it can be concluded that the high-quality data obtained at high resolution in this study

reflect true geomagnetic field variations during MIS 4 in the Black Sea area, characterized by pronounced paleosecular variation associated with a decreased field intensity. According to compilations of globally distributed paleointensity estimates (e.g., Channell et al., 2009; Laj et al., 2004) the intensity low around 65 ka is a global feature. In the Black sea area for the past 69 ka it is the second lowest minimum, with the Laschamp excursion at 41 ka being associated with lowest field values (Nowaczyk et al., 2013). Thus, the interpretation for MIS 4 is that the geomagnetic field decayed globally in intensity at around 65 ka. At this time, at northern high latitudes, literature listed above indicate the recording of excursional directions while at mid (and low) latitudes, here especially the Black Sea, only secular variation-typical directional swings, but with larger amplitudes and higher rates of change than normal could be reconstructed.

Data currently available is not sufficient in order to quantify the global situation during MIS 4 in terms of a spherical harmonics analysis in order to describe the geomagnetic field geometry in space and time. At least, variations predominant in declination in the Black Sea area (42°N) point towards sectoral and/or tesseral multipoles rather than towards zonal (axisymmetric) multipoles, because, the latter would result only in inclination anomalies. For latitudes higher than 75 to 80°N it is quite difficult to obtain useful fully oriented paleomagnetic data by rotating obtained directions from azimuthally unoriented cores to a mean declination of 0°. This is due to the fact that such sites are lying inside the typical migration area of the geomagnetic North pole with southerly declinations occurring even in a clear dipolar field configuration and with high field intensities. Therefore, analysis of magnetostratigraphic data from the high Arctic is a challenge. Often directional data is restricted to the presentation of ChRM inclination only. Precise age information is also an issue since Arctic sediments are barren of datable material such as foraminifera at many stratigraphic levels. Even if there would be sufficient material available at any site at northern high latitudes, the Norwegian-Greenland Sea excursion with an estimated age of around 65 ka occurred at a time that is clearly beyond what could be dated by the AMS ^{14}C technique (~50 ka). In summary, the available paleomagnetic data from MIS 4 is still too sparse even in order to develop a low order spherical harmonics field model. For this, much more data acquired at high resolution and precisely dated from various regions all over the globe is needed. Nevertheless, taking available data together, there is some evidence that the field might have been characterized by at least a distorted dipole geometry at low field intensities.

Since geomagnetic excursions are associated with a significantly reduced field strength, principally, high-energetic cosmic particles are able to better penetrate into the Earth's

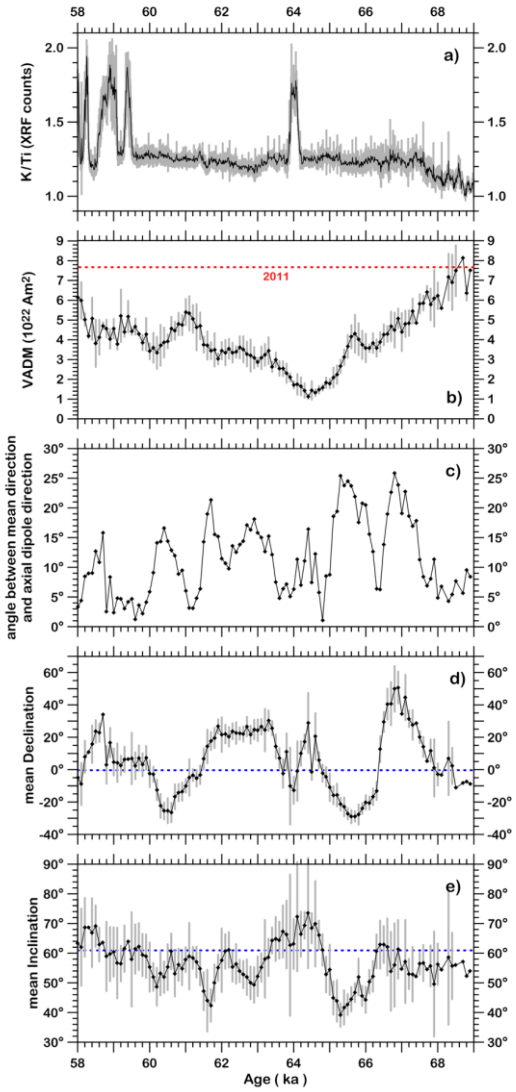

Figure 3.9 Data from Black Sea sediments from 69 to 58 ka: a) paleoclimatic context imaged by K/Ti ratios from XRF scanning stacked into 10 year bins (see also Fig. 3.3), together with paleomagnetic data (comp. Fig. 8) stacked into 100 year bins, with b) relative paleointensity (slope NRM/ARM), c) angle between calculated mean directions and the expected direction of a geocentric axial dipole field on a great circle (see text for further explanation), based on Fisherian means calculated from d) ChRM declinations and e) ChRM inclinations. The latter two are shown with corresponding α_{95} values indicated by vertical gray bars. Blue dashed lines in the directional stacks indicate the dipole inclination (+61°) and declination (0°), respectively, for a geocentric axial dipole field of normal polarity. In a) and b) vertical gray bars indicate the 1 σ standard deviation. The dashed red line in b) indicates the axial dipole moment of the present day field (see text).

atmosphere then (e.g., Lal, 1988; Masarik & Beer, 1999), producing more cosmogenic radionuclides than in a stronger field situation. The weaker the geomagnetic field is the larger the production rate is, but the link is not a linear function (e.g., Beer et al. 2002, Fig. 3.6). Beside ^{14}C, ^{10}Be (half life: 1.387×10^{6} yrs, Chmeleff et al, 2010; Korschinek et al., 2010) is the most important radionuclide on time scales of up to a few million years. In a recent study by Simon et al. (2016), summarizing data on ^{10}Be flux from various sites on Earth, MIS 4 is

characterized by one of the highest ^{10}Be flux anomalies during the past 400 ka (feature III in Fig. 3.6 of Simon et al., 2016), thus independently pointing towards a global geomagnetic field low. The strength of the VADM associated with the MIS 4 ^{10}Be flux maximum was calculated to about 3.5×10^{22} Am^2 by Simon et al. (2016), similar to what was estimated for the GLOPIS (global paleointensity stack) with 4×10^{22} Am^2 (Laj et al., 2004). Thus, VADM values from these global stacks are about 3 times higher than the value of 1.2×10^{22} Am^2 estimated from relative paleointensity data from sediments from the Black Sea, a single location at mid latitudes. But, sedimentation rates of investigated cores in this study are with 20 to 35 cm ka^{-1} much higher than the cores investigated by Simon et al. (2016) which are in the range of only 5 to 10 cm ka^{-1}. Therefore, a certain degree of smoothing of the ^{10}Be signal might be assumed that yielded a less pronounced field intensity low when reconstructed from the ^{10}Be flux data.

The geomagnetic field's dipole axis might be tilted to a certain degree with respect to the Earth's rotation axis. In general, theoretically calculated production rates of cosmogenic radionuclides are given as a function of geomagnetic latitude, that is, the angular distance from the dipole axis. The assumption of a (slighty tilted) dipolar field is a realistic approach since most of the time the geomagnetic field fulfils this criteria. However, during reversals and excursions, such as might be the case as discussed here, the simple dipolar geometry is obviously lost. Then relation between geographic and geomagnetic coordinates becomes complicated or even undefined, especially in a case of a more complex but weak multipole field. In addition the radial decay of multipoles is much faster with $r^{-(n+2)}$ with n being the degree of the multipole (n=1: dipoles, n=2: quadrupoles, n=3: octupoles, etc.). The distribution of low and high field intensities of a multipole field is also much more complicated than in a dipolar geometry. Thus, theoretically, the much lower VADM values derived from Black Sea sediments as a single location, might be an effect of the inferred multipole configuration with a regional low in the Black Sea area during the middle of MIS 4.

Another explantion for the lower VADM estimation from Black Sea sediments might result from a non-linear response during NRM acquisition to the geomagnetic field strength. Since the VADM range during MIS 4 is lower than reconstructed from global stacks, NRM acquisition in Black Sea sediments might be less efficient in low fields. Consequently, this should be accompanied with a noisier paleomagnetic record. But, the opposite is the case. Even paleomagnetic directions during the change from normal to reversed directions at the onset of the Laschamp excursion in Black Sea sediments, associated with reconstructed VADM values of just 0.50×10^{22} Am^2 are of high quality and reproducible from core to core (Nowaczyk et al., 2012, 2013) which is also valid for MIS 4 data. VADM reconstructions by Laj et al. (2004)

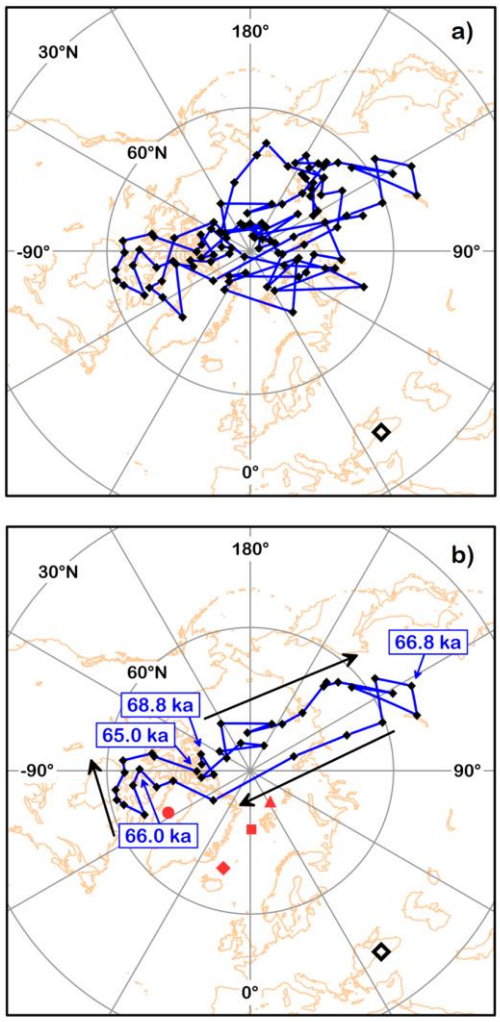

Figure 3.10 Course of the virtual geomagnetic pole (VGP) derived from Black Sea sediments a) from 69 to 58 ka, according to data shown in Fig. 9, and b) detailed look at the VGP path between 68.8 and 65.0 ka. VGP positions are plotted every 100 years and are connected with lines along great circles. A fairly fast movement could be reconstructed from 66.8 to 66.0 ka across a distance of about 60° (6660 km) with a maximum speed of 20° in 100 years between 66.4 and 66.3 ka. A geomagnetic excursion was reported from sediments deposited at northern high latitudes shortly after the MIS boundary 5/4 (71 ka), as indicated by red symbols: filled diamond - Bleil & Gard (1989), Nowaczyk & Frederichs (1999); square – Nowaczyk & Bauman (1992), Nowaczyk et al. (2003); triangle – Xuan & Channell (2012); filled circle – Simon et al. (2012). The black open diamond indicates the site of this study.

and Simon et al. (2016) for the time of the Laschamp excursion yielded values which are about 3 times higher, while the estimates for a field maximum around 50 ka yielded values of 11×10^{22} Am^2, comparable to what was reconstructed from the Black Sea sediments (Nowaczyk et al., 2013). Thus, the discrepancy in VADM reconstruction should be more likely caused by the lower sedimentation rates and related smoothing of signals in the records in the stacks used by Laj et al (2004) and Simon et al. (2016).

Remanence data from artificially deposited sediments often show a lower efficiency in remanence acquisition at higher fields (e.g., Barton et al., 1980; Johnson et al., 1948; Spassov & Valet 2012). Thus, if remanence acquisition in Black Sea sediments worked in a similar way paleointensities derived from sediments deposited in a weak geomagnetic field should be higher with respect to paleointensities from sediments deposited in a strong geomagnetic field. Then a downscaling of low (relative) paleointensities would be required. Consequently, Black Sea data then would point towards VADM values weaker than 1.2×10^{22} Am^2, which is an even larger discrepancy to reconstructions from ^{10}Be flux data.

3.5 CONCLUSIONS

In summary, high quality paleomagnetic data obtained from MIS 4 sediments deposited in the Black Sea at high resolution represent a phase of enhanced paleosecular variation. Associated VGP positions were quickly changing positions between opposite sides of the globe almost reaching excursional latitudes. These fast directional changes were accompanied with a fast decaying field, finally reaching the second lowest level of the past 69 ka. This is also seen in global compilations of paleointensity data as well as in reconstructions of the geomagnetic dipole moment from ^{10}Be flux data. Contemporaneous data from northern high latitudes indicate much larger deviations from a dipolar field geometry, probably even a regional field reversal. Thus, the geomagnetic field during the middle of MIS 4 might have been characterized by a non-dipole field configuration accompanied with fairly low field intensities, but, the current data base is far too sparse to quantify the field geometry in terms of a (low-order) spherical harmonics model. Field minima reconstructed from Black Sea sediments appear to be much too low when compared to reconstructions from globally distributed cores, either derived from relative paleointensity data from other sites or from estimates based on ^{10}Be flux data. Also, deposition experiments indicate that lower fields should be overestimated from sedimentary remanences. In order to clarify the discussed discrepancies it will be necessary to perform redeposition experiments as well as ^{10}Be determinations directly with Black Sea sediments in future studies.

ACKNOWLEDGEMENTS

We thank S. Plewe, M. Duwe, and T. Moldenhawer for their technical and logistical help during processing and sub-sampling of the cores. We also thank the captains and crews of *RV Meteor*, cruise M72/5 and *RV Maria S. Merian*, cruise MSM33, respectively, for their effords in providing optimal scientific working conditions. This work was partly funded by the German Research Foundation (Deutsche Forschungsgemeinschaft, DFG SPP 1266 "INTERDYNAMIC" grants AR 367/9-1 and AR 367/9-2), the Gary Comer Science and Education Foundation, U.S.A., and the Chinese Scholarship Council (CSC grant No. 201506180060).

4 Geomagnetic paleosecular variation record spanning from 40 to 20 ka - implications for the Mono Lake excursion from Black Sea sediments

Published in Earth and Planetary Science Letters 509 (2019), 114–124.

Liu Jiabo [1,*], Norbert Nowaczyk [1], Ute Frank [1], Helge Arz [2]

[1] GFZ German Research Centre for Geosciences, Section 'Climate Dynamics and Landscape Evolution', 14473 Potsdam, Germany.

*(jiabo@gfz-potsdam.de)

[2] Leibniz Institute for Baltic Sea Research Warnemünde, 18119 Rostock, Germany

SUMMARY

The Mono Lake geomagnetic excursion, characterized by low paleointensity and excursional virtual geomagnetic pole (VGP) positions at about 35 ka, has been cumulatively documented from global sites. However, the geomagnetic field geometry during this short-lived excursion is not conclusively described, since excursional directions are only sporadically reported. A full-vector paleosecular variation (PSV) record between 20 and 40 ka could be reconstructed from seven Black Sea sediment cores. The age models of these cores are based on radiocarbon dating and tephrochronology. Further age constrains were achieved by tuning ice rafted debris (IRD) counts and XRF logs (mainly Ca/Ti ratio) as climate proxies for Dansgaard-Oeschger (D-O) warming events, to the oxygen isotope record from Greenland ice cores (NGRIP). The PSV records of individual Black Sea cores were stacked by using 100-year bins. At about 34.5 cal. ka BP, the Mono Lake excursion is evidenced in the stacked Black Sea PSV record by both a relative paleointensity (rPI) minimum and directional shifts. Associated VGPs from stacked Black Sea data migrated from Alaska, via central Asia and the Tibetan Plateau, to Greenland, performing a clockwise loop. This agrees with data recorded in the Wilson Creek Formation, USA., and Arctic core PS2644-5 from the Iceland Sea, suggesting a dominant dipole field. On the other hand, the Auckland lava flows, New Zealand, the Summer Lake, USA., and Arctic core ODP-919 yield distinct VGPs located in the central Pacific Ocean due to presumably non-dipole field. Finally, Black Sea sediments younger than the Mono Lake excursion recorded only normal secular variations.

KEYWORDS

Mono Lake excursion; Black Sea; paleosecular variation

4.1 INTRODUCTION

The Mono Lake excursion was initially identified in the Wilson Creek Formation at Mono Lake (California, USA) when actually searching for the Laschamp excursion (Denham and Cox, 1971), and it was further confirmed by Liddicoat and Coe (1979) with a record from the same site showing directional anomalies. Although the uncertainty in age was in debate for decades and even confused with the Laschamp excursion (e.g., Kent et al., 2002; Zimmerman et al., 2006), the Mono Lake excursion has been progressively identified in age between about 33 and 35 ka BP., coupled with absolute dating methods from volcanic rocks (e.g., Kissel et al., 2011; Laj et al., 2014). As was the case for the Laschamp excursion, the distinct magnetic field behavior of the Mono Lake excursion has been evidenced from records comprising both geomagnetic excursions (e.g., Channell, 2006; Lund et al., 2017; Nowaczyk et al., 2012; Nowaczyk and Knies, 2000). In addition, a minimum in relative paleointensity associated with the Mono Lake excursion is ubiquitously reported in sedimentary records from the Black Sea (Nowaczyk et al., 2012), the Iceland Sea (core PS2644-5, Laj et al., 2000) and more globally in the global paleointensity stack GLOPIS-75 (Laj et al., 2004), as well as in absolute paleointensity data from volcanic rocks on Hawaii (Laj et al., 2002; Teanby et al., 2002), the Canary Islands (Kissel et al., 2011), New Zealand (Cassata et al., 2008), and the French Chaîne des Puys (Laj et al., 2014).

In the Auckland volcanic province, New Zealand, the VGP cluster identified as the expression of the Mono Lake excursion locates in the central Pacific Ocean (Cassata et al., 2008), close to the southernmost part of the VGP path of the excursion recorded at Site ODP-919 (Iceland Sea, Channell, 2006). Cassata et al. (2008) suggested, the pattern possibly implies a fairly dominating dipole field during the Mono Lake excursion, though they could not exclude the possibility of a more complex geomagnetic field geometry. Based on the VGPs obtained from the Summer Lake (western USA) and Site ODP-919 (discrete samples), Negrini et al. (2014) argued that the VGP positions during the Mono Lake excursion gather in clusters, locations which coincide with non-axial dipole features found in the Holocene geomagnetic field. Nevertheless, the Mono Lake excursion recorded at Site ODP-919, Iceland Sea (Channell, 2006), was described only by directional changes without an associated decrease in paleointensity, contrarily to all other marine records (Kissel et al., 2011). VGPs of the Mono Lake excursion obtained from the Teide volcanic complex on Tenerife, Canary Islands (off West Africa) are located in the northern Persian gulf (Kissel et al., 2011), close to VGPs of the Mono Lake excursion recorded in core PS2644-5, Iceland Sea (Laj et al., 2000b), and the Wilson Creek Formation (Lund et al., 1988). Thus, the available geomagnetic field patterns

during the Mono Lake excursion are obviously distinct but not yet sufficient enough to really develop a satisfying model of the Earth's magnetic field behavior (Kissel et al., 2011).

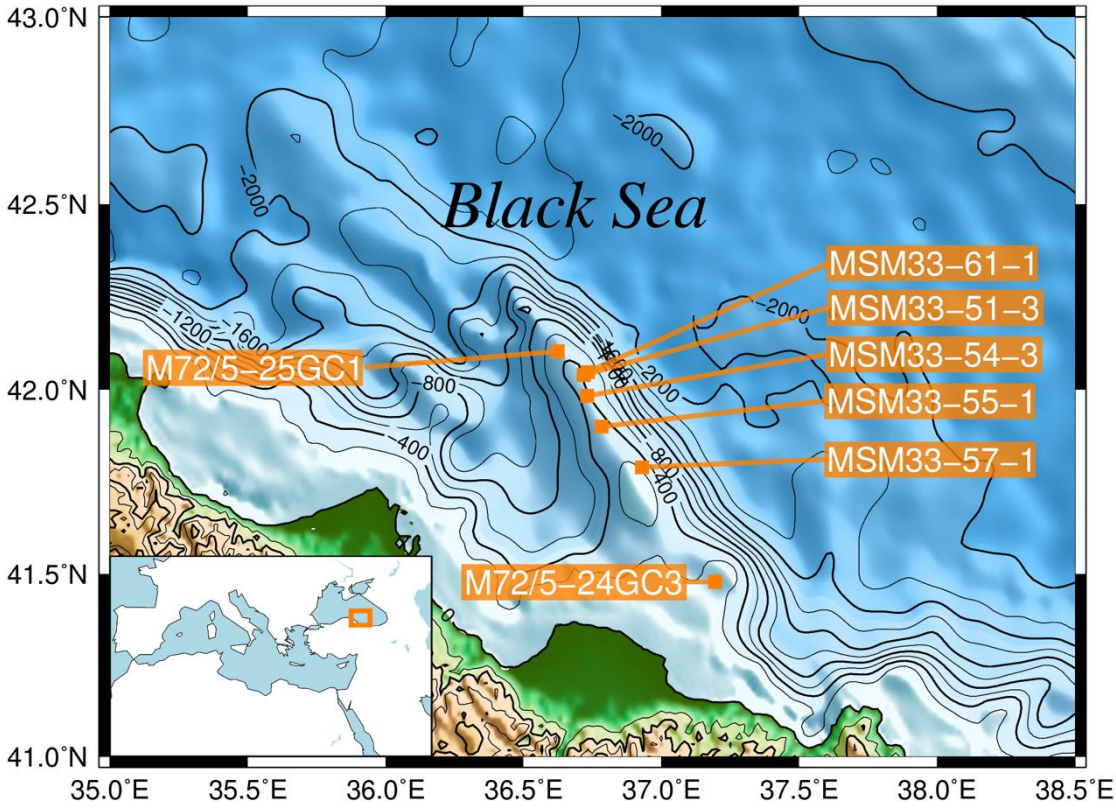

Figure 4.1 Positions of coring sites of sediment cores taken during expeditions M72/5 (RV METEOR) and MSM33 (RV Maria S. Merian) along the Archangelsky Ridge in the SE Black Sea.

The Mono Lake excursion recorded in Black Sea sediments, documented with both directional anomalies and a relative paleointensity minimum, has been discussed by Nowaczyk et al. (2012, 2013). Here we report an updated paleomagnetic data set from Black Sea sediments supplemented with data from five further cores from the same sampling region, which enables high-resolution PSV stacking for the time window between 20 ka and 40 ka. The Mono Lake excursion, centered at about 34.5 ka cal. BP, thus will be discussed on the basis of its detailed VGP path.

4.2 MATERIAL AND METHODS

The investigated Black Sea sediment cores were taken during two cruises of the German research vessels RV METEOR in 2007 (M72/5) and RV Maria S. Merian in 2013 (MSM33). A total of 21 gravity and piston cores, each with 12 cm diameter and lengths between 6.8 and 10.3 m were recovered from various water depths between 208 m and 847 m on the Archangelsky Ridge, SE Black Sea. In this paper, cores from seven sites shown in Fig. 4.1 are discussed.

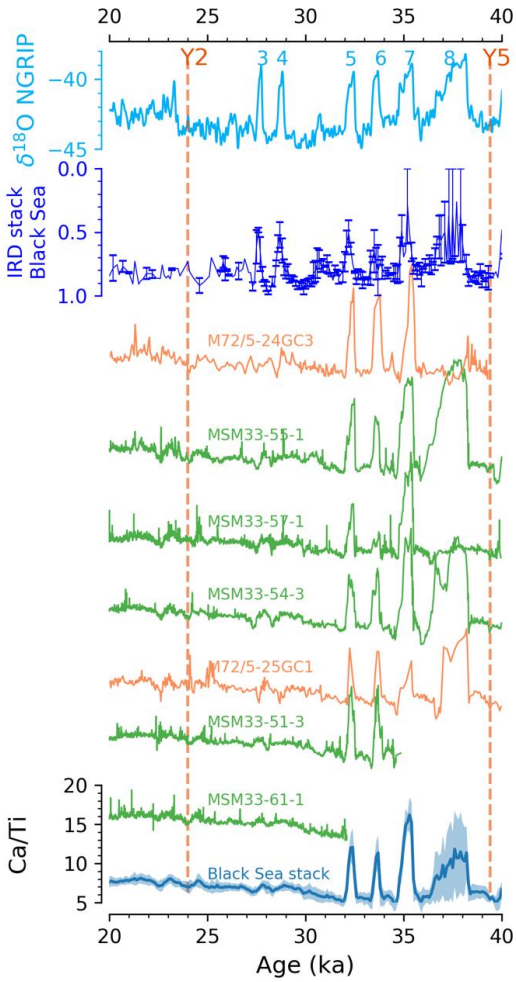

Figure 4.2 Oxygen isotope variations ($\delta^{18}O$) from Greenland ice cores (NGRIP, Svensson et al., 2008) shown on the top with numbers indicating Dansgaard-Oescher (D-O) warming events (Dansgaard et al., 1993). The Black Sea IRD (ice rafted debris) stack was derived from two M72 cores using 100 yr bins (M72/5-24GC3 and M72/5-25GC-1, Nowaczyk et al., 2012). Ca/Ti elemental ratios derived from X-ray fluorescence scanning of the two M72/5 cores (orange) and five MSM33 cores (green), are shown together with their 100 yr bins stack (blue) on the same scale. The Black Sea IRD stack and Ca/Ti stack are all plotted with 1 σ standard deviation bars. The records of Ca/Ti ratios from individual Black Sea cores are lined-up from bottom to top depending on the water depth of the coring sites from deep to shallow. Y2-tephra layer from the Cape Riva eruption, Santorini, Greece (e.g., Fabbro et al., 2013), Y5-tephra from Campanian Ignimbrite eruption, Phlegraean Fields, Italy (e.g., De Vivo et al., 2001).

Samples for paleomagnetic studies were taken continuously from the central axis of each core segment, using cubic plastic boxes with a volume of 6 cm3. The low-frequency magnetic volume susceptibility (κLF) for discrete samples were measured with an AGICO multi-function Kappabridge MFK-1A, applying a field of 200 Am-1 and a frequency of 976 Hz. Before, the magnetic volume susceptibility was measured in steps of 1 mm directly on the split-surface of the cores using a Bartington MS2E spot-reading sensor with a spatial resolution of 4 mm (Nowaczyk, 2001). Those data sets were used for correlation purposes only and are not shown here.

The natural remnant magnetization (NRM) and the anhysteretic remanent magnetization (ARM) were measured on a cryogenic 2G Enterprises 755 SRM long-core magnetometer. The NRM was determined after application of alternating field (AF) amplitudes of 0, 5, 10, 15, 20, 30, 40, 50, 65, 80, and 100 mT. Directions of the characteristic remnant magnetization (ChRM) were determined by principal component analysis (PCA) according to Kirschvink (1980). The ARM was imparted along the samples' z-axes with a static field of 0.05 mT and an AF field of 100 mT. Demagnetization then was performed in steps of 0, 10, 20, 30, 40, 50, 65, and 80 mT. The relative paleointensity (rPI) was defined by using the slope of NRM versus ARM of common demagnetization steps along a straight line.

Isothermal remnant magnetizations (IRM) were measured with a Molyneux spinner magnetometer. IRMs were imparted using a 2G Enterprises 660 pulse magnetizer. IRM intensities acquired in a peak field of 1.5 T are defined as the saturation IRM (SIRM). A reversed field of 0.2 mT was used to determine the S-ratio, defined as: $0.5 \times (1 - [\text{IRM-0.2T} / \text{SIRM1.5T}])$, with $0 \leq S \leq 1$. Detailed IRM acquisition curves and first order reversal curves (FORC) measurements were performed using a 4" Princeton Measurements Corporation 'MicroMag' alternating gradient magnetometer (AGM). IRM acquisitions curves were obtained by applying 61 logarithmically spaced field steps from 2 mT to 1 T. The IRM component analyses were calculated using the software "pyIRM", based on a Gaussian mixture model, available on https://github.com/botaoxiongyong/pyIRM. The protocol and calculation of irregular FORC (irFORC) and transient hysteresis FORC (tFORC) diagrams were performed following Zhao et al. (2017, 2015). All paleo- and rock magnetic investigations on discrete samples were performed at the Helmholtz Centre Potsdam, GFZ German Research Centre for Geosciences, Potsdam, Germany.

X-ray fluorescence (XRF) scanning of M72/2 cores was performed at a resolution of 10 to 20 mm (Nowaczyk et al., 2013, 2012). High-resolution XRF-logs from MSM33 cores were obtained from split archive core halves, using an ITRAX XRF Core Scanner (COX Analytics; e.g., Croudace et al., 2006). The core scanner was operated with a Cr-tube at 30 kV and 30 mA and an SDD Si drift detector. Exposure time was 15 seconds and down-core step size was 1 mm. XRF measurements of MSM33 cores were performed at the Leibniz Institute for Baltic Sea Research Warnemünde, Rostock, Germany. The XRF data obtained from MSM33 cores were presented before for marine isotope stage (MIS) 4 by Nowaczyk et al. (2018) and for MIS 2 by Liu et al. (2018).

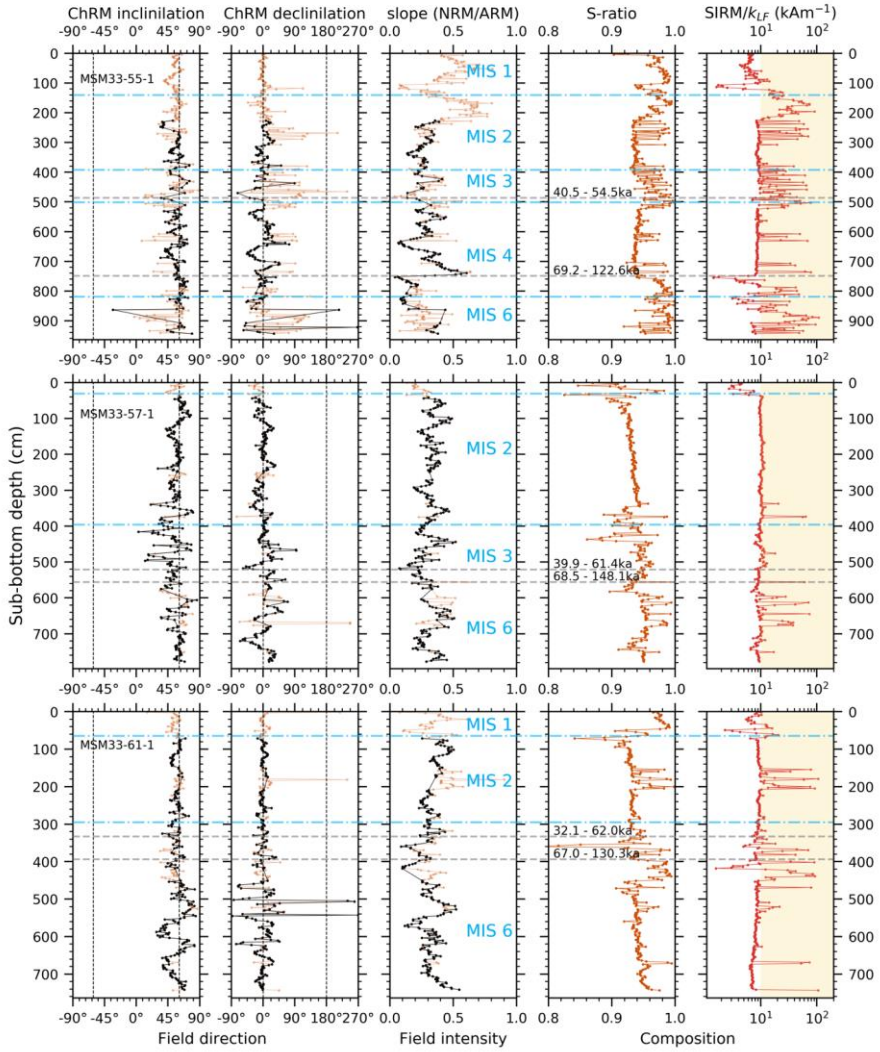

Figure 4.3 Down-core plots of paleomagnetic data, ChRM inclination and declination, slope (NRM/ARM), a proxy for relative geomagnetic field intensity, and rock-magnetic data, S-ratio and SIRM/κ_{LF}, from three MSM33 cores. Paleomagnetic data are plotted in orange for raw data and in black for greigite-filtered data. Grey vertical dashed lines in the directional plots indicate the dipole inclination (± 61°) and declination (0, 180°) for normal and reversed polarity, respectively. The S-ratio and the SIRM/κ_{LF} ratio are plotted in orange color, displaying all investigated samples. They reflect magneto-mineralogical variations mainly caused by hematite (S-ratio < 0.94) and greigite (yellow areas, SIRM/κ_{LF} > 10 Am^{-1}, S-ratio > 0.95) against a background of (titano-) magnetite (Nowaczyk et al., 2013, 2012). Horizontal dashed blue lines indicate marine isotope stage (MIS) boundaries. Grey horizontal dotted lines indicate inferred hiatuses with black labels indicating the estimated time intervals missing in the records. NRM – natural remanent magnetization, ARM – anhysteretic remanent magnetization, ChRM – characteristic remanent magnetization, SIRM – saturated isothermal remanent magnetization, κ_{LF} – low field magnetic volume susceptibility.

4.3 RESULTS

4.3.1 Age models

The initial stratigraphy of M72/5 cores is based on a sequence of 16 accelerator mass spectrometry (AMS) 14C dating in core M72/5-24-GC3, which span the time interval from

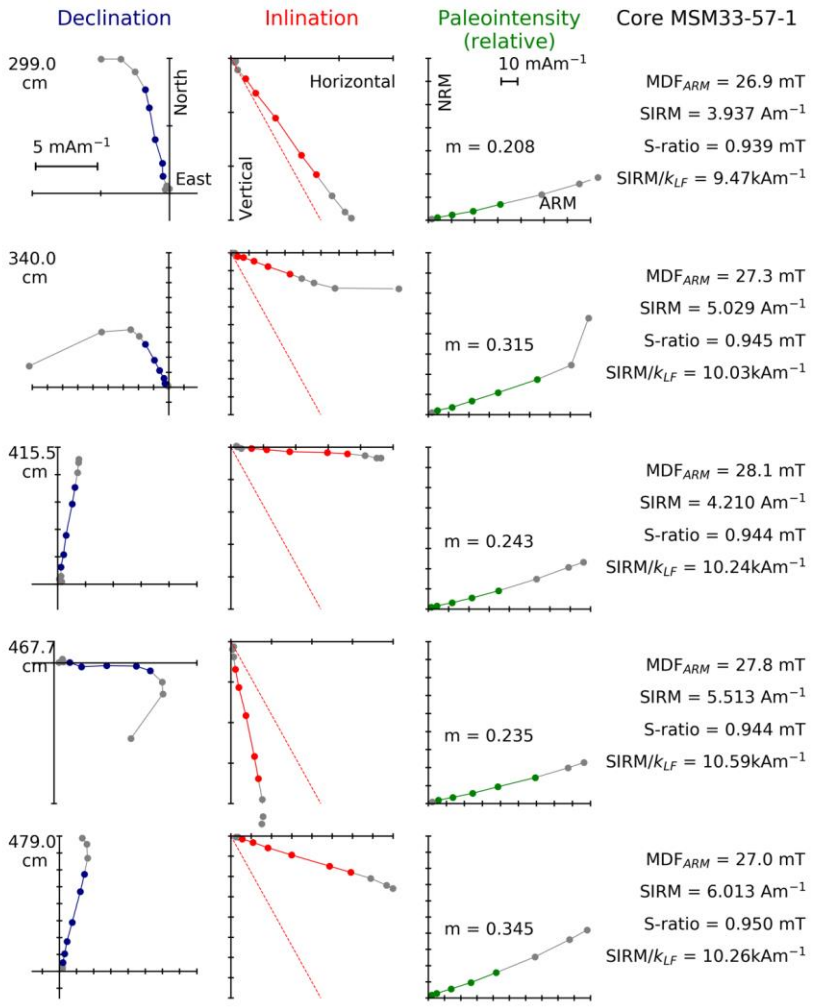

Figure 4.4 Results from alternating field (AF) demagnetization from the study interval between 20 and 40 ka in core MSM33-57-1, with sampling depths given at the outer left. The first column illustrates variations in declination with vector endpoint diagrams of North versus East. The second column illustrates variations in inclination with diagrams of vertical versus horizontal components. The third column illustrates relative paleointensity variations estimated by the slope m of NRM intensity versus ARM intensity. The fourth column lists some basic rock magnetic properties, with their detailed rock magnetic results shown in Fig. 4.5. Directional data is shown after adjustment of declinations from the whole core to a mean value of 0°. Gray symbols indicate raw data from AF steps from 0 to 100 mT (80 mT) for the directional (intensity) variations. Colored symbols indicate AF steps used for determination of the ChRM direction (first and second column) and relative paleointensity (third column), respectively. The red dotted line in the inclination plots represent the inclination of 61° of a geocentric axial dipole field. Note that for reasons of clarity axes for NRM and ARM in the intensity plots (third column) have different scaling, but with a constant ratio in all diagrams. MDF – median destructive field.

12.5 to 38.9 ka cal. BP (Nowaczyk et al., 2012). Identification of tephra material related to the Campanian Ignimbrite (C.I.) eruption, also termed ‘Y5’ at 39.3 ka (e.g., De Vivo et al., 2001) and the Cape Riva eruption of Santorini at about 21.8 ka (‘Y2’ tephra, e.g., Fabbro et al., 2013) in Black Sea sediment cores yielded further tie points for the age models (e.g., Cullen et al.,

2014; Nowaczyk et al., 2012). Further age constrains for M72/5 and MSM33 cores were obtained by correlating their XRF logs, mainly Ca/Ti and K/Ti ratios, and stacked ice rafted debris (IRD) counts, as proxies of the succession of Black Sea interstadial and stadial intervals, to the oxygen isotope record from Greenland ice cores (NGRIP) (Svensson et al., 2008). The detailed correlations between Black Sea records and the NGRIP are presented for M72/5 cores by Nowaczyk et al. (2012) and for several MSM33 cores by Nowaczyk et al. (2018). For the time interval between 20 and 15 ka cal. BP, the ages of M72/5 and MSM33 cores were further constrained by correlating their XRF logs and S-ratio records to dated meltwater events investigated by Bahr et al. (2006) and Soulet et al. (2013) in the western Black Sea (Liu et al., 2018). More extensive paleoclimatic interpretations based on multi-proxy studies are presented for the Holocene and the Eemian by Shumilovskikh et al. (2013, 2012) and for the period between 20 and 65 ka by Wegwerth et al. (2016, 2015).

In Fig.2, the correlations between NGRIP $\delta^{18}O$ and Black Sea IRD counts and XRF Ca/Ti ratios are shown for the interval from 40 to 20 ka cal. BP. The Black Sea IRD counts, stacked from cores M72/5-24GC3 and M72/5-25GC1, could be precisely tuned to every Dansgaard-Oeschger (D-O) warming events (Dansgaard et al., 1993) indicated by NGRIP $\delta^{18}O$ peaks. Though the two D-O warming events 3 and 4 between 27 and 29 ka are evidenced in IRD counts, their pattern does not show up in the XRF data from all Black Sea cores. From 30 to 40 ka cal. BP, all D-O events are document in the XRF Ca/Ti ratios from all studied cores, enabling a high-resolution correlation to the NGRIP $\delta^{18}O$ record. The age-depth models for all studied cores have been presented by Liu et al. (2018) for the past 50 ka.

4.3.2 Paleo- and rock magnetism

Paleomagnetic data sets, ChRM directions and rPI, and rock magnetic data sets, S-ratio and SIRM/κ_{LF} ratio, from three MSM33 cores (sites 55, 57, 61) are shown as down-core plots in Fig. 4.3. Complete magnetostratigraphic data from M72/5 cores were presented in detail by Nowaczyk et al. (2013, 2012). Further data from other MSM33 cores were discussed by Nowaczyk et al. (2018) (sites 51, 54, 64) and by Liu et al. (2018) (sites 57, 62, 63) focusing on geomagnetic field variations during MIS 4 and MIS2, respectively. Aiming to avoid compromising of paleomagnetic data by erroneous directions carried by greigite, samples with SIRM/κ_{LF} ratios >10 kAm^{-1} and S-ratios >0.95, shown to be affected by greigite (Nowaczyk et al., 2013, 2012), were removed from studied records. In Fig. 4.3 the unfiltered data sets are all plotted in orange while greigite filtered paleomagnetic data, ChRM inclination and declination as well as rPI, slope (NRM/ARM), are plotted in black. For the time interval from

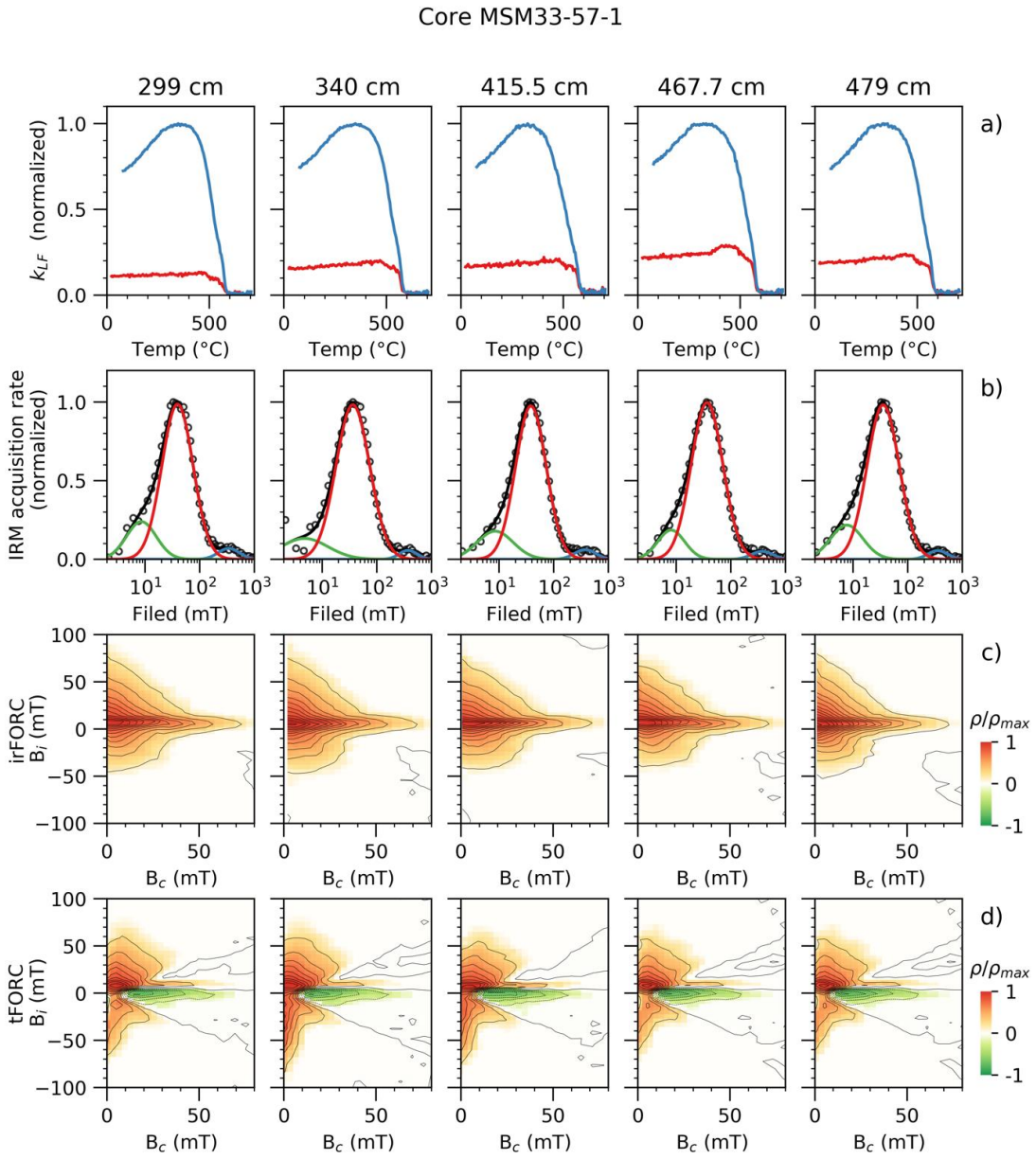

Figure 4.5 Compilation of a) high-temperature magnetic susceptibility curves, b) IRM decomposition curves, c) irregular FORC (irFORC) and d) transient hysteresis FORC (tFORC) diagrams, shown from top to bottom for the samples as listed in Fig. 4.4. In high-temperature magnetic susceptibility graphs, red (blue) lines denote heating (cooling) curves. In IRM decomposition graphs, circles indicate IRM acquisition rates determined from measured data. The green, red and blue lines represent three different components fitted to these data, whereas the black line is the fitted total spectrum. The irFORC and tFORC for all samples were calculated with a smooth factor (SF) of 2, and the FORC distributions ρ were normalized by their respective maximum ρ_{max} (for details, see Section 3.2).

20 to 40 ka, though greigite contamination is present here and there (e.g., core MSM33-55-1), the filtered data represents consistent paleosecular variation patterns.

In Fig. 4.4, samples with fairly low rPIs and shallow inclinations from core MSM33-57-1 are presented with detailed AF demagnetizations results and their corresponding rock magnetic data. The demagnetization diagram of representative samples show that vector end-points migrate straight towards the origins, with some visible viscous overprint, eliminated latest after about 15 mT (AF). For all studied samples, ChRM directions were generally defined from AF steps from 20 to 65 mT, yielding maximum angular deviation (MAD) angles smaller than 2°, thus indicating a very stable nature of the primary magnetization components. A conspicuous directional deviation can be recognized in the results from sample 467.7 cm, with a distinct declination deviation that reach values beyond 90°E. Though samples 340.0 cm, 467.7 cm, and 479.0 cm all demonstrate largely diverting inclinations, declinations are in normal PSV ranges. For comparison, the inclination of 61°, expected from a geocentric axial dipole field at Black Sea site, is marked by the red dotted lines in Fig. 4.4. Associated rock magnetic data from samples shown in Fig. 4.4, including high-temperature magnetic susceptibility curves, IRM decomposition curves, irFORC and tFORC diagrams, are presented in Fig. 4.5.

Results from high-temperature magnetic susceptibility measurements performed in Argon gas, illustrate a unique Curie-temperature at about 580 °C (Fig. 4.5a), indicating the dominance of magnetite. The IRM acquisition rates of all samples can be fitted with three components (Fig. 4.5b), though the dominant component (red lines) contributes to more than 80% of the total SIRM. The dominant component is commonly characterized by a median field between 34 mT and 40 mT and dispersion parameter (DP) between 0.28 and 0.31. The irFORC and tFORC were calculated with a smooth factor (SF) of 2 (following Zhao et al., 2017, 2015). The irFORC diagrams show all samples sharing a similar pattern, with FORC distributions spreading along the B_i axis up to 70 mT (Fig. 4.5c), denoting typical geological “pseudo-single domain” materials (e.g., Roberts et al., 2014). The tFORC diagrams (Fig. 4.5d), with a larger positive peak along the $B_i>0$ axis and a smaller positive peak along the $B_i<0$ axis, indicate that the “pseudo-single domain” materials are in vortex state (e.g., Zhao et al., 2017). Additionally, the tFORC diagrams, with a negative peak below $B_i=0$ axis and a statistically insignificant positive peak above $B_i=0$ axis, are likely indicating non-interacting stable single domain particles (e.g., Zhao et al., 2017).

The paleosecular variation (PSV) records, ChRM directions and the slope (NRM/ARM), as a measure of rPI, from all investigated cores considered for this study, converted into time series, are shown in Fig. 4.6 for the time interval from 40 to 20 ka cal. BP. Individual PSV records are plotted in orange for M72/5 cores and in green for MSM33 cores. The related 100-year bin stacked PSV records are plotted in blue in the bottom of Fig. 4.6. The stacked data is also

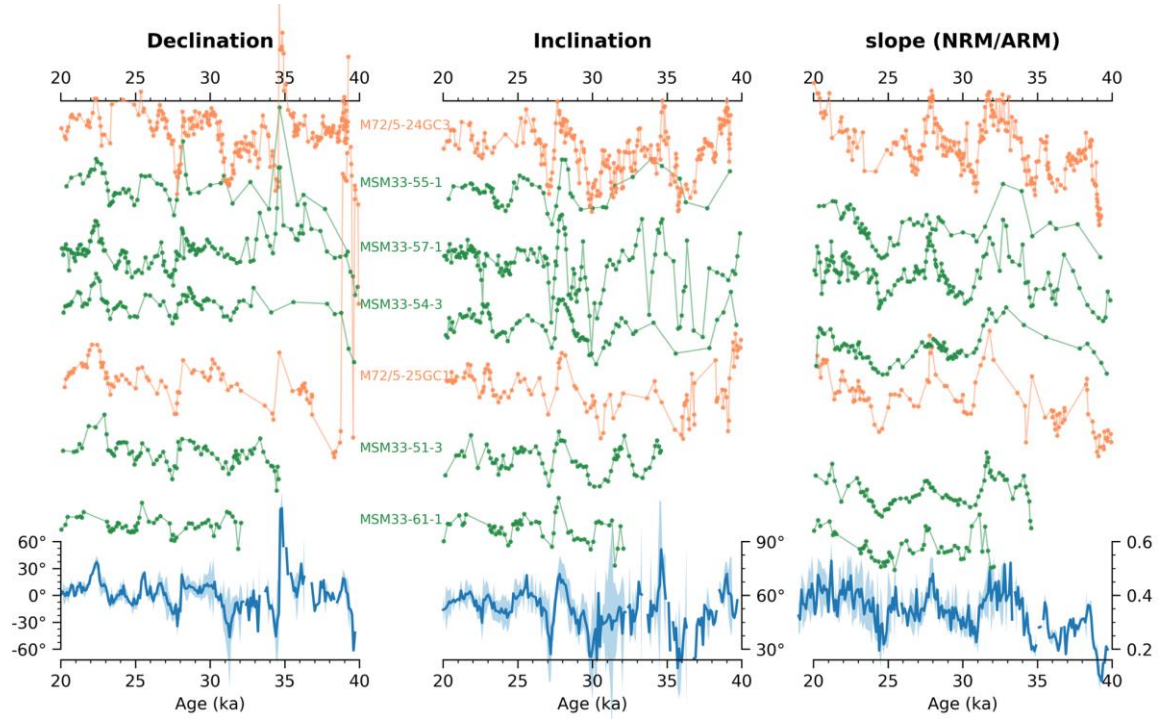

Figure 4.6 ChRM directions (declination and inclination) and relative paleointensity (rPI, approximated by the slope (NRM/ARM) during AF demagnetization shown individually for two M72/5 cores (orange) and five MSM33 cores (green) for the time window from 40 to 20 ka, together with 100-year bin stacks (blue). Inclination and Declination stacks are plotted with α_{95} error bars. The rPI stack is plotted with 1σ standard deviation bars. All individual records share a constant offset with their stacks. The plots of individual cores are lined-up from bottom to top depending on the water depth of the coring sites from deep to shallow (compare Fig. 1).

shown versus a common age axis in Fig. 4.7, including the number of samples per time bin. The features in the PSV stacks are all reproducible from record to record, resulting in fairly low α_{95} values for averaged directions using Fisher (1953) statistics, and low 1σ standard deviations (rPI), shown as light blue bars, except for larger errors between 30 and 32 ka cal. BP for the directional data. The number of samples per time bin commonly lies between 3 and 6. At around 34.5 ka cal. BP, the remarkable directional anomaly and a rPI minimum in the Black Sea PSV stack can be related to the Mono Lake excursion (Fig. 4.7). Some less pronounced paleointensity minima younger than 33 ka cal. BP are only associated with normal PSV fluctuations (+/- 20°).

In order to better compare the stacked Black Sea directional data with findings from other regions, virtual geomagnetic poles (VGPs) were calculated. For reasons of clarity, the Black Sea VGP path is only shown for the Mono Lake excursion between 33 and 36 ka in Fig. 4.8a, since no abnormal VGP positions are observed before or after this specific time interval. The VGP path from the Black Sea stack is shown together with VGP paths from individual Black Sea cores in Fig. 4.8a, and together with VGPs from the Wilson Creek Formation (Lund et al.,

1988), Iceland Sea core PS2644-5 (Laj et al., 2000b) and Tenerife lava flows (Kissel et al., 2011) in Fig. 4.8b, as well as VGPs from the Auckland volcanic field (Cassata et al., 2008), the Summer Lake (Negrini et al., 2014) and Site ODP-919 from discrete sample (Negrini et al., 2014) and u-channel (Channell, 2006) data in Fig. 4.8c. During the Mono Lake excursion, though VGP paths from individual cores are not entirely continuous, Black Sea-derived VGPs are all located on the Eurasian continent. The VGPs performed a clockwise loop from east Asia to the Tibetan Plateau and then migrated to the Arctic area, except for a single VGP position from core M72/5-24GC3 that is sited in East Africa (Fig. 4.8a).

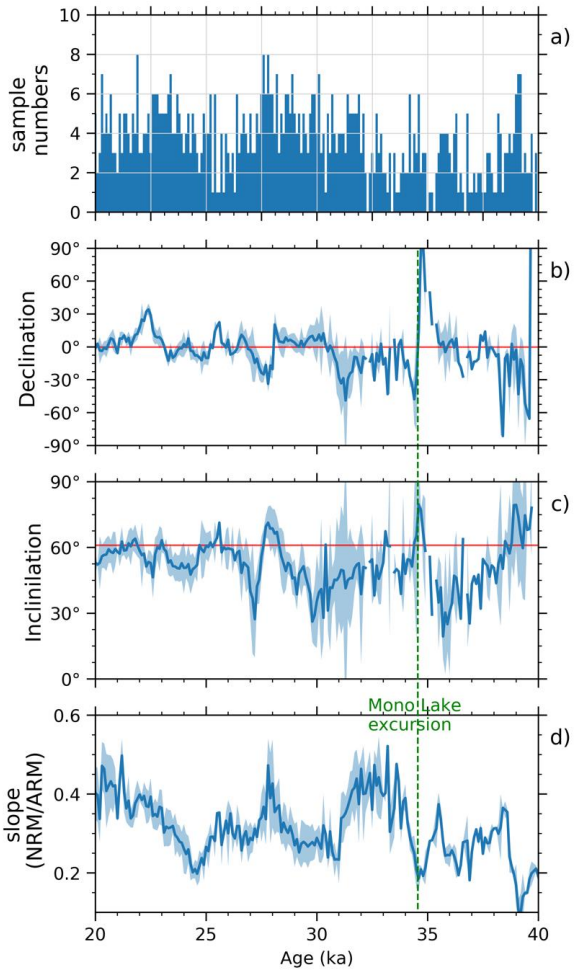

Figure 4.7 Stacked paleosecular variation record from 40 to 20 ka from Black Sea sediments on a common time axis (see also Fig. 4.6): a) record of numbers of samples per 100-year bin for paleomagnetic data stacking of b) declination, c) inclination (both with α_{95} error bars), and d) paleointensity (slope (NRM/ARM), with 1σ standard deviation bars). For comparison, in b) the declination of 0° and in c) the inclination of 61°, both expected from a geocentric axial dipole field of normal polarity at the Black Sea site, are marked by red lines.

4.4 DISCUSSION

4.4.1 The Black Sea paleointensity record

The stacked rPI record derived from seven Black Sea sediment cores for the time window from 40 and 20 ka (Fig. 4.9a) are shown together with the South Atlantic paleointensity stack (SAPIS, Stoner et al., 2002, Fig. 4.9b), the Global paleointensity stack (GLOPIS-75, Laj et al., 2004, Fig. 4.9c), and with relative paleointensity stacks of sediment records (Fig. 4.9d) as well as virtual axial dipole moments (VADMs) from lava flows taken from the GEOMAGIA50 database (Brown et al., 2015, 9e). Note that the SAPIS and the GLOPIS-75 are plotted in Fig.9 based on the GICC05 timescale (NGRIP, 2004). The sedimentary rPI records from GEOMAGIA50 database were initially normalized in order to enable the stacking on a common amplitude scale. In Fig. 4.9, a general agreement between the Black Sea rPI stack and reference paleointensity records are evidenced, though with slight age offsets. At about 34.5±1 ka, a distinct paleointensity low, linked to the Mono Lake excursion in SAPIS (Stoner et al., 2002) and GLOPIS-75 (Laj et al., 2004), are observed in all paleointensity curves (Fig. 4.9). The paleointensity low, centered at about 34.5 ka in Black Sea rPI stack, is further accompanied by noticeable directional anomalies (Figs. 7, 8, 9). This pattern, but on a sparser data base, has been discussed as the Mono Lake excursion in M72/5 cores (Nowaczyk et al., 2013, 2012) and is now further validated in MSM33 cores (Fig. 4.6).

After the Mono Lake excursion, a paleointensity minimum is observed in the Black Sea and the SAPIS rPI stack at about 25.1 ka, though it is not evident in GLOPIS-75 and the GEOMAGIA50 (Fig. 4.9). The paleointensity low was also found in core MD04-2822 (Rockall Trough, Northeast Atlantic) at about 26.5 ka, and was reported as an excursion with directional anomalies (Channell et al., 2016). Nevertheless, in Black Sea sedimentary records, the rPI low at about 24.5 ka is only associated with directional changes typical for paleosecular variation (Fig. 4.7). Thus, after about 32 ka, no directional shifts are coeval with rPI minima observed in the Black Sea PSV stack, denoting simply normal secular variations. Also the postulated Hilina Pali excursion (Singer et al., 2014) at around 18.5 ka is expressed only as more pronounced paleosecular variations, with VGPs not exceeding latitudes lower than 60°N (Liu et al., 2018).

4.4.2 Directional behavior during the Mono Lake excursion

The Mono Lake excursion, recorded in Black Sea sediments centered at 34.5 ka, is evidenced by remarkably low paleointensities associated with directional anomalies (Fig. 4.7). For the time interval between 33 ka and 36 ka, covering the Mono Lake excursion, the VGP paths

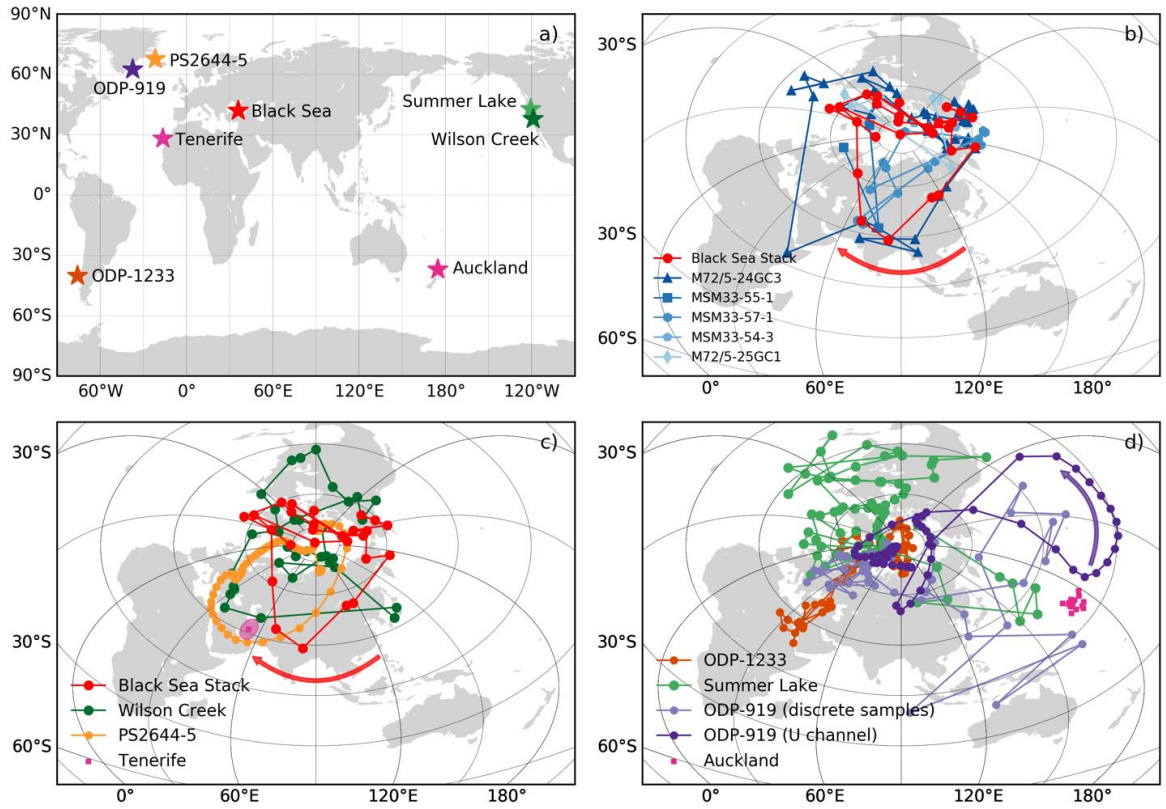

Figure 4.8 Migration of the virtual geomagnetic poles (VGPs) derived from b) individual Black Sea cores (blue) and the stacked Black Sea record (red) from 36 to 33 ka, and c) stacked Black Sea record, shown together with VGP paths obtained from the Wilson Creek Formation, USA (Lund et al., 1988), Iceland Sea core PS2644-5 (Laj et al., 2000a), and the VGP positions from Tenerife lava flows, with the (dp, dm) ellipse of confidence (Kissel et al., 2011). d) VGP paths derived from the continental slop of southern Chile, Site ODP-1233 (Lund et al., 2007; S. P. Lund et al., 2006), the Summer Lake, USA (Negrini et al., 2014), the Iceland Sea, Site ODP-919 (discrete samples by Negrini et al., 2014; u-channel by Channell, 2006), and VGP positions from the Auckland volcanic field (Cassata et al., 2008). The respective coring/sampling sites are shown in a). The arrows indicate the sense of VGP movement.

obtained from individual Black Sea cores are shown in Fig. 4.8b. Although, during the Mono Lake excursion, VGP paths are not continuous in some cores due to hiatuses and samples omitted by greigite filtering, excursional VGPs are observed in three Black Sea cores (Fig. 4.8b). The VGP throughout the Mono Lake excursion based on stacked data first moved from high latitudes to East Asia, subsequently moved southwestwards to the Tibetan Plateau, then crossed central Asia and North Europe, and finally moved back to the Arctic. Note that the stacked Black Sea VGP positions reach lower-most latitudes of 29°N (α_{95}=17.5), while one single VGP from core M72/5-24GC3 even reach a latitude of only 6°N in East Africa.

In Fig. 4.8c, the VGP path of the Mono Lake excursion derived from Black Sea sediments is compared with VGPs obtained from the Wilson Creek Formation, USA (Lund et al., 1988),

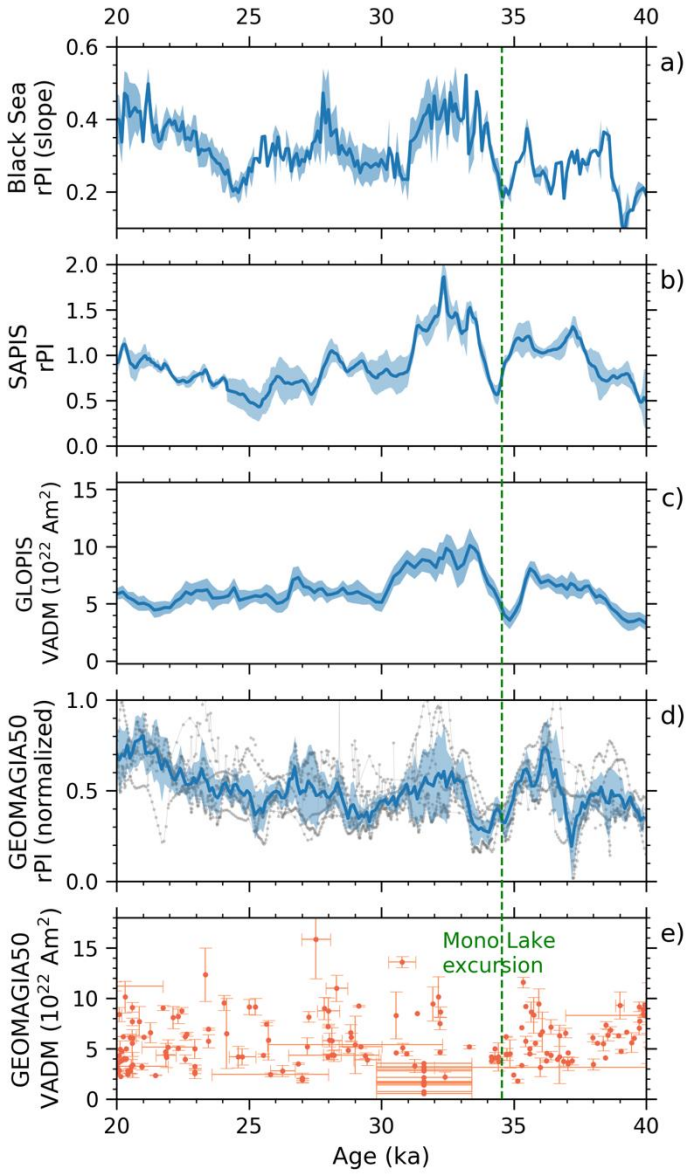

Figure 4.9 Stacked paleointensity records for the time window from 20 to 40 ka: a) Black Sea relative paleointensity (rPI) stack; b) the South Atlantic paleointensity stack (SAPIS, Stoner et al., 2002); c) the global paleointensity stack (GLOPIS-75, Laj et al., 2004); d) stacked rPI record from sediments and e) virtual axial dipole moments (VADM) from lavas both taken from the GEOMAGIA50 database (Brown et al., 2015). The SAPIS and the GLOPIS-75 are plotted on the GICC05 timescale (NGRIP, 2004). Prior to stacking, the rPI records from sediments from the GEOMAGIA50 database were normalized to the same scale for the studied time interval.

from core PS2644-5, Iceland Sea (Laj et al., 2000a) and from Tenerife lava flows, Canary Islands (Kissel et al., 2011).

The Mono Lake excursion, originally reported in the Wilson Creek Formation (west USA), is characterized by directional shifts at around 33 ka cal. BP (Benson et al., 2003; Liddicoat and Coe, 1979; Lund et al., 1988). The VGPs calculated from Wilson Creek data (Lund et al., 1988) are shown in Fig. 4.8c for the time interval between 33.5 ka and 31 ka (ages following Benson

et al., 2003). During the Mono Lake excursion, its VGPs migrated clockwise from the Arctic to Japan (35°N), and westwards across central Asia to the eastern Mediterranean Sea (32°N), then back to the Arctic across eastern Europe (Fig. 4.8c). At end of the Mono Lake excursion, the VGPs of Wilson Creek data migrated counterclockwise from Alaska to Mississippi with a southernmost latitude of 32°N, and then along the Atlantic coast back to the Arctic area (Fig. 4.8c). The Mono Lake excursion recorded in the Wilson Creek Formation is further evidenced in Pyramid Lake sediments (west USA) with a comparable pattern (Lund et al., 2017). Coupled with radiocarbon dates, dated intercalated ashes, and correlating with other PSV records, the PSV record from Pyramid Lake reveals both the Mono Lake (34.1±0.4 ka) and the Laschamp excursion (40.9±0.5 ka) by anomalous paleomagnetic directions (Lund et al., 2017).

In the Arctic Ocean, Nowaczyk et al (1994) and Nowaczyk and Knies (2000) reported the Mono Lake and the Laschamp excursions from two sediment cores (PS2212-3-KAL and PS2138-1-SL) with pronounced directional swings and low paleointensity. Though the excursions are evident in ChRM inclinations, the ChRM declinations are fairly scattered due to the high northern latitude coring sites. Thus, it is impossible to calculate a well constrained VGP path from these records. In the Iceland Sea, core PS2644-5, integrated in NAPIS-75 stack, exhibits a slight directional shift with an intensity minimum at about 34 ka that was associated with the Mono Lake excursion (Laj et al., 2000a). The VGPs from core PS2644-5 shown in Fig. 4.8c for the period spanning the Mono Lake excursion, migrated clockwise from the Arctic to the Arabian Peninsula (24°N), across Siberia, and then across the eastern Mediterranean Sea and east Europe, back to the Arctic (Fig. 4.8c). Hence, the VGP path from core PS2644-5 is comparable to the Wilson Creek data, though smoother in shape (due to U-channel data) but reaching lower latitudes.

On the island of Tenerife (Canary Islands, off West Africa), the Mono Lake excursion was reported in three lava flows ranging in age between 32±1.2 and 33.2±3.4 ka (Kissel et al., 2011). Their ages obtained from K/Ar and $^{40}Ar/^{39}Ar$ dating, on a statistic base, cannot be distinguished from each other, though the paleomagnetic results denote that the three lava flows were erupted at different times during the Mono Lake excursion. Specifically, one of the lava flows is characterized by remarkable directional deviations coinciding with a paleointensity low (7.8 μT). Its VGP is located in the north of the Persian Gulf (32.2°N, α_{95}=4.7), close to the excursional VGPs from core PS2644-5 (Laj et al., 2000a), the Wilson Creek Formation (Lund et al., 1988) and the Black Sea stack (Fig. 4.8c). Although the other two lava flows manifest low paleointensities of about 12 and 21 μT, their VGPs are sited at high latitudes of 82°N and 73°N, respectively (Kissel et al., 2011). For comparison, the present day field value at Tenerife

is 38.56 μT (value calculated using the NOAA geomagnetic field calculator, based on IGRF12; https://www.ngdc.noaa.gov/geomag-web/#igrfwmm).

Thus, during the Mono Lake excursion, the VGPs obtained from the Black Sea, the Wilson Creek Formation (USA), core PS2644-5 (Iceland Sea), and the Tenerife lava flow (off West Africa), roughly reach low latitudes of ~30°N in western and central Asia (Fig. 4.8c). Interestingly, except for the volcanic Tenerife data, those sedimentary VGP paths exhibit a clockwise loop on the Eurasian continent, though with some offset (Fig. 4.8c). On the other hand, the VGPs during the Mono Lake excursion as derived from site ODP-919 (Iceland Sea) (Channell, 2006; Negrini et al., 2014), the Summer Lake (west USA, Negrini et al., 2014), and lavas in the Auckland volcanic field (New Zealand, Cassata et al., 2008) are located in a cluster in the equatorial Pacific Ocean (Fig. 4.8d), demonstrating no specific migration path and distinct VGP positions when compared to the Black Sea data.

In the Iceland Sea, paleomagnetic data obtained from site ODP-919, both the Mono Lake and the Laschamp excursion are documented with directional anomalies (Channell, 2006). During the Mono Lake excursion, the VGP path from site ODP-919 (U-channel data, Channell, 2006) migrated counterclockwise from Alaska to the central Pacific Ocean, off west Hawaii, then moved further south to the equatorial region, then northward to the Arctic (Fig. 4.8d). The VGPs obtained from discrete samples from site ODP-919, presented by Negrini et al (2014), however, show scattered positions in Southeast Asia without an evident path. Nonetheless, the Mono Lake excursion recorded at site ODP-919 was solely manifested in directional swings, without a coeval paleointensity minimum. It might be possible that the PSV record from site ODP-919 was partly biased due to sedimentary artifacts at this specific site during this short lived excursion (Kissel et al., 2011).

In the western USA, the Mono Lake excursion is additionally evidenced in Summer Lake sediments (Oregon) with directional anomalies associated with a paleointensity low (Negrini et al., 2014). During the Mono Lake excursion, associated VGPs were moving in three clusters, specifically, from the western equatorial Pacific cluster, via the North Atlantic/Europe cluster, finally to the southern North America cluster (Fig. 4.8d, Negrini et al., 2014). Similarly, the VGPs derived from discreet samples from site ODP-919 are also plotting in the same clusters during the Mono Lake excursion, though with some offset in phase (Fig. 4.8d, Negrini et al., 2014). Negrini et al (2014) suggested that the locations of these three clusters are coinciding with non-axial dipole features found in the Holocene geomagnetic field.

In the Southern Hemisphere, cores taken at site ODP-1233 at the southern Chile Trench provided high-resolution PSV records for the last 50 ka (Lund et al., 2007; S. P. Lund et al., 2006). The Mono Lake and the Laschamp excursions are evidenced by distinct directional swings at about 35 ka cal. BP and 41 ka cal. BP, respectively. The directional pattern of the two excursions are also reproduced in site ODP-1234 cores some 500 km away. However, the directional variability for the two excursions at ODP sites 1233 and 1234 is significantly different in pattern from that of the Mono Lake and the Laschamp excursion from the Northern Hemisphere sites (Lund et al., 2007). The VGPs, calculated from a composite directional splice from ODP-1233 cores (Lund et al., 2007), are shown for the Mono Lake excursion in Fig. 4.8d. During the Mono Lake excursion, VGPs from site ODP-1233 ate located around northeast Africa and the Middle East. Although VGPs from site ODP-1233 are close to those from the Wilson Creek record and core PS2644-5 (Fig. 4.8c), no evident migrating path is visible.

In New Zealand, eight volcanic centers in the Auckland volcanic province yielded excursional field directions that define three spatially distinct clusters (Cassata et al., 2008; Shibuya et al., 1992). The lava flows of cluster 1, with an $^{40}Ar/^{39}Ar$ age of 31.6±1.8 ka, was correlated to the Mono Lake excursion (Cassata et al., 2008). The VGPs of cluster 1, sited in the Pacific Ocean west of Hawaii (Fig. 4.8d), is different from the VGPs from the Tenerife lava flows, the Black Sea stack, and the Wilson Creek during the Mono Lake excursion. Note that the VGPs from lavas that recorded the Laschamp excursion in Auckland volcanic field also do not closely match with VGPs corresponding to the Laschamp excursion obtained from eight globally distributed marine sediment cores (Channell, 2006; Laj et al., 2006). Cassata et al. (2008) suggested that this should be due to non-axial dipole fields of a more complex geometry, perhaps influenced by long-lived lower mantle features beneath Australasia (Hoffman and Singer, 2004). If this is true, it may also explain the different VGPs recorded in the Auckland volcanic field during the Mono Lake excursion. In addition, compared to ages of the Mono Lake excursion reported in the French Chaîne des Puys (34.2±1.2 ka, Laj et al., 2014), site ODP-919 (33.5-32.5 ka, Channell, 2006) and the GLOPIS-75 stack (35-33 ka, Laj et al., 2004), the age of the Auckland cluster 1 (31.6±1.8 ka) is relatively young.

During the Mono Lake excursion, the VGPs recorded in sediments at site ODP-919 (Iceland Sea, Channell, 2006), the Summer Lake (west USA, Negrini et al., 2014) and in the lavas of the Auckland volcanic field (New Zealand, Cassata et al., 2008), are sited in the west Pacific cluster, however, with scattered locations (Fig. 4.8d). Their VGPs are thus different from those that were recorded in the Black Sea sediments (Fig. 4.8b). But, the Mono Lake excursion recorded at site ODP-919 is likely only partially recorded due to some possible sedimentary

artifacts during the Mono Lake excursion (Kissel et al., 2011). In the Auckland lava flows, the age of cluster 1 (31.6±1.8 ka) associated with the Mono Lake excursion is somewhat younger than other comparable records. Additionally, VGPs obtained from core PS2644-5 and site ODP-919, that are closely located in the Iceland Sea exhibit significantly distinct patterns, which is likely resulting from different data fidelity. The similar scenario was also observed in VGPs recorded by the Summer Lake and the Wilson Creek that are about 500 km away in western USA.

In summary, during the Mono Lake excursion, the VGPs obtained from the Black Sea sediments, the Wilson Creek Formation, the Iceland Sea sediments (core PS2644-5), Tenerife lava flows and southern Chile continental slope sediments (site ODP-1233), are located mainly around the Arabian Peninsula (Fig. 4.8c, d). Additionally, VGP paths from the Black Sea, the Wilson Creek Formation and core PS2644-5 exhibit a clockwise loop on the Eurasia continent. The coinciding excursional VGPs from a variety of sites would suggest the conclusion that the Mono Lake excursion, like the Laschamp and the Iceland Basin excursions (e.g., Laj and Channell, 2015), has a globally comparable pattern of field behavior. On the other hand, diverging VGP positions are observed at site ODP-919, the Summer Lake and the Auckland volcanic field (Fig. 4.8d). Besides, VGP paths obtained from sites ODP-919, ODP-1233 and the Summer Lake are distinct and demonstrate no comparable patterns. The VGP behaviors obtained from those sites are thus likely indicating a non-dipole field during the Mono Lake excursion. Hence, aiming to better define these geomagnetic field geometry changes across the short-lived Mono Lake excursion, further precisely dated lava flows and high-resolution sediment records are required.

4.5 CONCLUSION

A fairly consistent paleosecular variation record, comprising inclination, declination, and relative paleointensity data, could be reconstructed from seven Black Sea sediment cores for the time window between 20 and 40 ka cal. BP. The data set includes the Mono Lake excursion, evidenced by a paleointensity minimum and significant directional shifts at around 34.5 ka. During the Mono Lake excursion, the VGP path from Black Sea sediments performs a clockwise loop with VGPs migrating from Alaska, via Siberia, to the north of India, then west-northward across central Asia towards Greenland. This pattern of the Mono Lake excursion recorded in Black Sea sediments is in good agreement with the ones recorded in the Wilson Creek Formation, the Iceland Sea (core PS2644-5), and Tenerife lavas. These paleomagnetic data sets suggest a global coherence of field behavior during the Mono Lake excursion. On the other hand, distinct excursional VGPs recorded from some further sites are in conflict with this

interpretation and thus indicate a non-dipolar geomagnetic field pattern with regionally diverging vector behavior. Further high fidelity paleomagnetic data are therefore required in the future to determine the exact field pattern during the Mono Lake excursion. After the Mono Lake excursion, the stacked Black Sea PSV record exhibits only normal secular variation for the studied time interval, with VGPs at high northern latitudes only.

ACKNOWLEDGEMENTS

We appreciate Robert M. Negrini for providing VGP data from the Summer Lake and Site ODP-919 (discrete samples). We also thank Zhao Xiang for discussing obtained FORC diagrams. And we thank S. Plewe, M. Duwe, T. Moldenhawer, and F. Brendel for their technical and logistical help during processing and sub-sampling of the cores. We also thank the captains and crews of *RV Meteor*, cruise M72/5 and *RV Maria S. Merian*, cruise MSM33, for their efforts in providing optimal scientific working conditions. This work was partly funded by the German Research Foundation (Deutsche Forschungsgemeinschaft, DFG SPP 1266 “INTERDYNAMIC” grants AR 367/9-1 and AR 367/9-2), the Gary Comer Science and Education Foundation, U.S.A., and the Chinese Scholarship Council (CSC grant No. 201506180060).

5 A 20–15 ka high-resolution paleomagnetic secular variation record from Black Sea sediments – no evidence for the 'Hilina Pali excursion' ?

Published in Earth and Planetary Science Letters 492 (2018), 174-185

Liu Jiabo[1], Norbert R. Nowaczyk[1], Ute Frank[1], Helge W. Arz[2]

[1] GFZ German Research Centre for Geosciences, Section 'Climate Dynamics and Landscape Evolution', 14473 Potsdam, Germany.

[2] Leibnitz Institute for Baltic Sea Research Warnemünde, 18119 Rostock, Germany.

SUMMARY

A comprehensive magnetostratigraphic investigation on sixteen sediment cores from the southeastern Black Sea yielded a very detailed high-quality paleosecular variation (PSV) record spanning from 20 to 15 ka. The age models are based on radiocarbon dating, stratigraphic correlation, and tephrochronology. Further age constraints were obtained by correlating four meltwater events, described from the western Black Sea, ranging in age from about 17 to 15 ka, with maxima in K/Ti ratios, obtained from X-ray fluorescence (XRF) scanning, and minima in S-ratios, reflecting increased hematite content, in the studied cores. Since the sedimentation rates in the investigated time window are up to 50 cm ka^{-1}, the obtained PSVs records enabled a stacking using 50-year bins. A directional anomaly at 18.5 ka, associated with pronounced swings in inclination and declination, as well as a low in relative paleointensity (rPI), is probably contemporaneous with the Hilina Pali excursion, originally reported from Hawaiian lava flows. However, virtual geomagnetic poles (VGPs) calculated from Black Sea sediments are not located at latitudes lower than 60° N, which denotes normal, though pronounced secular variations. During the postulated Hilina Pali excursion, the VGPs calculated from Black Sea data migrated clockwise only along the coasts of the Arctic Ocean from NE Canada (20.0 ka), via Alaska (18.6 ka) and NE Siberia (18.0 ka) to Svalbard (17.0 ka), then looping clockwise through the Eastern Arctic Ocean.

KEYWORDS

paleosecular variation, geomagnetic excursion, relative paleointensity, Hilina Pali excursion, Black Sea

5.1 INTRODUCTION

A geomagnetic field excursion is a 'brief' (<10^4 years) but significant deviation of paleomagnetic directions from the direction of a geocentric axial dipole (GAD). Associated virtual geomagnetic poles (VGPs) then move out of the area of normal secular variation (Laj and Channell, 2015b), i.e., to latitudes below 45°. With increasing numbers of high-fidelity paleomagnetic records, numerous excursions have been discovered in the last few decades. Some well-validated excursions, such as the Laschamp excursion (e.g., Cassata et al., 2008; Nowaczyk et al., 2012; Plenier et al., 2007) and Iceland Basin excursion (e.g., Channell, 2014, 2006), have been demonstrated to have global appearance and their VGPs reach high southern latitudes (Laj et al., 2006), whereas some postulated excursions, associated with less pronounced paleointensity lows, are sporadically reported due to inadequate paleomagnetic recordings (Roberts, 2008).

Low paleointensity values at 17.86±0.67 ka, recorded in a pair of lava flows at Hilina Pali from Kilauea Volcano, Hawaii (19.2ºN, 204.7ºE), and shallow inclinations in one of the flows were firstly reported by Coe et al. (1978). The same feature at 20 ka was later documented as 'Excursion A' in SHO (Scientific Observation Hole) cores of Hawaii by Teanby et al. (2002) and Laj et al. (2002), who suggested it may represent the postulated Hilina Pali excursion.

However, the Hilina Pali excursion is not yet well established, though some possible excursions have been observed around the same time. With only roughly dated ages, Clark and Kennett (1973) found inclination changes between 12.5 and 17.0 ka in two cores from the western Gulf of Mexico. In a sediment core from Lake Baikal (Siberia, Russia), a sharp declination swing of 85º (in five samples) at 20 ka, corresponding to an interval of shallow inclination between 22 and 18 ka, were documented by Peck et al. (1996). From an Arctic Ocean site, a short excursion at around 20 ka (uncalibrated) accompanied with low relative paleointensity and negative inclination was reported in four sediment cores (Nowaczyk et al., 2003; Nowaczyk and Knies, 2000). In southern South America, a directional swing at around 20 ka is observed in several cores, Laguna Potrok Aike (Lisé-Pronovost et al., 2013), ODP Site 1233 (S. Lund et al., 2006) and ODP Site 1089 (Stoner et al., 2003). Lisé-Pronovost et al. (2013) suggest that the associated low in paleointensity from Laguna Potrok Aike could correspond to the Hilina Pali excursion recorded in the Hawaii lava flows (Laj et al., 2002; Teanby et al., 2002). In the Chaîne des Puys, France, three lava flows erupted at around 18 ka, characterized by low paleointensities (Laj et al., 2014). Singer et al. (2014) suggest that this feature may also correspond to the postulated Hilina Pali excursion although VGP positions are only as far South as 62°N for just one of the lava flows. With new 40Ar/39Ar dating of the lava flows from

Tianchi volcano, China, an excursion, originally reported at 123 ka as the Blake excursion by Zhu et al. (1999), was redated to 17.0±1.1 ka and named as 'Hilina Pali/Tianchi excursion' by Singer et al. (2014). The Hilina Pali/Tianchi excursion is, therefore, the first and only record that yielded transitional VGPs located at South Korea and Tasmania, respectively.

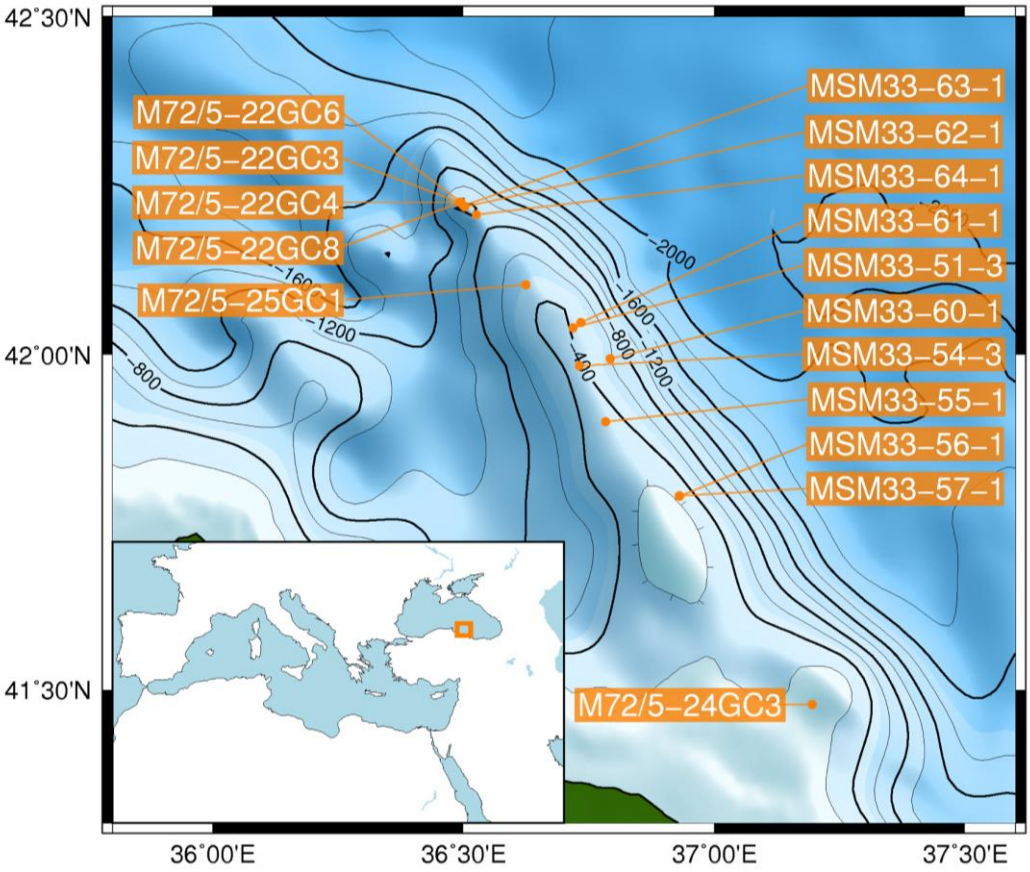

Figure 5.1 Positions of coring sites along the Archangelsky Ridge in the SE Black Sea during cruises of *RV Meteor* (M72/5, 2007) and *RV Maria S. Merian* (MSM33, 2013).

Here, we present well-dated high-resolution magnetostratigraphic data, directions and relative paleointensities, from sixteen sediment cores recovered from the SE Black Sea, covering the time interval from 20 to 15 ka at high resolution. Thus, these cores are an ideal archive in order to test whether the postulated Hilina Pali excursion finds an expression in the paleomagnetic record from the Black Sea area.

5.2 METHODS

For this detailed study a collection of sixteen cores, recovered from the SE Black Sea, with exceptional high sedimentation rates of up to 50 cm ka-1 in marine isotope stage (MIS) 2, were selected. Six of them were cored in 2007 during the German RV Meteor cruise M72/5 and ten were taken in 2013 during the German RV Maria S. Merian cruise MSM33. All cores have a

diameter of 12 cm. They were recovered from water depths between 208 and 847 m along the Archangelsky Ridge (Fig. 5.1, see also Table 1.1).

X-ray fluorescence (XRF) scanning of M72/2 cores was performed at a resolution of 10 to 20 mm (Nowaczyk et al., 2013, 2012). High-resolution XRF-logs from MSM33 cores were obtained from split archive core halves, using an ITRAX XRF Core Scanner (COX Analytics; e.g., Croudace et al., 2006). The core scanner was operated with a Cr-tube at 30 kV and 30 mA and an SDD Si drift detector. Exposure time was 15 seconds and down-core step size was 1 mm. XRF measurements of MSM cores were performed at the Leibnitz Institute for Baltic Sea Research Warnemünde, Rostock, Germany. Here, also the low-field magnetic volume susceptibility κLF was first measured in steps of 1 mm directly on the split-surface of the cores using a Bartington MS2E spot-reading sensor with a spatial resolution of 4 mm, integrated into an automated core logging system. These data sets were used for correlation.

Magnetic volume susceptibility was also determined on 6 cm3 discrete paleomagnetic samples (cubic plastic boxes), taken continuously from the central axis of each core segment, using an AGICO multi-function Kappabridge MFK-1A, measured with a field of 200 Am-1 and a frequency of 976 Hz.

Measurements of the natural remanent magnetization (NRM) and the anhysteretic remanent magnetization (ARM) were performed with a cryogenic 2G Enterprises 755 SRM long-core magnetometer. The NRM was determined after application of alternating field (AF) amplitudes of 0, 5, 10, 15, 20, 30, 40, 50, 65, 80, and 100 mT. Directions of the characteristic remanent magnetization (ChRM) were determined by principal component analysis (PCA) according to Kirschvink (1980). The ARM was imparted along the samples’ z-axes with a static field of 0.05 mT and an AF field of 100 mT. Demagnetization then was performed in steps of 0, 10, 20, 30, 40, 50, 65, and 80 mT. The slope of NRM versus ARM of common demagnetization steps was then used to determine the relative paleointensity (rPI). Mostly, demagnetization steps from 20 to 65 mT were used to determine the rPI.

An isothermal remanent magnetization (IRM) was imparted using a 2G Enterprises 660 pulse magnetizer and then measured with a Molyneux spinner magnetometer, due to its capability of measuring strong magnetization that would over-range the cryogenic magnetometer. IRM intensities acquired in a peak field of 1.5 T are defined as the saturation IRM (SIRM). A reversed field of 0.2 mT was used to determine the S-ratio, defined as: $0.5 \times (1 - [\text{IRM-0.2T} / \text{SIRM-1.5T}])$, with $0 \leq S \leq 1$. First order reversal curve (FORC) measurements were performed on irregularly spaced field grids using a Princeton Measurements Corporation 'MicroMag'

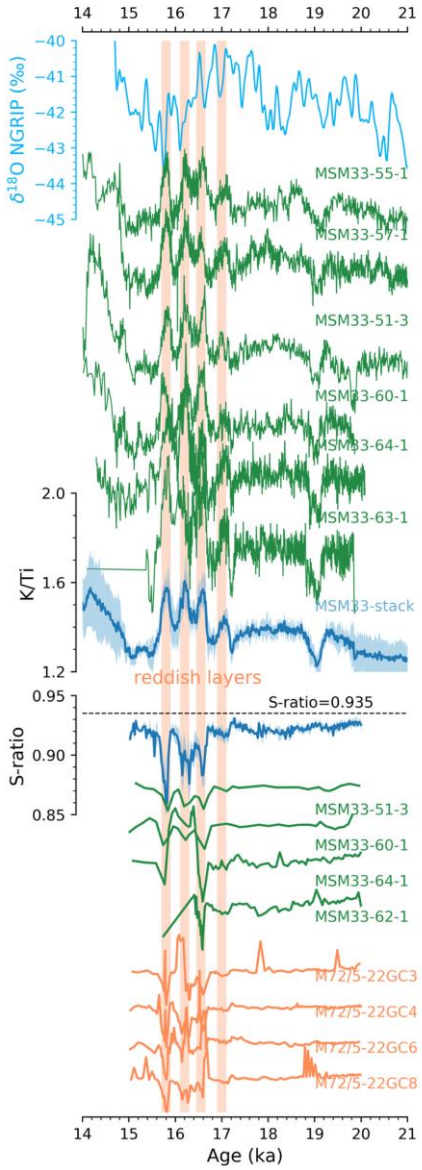

Figure 5.2 K/Ti elemental ratios from X-ray fluorescence (XRF) scanning, together with 10 year bins stacked K/Ti ratios of MSM33 cores (K/Ti stacks, blue lines with 1 σ standard deviation bars), shown for the time window from 21 to 14 ka. S-ratios from MSM33 cores (green) and M72/5 cores (orange) are shown with 25 year bins stack (S-ratio stack, blue lines with 1 σ standard deviation bars) spanning from 20 to 15 ka, note S-ratios > 0.935 were omitted for stacking. NGRIP indicates the oxygen isotope record from Greenland ice cores (Svensson et al., 2008, 2006). Four vertical orange bars, illustrating the meltwater events in the NW Black Sea (Soulet et al., 2013), are correlated to K/Ti peaks and S-ratio lows in SE Black Sea sediment. All K/Ti ratios and S-ratios of individual cores are plotted using the same scale as their stacks, respectively.

alternating gradient magnetometer (AGM). The protocol and calculation of FORC diagrams were performed following Zhao et al. (2015). All paleo- and rock magnetic investigations on discrete samples were performed at the Helmholtz Centre Potsdam, GFZ German Research Centre for Geosciences, Potsdam, Germany

5.3 RESULTS

5.3.1 Establishment of age models

The age models of M72/5 and MSM33 cores were achieved by tuning their XRF logs, mainly Ca/Ti and K/Ti ratios as proxies for Dansgaard-Oeschger warming events (Dansgaard et al., 1993), to the oxygen isotope record from Greenland ice cores (NGRIP, Svensson et al., 2008, 2006). The detailed correlations between Black Sea sediments and NGRIP have been presented by Nowaczyk et al. (2012) for M72/5 cores, and by Nowaczyk et al. (2018) also for MSM33 cores. In addition, the age models of the six M72/5 cores were constrained by 16 accelerator mass spectrometry (AMS) ^{14}C dating on one core, the identification of the well-dated Campanian Ignimbrite tephra and the documentation of the Laschamp geomagnetic excursion centered at 41 ka cal. BP in five of these cores (Nowaczyk et al., 2012).

Based on the age models that have been obtained for the core compilation, the chronology for the time window spanning from 20 to 15 ka cal. BP could be further refined by tuning K/Ti ratios and S-ratios from reddish layers documented in the sediments from the Archangelsky Ridge, SE Black Sea, to similar layers in NW Black Sea sediments. According to Bahr et al. (2006, 2005) and later by Soulet et al. (2013), these reddish layers were caused by large meltwater discharges into the Black Sea, originating from the stepwise decay of the Fennoscandian ice sheet. Each reddish layer is characterized by high XRF Ti/Ca ratios due to sediment provenance changes. In core MD04-2790, four of such red layers between 17.5 and 15 ka cal. BP were recognized, each with a duration of about 220 years (Soulet et al., 2013). The four reddish layers recognized from core MD04-2790 are indicated by orange bars in Fig. 5.2. Between 20 and 15 ka cal. BP, four intervals of K/Ti ratio peaks and low S-ratios, as a proxy for an increased hematite content, responsible for the reddish hues of the sediments, could be identified also in M72/5 and MSM33 cores. Consequently, these were then correlated to the reddish layers reported by Soulet et al. (2013). In the cores investigated for this study, the reddish layers can be also recognized from Ti/Ca ratios but they are much better seen here in K/Ti ratios. Thus, after fine tuning, the K/Ti ratios from individual MSM cores were stacked instead. M72/5 cores were not included in the stack since they were scanned with a different scanning device and also at a lower resolution. Individual K/Ti records from both ship expeditions together with the stack obtained from MSM33 cores with 1σ standard deviation are shown in Fig. 5.2. Examples of some individual S-ratio records, as a proxy for the content of ruddling hematite, are also included. The S-ratio stack was then calculated with values only lower than 0.935, since greigite-bearing samples, distorting the S-ratio record, have generally higher values. Thus, there is a very good fit of reddish layers identified in SE Black Sea

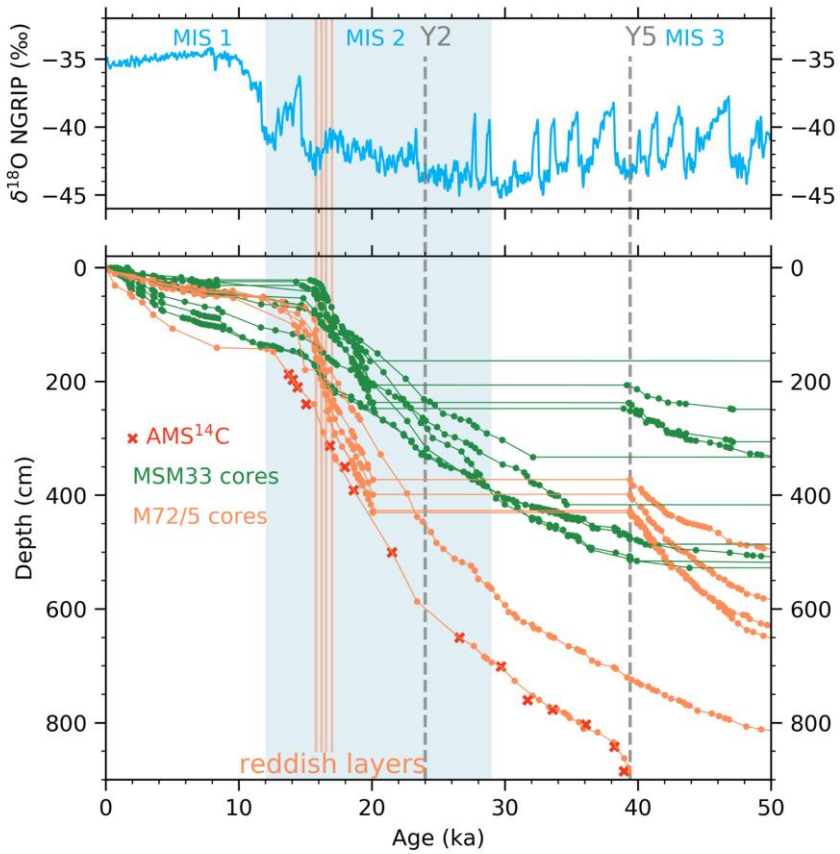

Figure 5.3 Oxygen isotope variations from Greenland ice cores (NGRIP) (top) as the main reference record, shown together with age models for six M72/5 cores (orange) and nine MSM33 cores (green) in the bottom. Sixteen AMS ^{14}C ages from core M72/5-24GC3 are indicated by red crosses. The detailed correlation between XRF scanning data of Black Sea sediment and NGRIP have presented by Nowaczyk et al. (2012, 2013, 2017). Y2-tephra layer from the Cape Riva eruption, Santorini, Greece (e.g., Fabbro et al., 2013), Y5-tephra from Campanian Ignimbrite eruption, Phlegraean Fields, Italy (e.g., Fisher et al., 1993). Reddish layers, representing meltwater events in the NW Black Sea (Soulet et al., 2013), are indicated by four orange bars.

sediments with the corresponding layers in core MD04-2790 from the NW Black Sea, indicated by the orange bars in Fig. 5.2. Ages for these layers from Soulet et al. (2013) were included into the age models from M72/5 and MSM33 cores which are shown in Fig. 5.3. For reasons of clarity, the age models are shown only back to 50 ka cal. BP, although some of the cores extend further back in time. A major hiatus between about 39 and 20 ka cal. BP can be observed in almost half of the studied cores, one reason to restrict the studied time interval back to only 20 ka cal. BP. This and further minor hiatuses are interpreted as the result of slumping due to strong earthquakes in this tectonically very active area (see also: Nowaczyk et al., 2013, 2012). The younger limit of the present study is defined by a major decline in sedimentation rates from up to 50 cm ka^{-1} to less than 10 cm ka^{-1} after about 15 ka cal. BP.

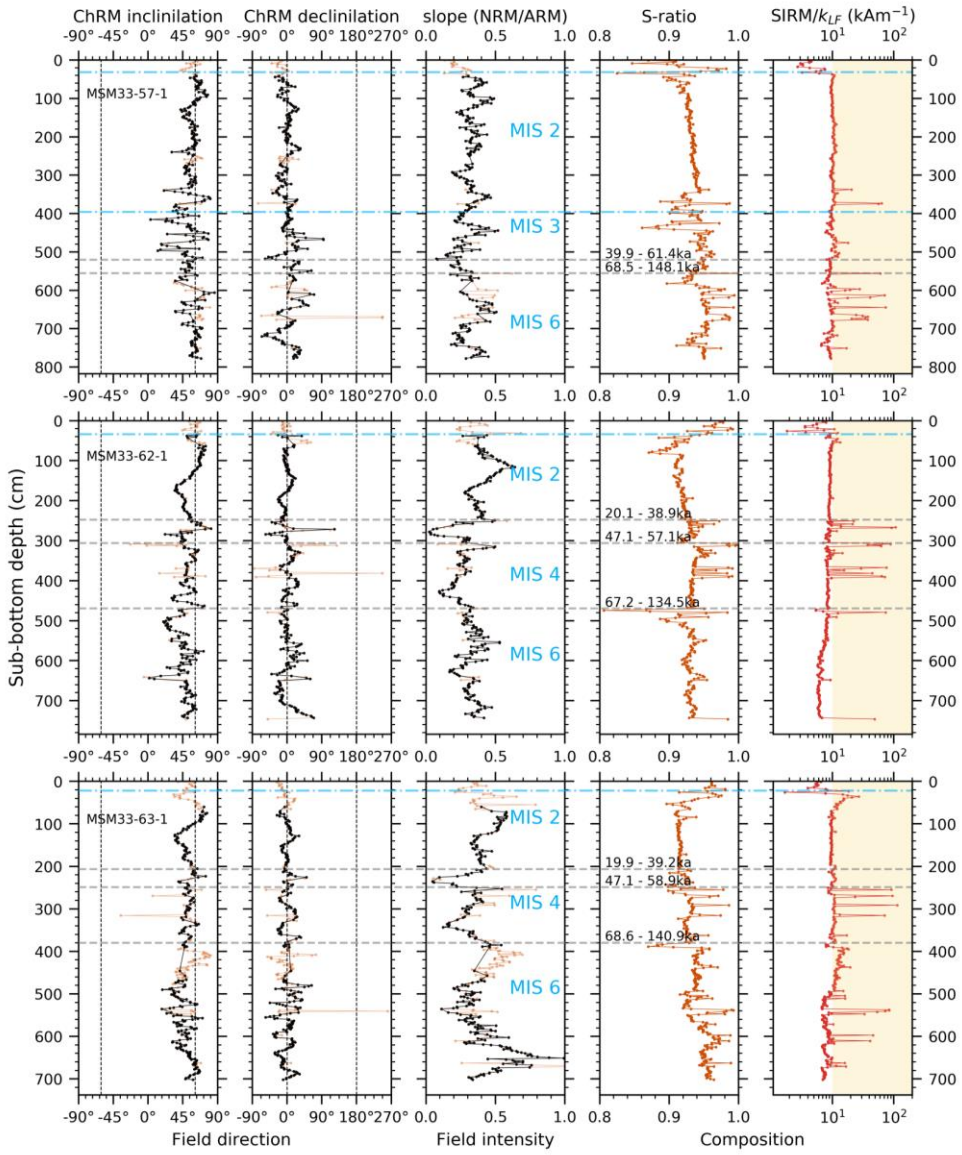

Figure 5.4 Down-core plots of paleomagnetic (ChRM inclination and declination, slope NRM/ARM) and rock-magnetic (S-ratio and SIRM/κ_{LF}) data from three MSM33 cores. For paleomagnetic data after filtering greigite samples (see chapter 3.2) are plotted in black, otherwise in orange color. Green vertical dashed lines in the directional plots indicate the dipole inclination (± 61°) and declination (0, 180°) for normal and reversed polarity, respectively. The slope of NRM versus ARM (middle), is taken as a proxy for relative paleointensity. The S-ratio and the SIRM/κ_{LF} ratio are plotted in orange color with all measured samples. They reflect magneto-mineralogic variations mainly caused by hematite (S-ratio < 0.94) and greigite (yellow areas, SIRM/κ_{LF} > 10 Am^{-1}, S-ratio > 0.95) against a background of (titano-) magnetite. Horizontal dashed blue lines indicate marine isotope stage (MIS) boundaries. Grey horizontal dotted lines indicate inferred hiatuses with black labels indicating the estimated time intervals missing in the records. NRM – natural remanent magnetization, ARM – anhysteretic remanent magnetization, ChRM – characteristic remanent magnetization, SIRM – saturated isothermal remanent magnetization, κ_{LF} – low field magnetic volume susceptibility.

5.3.2 Paleo- and rock magnetism

Complete magnetostratigraphic data from M72/5 cores were already presented in detail by Nowaczyk et al. (2013, 2012). Data from three MSM33 cores (sites 51, 54, 64) were discussed by Nowaczyk et al. (2018), focusing on geomagnetic field variations during MIS 4, also documented at high resolution. New paleomagnetic data sets, ChRM directions and relative paleointensity, and rock magnetic data, S-ratio and SIRM/κ_{LF} ratio, for three further MSM33 cores (sites 57, 62, 63) are shown as down-core plots in Fig. 5.4. Due to low sedimentation rates or hiatuses, as explained above, the Laschamp excursion is missing or documented only fragmentary in most of these MSM33 cores. Nevertheless, the sediments during late MIS 2 were continuously deposited in all studied cores, covering several meters (see also Fig. 5.3). To avoid compromising of paleomagnetic data by erroneous directions carried by greigite, the filter criteria defined by Nowaczyk et al. (2012) were applied also to MSM33 cores, that is, samples with SIRM/κ_{LF} ratios >10 kAm^{-1} and S-ratios >0.95, shown to be affected by greigite, were removed from the records. In Fig. 5.4 the unfiltered data sets are all plotted in orange while greigite-filtered paleomagnetic data, ChRM inclination and declination as well as relative paleointensity (slope NRM/ARM) are plotted in black. During the late MIS2, only a few samples are characterized by SIRM/κ_{LF} ratios larger than 10 kAm^{-1} (Fig. 5.4). Finally, for the time interval between 20 and 15 ka cal. BP, 891 samples out of a total of 1062 samples were left after excluding greigite-bearing samples.

The filtered data set consistently shows large directional swings, mostly indicated by shallow inclinations, as well as low rPI values in all studied cores. For this time interval, representative detailed AF demagnetization data of individual samples from core MSM33-57-1 and their corresponding FORC diagrams are presented in Fig. 5.5. The demagnetization diagrams show that vector end points migrate straight towards the origins, with almost no viscous overprint visible, in all samples. ChRM directions were mostly defined between 20 to 65 mT and yielded maximum angular deviation (MAD) angles smaller than 2°, indicating a very stable nature of the primary components. Directional swings are demonstrated in samples 129 cm and 152 cm with both divergent declinations and inclinations. The conspicuous declination deviations in these two samples are reaching values of around 30°E, and inclinations are likewise getting shallow. For comparison, the inclination of 61°, expected from a geocentric axial dipole field, is marked by the red dotted lines in Fig. 5.5.

The FORC diagrams for MSM33-57-1 samples, performed on irregularly spaced field grids and calculated with a smooth factor (SF) of 2 (following Zhao et al., 2015),

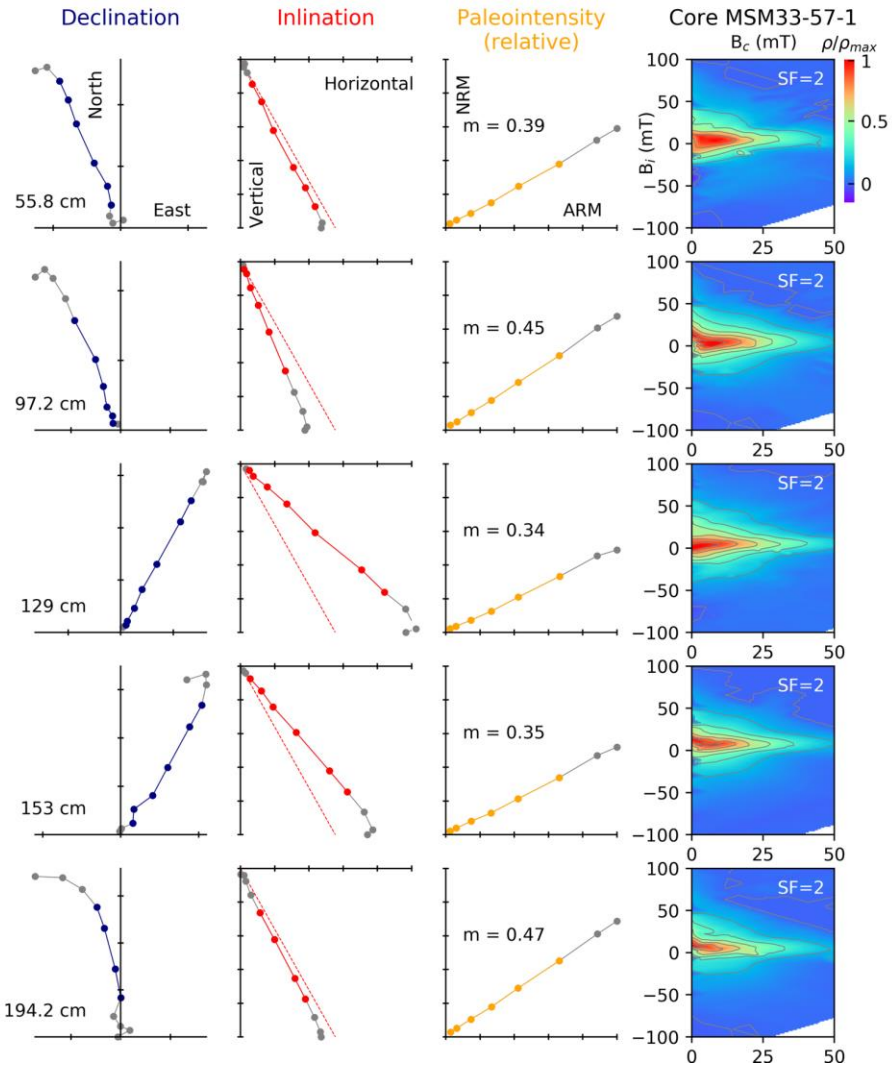

Figure 5.5 AF demagnetization results from five representative samples from the study interval 20 to 15 ka in core MSM33-57-1, with sampling depths given at the outer left. The first column illustrates variations in declination with vector endpoint diagrams of North versus East. The second column illustrates variations in inclination with diagrams of horizontal versus vertical components. The third column illustrates relative paleointensity variations with diagrams of NRM intensity versus ARM intensity. The fourth column displays irregular FORC diagrams for each sample. Directional data is shown after adjustment of declinations from the whole core to a mean value of 0°. Gray symbols indicate raw data from AF steps from 0 to 100 mT (80 mT) for the directional (intensity) variations. Colored symbols indicate AF steps used for determination of the ChRM direction (left & middle) and relative paleointensity (right), respectively. The red dotted line in the inclination plots represent the inclination of 61° of a geocentric axial dipole field. Note that for reasons of clarity axes for NRM and ARM in the intensity plots (right) have different scaling, but with a constant ratio in all diagrams. Irregular FORC diagrams for all samples were calculated with a smoothing factor (SF) of 2, and the FORC distributions ρ were normalized by their respective maximum ρ_{max}.

are shown in the right column of Fig. 5.5. They demonstrate FORC distributions spreading along the B_i axis up to 50 mT, with coercivity peaking at B_c ~10 mT. The pattern has been

interpreted as typical behavior of geological pseudo-single domain (PSD) materials (e.g., Zhao et al., 2015), or further evidenced as vortex state materials (e.g., Zhao et al., 2017).

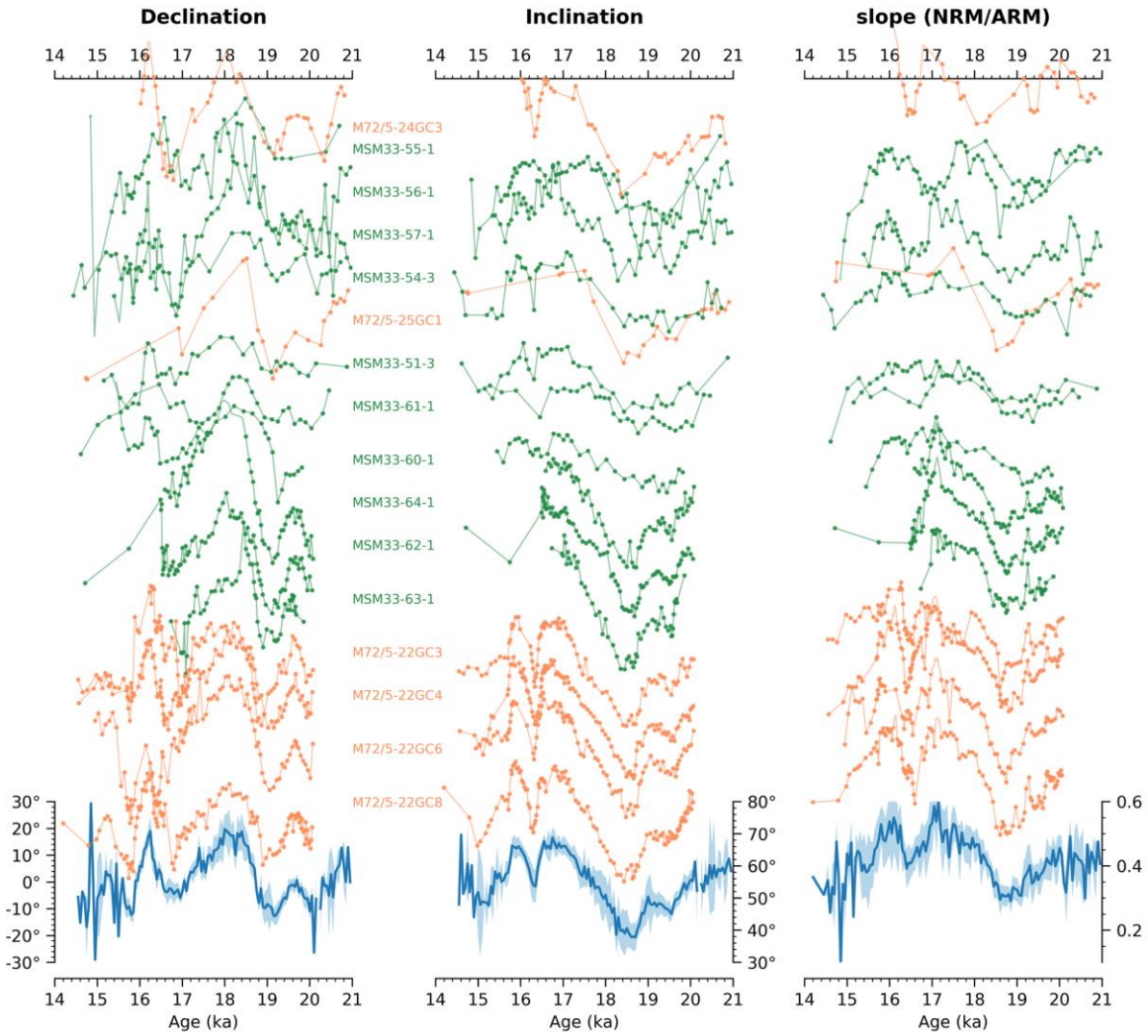

Figure 5.6 ChRM directions (declination and inclination) and relative paleointensity (rPI, approximated by the slope of NRM versus ARM during AF demagnetization) are shown for six M72/5 cores (orange) and ten MSM33 cores (green) for the time window from 21 to 14 ka, together with 50 year bins stacks (blue). Inclination and Declination stacks are plotted with α_{95} bars. The rPI stack is plotted with 1σ standard deviation bars. All individual records share a constant offset with their stacks, respectively. The plots of individual cores are sequenced from bottom to top depending on the water depth of the coring sites from deep to shallow.

The paleosecular variation (PSV) records ranging from 20 to 15 ka cal. BP, comprising ChRM directions (declination and inclination) and slope of NRM/ARM, as a measure of rPI, from all investigated cores are shown in Fig. 5.6. Individual records of M72/5 cores are plotted in orange and MSM33 cores in green. 50 year bins stacked ChRM directions and rPI (slope NRM/ARM) are plotted in blue in the lower part of Fig. 5.6. The stacked data is also shown versus a common age axis in Fig. 5.7. The features in the PSV stacks are all reproducible from

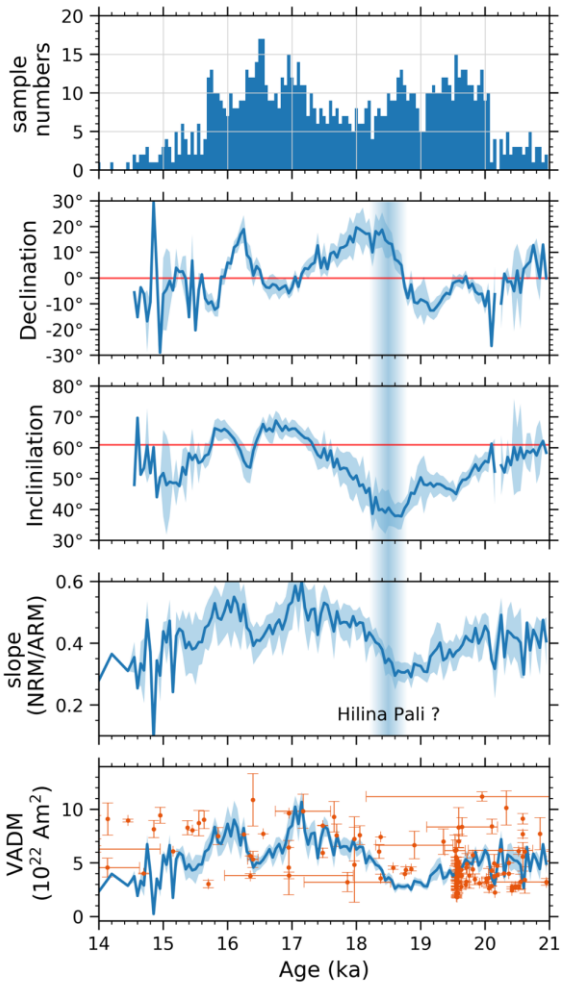

Figure 5.7 Stacked paleosecular variation record from 21 to 14 ka from Black Sea sediments: a) numbers of samples per 50 year time bin used for paleomagnetic data stacking of b) declination, c) inclination, and d) relative paleointensity (rPI), derived from NRM/ARM slopes, and e) rPIs converted into virtual axial dipole moments (VADM). Error bars in b) and c) are α_{95} values, and error bars in d) are marking the 1σ standard deviation. For comparison, in b) the declination of 0° and in c) the inclination of 61°, both expected from a geocentric axial dipole field, are marked by red lines. Orange symbols with error bars in e) mark volcanic VADM records taken from the GEOMAGIA50 database (Brown et al., 2015).

record to record, resulting in the low α_{95} values (directions) and low 1σ standard deviations (rPI), respectively, shown as blue bars in Figs. 6 and 7. The number of samples per time bin in the PSV stacked record are indicated by the histogram in Fig 7a. For bins between 20 and 15.7 ka cal. BP, the number of samples per time bin lies between 4 and 17, while younger and older time bins are based on significantly less samples (0-4). Stacked inclinations are getting shallowest at 18.5 ka cal. BP, with declinations shifting rapidly to Easterly directions, as well as rPI reaching lowest values (Fig. 5.7). Another anomaly with a similar characteristic, but less significant, is visible at 16.4 ka cal. BP.

The Black Sea relative paleointensity (rPI) record was converted into virtual axial dipole moments (VADM). Absolute VADM values were calculated using volcanic data from the GEOMAGIA50 database (Brown et al., 2015) for the time window from 21 to 14 ka. The ratio of the average from absolute VADMs to the average of relative paleointensities from the Black Sea were used to scale the relative paleointensities into VADM values as described by Nowaczyk et al. (2013). The VADM record from Black Sea sediments are shown together with VADMs of GEOMAGIA50 from volcanic rocks as orange symbols (with error bars for age and VADM) in Fig. 5.7e. There appears to be some general agreement between data from volcanic rocks and Black Sea sediment derived data. However, Fig. 5.7e also illustrates the difficulty in comparing continuously determined, well dated relative paleointensities with absolute paleointensities derived from volcanic rocks, representing only spot readings of field variations, partly flawed with large age uncertainties.

The virtual geomagnetic poles (VGP) from the Black Sea data were calculated using Fisher statistics (Fisher, 1953), averaging ChRM inclinations and declinations from the time interval only from 20 to 16 ka cal. BP, since sample numbers for per 50 year bin stacking are generally more than 6 in this period. Thus, the VGP path obtained from Black Sea cores reaches a resolution of 50 years per step (Fig. 5.8a). From 20 ka cal. BP on, the VGP migrated clockwise along the shores of the Arctic Ocean, starting in NE Canada, with a minimum latitude of 64° N. The VGP path of the Black Sea is shown together with other VGP paths obtained from lake sediments (Fig. 5.8a), while in Fig. 5.8b VGPs are plotted that were obtained from volcanic rocks. Their detailed information is listed in Table 5.1.

5.4 DISCUSSION

A high-resolution as well as high-quality paleosecular variation record including relative paleointensity could be reconstructed from a total of sixteen cores from the Black Sea, spanning from 20 to 16 ka cal. BP. At 18.5 ka cal. BP, an anomaly indicated by directional swings associated with a low in relative paleointensity is contemporaneous to the Hilina Pali excursion, first reported by Coe et al. (1978) from Hawaiian lava flows. Aiming to comprehend the existence and extent of the Hilina Pali excursion, data published in literature, including ages and dating methods, is listed in Table 5.1, comprising results obtained from both lava flows and sediments. The Hilina Pali excursion was confidently dated in Hawaii. The age of lava flows reported by Coe et al. (1978) as 17.86±0.67 ka was calibrated as 19.3±1.6 ka using IntCal13, ±2σ by Singer et al. (2014). At around 20 ka, Teanby et al. (2002) and Laj et al. (2002) reported an excursion characterized by low paleointensities and shallow inclinations in Scientific Observation Hole (SOH) drill cores SOH1 and SOH4 from Kilauea Volcano, Hawaii.

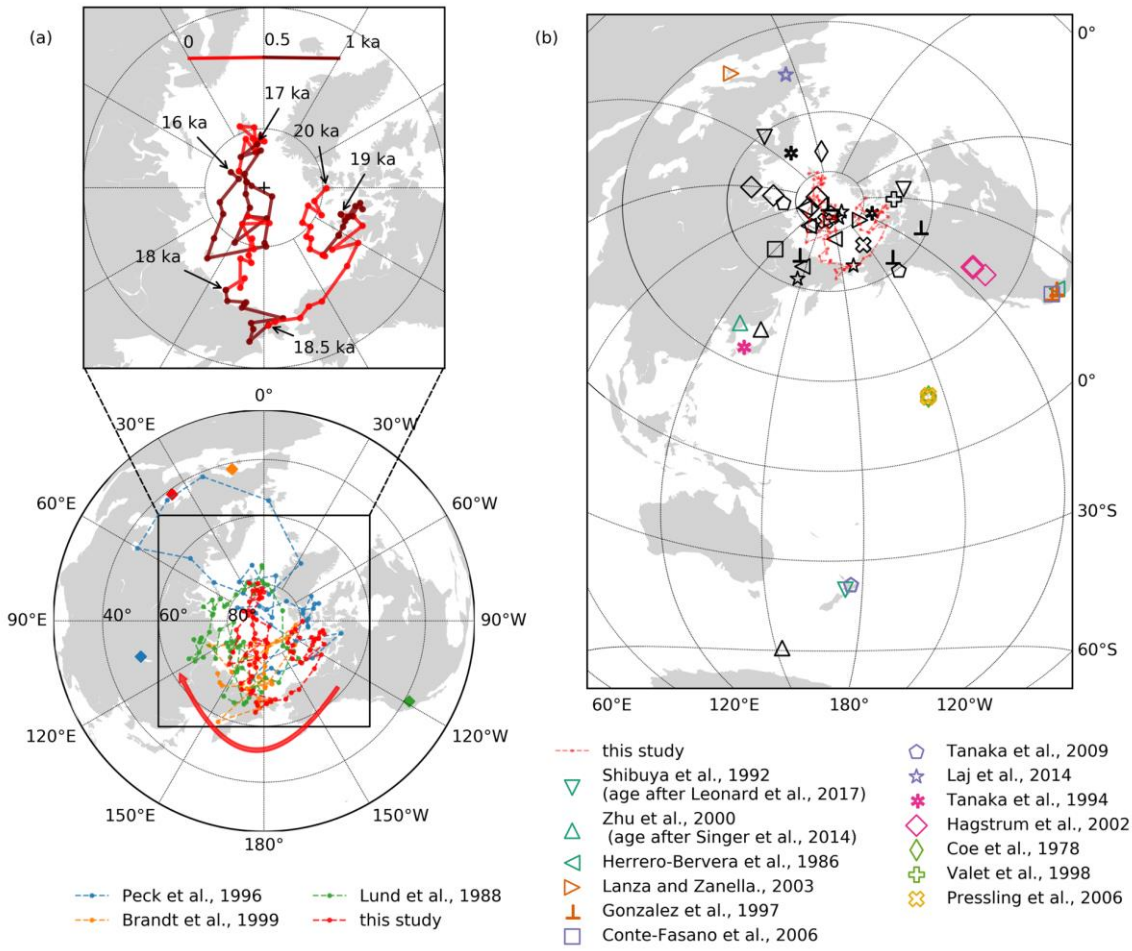

Figure 5.8 a) Virtual geomagnetic pole (VGP) positions derived from stacked ChRM directions (declination and inclination) of SE Black Sea cores spanning from 20 to 16 ka (upper panel), and together with another three sediment records in different colors (lower panel, see references and Table 5.1). Diamonds indicate the coring sites whereas the corresponding VGP paths are plotted with dotted lines of the same color. In the upper panel, the migration of SE Black Sea VGPs is illustrated with alternating light-red and dark-red colors indicating 500 year intervals. b) VGPs derived from lava flows, black symbols, with same symbols in color indicating the corresponding site.

They suggested the excursion is probably the same as the Hilina Pali excursion reported by Coe et al. (1978). In the lava flows reported by Coe et al. (1978) inclinations reach values as shallow as 1.1°, but with associated VGP latitudes being still sited at latitudes higher than 70.3° N. Paleomagnetic data reported from Hawaii by Pressling et al. (2006) and Valet et al. (1998), ranging in age from 20 to about 15 ka (Fig. 5.8), also indicate VGP latitudes all higher than 60° N. The SOH cores, unfortunately, are lacking declination data, and thus, do not allow the calculation of VGP positions. Generally, the postulated Hilina Pali excursion studied in lava flows of Hawaii is only documented with shallow inclinations and a low paleointensity, but is actually not related to transitional VGP latitudes of less than 45°N.

Four investigated lava flows from the Transmexican Volcanic Belt of central Mexico (Gonzalez et al., 1997), ranging in age from 22 to 17 ka, recorded a very low paleointensity, recalculated into a virtual dipole moment (VDM) of 3.1±0.4×1022 Am2, but with an inclination of 64.4° at 21.8 ka. The shallowest inclination of 16.6° related to a VDM of about 6.2±1.6×1022 Am2 was recognized at 19.53 ka (Table 5.1). Around the same time, a comparably low VDM of 3.68×1022 Am2 was reported by Coe et al. (1978) for the Hilina Pali excursion, and thus is likely corresponding to the same 'excursion'. Nevertheless, all VGPs determined from the four lava flows are located at latitudes higher than 60°N (Fig. 5.8, Table 5.1). Similar to these results, VGP positions obtained from other Mexican lava flows, with ages around 19.5 ka (Herrero-Bervera et al., 1986), and from lavas in Idaho and Utah, U.S.A., with ages from about 18 to 15 ka (Hagstrum and Champion, 2002), are distributed without exception at high northern latitudes (Fig. 5.8, Table 5.1).

The VGPs recorded in the lava flows at Tianchi Volcano, Eastern China, was originally reported as representing the Blake excursion by Zhu et al. (2000). With new Ar40/Ar39 dating, Singer et al. (2014) suggested it is the 'Hilina Pali/Tianchi excursion' at 17.1±0.9 ka, thus being contemporaneous to the excursion reported by Coe et al. (1978). The data from sites 3 and 4 of Tianchi Volcano are characterized by anomalous inclination and declination values and yielded VGPs located in South Korea and Tasmania, respectively (Fig. 5.8, Table 5.1), thus clearly representing transitional VGP positions. The transitional directional data is also associated with low VDMs of 3.4×1022Am2 and 6.1×1022Am2, respectively (Zhu et al., 2000). Tanaka et al. (1994) reported on two lava flows from Daisen Volcano, Japan (close to the Tianchi Volcano, Eastern China), dated at 21 and 17 ka, with VADMs as low as 3.83 and 3.23×1022 Am2, respectively. Although this is close to the value of the Hilina Pali excursion (3.68×1022 Am2), as reported by Coe et al. (1978), associated VGP positions are located north of 70°N (Fig. 5.8, Table 5.1).

Laj et al. (2014) published paleomagnetic data obtained from volcanic rocks in the French Chaîne des Puys. Their ages range from 75 to 10 ka, with four lava flows with ages between 18 and 17 ka (Table 5.1). Paleointensities determined from Lava flows at Blanzat, Moulet-Marcenat, and Mazaye calculate into VADM values of 3.9±0.3, 4.0±0.5 and 4.9×1022 Am2, respectively, while the lava at Fontfreyde yielded a value of 6.6±1.0×1022 Am2. Singer et al. (2014) suggested the low paleointensities recorded in these lava flows may also correspond to the Hilina Pali/Tianchi excursion. However, all VGPs derived from these lava flows in the French Chaîne des Puys are clustering in a small area, with none of their latitudes being lower than 60°N. Further VGPs obtained from two lava flows from Vulcano (Aeolian islands), Italy,

with ages of 21.3±3.4 and 15.5±1.5 ka, both have VGP latitudes higher than 79°N (Lanza and Zanella, 2003).

In New Zealand four lava flows from the Okataina volcanic center, with rough datings between 21 and 15 ka, yielded VGP latitudes higher than 59°N (Tanaka et al., 2009). Also two lava flows, the One Tree Hill and Mangere, dated between 18.3 and 17.1 ka, from the Auckland volcanic field, yielded VGP latitudes higher than 70°N (Shibuya et al., 1992). With new Ar40/Ar39 datings, however, the One Tree Hill and Mangere lava flows were redated to 52.8±3.8 and 70.3±3.6 ka, and lava flows of the Mt Smart, Green Mtn and Mt Eden from the same site were dated between 22 and 16 ka (Leonard et al., 2017). Thus, Leonard et al. (2017) suggested the Mt Smart and Mt Eden with shallow inclinations are consistent with the Hilina Pali excursion reported by Teanby et al. (2002), and the Green Mtn erupted either before or after this brief excursion. Nevertheless, paleomagnetic data from the Mt Smart and Mt Eden (Shibuya et al., 1992) yielded VGP latitudes of 68º and 61.2º respectively (Table 5.1).

Regarding published paleomagnetic records from lava flows dated between 22 and 15 ka (Table 5.1) almost all studies yielded VGP positions north of 60°N (Fig. 5.8), though being characterized by fairly low paleointensities. Only paleomagnetic data from Tianchi volcano, China, indicate transitional directions. Thus, in summary, there is no consistent evidence yet that allows to characterize the postulated Hilina Pali excursion either as a global or just a regional geodynamo instability.

Lava flows record geomagnetic field variations within a short time during cooling, and ages of volcanic rocks having erupted closely in time cannot be resolved due to limitations in the precision of the dating methods. Thus it is quite complicated to obtain continuous VGP paths from lava flows, specifically during a short-lived excursion. Therefore, in addition to lava flows, sedimentary data are discussed as well in order to prove the existence and extend of the postulated Hilina Pali excursion.

In principle, sediments can provide continuous records of geomagnetic field variations, despite the deficiency of only providing records of relative paleointensity variations. With only a few age estimates, Clark and Kennett (1973) reported directional swings occurring between 17.0 and 12.5 ka in two cores from the Gulf of Mexico. In core K138, the distinct inclination change was dated between 17 and 15 ka while the associated systematic declination change occurred between 22.5 and 15 ka. In core K136, the inclination variations were dated between 17 and 12.5 ka (Clark and Kennett, 1973). In the maar lake Laguna Potrok Aike, Argentina, South America (Table 5.1), Lisé-Pronovost et al. (2013) reported a directional swing accompanied

by low relative paleointensities at 20 ka and suggested it is probably associated with the Hilina Pali excursion. According to Lisé-Pronovost et al. (2013), the feature recorded in Laguna Potrok Aike are probably also observed in cores from ODP Site 1233 in the Southeast Pacific (S. Lund et al., 2006) and ODP Site 1089 in the southern South Atlantic (Stoner et al., 2003).

Possible records of the Hilina Pali excursion were reviewed by Singer et al. (2014), including the Arctic Ocean (Nowaczyk et al., 2003; Nowaczyk and Knies, 2000) and Lake Baikal (Peck et al., 1996). However, the paleomagnetic data of cores from the Arctic Ocean may be compromised by the accuracy of the 14C ages (Nowaczyk et al., 2003) and magnetic mineral diagenesis (Xuan et al., 2012).

Peck et al. (1996) reported a magnetostratigraphic secular variation record from Lake Baikal covering the last 84 ka, including a geomagnetic excursion at 20 ka. The excursion was indicated by a sharp swing of 85° in declination (in five samples) and an interval of shallow inclinations between 18 and 22 ka. Despite some age uncertainties, due to lower sedimentation rates, the excursion recorded in Lake Baikal sediments may correlate with the Hilina Pali/Tianchi excursion in Tianchi volcano (Singer et al., 2014). The VGP path of Lake Baikal spanning from 22 to 18 ka are presented in Fig. 5.8 with five samples remarkably deviating from the area of normal secular variation. Their VGPs migrated from western Greenland to central Asia, making a clockwise loop, then back to the geographic north pole. Afterwards, it moved along the Arctic ocean coast from North America to the Far East Siberia coast and then back to the west of Greenland. During the excursion, however, the VGP path recorded in Lake Baikal sediments are divergent from that of Tianchi volcano. Despite the age uncertainty of Lake Baikal sediments, the sharp swing in declination at 20 ka is also paralleled by high magnetic susceptibility. Highest magnetic susceptibility was dated between 18.03 and 21.28 ka in core 339P2 (Peck et al., 1996). This feature might be due to diagenetic processes and the post-depositional forming of greigite (Fe3S4) in Lake Baikal sediments (Demory et al., 2005b). Thus, the excursional VGPs at 20 ka is probably biased by post-depositionally formed greigite.

Magnetostratigraphic records reaching back to 31 ka were obtained from two sediment cores from Lago di Mezzano, Italy (Brandt et al., 1999, Table 5.1). Shallow inclinations at 18.5 ka are reproducibly recorded in both cores, notwithstanding the nonfluctuating declination variations. The VGPs of the Lago di Mezzano were calculated using 100 years stacked PSV records from the two cores. For the time window from 20 to 17 ka, the VGP path is presented in Fig. 5.8, exhibiting an irregular route. Nevertheless, the VGPs for this time interval are all sited at latitudes higher than 58° N. During the interval of shallowest inclinations, the

corresponding VGPs were migrating north of Far East Siberia, with VGP position sited at the Kamchatka Peninsula.

The PSV record from Mono Lake reported by Lund et al. (1988) demonstrated a distinctive directional anomaly representing the Mono Lake excursion. Besides this, shallow inclinations and corresponding changes of declinations were observed at around 18 ka. The corresponding VGP path is shown in Fig. 5.8. During this time interval, the VGPs migrated from the east of Greenland and moved quickly to the north of Far East Siberia, along the North American coast and then shifted along the Russian coast, and back to the west of Greenland. Obviously, the VGP path obtained from Mono Lake sediments shows no VGP position falling out of the area of normal secular variation (Fig. 5.8).

In the Black Sea, the directional anomaly and intensity low at 18.5 ka cal. BP is contemporary to the postulated Hilina Pali excursion. The PSV record with 50 year resolution stacked from sixteen cores was converted into a VGP path for the time window from 20 to 16 ka cal. BP. The VGPs migrate from northwest Greenland, along the North American coast, then reaching the north of Far East Siberia (Fig. 5.8). Afterwards, it moves back and clusters around the geographic North Pole. The clockwise migration of the VGPs is shown in Fig 8 with an arrow indicating the major sense of motion. Though the VADMs calculated from SE Black Sea data indicate low values of about 2.8×1022 Am2 at 18.5 ka cal. BP (Fig. 5.7), the corresponding VGP is sited still at a fairly high latitude of 64° N in Far East Siberia (Fig. 5.8).

During the Laschamp and Mono Lake excursions both recorded in SE Black Sea sediments, the VGP paths exhibited remarkable deviations from the area of normal secular variation (Nowaczyk et al., 2013, 2012). In contrast, the VGPs during the postulated Hilina Pali excursion derived from Black Sea sediments were migrating only inside the 64° N small circle, thus reflecting no excursional field behavior (Fig. 5.8).

All the VGP paths reported from sediment cores shown in Fig. 5.8 exhibit no transitional VGPs throughout the time window of the postulated Hilina Pali excursion, except for five questionable samples from Lake Baikal sediments. Directional swings, generally associated with shallow inclinations and low rPI values, are observed in all sediment cores between 20 and 18 ka. Although the VGP paths are diverse among the different cores, the VGP paths migrated fast from North America to Far East Siberia at around 18 ka, as evidenced by the records from the SE Black Sea, Lake Baikal and Mono Lake. In addition, all VGP positions derived from sediment cores are located within the area of normal secular variation with latitudes not lower than 58° N for this time interval.

Table 1
Informations of VGPs between 22 and 15 ka from lava flows and sediments

Site	Slat °N	Slong °E	Inc °	Dec °	α95 °	VDM/VADM§ $10^{22}Am^2$	Age ka	dating method	Plat °	Plong °	ref
lava flows											
Hilina Pali I, Hawaii	19.3	204.7	8.5	7.9	4.4	3.68 ± 1.08	17.9 ± 0.67	UnCal ^{14}C	73.1	357.6	1)
Chichinautzin Formation Volcanics, Mxico	19.0	261.0	17.1	338.7	4.2	-	19.5 ± 0.16	Cal ^{14}C	66.9	147.2	2)
	19.0	261.0	22.4	358.2	7.8	-	19.5 ± 0.16	Cal ^{14}C	82.3	93.8	
	19.0	261.0	23.9	352.0	4.5	-	19.5 ± 0.16	Cal ^{14}C	79.8	131.0	
	19.0	261.0	36.1	346.6	6.0	-	19.5 ± 0.16	Cal ^{14}C	77.4	176.9	
Auckland volcanic field, New Zealand	-39.6	174.8	-60.1	28.9	2.3	-	16.4 ± 1.8	$^{40}Ar/^{39}Ar$	68.0	277.8	3)
	-39.6	174.8	-74.7	329.1	2.5	-	21.2 ± 3.3	$^{40}Ar/^{39}Ar$	61.2	25.6	
Daisen Volcano, Japan	35.4	133.6	44.8	339.2	2.3	3.83 ± 0.31§	21 ± 1	Cal ^{14}C	77.4	245.8	4)
	35.5	133.5	48.9	13.5	4.8	3.23 ± 0.31§	17 ± 1	Cal ^{14}C, Stratigraphy	70.1	22.3	
Chichinatutzin Formation Volcanics, Mexico	19.2	260.5	64.4	353.3	3.4	3.1 ± 0.4	21.9 ± 0.38	Cal ^{14}C	62.2	250.5	5)
	19.2	260.6	16.6	342.6	4.2	6.2 ± 1.6	19.5 ± 0.16	Cal ^{14}C	70.0	131.0	
	19.2	260.8	33.7	359.1	5.8	6.7 ± 1.3	18.9 ± 0.6	Cal ^{14}C	88.8	128.2	
Michoacan-Guanajuato volcanic field, Mexico	19.7	258.6	58.2	339.7	4.6	7.7 ± 1.2	17.2 ± 0.43	Cal ^{14}C	64.0	222.8	
Mauna Loa volcano, Hawaii	19.1	204.6	44.7	18.8	5.7	5.4 ± 0.7§	16.4 ± 0.08	Cal ^{14}C	71.2	268.5	6)
Tianchi Volcanics, China	42.0	128.1	86.3	78.9	3.2	3.4 ± 0.05	17.1 ± 0.9	$^{40}Ar/^{39}Ar$	43.0	137.9	7)
	42.0	128.1	-25.1	167.5	8.1	6.1 ± 0.1	17.1 ± 0.9	$^{40}Ar/^{39}Ar$	-59.2	152.3	
Moon lava field, Idaho, USA	43.0	246.4	-	-	-	-	18.1 +0.68/-0.62	Cal ^{14}C	85.9	57.6	8)
Tabernacle Hill lava field, Utah, USA	38.9	247.5	-	-	-	-	17.2	Cal ^{14}C	66.6	60.7	
Cerro Grande lava field, Idaho, USA	43.3	247.2	-	-	-	-	16.1 +0.93/-1.58	Cal ^{14}C	83.5	97.2	
Moon lava field, Idaho, USA	43.5	246.5	-	-	-	-	15.4 +1.54/-0.5	Cal ^{14}C	73.4	67.7	
II Piano cldera, Italy	38.4	15.0	52.2	2.4	1.3	-	21.3 ± 3.4	K/Ar	84.0	175.0	9)
Lentia complex, Italy	38.4	15.0	48.1	353.3	2.1	-	15.5 ± 1.5	K/Ar	79.2	227.8	
Mauna Loa Volcanics, Hawaii	19.7	204.9	41.0	354.2	2.4	-	20.2 ± 0.5	Cal ^{14}C	83.4	158.7	10)
	19.1	204.4	56.0	1.1	1.7	-	16.4	Cal ^{14}C	72.5	207.3	
Michoacan-Guanajuato volcanic field, Mexico	19.7	258.6	4.6	345.5	2.2	-	17.2 ± 0.43	Cal ^{14}C	67.5	119.6	11)
Okataina Volcanic Centre, New Zealand	-38.1	176.4	-49.6	352.6	9.2	-	21	Stratigraphy	80.2	135.6	12)
	-38.1	176.5	-25.2	20.2	6.4	-	21	Stratigraphy	59.4	217.8	
	-38.2	176.6	-53.7	359.8	5.8	-	18 ± 3	Stratigraphy	86.1	174.2	
	-38.3	176.5	-58.2	342.7	4.4	-	15	Stratigraphy	76.5	78.3	
Blanzat 1, French Chaîne des Puys	45.8	3.1	59.1	-2.0	6.0	3.9 ± 0.3§	18.4 ± 5.4	$^{40}Ar/^{39}Ar$	83.9	197.7	13)
Moulet-Marcenat, French Chaîne des Puys	45.9	3.0	39.1	17.0	3.6	4.0 ± 0.5§	18.5 ± 3.1	K/Ar	62.6	146.9	
Fontfreyde, French Chaîne des Puys	45.7	3.0	40.9	-3.0	7.6	6.6 ± 1.0§	18.1 ± 4.5	TL	67.5	190.2	
Mazaye, French Chaîne des Puys	45.8	2.9	60.6	-3.6	9.8	4.9 ± - §	17.3 ± 4	TL	85.1	216.3	
sediment											
Mono Lake, California	38.0	119.0	-	-	-	-	17 – 19	Cal ^{14}C, Ashstratigraphy	-	-	14)
Lake Baikal, Russia	52.5	106.1	-	-	-	-	18 – 22	Uncal ^{14}C, AMS ^{14}C, Pollen stratigraphy	-	-	15*)
Lago Di Mezzano, Italy	42.6	11.8	-	-	-	-	17 – 20	Cal AMS ^{14}C	-	-	16*)
Black Sea	42.0	36.0	-	-	-	-	16 – 20	Cal AMS ^{14}C, Stratigraphy, Tephrochronology	-	-	◊)

Table 5.1 Slat and Slong = site latitude and longitude; Inc and Dec = mean inclination and declination; α95 = 95% confidence cone of Fisher distribution; VDM/VADM§ = virtual dipole moment/ virtual axial

dipole moment, value with marker '§' indicating VADM and VDM elsewhere; TL = Thermoluminescence; Plat and Plong = latitude and longitude of the VGP. ref: 1) Coe et al. (1978); 2) Herrero-Bervera et al. (1986); 3) Shibuya et al. (1992); 4) Tanaka et al. (1994); 5) Gonzalez et al. (1997); 6) Valet et al. (1998); 7) Zhu et al. (2000) with age after Singer et al. (2014); 8) Hagstrum et al. (2002); 9) Lanza and Zanella. (2003); 10) Pressling et al. (2006); 11) Conte-Fasano et al. (2006); 12) Tanaka et al. (2009); 13) Laj et al. (2014); 14) Lund et al. (1988); 15*) Peck et al. (1996); 16*) Brandt et al. (1999); ◊) this study. * denote data from GEOMAGIA50 database (Brown et al., 2015).

Taking all data together, in the time interval spanning from 22 to 15 ka, a directional anomaly with low paleointensity is commonly observed in both lava flows and sediment cores. However, evidence for transitional VGPs from lava flows were solely derived from a single site, the Tianchi volcano, so far. Stacked directions and relative paleointensities from the studied SE Black Sea sediment cores, show only normal, though pronounced secular variations. Since Black Sea sediment cores have successfully recorded the MIS3 Mono Lake and Laschamp excursions (Nowaczyk et al., 2013, 2012), the Hilina Pali, if an excursion of global extent, should have been recorded with (much) more pronounced directional variations in the SE Black Sea as well. One reason that a sedimentary sequence has not captured every excursion that has been observed in lava flows somewhere else may result from low sedimentation rates, leading to a significant smoothing of directional information (Roberts, 2008). But, the sedimentation rates of studied Black Sea cores reach up to 50 cm ka-1 during this period (Fig. 5.3), and hence the VGP path obtained from the stacked PSV record provides a resolution of 50 years per step. Thus, Black Sea sediments are, theoretically, able to record any excursion that lasts longer than 50 years. Furthermore, except the Tianchi volcano and five samples from Lake Baikal, the VGP positions from distant locations are exclusively located at latitudes higher than 58° N for this time interval. Therefore, on the one hand, it is reasonable to rule out the existence of a significant reversed dipole component contributing the total field during the postulated Hilina Pali excursion. On the other hand, if non-dipole fields were dominant, widely differing VGP paths should be observed at different sites (Laj and Channell, 2015b). This is more probable the scenario for the time window comprising the postulated Hilina Pali excursion. However, for detailed geomagnetic field models, much more precisely dated high-quality paleomagnetic records at high resolution are required.

5.5 CONCLUSIONS

Sixteen sediment cores from the Black sea partly recorded geomagnetic field variations at high resolution. For the selected time window from 20 to 16 ka, with sedimentation rates of up to 50 cm ka-1, pronounced directional swings and low relative paleointensities at around 18.5 ka could be reconstructed. At about the same time, lava flows at Hilina Pali, Hawaii, recorded also low inclinations and low paleointensities (Coe et al., 1978), which was later interpreted as

a geomagnetic field excursion. However, the high-resolution VGP path from Black Sea sediments is always sited at latitudes higher than 60° N for the whole time window from 20 to 16 ka, as do also the VGPs from Hilina Pali, Hawaii. Thus, no transitional VGPs were observed, neither in the Black Sea area, nor at the type locality. Also other sedimentary records, e.g. from southern Europe and North America, did not yield transitional VGP positions, that is, VGP latitudes lower than 45°N. Therefore, most of the available paleomagnetic records do not support the presence of a geomagnetic excursion between 20 and 16 ka. Only one, probably questionable sedimentary record and a single data set from volcanic rocks give indications for an anomalous field behavior in this time interval.

ACKNOWLEDGEMENTS

We thank S. Plewe, M. Duwe, T. Moldenhawer, and F. Brendel for their technical and logistical help during processing and sub-sampling of the cores. We also thank the captains and crews of RV Meteor, cruise M72/5 and RV Maria S. Merian, cruise MSM33, respectively, for their effords in providing optimal scientific working conditions. This work was partly funded by the German Research Foundation (Deutsche Forschungsgemeinschaft, DFG SPP 1266 “INTERDYNAMIC” grants AR 367/9-1 and AR 367/9-2), the Gary Comer Science and Education Foundation, U.S.A., and the Chinese Scholarship Council (CSC grant No. 201506180060).

6 Full-vector paleosecular variation from 14.5 ka back to 68.9 ka as reconstructed from Black Sea sediments

Currently under review by Quaternary Science Reviews

Liu Jiabo [1], Norbert R. Nowaczyk [1,*], Ute Frank [1], Helge W. Arz [2]

[1]GFZ German Research Centre for Geosciences, Section 'Climate Dynamics and Landscape Evolution', 14473 Potsdam, Germany.

*(norbert.nowaczyk@gfz-potsdam.de)

[2]Leibnitz Institute for Baltic Sea Research Warnemünde, 18119 Rostock, Germany.

Abstract

Full vector paleomagnetic records, comprising directional data and relative paleointensity (rPI), were derived from 16 sediment cores recovered from the southeastern Black Sea. The obtained data were used to create a stack covering the time window between 68.9 and 14.5 ka. Age models are based on radiocarbon dating and correlations of warming/cooling cycles monitored by high-resolution X-ray fluorescence (XRF) elementary ratios as well as ice-rafted debris (IRD) in Black Sea sediments to the sequence of 'Dansgaard-Oeschger' (DO) events defined from Greenland ice core oxygen isotope stratigraphy. Due to environmental and tectonic impacts, resulting in variation in sedimentation rates and hiatuses, the PSV record stacked from Black Sea sediments is characterized by resolutions ranging from 40 to 100 years for five different time intervals. The stacked Black Sea paleointensity record is in general agreement with global and other regional paleointensity stacks, though with some obvious deviations on a centennial scale. In addition, reconstructed prominent lows of paleointensity at about 64.5 ka, 41.6 ka and 34.5 ka are coeval with the Norwegian–Greenland Sea excursion, the Laschamp excursion, and the Mono Lake excursion, respectively. The excursions are further evidenced by an abnormal PSV index, though only the Laschamp and the Mono Lake excursions exhibit excursional virtual geomagnetic pole (VGP) positions. The stacked Black Sea paleomagnetic record was converted into one component parallel to the direction expected from a geocentric axial dipole (GAD) and two components perpendicular to it, representing only non-GAD components of the geomagnetic field. Thus, the Laschamp and the Norwegian–Greenland Sea excursions are both characterized by extremely low GAD components, while the Mono Lake excursion is marked by large non-GAD contributions. Notably, negative values of the GAD component, indicating a fully reversed geomagnetic field, are observed only during the

Laschamp excursion. The data from Black Sea sediments strongly suggest that the geomagnetic field behaved differently during these three excursions.

Keywords

paleosecular variation; geomagnetic excursion; Black Sea; paleointensity

6.1 Introduction

Geomagnetic paleosecular variation (PSV) records obtained from paleomagnetic archives, such as archaeological artefacts, volcanic rocks, and sediments, are an expression of geodynamo processes inside the Earth's liquid outer core (Merrill and McFadden, 1999). These paleomagnetic time series provide insights into the properties of the Earth's magnetic field, from normal behavior with a dominating dipolar geometry, over field crises, such as pronounced intensity lows and geomagnetic excursions with a distorted field geometry, to the complete reversal of the dominating dipole contribution (e.g., Laj and Channell, 2015; Roberts, 2008; Valet et al., 2005).

Paleomagnetic studies from sediments, which ideally permit precise dating of the sequence and the development of good sequential records of both paleomagnetic directional and intensity variability, have significantly improved our understandings of the PSV (e.g., Channell et al., 2012; Lund et al., 2006; Valet et al., 2008). Besides, sedimentary PSV records provide a level of detail and temporal continuity that is unavailable from other paleomagnetic archives, such as lava flows or archeological artifacts. With greater global coverage and further back in time, PSV records enable the assessment of the signals of dipolar versus non-dipolar geomagnetic field contributions (Roberts et al., 2013). Specifically, the relative paleointensity (rPI, Tauxe, 1993), obtained from sediments in the past decades have yielded a lot of new information about the dynamics in geomagnetic field behavior (Roberts et al., 2013) and served as a reference signal that has become widely used for dating purposes of sedimentary sequences (e.g., Channell et al., 2009; Laj et al., 2004, 2000; Stoner et al., 2002). Furthermore, high resolution and high-fidelity records of sedimentary PSV records allowed the estimation of durations and field geometries of geomagnetic field excursions (e.g., Bourne et al., 2012; Channell, 2014, 2006; Channell et al., 2017; Laj et al., 2006; Nowaczyk et al., 2012). Nevertheless, obtained stacks of PSV records often represent only smoothed time series due to large areal stacking and/or low sedimentation rates (e.g., Channell et al., 2018; Laj et al., 2004; Panovska et al., 2018). Therefore, geomagnetic excursions, to a certain degree, are not yet satisfactorily understood in terms of their occurring frequency, individual duration, and pattern of field behavior (e.g., Channell et al., 2017; C. Kissel et al., 2011; Laj et al., 2014; Roberts, 2008). Accordingly, high resolution PSV records, normally with sedimentation rates >10 cm/kyr

(Roberts, 2008), are in need of a better understanding of the effects of smoothing on paleomagnetic records and reconstructing the higher frequency components in the spectrum of geomagnetic field variations.

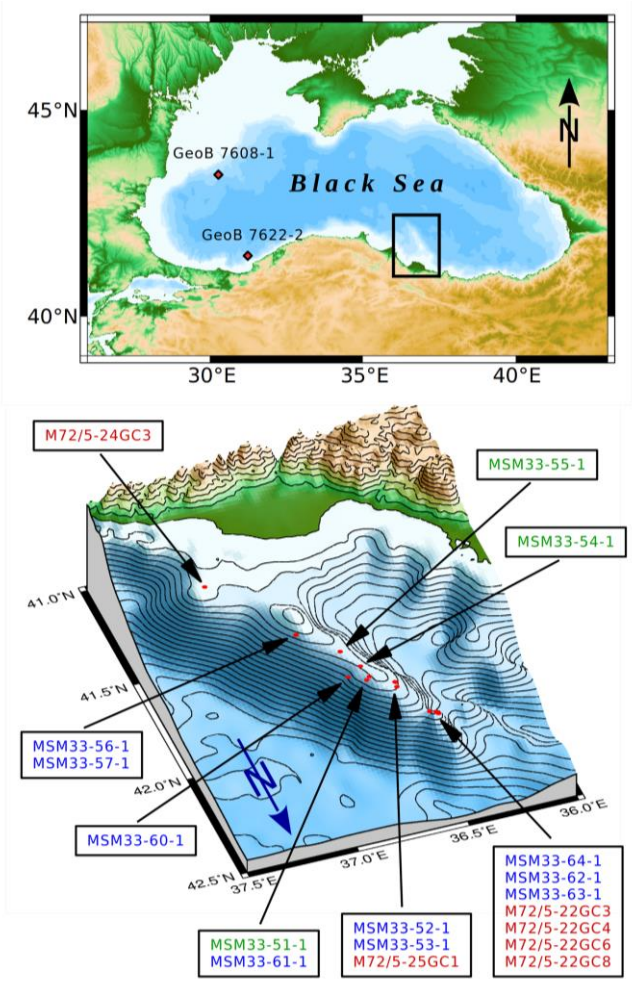

Figure 6.1 Location of the study area (black rectangle) in the south-eastern Black Sea (top) with additional positions of GeoB cores, that were used for age reference, recovered during expedition M51/4 (black labels). Investigated sediments cores were recovered along the Archangelsky Ridge during expeditions M72/5 (red labels) and MSM33 (green labels for piston cores and blue labels for gravity cores). Note that in the perspectival close-up view of the study area (bottom) North is to the lower right.

In this paper, we discuss PSV records reconstructed from a total of 16 (out of 18 investigated) sediment cores from the SE Black Sea spanning the time interval from 68.9 to 14.5 ka, provided with temporal resolutions ranging from 40 to 100 years. As a first result, a high-quality and high-resolution record of the Laschamp excursion (~41 ka) and a high-resolution record of relative paleointensity from 14 to 68 ka, based on 6 sediment cores, could be presented (Nowaczyk et al., 2013, 2012). Though supplemented with data obtained from 13 further cores from the same region, the extended data set had to be compiled in five time intervals with different temporal resolution and with variable data quality. This is due to highly variable

sedimentation rates, detected hiatuses, and partly massive contamination by chemically formed greigite that made parts of the obtained records useless. The greigite-bearing samples in Black Sea sediments are generally characterized by ideal single domain (SD) particles and extremely high magnetic susceptibility. Hence, detailed mineral magnetic analyses were performed on all studied cores that enabled omitting greigite-bearing samples for paleomagnetic studies (e.g., Liu et al., 2018, 2019.; Nowaczyk et al., 2018, 2013, 2012).

The obtained PSV record for the time interval from 58 to 69 ka, about equivalent with MIS (marine isotope stage) 4, with fast directional changes, though not yet being 'excursional', associated with low field intensities at 64.5 ka was reported by Nowaczyk et al. (2018). For the time interval from 14 to 20 ka (about coeval with MIS 2), the Black Sea PSV record exhibits only normal variations and no evidence for the postulated 'Hilina Pali' excursion at 18.5 ka (Liu et al., 2018). The PSV data from 20 to 40 ka, with the Mono Lake excursion documented with excursional directions and low paleointensity at about 34.5 ka, is presented by Liu et al. (2019.). In addition to the mentioned magnetostratigraphic studies, the studied cores were also subjected to tephrochronological (e.g., Cullen et al., 2014) and paleoclimate studies (e.g., Shumilovskikh et al., 2013, 2012, Wegwerth et al., 2016, 2015, 2014), which further refined their age models.

The main focus of this paper is the presentation of data from the time interval from 42 to 58 ka, a short discussion of a (partly) greigite-based record of the Laschamp excursion in one of the cores, the summary of all paleomagnetic data obtained from the whole collection of cores, and a comparison of the obtained paleomagnetic composite record from the SE Black Sea with other regional and global paleointensity stacks. Finally, the Black Sea full-vector PSV record will be discussed on basis of a transformed record, with one component parallel to the direction expected from a geocentric axial dipole (GAD) and two components perpendicular to it representing only non-GAD components of the geomagnetic field intending to provide some general insights into the geomagnetic field behavior across the documented three excursions.

6.2 Material and methods

6.2.1 Sediments under investigation

For this study, a total of eighteen sediment cores recovered during two ship expeditions from the Archangelsky Ridge in the SE Black Sea were investigated. The expedition M72/5 of German research vessel *RV METEOR* in 2007 provided six cores, and the expedition MSM33 of German research vessel *RV Maria S. Merian* in 2013 provided a total of fifteen cores from the SE Black Sea. The sediment cores were taken from water depths between 208 and 848 m,

with core lengths ranging from 682 to 1027 cm (Table 1.1). All six M72/5 cores and twelve MSM33 cores (Fig. 6.1) have been investigated up to now.

Sediments investigated for this study cover mostly the last glacial, MIS 4 to 2, and the Holocene (MIS 1). During the last glacial to the early Holocene, the Black Sea was disconnected from the Mediterranean Sea, with its lake level temporarily lying at around -100 m below modern sea level (e.g., Major et al., 2006; Shumilovskikh et al., 2012). Thus, fine-grained siliciclastic sediments with variable carbonate content (25 – 40%, Nowaczyk et al., 2012) were deposited under limnic and oxic water conditions for this time window at the study site. Due to global sea-level rising during the last deglaciation and a subsequent ingression of marine seawater through the sill of the Bosporus (modern water depth 36 m) at around 8.2 ka (e.g., Kwiecien et al., 2008; Major et al., 2006), the Black Sea was turned into the World's largest anoxic basin. Since then finely laminated organic-rich sapropelitic sediments and coccolith oozes were deposited (e.g., Bahr et al., 2005; Shumilovskikh et al., 2013).

6.2.2 XRF-logging

In general, the archive halves of split cores were used for down-core X-ray fluorescence (XRF) scanning. The M72/5 cores were processed at the MARUM lab of Bremen University, Germany, using an Avaatech XRF core scanner configured with an Amptek detector. Counts of major elements were obtained every 1 to 2 cm with an integration time of 15 seconds and a X-ray current of 0.15 mA (Röhl and Abrams, 2000). The MSM33 cores were processed at the Leibnitz Institute for Baltic Sea Research Warnemünde, Rostock, Germany, using an ITRAX XRF Core Scanner (COX Analytics; e.g., Croudace et al., 2006). The XRF core logger was operated with a Cr-tube at 30 kV and 30 mA and a SDD Si drift detector, with an exposure time of 15 seconds and a step size of 1 mm. Data obtained from this method was mainly used for correlation purposes.

6.2.3 Paleo- and rock magnetism

For correlation purposes all cores were logged also for magnetic susceptibility at 1 mm intervals applying fully automated split-core logging systems. Measurements were performed on the split-surface of the core segments using a Bartington MS2E-1 spot-reading sensor. For paleo- and rock magnetic purposes clear rectangular plastic boxes (inner dimension 20×20×15 mm) with a volume of 6 cm^3 were used. In most cases boxes were pressed into one half of the core sections side-by-side with a spacing of 24 to 30 mm. Intervals that were identified from the logging results to be promising in advance, e.g., having recorded an excursion, were sampled at high-resolution in two parallel rows with the square-shaped boxes being rotated by 45°, yielding an effective resolution of 16 to 17 mm (Nowaczyk et al., 2012). An AGICO

Multi-function Kappabridge MFK1-A was then used to determine the low-field magnetic susceptibility κ_{LF}, and its anisotropy (AMS), of these samples.

The natural remanent magnetization (NRM) and the anhysteretic remanent magnetization (ARM) were measured with a 2G Enterprises 755 SRM (cryogenic) long-core magnetometer equipped with a sample holder for eight discrete samples at a separation of 20 cm. The magnetometer's in-line tri-axial alternating field (AF) demagnetizer was used to demagnetize the NRM and ARM of the samples. The NRM was measured after application of AF peak amplitudes of 0, 5, 10, 15, 20, 30, 40, 50, 65, 80, and 100 mT. Directions of the characteristic remanent magnetization (ChRM) were determined by principle component analysis (PCA) according to Kirschvink (1980). The error range of the ChRM is given as the maximum angular deviation (MAD). The ARM was imparted along the samples' z-axis with a static field of 0.05 mT and an AF field of 100 mT. Demagnetization then was performed in steps of 0, 10, 20, 30, 40, 50, 65, and 80 mT. The median destructive field of the ARM (MDF_{ARM}) was determined to estimate the coercivity of the sediments. The slope of NRM versus ARM of common demagnetization steps was used to determine the relative paleointensity (rPI). In most cases, demagnetization steps from 20 to 65 mT were used to determine the rPI. The ARM intensity normalized by the static field used to produce the ARM yields the anhysteretic susceptibility κ_{ARM}. Since the ARM mostly affects fine-grained particles, whereas the magnetic susceptibility κ_{LF} is influenced by all particles, high (low) values of the κ_{ARM}/κ_{LF} ratio indicates fine- (coarse-) grained particles.

A 2G Enterprises 660 pulse magnetizer was used to impart an isothermal remanent magnetization (IRM) along the samples' z-axes. Since IRM intensities often exceed the measuring range of cryogenic magnetometers, the samples' IRMs were measured with a Molyneux spinner magnetometer. A peak field of 1.5 T was used to saturate the samples. The acquired magnetization is defined as the saturated IRM (SIRM). A backfield of -0.2 T was applied in order to determine the S-ratio, defined as 0.5×(1-(IRM(-0.2 T)/SIRM)). The S-ratio is close to 0 for pure haematite (Fe_2O_3) and close to 1 for both magnetite (Fe_3O_4) and greigite (Fe_3S_4). In order to be able to discriminate between these two minerals, the ratio of saturation magnetization over magnetic susceptibility $SIRM/\kappa_{LF}$ was determined. Magnetite and greigite have similar SIRMs but the κ_{LF} of greigite is significantly lower than that of magnetite. Thus the presence of greigite can be indicated by $SIRM/\kappa_{LF}$ ratios significantly higher than those for magnetite (Nowaczyk et al., 2012). Like for the κ_{ARM}/κ_{LF} ratio, high (low) values of the ARM/SIRM ratio indicate more fine- (coarse-)grained particles. All paleo- and rock magnetic

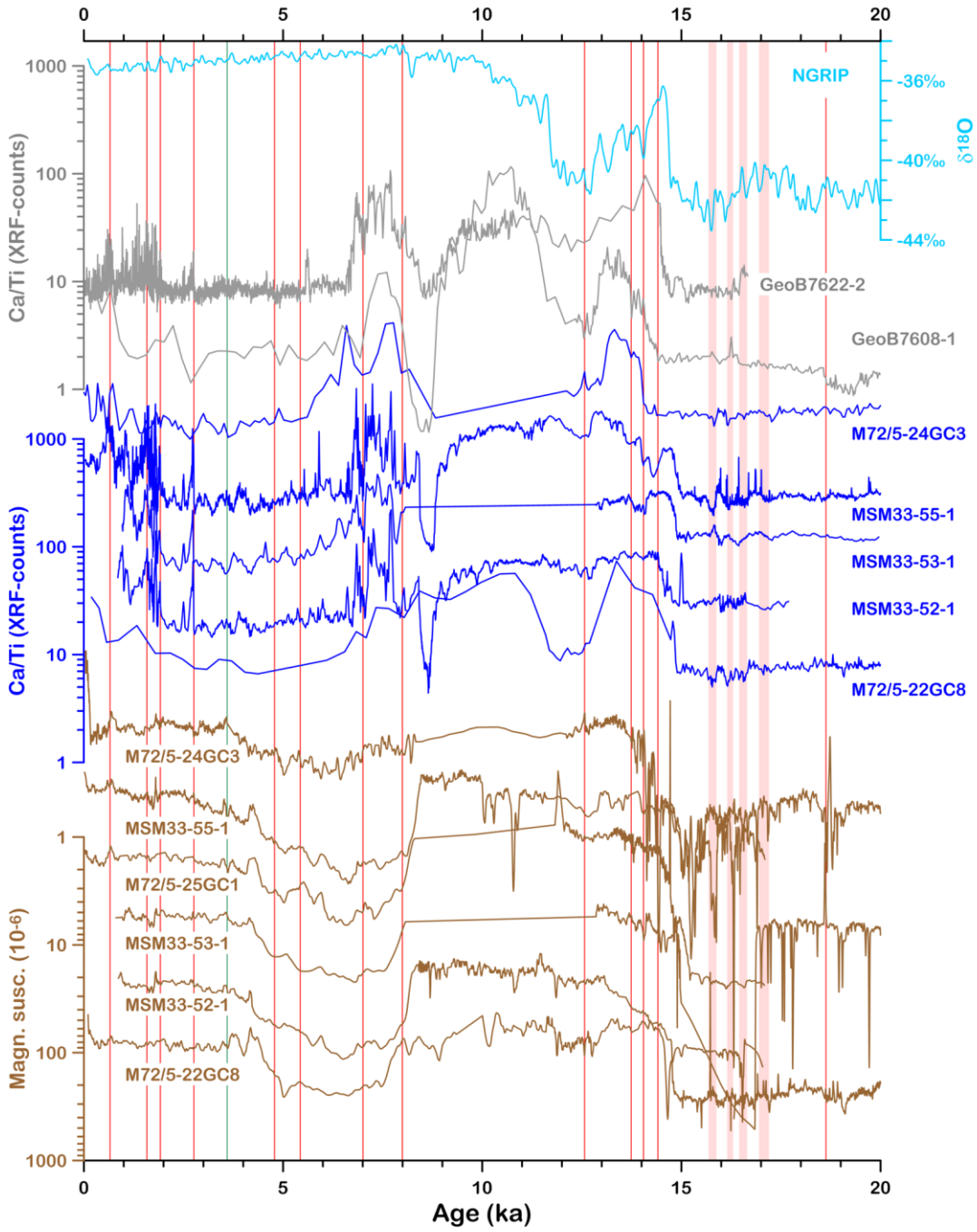

Figure 6.2 Age constrains for the time interval between 0 and 20 ka obtained from Ca/Ti ratios (XRF-logging) and magnetic susceptibility records from selected cores correlated to the oxygen isotope ($\delta^{18}O$) record from Greenland ice-cores (NGRIP) according to the GICC05 age model (Svensson et al., 2008). Vertical red lines mark age model tie points from AMS (accelerator mass spectrometry) ^{14}C ages from Core M72/5-24GC3 (older than 10 ka, Nowaczyk et al., 2012) and Core GeoB7622-2 (younger than 10 ka, Lamy et al., 2006), with a green line for the age of the Santorini tephra found in the latter. Vertical pink bars between 15 and 18 ka mark the positions of 'reddish layers' according to Soulet et al. (2013) and Liu et al. (2018).

investigations on discrete samples were performed at the Helmholtz Centre Potsdam, GFZ German Research Centre for Geosciences, Potsdam, Germany.

6.3 Results

6.3.1 Age models

For dating of investigated Holocene and late-glacial sediments from the SE Black Sea, accelerator mass spectrometry (AMS) ^{14}C ages from cores GeoB7608-1 (Bahr et al., 2005) and GeoB7622-2 (Lamy et al., 2006), recovered from the western Black Sea during *RV METEOR* cruise M51/4 (Fig. 6.1), were transferred to the studied cores from expeditions M72/5 and MSM33 by correlation of their Ca/Ti ratios obtained from XRF scanning (Fig. 6.2). Identification of the tephra layer related to the Minoan eruption of Thera/Santorini at around 1600 BCE (e.g., Höflmayer, 2012) in core GeoB7622-2 (Lamy et al., 2006) and M72/5-25GC1 (Cullen et al., 2014) yielded a further tie point for the age models (green vertical line in Fig. 6.2).

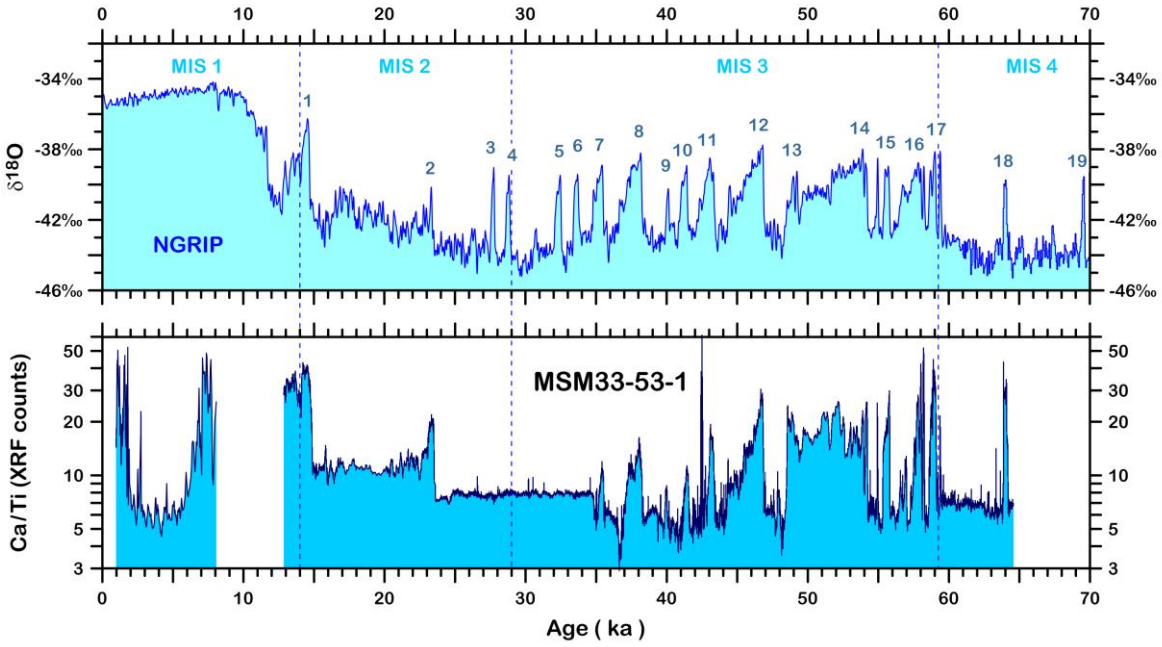

Figure 6.3 Record of Ca/Ti ratio as derived from X-ray fluorescence (XRF) logging from Core MSM33-53-1 after correlation to the oxygen isotope ($\delta^{18}O$) record from Greenland ice-cores (NGRIP) according to the GICC05 age model (Svensson et al., 2008). Vertical dashed lines mark the boundaries of marine isotope stages (MIS) 1 to 4. Numbers in the NGRIP $\delta^{18}O$ record from 1 through 19 denote the so-called Dansgaard-Oeschger events (Dansgaard et al., 1993).

In addition, high-resolution magnetic susceptibility records, exemplarily shown for six cores in the lower part of Fig. 6.2, were used to cross-check the correlations by Ca/Ti ratios. It is obvious that several cores are affected by a hiatus from about 8.0 to 12.5 ka (e.g., M72/5-24GC3, M72/5-25GC1, MSM33-53-1). Four reddish sediment layers related to meltwater events during the decay of the Fennoscandia ice sheet, with ages from about 15 to 17 ka (Fig.

6.2), described from the western Black Sea (Bahr et al. 2006; Soulet et al., 2013), could also be found in the SE Black Sea (Liu et al., 2018). Here, they were identified from their maxima in K/Ti ratios as well as by their minima in S-ratios, reflecting an increased haematite content that causes the visible reddish hues of the corresponding sediments (Fig. 6.2).

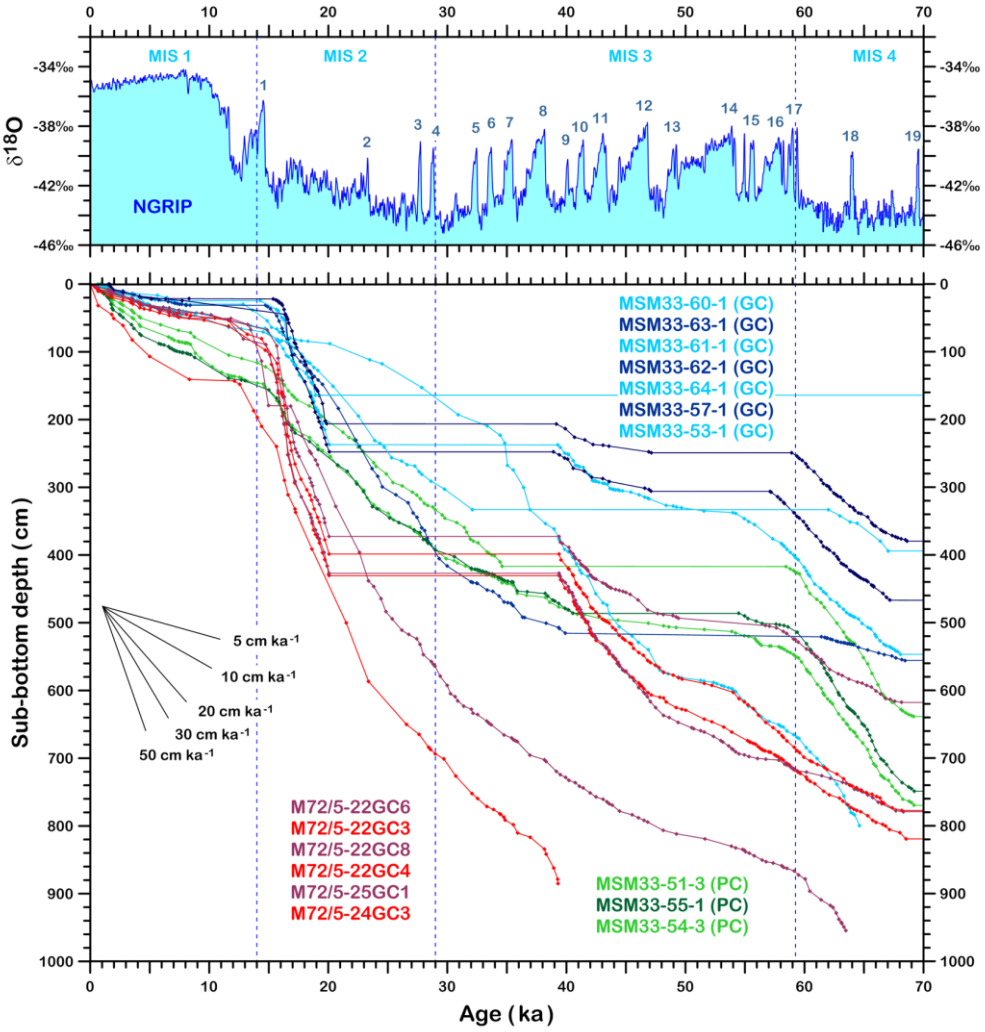

Figure 6.4 Age-depth relationships for all sediment cores considered in this study (see also Figs. 2 and 3) showing the highly variable sedimentation rates from 5 to 50 cmka^{-1} (compare bundle of lines in the left). A major hiatus from about 20 to 39 ka was detected in numerous cores. Another hiatus from 69 to about 115 ka was detected in all sediment cores from the Archangelsky Ridge. Therefore, for this study, the age models are only shown until 70 ka. Blue (green) colours were used for gravity (piston) cores from Expedition MSM33. Red colours were used for gravity cored from expedition M72/5. The oxygen isotope ($\delta^{18}O$) record from Greenland ice-cores (NGRIP) according to the GICC05 age model (Svensson et al., 2008) as the major reference record is shown in the top. Vertical dashed lines mark the boundaries of marine isotope stages (MIS) 1 to 4. Numbers from 1 through 19 denote the so-called Dansgaard-Oeschger events (Dansgaard et al., 1993).

AMS ^{14}C ages from core M72/5-24GC3 and partly from core GeoB7608-1 support the age models between 12.5 and 39.4 ka (Bahr et al., 2005; Nowaczyk et al., 2012). Further-on, detailed counting of ice-rafted debris (IRD, 'drop-stones') on cores M72/5-22GC8, M72/5-

24GC3, and M72/5-25GC1 (Nowaczyk et al., 2013, 2012) yielded a clear pattern of warming/cooling cycles that could be unequivocally correlated to the sequence of 'Dansgaard-Oeschger' (DO) events (Dansgaard et al., 1993) defined from Greenland ice core oxygen isotope stratigraphy (Svensson et al., 2008). These results provided mainly age constraints from about 25 to 69 ka (DO events 3 to 18, see Fig. 6.3). This sequence of DO events is also clearly seen in the Ca/Ti ratio from XRF scanning in all investigated cores, if not missing due to hiatuses (e.g., Nowaczyk et al., 2018, 2012). As an example of MSM33 data, the Ca/Ti ratio from XRF counts from core MSM33-53-1 correlated to the NGRIP oxygen isotope record is shown in Fig. 6.3. In this core, a hiatus from about 8.1 to 12.6 ka could be identified by correlation of Ca/Ti ratios and magnetic susceptibility to cores GeoB7608-1 and GeoB7622-2 (Fig. 6.2). Nearly constant values of Ca/Ti ratios from about 23.5 to 34.0 ka probably indicate a homogenized interval, e.g., due to slumping.

Obtained age models of investigated sediment cores from expeditions M72/5 and MSM33 are shown in Fig. 6.4 back until 70 ka. Apparently, the end of the last glacial lead to a dramatic decrease in sedimentation rates from about 50 $cmka^{-1}$ in MIS 2 down to 5 to 10 $cmka^{-1}$ in MIS 1. MIS 3 is mostly characterized by sedimentation rates from 20 to 30 $cmka^{-1}$, with lowest values in early MIS 3 characterized by generally higher temperatures and longer warm phases (DO events 12 to 17), while glacial conditions in the preceding MIS 4 led to higher sedimentation rates. In numerous cores hiatuses were detected. These gaps in the sedimentary sequences at the slope of the Archangelsky Ridge (Fig. 6.1) are interpreted as the effect of slumping down of sediments mobilized by the tectonic (earthquake) activity in this region. The most significant hiatus is between about 69 ka and the early to middle Eemian interglacial (MIS 5e, 115-120 ka). Thus, in none of the recovered cores early MIS 4 and MIS 5a to 5d sediments can be found. The Eemian is, like the Holocene, build up by soft organic-rich sapropelitic sediments, whereas the glacial sediments are built up by fairly stiff clays. Presumably, this strong difference in shear resistance led to the slumping down over large areas of the Archangelsky Ridge of the sediments deposited since MIS 5d until early MIS 4 triggered by a strong earthquake at around 69 ka (Fig 1). The lower sections in all studied cores, except cores M72/5-24GC3, M72/5-25GC1, and MSM33-53-1 (Fig. 6.4) contain also sediments from early MIS 5 back to middle/early MIS 6 (e.g., Shumilovskikh et al., 2013; Wegwerth et al., 2014) which are subject of ongoing stratigraphic, paleomagnetic, and paleoenvironmental investigations.

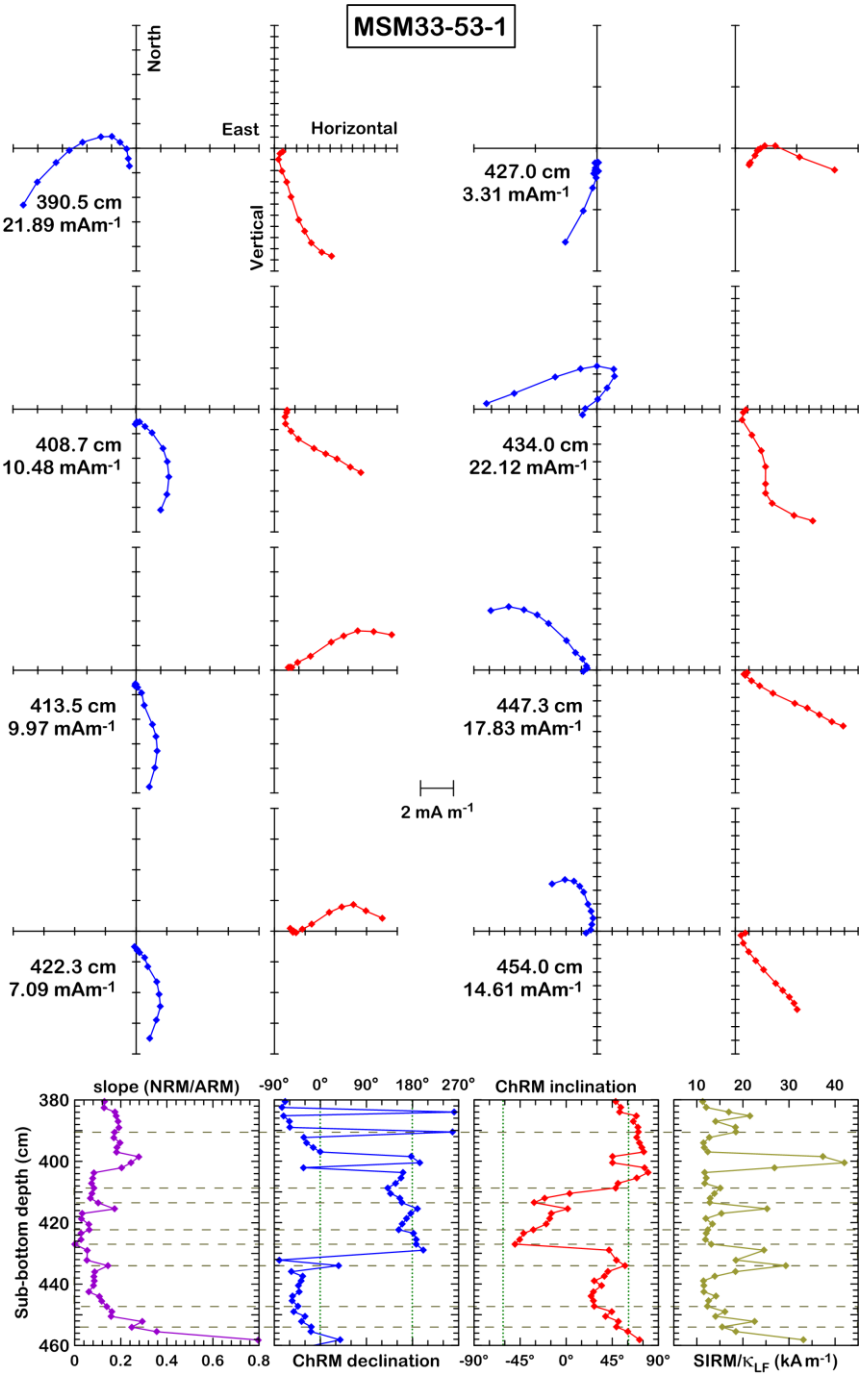

Figure 6.5 Vector endpoint diagrams from eight samples across the Laschamp excursion during the course of alternating field demagnetization. The examples are taken from Core MSM33-53-1 with abundant greigite precipitation. Results are shown for the declination in the horizontal (North vs. East) plane (blue), together with the inclination (Vertical vs. Horizontal, red). Positions of these samples are marked by horizontal dashed lines in the down-core plots of the slope (NRM/ARM), as a measure of relative palaeointensity, ChRM declinations and inclinations, and the SIRM/κ_{LF} ratio, as a measure for the presence of greigite (>10 kAm^{-1}), in the bottom. ChRM – characteristic remanent magnetization.

6.3.2 Magnetostratigraphy of core MSM33-53-1

The typical approach to remove viscous overprints is to stepwise demagnetize samples with alternating fields (AF) of increasing peak-amplitude. Samples carrying a reversed

magnetization need amplitudes of at least 20 mT to partly even 50 mT in order to completely remove the normal polarity overprint (e.g., Nowaczyk et al., 2003). Normally, the remaining NRM then is demagnetized in further steps of up to 100 mT peak AF amplitude in order to provide the data base for principle component analysis yielding the direction of the characteristic remanent Magnetization (ChRM). In many cases of a NRM partly or mostly carried by greigite the acquisition of a gyro-remanent (GRM) magnetization is observed at these steps (e.g., Roberts et al., 2011; Snowball, 1997). GRM acquisition visibly starts at peak AF fields of about 40 to 65 mT (e.g., Krs et al., 1990; Ron et al., 2007), mostly acquired perpendicular to the last axis that was demagnetized. Thus, demagnetization data, needed for determining the ChRM direction by PCA analysis, actually gets compromised by the GRM acquisition in greigite. And, it is rarely possible to obtain useful paleomagnetic directions from such samples, especially in cases of samples carrying a reversed stable direction superimposed by a soft normal overprint. As a case study for such a conflict between the need to go to higher peak fields to isolate the ChRM direction, on the one hand, and the acquisition of unwanted artificial GRMs, on the other hand, results from core MSM33-53-1 shall be discussed here.

Fig. 6.5 shows AF demagnetization data as vector endpoint diagrams from eight samples from core MSM33-53-1. The diagrams are plotted together with an excerpt of down-core paleo- and rock magnetic data, relative paleointensity (slope (NRM/ARM)), ChRM declination and inclination, and the greigite-indicating SIRM/κ_{LF} ratio, between 380 and 460 cm. Like in four cores of expedition M72/5, the Laschamp excursion, centered at 41 ka (Nowaczyk et al., 2012), is identified from steep negative inclinations and declinations around 180° from about 410 to 430 cm. Obviously, the Laschamp excursion is affected by greigite present in the sediments which is indicated by frequent SIRM/κ_{LF} ratios > 10 kAm^{-1}. This is also expressed by GRM-acquisition throughout AF demagnetization of these samples, that is, vector endpoints do not migrate straight to the origin of the diagrams. Instead, the vector endpoint diagrams show a typical ‘fish hook’ appearance (Fig. 6.5).

The full down-core plot of data obtained from core MSM33-53-1 is shown in Fig. 6.6. In the left panel, the NRM (black) and ARM (blue) intensities are plotted together with the estimate of relative paleointensity as derived from the slope of NRM versus ARM of common demagnetization steps. In the middle panel of Fig. 6.6, ChRM inclinations and declinations are displayed. The down-core variations of the S-ratio and the SIRM/κ_{LF} ratio are plotted in the right panel. The latter is plotted twice, once on a full-range (3 – 100 kAm^{-1}) logarithmic axis (Fig. 6.6, outer right) and once with a linear axis cropped to a range between 8 and 28 kAm^{-1}, in order to better show the variations of this parameter ratio. For filtering out greigite-bearing

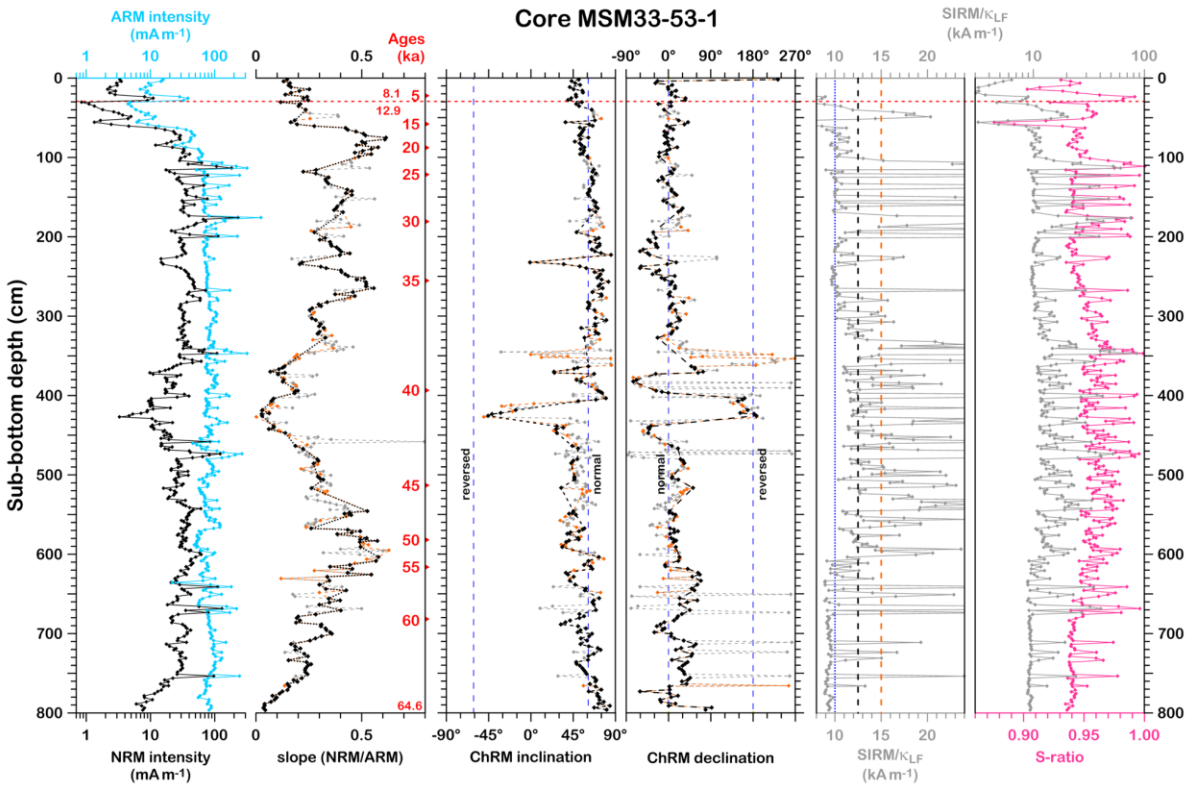

Figure 6.6 Down-core variations of palaeo- and rock magnetic parameters derived from Core MSM33-53-1 (from left to right): NRM intensity, ARM intensity, relative palaeointensity estimated by the slope of NRM/ARM during alternating field demagnetization, ages (red numbers), ChRM inclination and declination, SIRM/κ_{LF} ratio on a linear axis from 8 to 24 kAm^{-1} only, and on a logarithmic axis (full scale), together with the S-ratio. In the ChRM plots black (orange) curves represent samples with SIRM/κ_{LF} ratios below 12.5 (15.0) kAm^{-1}, whereas grey curves represent unfiltered data. In the linear SIRM/κ_{LF} plot the black (orange) vertical dashed line marks the cut-off levels used for filtering out greigite bearing samples (>10 kAm^{-1}) in Core MSM33-53-1. The blue dotted vertical line at 10 kAm^{-1} marks the cut-off level used for all other cores in this study. The horizontal red dashed line indicates a hiatus from about 8.1 to 12.9 ka. NRM – natural remanent magnetization, ARM – anhysteretic remanent magnetization, ChRM – characteristic remanent magnetization, SIRM – saturated remanent magnetization. κ_{LF} – low-field magnetic susceptibility.

samples from Black Sea sediments, Nowaczyk et al. (2013, 2012) defined a SIRM/κ_{LF} ratio threshold level of 10.0 kAm^{-1}, with samples below (above) 10 kAm^{-1} being free of (increasingly contaminated by) greigite. This threshold level is marked by a dotted blue line in the down-core plot of the SIRM/κ_{LF} ratio (Fig. 6.6, inner right). Applying this strict criterion (SIRM/κ_{LF} > 10 kAm^{-1}) would eliminate every sample between 300 and 600 cm, including the well documented record of the Laschamp excursion. Therefore, in order to check the performance of less restrictive criteria, threshold levels of 12.5 and 15.0 kAm^{-1} were then applied to the data. Cutting off data with SIRM/κ_{LF} ratios above 15.0 kAm^{-1} (orange dashed lines) excludes many of greigite-related spikes in the paleomagnetic data (slope (NRM/ARM), ChRM inclinations and declination, Fig. 6.6, middle), but still some erratic data points are left, e.g., at around 350

cm (see Fig. 6.6). Thus, the filter level of 15.0 kAm^{-1} leaves 252 out of 369 samples, or 68.3 percent of the data. Using the 12.5 kAm^{-1} threshold results in fairly consistent (looking) paleomagnetic record (black dashed lines in Fig. 6.6). However, only 200 out of 369 samples are left, equal to just 54.2 percent of the data.

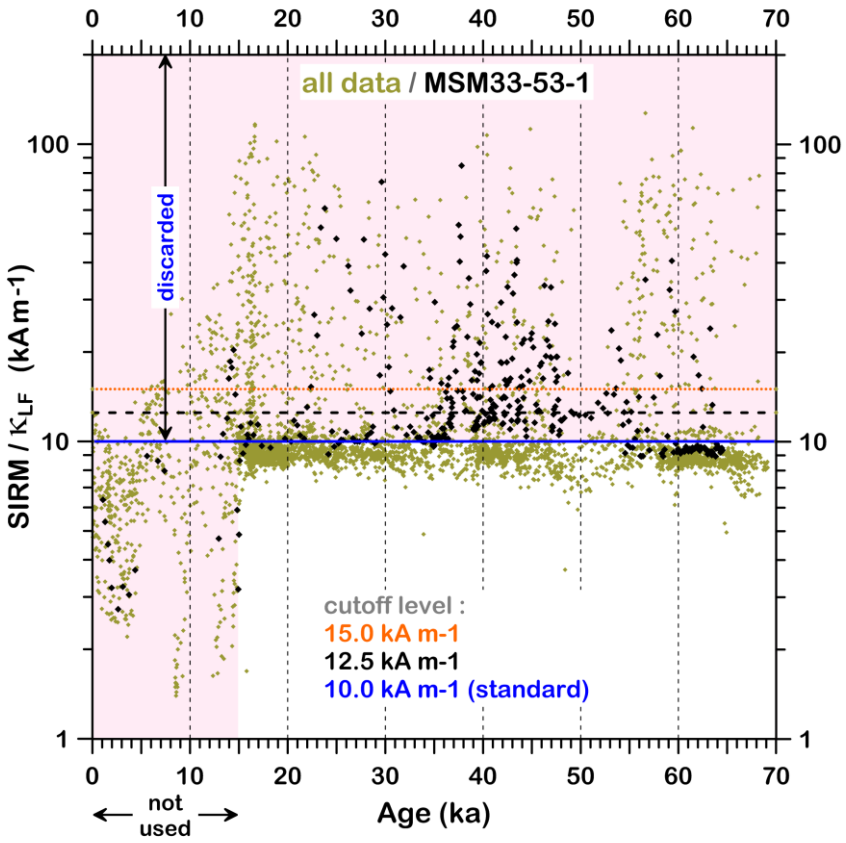

Figure 6.7 SIRM/κ_{LF} ratios from all samples investigated in this study reaching back to 69 ka. Because of too low sedimentation rates, the time window from 0 to 15 ka was not used. Also, in general samples with SIRM/κ_{LF} ratios above 10 kAm^{-1} (standard cut-off level, blue line) were not considered for stacking of palaeomagnetic directions and relative palaeointensity estimates due to secondary greigite. Almost all samples from Core MSM33-53-1, including all samples documenting the Laschamp excursion, would be discarded using these criteria. Therefore, more tolerant cut-off levels of 12.5 (black dashed line) and 15.0 kAm^{-1} (orange dashed line), respectively, were tentatively used for samples to be considered for palaeomagnetic interpretation (compare Fig. 6).

Determined SIRM/κ_{LF} ratios of all investigated samples (from 16 cores) versus age between 0 and 70 ka are shown in Fig. 6.7 in olive green, with data from MSM33-53-1 highlighted in black, together with the standard cut-off level of 10.0 kAm^{-1} (blue solid line) and the less restrictive cut-off levels of 12.5 kAm^{-1} (black dashed line) and 15.0 kAm^{-1} (orange dotted line). Thus, compared to many other samples investigated, data from core MSM33-53-1 appears questionable rather than being reliable. The dense population of data points below the most robust cut-off level of 10.0 kAm^{-1} also illustrates that despite the fact that 16 cores provided

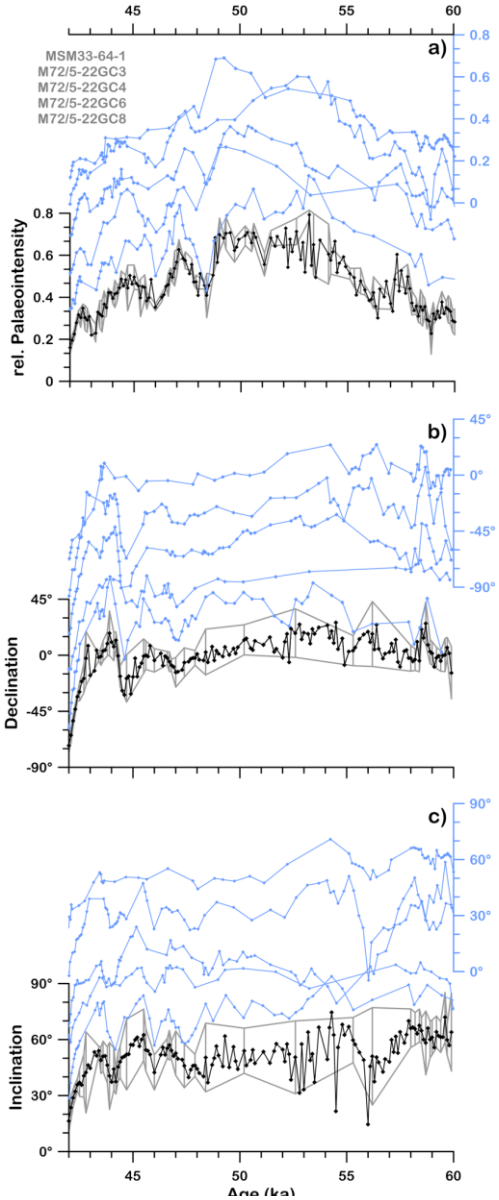

Figure 6.8 Palaeomagnetic data from the SE Black Sea for the time interval from 42 to 60 ka: a) relative palaeointensities, b) declinations, and c) inclinations from five cores as listed in a), shown as blue curves, together with the respective stacks in black, plotted with identical scaling and a constant offset. Where available, the 1σ standard deviation for relative palaeointensities in a) and the α_{95} for directional data in b) and c) are shown in grey. All other cores shown in Fig. 6.1 are either younger than 42 ka, are contaminated too much by greigite (e.g. MSM33-53-1, Fig. 6.6), or are characterized by low sedimentation rates or a hiatus (see Fig. 6.4).

useful data, certain time intervals are sparsely covered by data, such as from 33 to 39 ka and from about 47 to 55 ka, respectively. The time interval between 0 and 15 ka is represented by sediments with relatively low sedimentation rates (5-10 cmka^{-1}, Fig. 6.4), low concentration of magnetic minerals (see NRM and ARM in Fig. 6.6, top left), or a totally different lithology, that is, organic-rich sapropelitic sediments compared to organic-poor clays during the last glacial. Therefore, this largely heterogeneous interval was completely omitted for further paleomagnetic interpretations.

6.3.3 Compiling the paleosecular variation record from 15 to 69 ka

Due to the heterogeneous data set compiled in the past decade from sixteen sediment cores from the SE Black Sea, publications were split into several studies. The most noteworthy result that was published in detail by Nowaczyk et al., (2012), is the high-resolution record of the Laschamp geomagnetic excursion from four parallel M72/5 cores in the time interval from 39.4 to 42.5 ka, partly with a temporal resolution of 20 years. The time interval from about 69 to 58 ka recovered from nine cores, comprising a pronounced low in paleointensity at around 65 ka, was published by Nowaczyk et al. (2018) with a temporal resolution of 100 years. The time interval from 20 to 15 ka, documented in all studied cores, is characterized by the highest temporal resolution (Liu et al., 2018). The fairly low paleointensity at about 18.5 ka is contemporary to the postulated 'Hilina Pali excursion' (e.g, Coe et al., 1978; Singer et al., 2014). However, Liu et al., (2018) could show that, despite the high sedimentation rates of around 50 cmka^{-1}, no evidence for excursional features could be found in SE Black Sea sediments. The VGPs associated with a shallow inclination and low paleointensity interval still plot exclusively at latitudes higher than 60°N. The remaining intervals from 20 to 39 ka and from 42.5 to 58 ka, respectively, are less well documented, due to hiatuses and/or low sedimentation rates (Fig. 6.4), or are compromised by the presence of greigite, such as in core MSM33-53-1 (Figs. 6, 7). Paleomagnetic data from 20 to 39 ka, based on the data of seven cores, including a record of the Mono Lake excursion, were compiled by Liu et al. (2019.).

The time interval from 42.5 to 58 ka shall be discussed in this study. Only five cores, MSM33-64-1 and the four parallel cores from site M72/5-22 (comp. Fig. 6.1), contribute useful data to this time interval (Fig. 6.8). Detailed down-core information on paleo- and rock magnetic results from these cores is given by Nowaczyk et al. (2018, 2013, 2012) and Liu et al. (2018). ChRM inclinations and declinations, as well as relative paleointensity records from these five cores versus age from 42 to 60 ka, together with the respective stacks (applying Fisher (1953) statistics to direction data) into 100-year bins are shown in Fig. 6.8. Where possible, for numbers of samples n≥3 (n≥ 2), α_{95} error bars (1σ error bars) are shown in the direction (paleointensity) stacks. It is evident that between about 47 to 55 ka the directional stacks are only sparsely defined (Fig. 6.8 b, c). Due to the low data density it was only possible to obtain α_{95} errors for a few mean paleomagnetic directions. Nevertheless, directions from consecutive samples, stacked together from five different cores, do not differ very much from each other. Thus, the obtained paleosecular variation record between 42.5 and 58 ka appears fairly reliable, representing geomagnetic field variations.

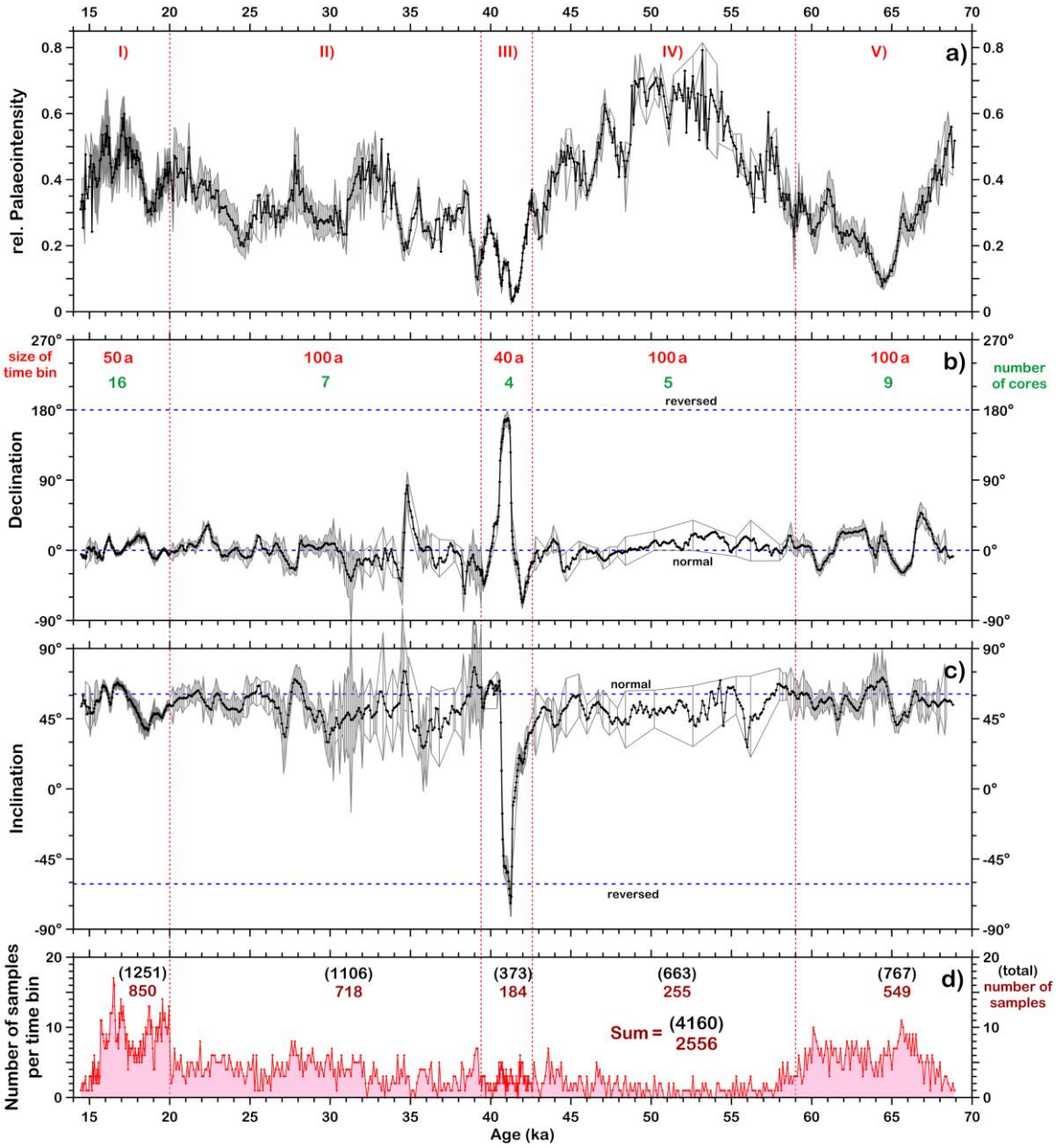

Figure 6.9 Summary of palaeomagnetic data obtained from a total of 16 sediments cores recovered from the SE Black Sea: a) relative paleointensity, b) declination, c) inclination, d) number of samples per time bin. Where available, the 1σ standard deviation for relative palaeointensities in a) and the α_{95} for directional data in b) and c) are shown in grey. Due to highly variable sedimentation rates and data coverage (comp. Fig. 6.4) the record was divided into five sub-sections of different temporal resolution, labelled with roman numbers from I to V: I – Liu et al. (2018), II – Liu et al. (2019), III – Nowaczyk et al. (2012), IV – this study, V – Nowaczyk et al. (2018). The temporal resolution (red numbers) and the number of sediment cores (green numbers) is indicated in b), and the number of (investigated) used samples per sub-section is given in d) by (black) red numbers. The directions for a geocentric axial dipole field at the study site are indicated by blue dashed lines in b) and c).

The complete paleomagnetic record obtained from the SE Black Sea from 15 to 69 ka is shown in Fig. 6.9. In addition to the paleointensity and the directional stacks, the number of samples per time bin is also indicated in the bottom. For the five sub-sections of the stacks, labeled with

Roman numbers in Fig. 6.9a, also their temporal resolutions and numbers of cores used for stacking are listed in Fig. 6.9b (see also Table 1.1). In Fig. 6.9d the total number of samples and the number of samples per sub-section used for stacking are listed in black and red, respectively. Thus, a total of 2556 out of 4160, or 61.4% of all investigated discrete samples were considered for stacking.

The stacked records shown in Figures 9 and 10 comprises 649 time-bins. Due to the lack of data in several intervals, 50 bins were interpolated linearly. In most cases only 1 value, for inclination, declination, and paleointensity each, had to be interpolated. Rarely 2 or 3 values were missing. Interpolation was needed since the stack was finally smoothed with a weighted three-point running-average (0.25×(n-1)+0.5×n+0.25×(n+1)), in order to suppress the scatter in the records to some degree.

6.4 Discussion

6.4.1 Directional variations

The most prominent features in the PSV records from the SE Black sea (Fig. 6.9) are the Laschamp excursion with a short but full reversal located in a pronounced field intensity low at around 41 ka (Nowaczyk et al., 2013, 2012), and the Mono Lake excursion, mostly expressed as a swing in declination at around 34.5 ka (Liu et al., 2019.). Further-on, there is a deep minimum in the paleointensity at around 64.5 ka, associated with larger swings in declination (Nowaczyk et al., 2018), probably the mid-latitude expression of a geomagnetic excursion seen at northern high-latitudes, the so-called 'Norwegian-Greenland-Sea excursion' (e.g., Nowaczyk et al., 2003; Simon et al., 2012; Xuan et al., 2012). A well-defined minimum in inclination at around 18.5 ka, occurring within a minimum in paleointensity, is coeval with the postulated 'Hilina Pali excursion' (e.g., Coe et al., 1978; Singer et al., 2014), though without excursional directions (Liu et al., 2018). There are further inclination minima between 25 and 40 ka (Fig. 6.9a), but less well constrained, considering α_{95} values, but stacked data still exhibit fairly consistent and smooth variations with data collected from seven cores. From about 47 to 55 ka, directional variations in times of highest field intensity of the studied time interval, are apparently less pronounced. Although only for a few directional data an α_{95} could be defined, also here consecutive samples combined from five different cores yielded a fairly smooth directional record. The Black Sea paleointensity stack formerly published by Nowaczyk et al. (2013) was based on six M72/5 cores. The improved record out of these cores, supplemented by further ten cores from the MSM33 expedition now is based on 2556 samples, almost doubling the number of samples and, providing directional data for the whole-time interval from 15 to 69 ka.

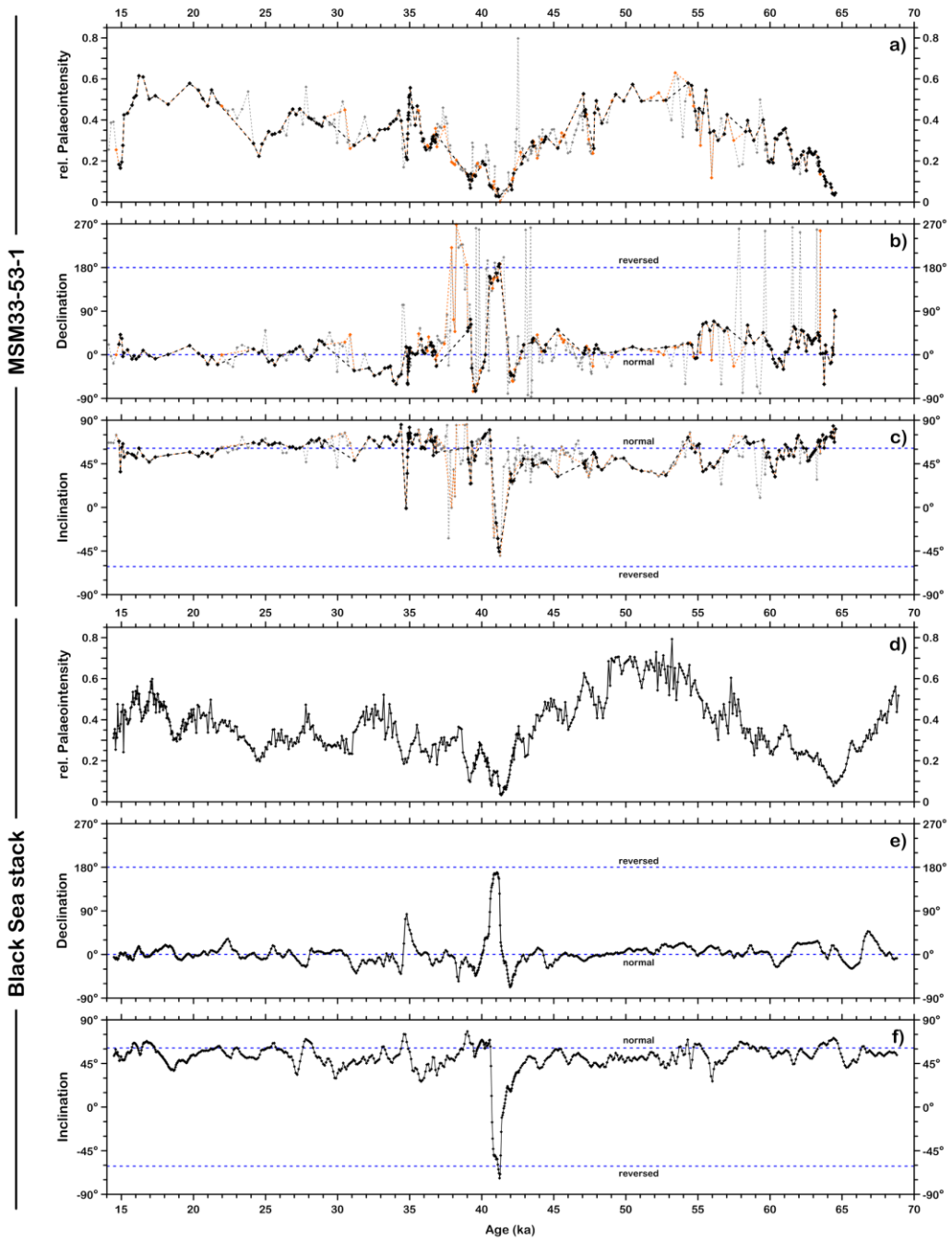

Figure 6.10 Palaeosecular variation data, a) relative palaeointensity, b) declination, and c) inclination from Core MSM33-53-1 compared to the stack from other Black Sea sediment cores (d through f) based on strict filter criteria, SIRM/κ_{LF} ratio <10.0 kAm^{-1}, for excluding greigite-based data. This filter level would have excluded almost all data from Core MSM33-53-1 between 35 and 55 ka (see Figs. 6 and 7). Therefore, data from Core MSM33-53-1 is shown as raw data (grey), for samples with SIRM/κ_{LF} ratio <15.0 kAm^{-1} (orange), and for samples with SIRM/κ_{LF} ratio <12.5 kAm^{-1} (black).

In Fig. 6.10, the new stack, solely based on data cleaned from greigite-bearing samples (Fig. 6.10d,e,f), is plotted together with the data from core MSM33-53-1 (Fig. 6.10a,b,c), being affected by greigite. The fact that magnetite and greigite-bearing samples together recorded the Laschamp excursion indicates that greigite particles very likely have formed shortly after the

deposition of magnetite. Since the overall redox conditions of the body of water above the study site was oxic during deposition of the sediments (Wegwerth et al., 2016), greigite must have been formed within the sediment in micro-environments such as inside organic remnants (e.g., Nowaczyk, 2011). On the other hand, inclination and declination anomalies around 38 ka in core MSM33-53-1 (Fig. 6.10b, c), according to SIRM/κ_{LF} ratios > 10 kAm^{-1}, are characterized by some amount of greigite. Apparently, this feature looks like a ghost image of the Laschamp excursion. However, this is impossible since the greigite is sited within sediments at around 38 ka definitely deposited after the Laschamp excursion. Thus, it is not safe to assume that greigite generally carries a syn-depositional and reasonable paleomagnetic signal, since greigite can form after deposition of the sediments at any time when dissolved iron and sulfide are available during diagenesis (Roberts et al., 2011). In order to avoid greigite, the restrict filter rule that SIRM/κ_{LF} ratios < 10 kAm^{-1} is subjected for paleomagnetic studies in all Black Sea cores (e.g., Liu et al., 2018, 2019.; Nowaczyk et al., 2018, 2013, 2012).

6.4.2 Paleointensity

The relative paleointensity records derived from a variety of sediments and non-sedimentary archives (e.g., ice cores) have demonstrated that the geomagnetic field varied in a globally coherent manner on millennial and longer timescales (e.g., Laj et al., 2014, 2004; Ménabréaz et al., 2012; Muscheler et al., 2005; Roberts et al., 2013). To obtain high fidelity paleomagnetic data from sediment cores, high deposition rates without significant reductive diagenesis inside the sediments, moderate variations in concentration of magnetic particles (ideally magnetite), and superb chronologies are generally required (Roberts et al., 2013). In order to check the reliability of single rPI records, a common method is to stack multiple sedimentary records. Available rPI records, like the NAPIS (North Atlantic paleointensity stack, Laj et al., 2000), the SAPIS (South Atlantic paleointensity stack; Stoner et al., 2002), and the GLOPIS-75 (global paleointensity stack since 75 ka; Laj et al., 2004), are all stacked from a variety of cores from hemispherically and globally distributed sites, respectively. Those stacks, however, represent a global averaged geomagnetic field intensity, and thus likely compromise the high frequency component of non-dipolar signals. Exemplarily, the GLOPIS-75 which has been stacked from 24 individual marine records from the North and South Atlantic Oceans, the Mediterranean Sea and the Indian Ocean, is plotted with 1σ envelops from the average after the 8th iteration of rejecting outliers in Fig. 6.11a (Laj et al., 2004). The resolution attained by GLOPIS-75, at least in certain intervals, is close to the maximum theoretical limit which can be attained on a global scale. Short-lived fluctuations of GLOPIS-75, appear globally coherent, with periods in the order of 600 to 700 years, usually associated with dipole field fluctuations

(Laj et al., 2004). On the other hand, geomagnetic field variations on shorter time scales are linked to non-dipole terms which typically fluctuate on a more restricted geographical scale (Laj et al., 2004).

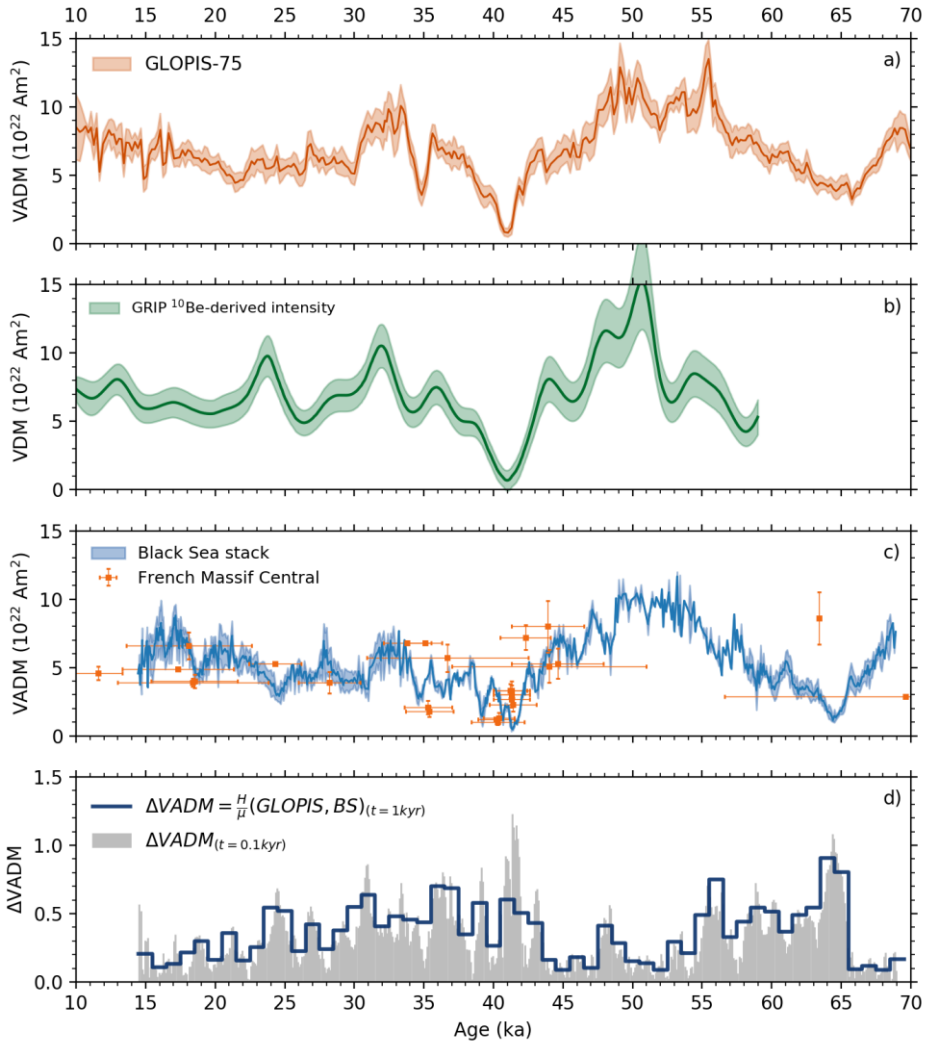

Figure 6.11 Comparison of palaeointensity data, a) GLOPIS-75 stack with 2σ envelop (Laj et al., 2004). b) 10Be-derived geomagnetic field intensity curves obtained from Greenland ice cores (Muscheler et al., 2005), the band of GRIP 10Be-derived VADM includes the geomagnetic field intensities that are based on different combinations of the 10Be data (Muscheler et al., 2004) and different production rate calculations (Masarik and Beer, 1999). c) blue curve: Black Sea rPI stack converted into virtual axial dipole moments (VADM) with 1σ error envelop, orange squares with error bars indicate VADM values from lava flows of the French Massif Central (Laj et al., 2014). d) Discrepancies between the GLOPIS-75 and the VADMs from Black Sea (BS), indicated by the ratio (ΔVADM) of Hausdorff distance (H) and average mean (μ) of VADMs from GLOPIS-75 and Black Sea stacks for every 1 kyr (blue line) and 0.1 kyr (grey bins). The ΔVAMD is a dimensionless number and higher (lower) values indicate greater (smaller) deviations. Note, that all data are plotted with GICC05 age model (Svensson et al., 2008).

In contrast to the mentioned hemispherical/global stacks, the paleointensity records, derived from the ^{10}Be flux from Greenland ice cores (Fig. 6.11b; Muscheler et al., 2005), lava flows

from the French Massif Central (Laj et al., 2014) , and sediment cores from the Black Sea (Fig. 6.11c), are reconstructed from restricted areas. In order to convert the Black Sea rPI values into virtual axial dipole moments (VADMs), a conversion factor of $14.52\times10^{22}Am^2$, derived by comparison to absolute paleointensities from the GEOMAGIA database (Brown et al., 2015), was adopted (e.g., Nowaczyk et al., 2013). Note that all records in Fig. 6.11 are plotted using the GICC05 timescale (Svensson et al., 2008). The GRIP ^{10}Be-derived paleointensity data was calculated assuming that the radionuclide flux (^{10}Be) to Greenland Summit is proportional to the global changes in geomagnetic field strength (Wagner et al., 2001). The band of GRIP ^{10}Be-derived VADM includes the geomagnetic field intensities that are based on the different combinations of the ^{10}Be data (Muscheler et al., 2004) and the different production rate calculations (Masarik and Beer, 1999).

In Fig. 6.11, a general agreement can be observed between paleointensity records stacked from global sites (GLOPIS-75) and a single site (NGRIP, French Massif Central, Black Sea). Specifically, the lowest paleointensity at about 41 ka, corresponding with the Laschamp excursion, are ubiquitously evidenced in all records. The Mono Lake excursion at about 34.5 ka is indicated by a fairly low paleointensity as well. The second deepest paleointensity low at about 65 ka in the Black Sea record is also evident in the GLOPIS-75. Thus, the consistent paleointensity variations, mainly on millennial time scales, are likely representing a dominating geomagnetic dipole signal that has been recorded in a globally coherent manner in different types of sediments as well as in non-sedimentary archives (Roberts et al., 2013).

Nevertheless, on centennial timescales, deviations are recognizable among the discussed paleointensity records. During the Mono Lake excursion, GRIP ^{10}Be-derived intensity and Black Sea paleointensity dropped less significantly compared to the GLOPIS-75. From 42 to 35 ka, both the GLOPIS-75 and GRIP ^{10}Be-derived intensity records exhibit a continuous and rather smooth increase in amplitude, whereas the Black Sea VADM record exhibits noticeable fluctuations. Another major deviation among the records can be seen from 30 to 15 ka, where paleointensity variations from different records are not coherent. In order to quantify the differences between the GLOPIS-75 and the Black Sea VADM record, the Hausdorff distance (Taha and Hanbury, 2015) is introduced. From 14.5 to 69 ka, the Hausdorff distance (H) between the two paleointensity curves and their respective mean values (μ) were calculated in centennial (every 0.1 kyr) and millennial (every 1 kyr) time scales. Due to the widely distinct mean values for different time intervals, the ratio (ΔVADM) of H to μ, a dimensionless number, is taken to indicate the variations between paleointensity curves given by the GLOPIS-75 and the Black Sea VADM records. The higher the ΔVADM values are the greater the difference

between both records is, and vice versa. The centennial ΔVADM (grey bars), though with evident high frequency variations, shows a generally agreement with the millennial ΔVADM (blue curve) in Fig. 6.11.

During the Laschamp excursion, the GLOPIS-75 and the Black Sea VADM demonstrate the highest centennial ΔVADM, but fairly low millennial ΔVADM values (Fig. 6.11d). This is likely due to the fact that the high frequency variations (mainly on a centennial scale) seen in the Black Sea VADM record are not recorded in the GLOPIS-75. The absence of high frequency variations in the GLOPIS-75 is probably a result of global areal averaging (Laj et al., 2004). On the other hand, the largest millennial ΔVADM values are centered at about 64.5 ka, where the Black Sea VADMs are estimated to be much lower than in the GLOPIS-75 (Nowaczyk et al., 2018). In contrast, between about 44 and 54 ka, high paleointensities in both records are corresponding to the lowest ΔVADM values. Additionally, the ΔVADM record shows a general decrease from about 65 to 50 ka, as well as from about 30 to 14.5 ka, whereas both paleointensity records exhibit a long-term increase in amplitude. Therefore, the ΔVADM demonstrate a generally counter relationship with the two records of field paleointensities. Theoretically, a dominant dipolar geomagnetic field is often associated with high paleointensities, which are thus recorded in a variety of archives with global coherence (e.g., Roberts et al., 2013). Thus, it is reasonable to expect less discrepancies between the two paleointensity records when the dipole field contribution is dominating, in general with high paleointensities. On the other hand, large ΔVADM values, evidenced for intervals with extremely low paleointensities and high frequency variations in the Black Sea VADM record, are probably caused by stronger regional non-dipolar features, relative to the weak dipolar contribution.

6.4.3 Vector Transformation of paleosecular variations

For the further discussion, VADMs of the Black Sea stack (Fig. 6.11c) were transformed into field strength F, first by dividing obtained VADMs by $8\times10^{22}Am^2$, the dipole moment from about A.D. 2000, and then by multiplying with 48 μT, the field strength for the SE Black Sea area (42°N, 36°E) in A.D. 2000 (according to the IGRF, https://www.ngdc.noaa.gov/geomag-web/?model=igrf). The obtained paleointensity values then range between about 3 μT, for the N-R (normal-reverse) transition of the Laschamp excursion at 41.6 ka, and about 60 μT at round 50 ka (Fig. 6.13d). Further on, field strength F, together with inclination I and declination D, the geomagnetic field components given in spherical coordinates, were converted into Cartesian coordinates (X, Y, Z), with +X=North, +Y=East, and +Z downward (Fig. 6.12). In a final step, data was transformed into a rotated Cartesian coordinate system (X',Y',Z') as laid

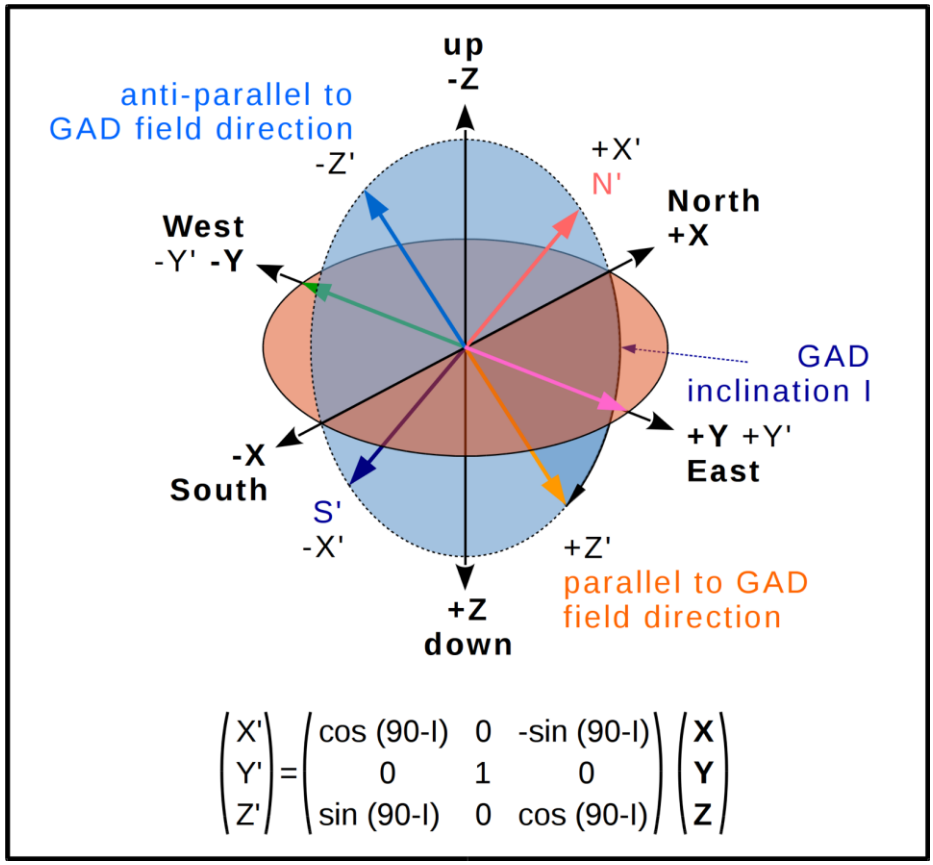

Figure 6.12 Sketch illustrating the coordinate transformation performed on the Black Sea palaeosecular variation record. Data were rotated around the Y-axis (EW) so that the obtained Z' component is parallel to the field direction of a geocentric axial dipole (GAD) of normal polarity with an inclination I of 61° (Latitude of 42°N). The transformation matrix is shown in the lower part of the sketch. The obtained X' and Y' components then are definitely field contribution from non-axial dipole contributions.

out in Fig. 6.12. Now, Z' is parallel to the expected field direction of a geocentric axial dipole (GAD) at the study site (42°N, 36°E). Paleosecular variations in X' and Y' (=Y) are then definitely related only to non-axial dipole contributions to the geomagnetic field. However, although Z' is parallel to the GAD field line, this component can also comprise contributions from higher order multi-poles. At least, zonal harmonics of higher order contribute only the X' component, due to their rotational symmetry with Y' = 0 (Table 6.1).

The field vector components (X', Y', Z'), transformed from the Black Sea paleomagnetic record, are shown in Fig. 6.13a through c, together with their total field strength F in Fig. 6.13d. The frequency distributions of the three transformed field vectors (X', Y', Z') are shown together with the inclination distribution in Fig. 6.14. There appears to be a persistent trend in the X' component for more positive than negative values (Figs. 13a, 14a), This is due to inclinations being persistently lower (by about 10°) than the inclination of 61° expected from a pure GAD field (Figs. 13f, 14e). One likely explanation is inclination-shallowing during

compaction of the mainly siliciclastic sediments. A similar effect is being observed in re-sedimentation experiments with the studied Black Sea sediments under controlled field conditions (work in progress).

	X'	Y'	Z'
GAD			*
Zonal harmonics	*		*
Non-zonal harmonics	*	*	*

Table 6.1 Distribution of dipolar (GAD, geocentric axial dipolar) and non-dipolar contributions of the geomagnetic field to the Cartesian vector components (X', Y', Z') as defined in Figure 6.11.

The distribution of Y', the EW component, does not show any offset. This is definitely caused by the fact that cores were taken without azimuthal orientation. But, a subsequent re-orientation was performed by mathematically correcting ChRM declinations of each core to a total mean of 0°. Nevertheless, the Y' (EW) component is apparently characterized by a low-frequency component with a period of around 2500 years.

In addition to field intensities, the VGP longitude and latitude, presented in Fig. 6.13e and 13f, are calculated from the stacked Black Sea inclination and declination data. Besides aiming to distinguish between normal PSV, excursions, and reversals, the PSV index (Panovska and Constable, 2017) was calculated from the stacked Black Sea data (Fig. 6.13g). The PSV index (P_i) combines the VGP latitudes and the virtual dipole moment (VDM), normalized to the present-day dipole moment ($8\times10^{22}Am^2$). For a stable geomagnetic field, dominated by an axial dipole, the PSV index calculates to values of $P_i \leq 0.3$. On the other hand, geomagnetic excursions, conventionally defined by VGP latitudes being lower than 45ºN and dipole moment of maximum half of the present day value, would give a P_i of ≥ 0.5 (Panovska et al., 2018).

The most striking feature in the PSV record from glacial Black Sea sediments is the Laschamp excursion centered at about 41 ka with very low (total) field intensity estimates of down to B = 3 µT (Fig. 6.13d). Looking at the transformed field vectors (X', Y', Z') the image becomes more differentiated. The field strength of B = 12.5 µT from 41.1 to 40.8 ka is related to clearly negative values in the Z' component of -10 µT (Fig. 6.13c), that is, the field was reversed, with VGP latitudes being higher than 60°S for about half a millennium (Fig. 6.13f). It is interesting to note, on the one hand, that the major field decay in the total field (Fig. 6.13d) is mainly

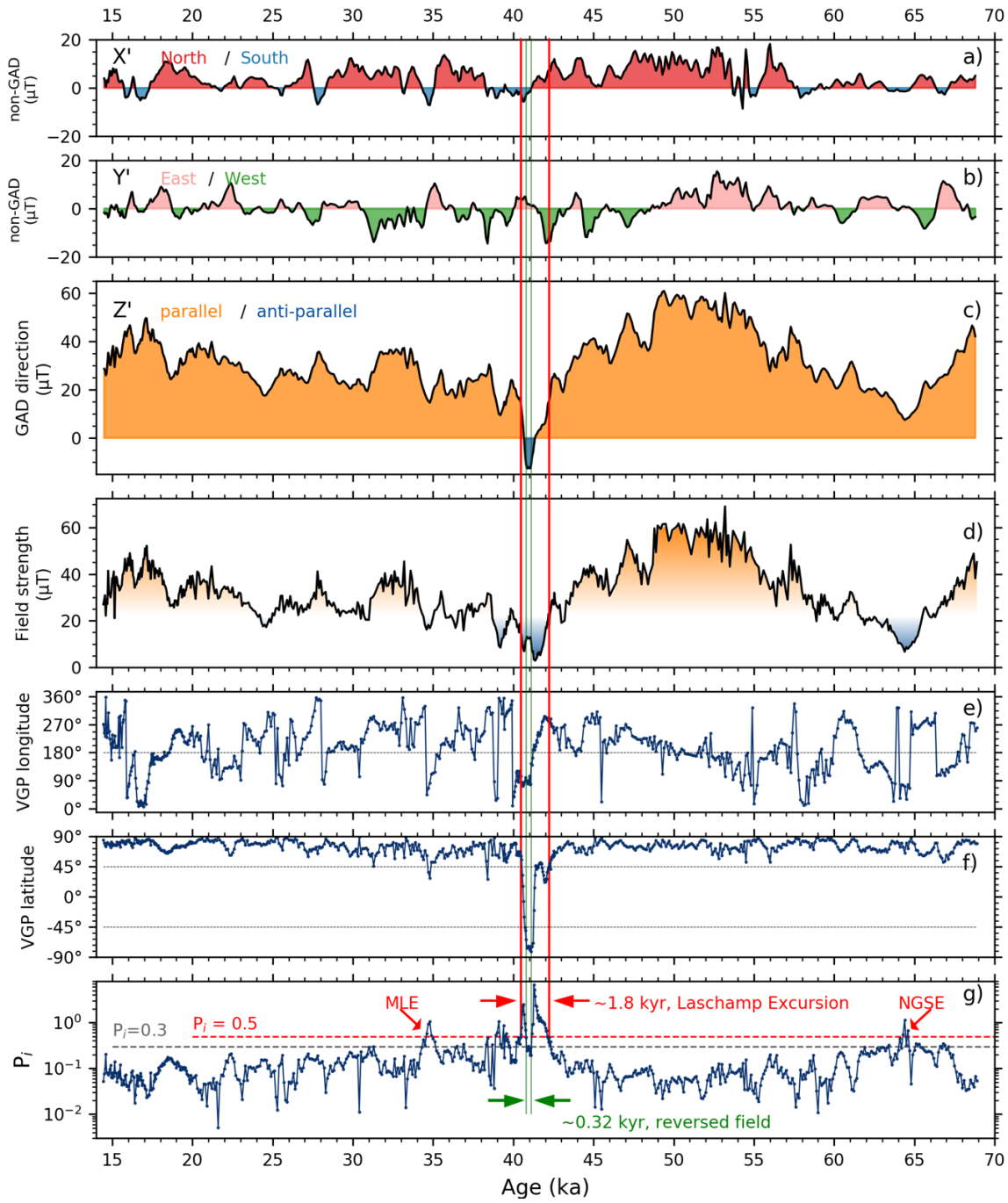

Figure 6.13 Paleosecular variation record from Black Sea sediments from 15 to 69 ka given in µT for the non-axial dipole contributions a) X' and b) Y' and c) the Z' component parallel to the field direction of a geocentric axial dipole (GAD) of normal polarity (comp Fig. 6.11). For comparison, the original data set obtained are shown as d) field strength, e) longitude and f) latitude of the related virtual geomagnetic pole (VGP). g) the palaeosecular variation (PSV) index P_i, calculated from the paleointensities and the VGP latitudes of stacked Black Sea data, implying stable (excursional) geomagnetic field with values of $P_i \leq 0.3$ ($P_i \geq 0.5$). MLE – Mono Lake excursion, NGSE - Norwegian–Greenland Sea excursion.

related to a decay in the Z' component prior to/during the N-R reversal (Fig. 6.13c). Thus, associated frequency distributions (Z' and F) are also very similar (Fig. 6.14c, d). In contrast

to this, the non-axial dipole contributions seen in X' and Y' appear to show more or less constant amplitude variations of about ±12 μT (relative to their respective means, Fig 14a, b) even across the Laschamp excursion (Fig. 6.13). In Fig. 6.13g, the Laschamp excursion is also evidenced in the PSV index with P_i with values larger than 0.5. Compared to the P_i calculated from global and regional stacks by Panovska et al. (2018), the P_i record from Black Sea sediments denotes a short interval of normal secular variations (with $P_i \leq 0.3$) during the reversed field phase of the Laschamp excursion (Fig. 6.13g). This short interval, spanning from 41.16 to 40.84 ka, is bracketed with green lines in Fig. 6.13. Interestingly, this short interval is also coinciding with the VGP latitudes higher than 60°S and negative values in the Z' component, respectively. Thus, the pattern is likely indicating even a stable reversed magnetic field configuration during the Laschamp excursion. Valet et al. (2008) suggested that an excursion is an 'aborted' polarity interval bracketed by two reversals, and the 'aborted' polarity interval should not be regarded as a real polarity state. However, the high-resolution PSV record obtained from Black Sea sediments indicate that the recorded Laschamp excursion with fully reversed VGP latitudes (higher than 60°S) for about 0.44 kyr (Nowaczyk et al., 2012), represents a stable reversed field for about 0.32 kyr (Fig. 6.13f).

The full duration of the Laschamp excursion was previously estimated by Nowaczyk et al. (2012) as being 1.64 kyr, mainly based on the derived transitional directions. In contrast, based on the PSV index P_i derived from the Black Sea stack, the duration of the Laschamp excursion can be estimated from 42.24 to 40.48 ka (Δt=1.76 kyr), with $P_i \geq 0.5$, and the fully reversed stable magnetic field from 41.16 to 40.84 ka (Δt=0.32 kyr), with $P_i \leq 0.5$. During this reversed field interval, the field strength derived from Black Sea site is characterized by a fairly high maximum value of about 12.5 μT, compared to the rather low field strength of about 3 μT at 41.6 ka.

Obviously, the temporal field maximum from 41.1 to 40.8 ka, associated with reversed directions, is not visible in globally stacked records (Fig. 6.11). One reason for this is an averaging out of this short feature during stacking. In addition, several of the individual records that went into the GLOPIS-75 stack, are lacking reversed directions during the interval of the Laschamp excursion. Thus, there has been probably already a smoothing effect during remanence acquisition in the sediments during deposition at those sites. If the lock-in time window comprises about 500 years, or more, weak reversed polarity field vectors are averaged together with stronger normal polarity field vectors, resulting mostly in normal polarity directions associated with a single low in relative paleointensity. In Black Sea sediments, the lowest field strength at 41.3ka is characterized by a P_i index peak value of 6.08 and by an

extremely fast VGP movement during the N-R reversal, whereas the R-N reversal took place at higher field strength with a Pi index of 2.5. Therefore, the lowest paleointensity values are not necessarily indicating the center of an excursion.

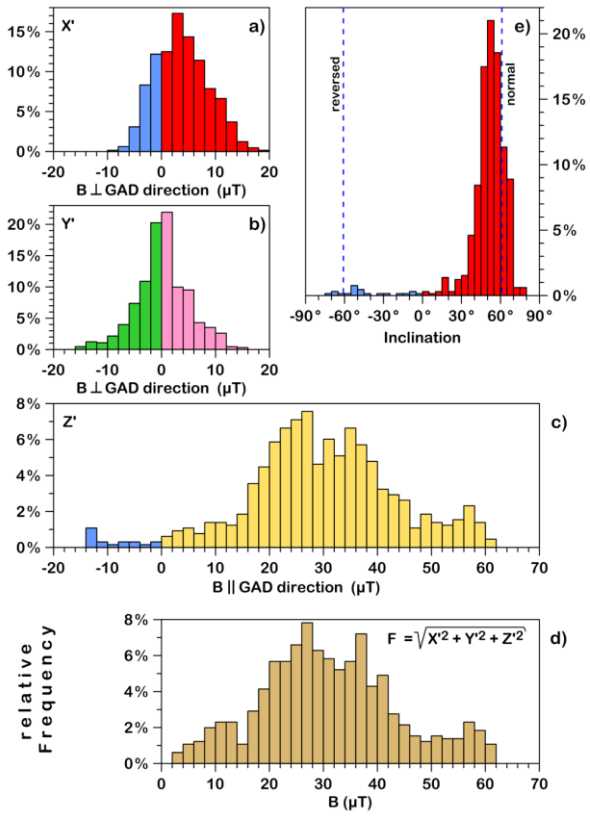

Figure 6.14 Frequency distributions of geomagnetic field components transformed into components perpendicular (a and b) and parallel (c) to the field of a geocentric axial dipole (GAD) of normal polarity (comp Fig. 6.11), the total field intensity F (d), and the inclination (e). In e) the inclinations for the study area expected from a GAD field of normal and reversed polarity, respectively, are indicated by vertical blue dashed lines.

The second deepest intensity minimum is observed at around 64.5 ka (B = 8 µT). The paleointensity low is contemporary with the so-called 'Norwegian–Greenland Sea excursion' (Løvlie, 1989), that was reported with shallow to steep negative inclinations from northern high-latitudes (e.g., Nowaczyk et al., 2003; Simon et al., 2012; Xuan et al., 2012). Compared to the paleointensity low during the Laschamp excursion, the two minima are fairly similar, but the record of the Z' component shows the difference. The Z' component is relatively low at 64.5 ka but still positive. Occasionally, the perpendicular (non-dipolar) components X' and Y' are also very small in amplitude at this time so that no abnormal directions were recorded. The PSV index of Black Sea stacks also exhibits values of $P_i \geq 0.5$ in a few samples at bout 64.5 ka, normally indicating an excursion event (Panovska et al., 2018). However, the Black Sea VGP positions show no deviations from a normal polarity for the 'Norwegian–Greenland Sea excursion' (Nowaczyk et al., 2018). Hence, the $P_i \geq 0.5$ is likely due to extremely low

paleointensity and fast directional changes. A similar pattern was also observed at about 39 ka, shortly after the Laschamp excursion.

In contrast, the Mono Lake excursion at about 34.5 ka is characterized by intermediate field intensities (B = 20 µT), which is much higher than during the Laschamp excursion (B = 3 µT) and the 'Norwegian–Greenland Sea excursion' (B = 8 µT). During the Mono Lake excursion, the GAD parallel contribution (Z') is slightly decreasing. However, the non-dipolar contributions in X' and Y' exhibit abrupt changes from 35 to 34 ka where are even faster than during the Laschamp excursion. Thus, the Mono Lake excursion is likely more related to a temporal dominance of multipolar components of the geodynamo rather than due to a decay of dipolar field contributions (e.g., Liu et al., 2019.). In addition, VGP latitudes during the Mono Lake excursion are lower than 45°N for about 0.4 kyr, defining it as a very short excursion (e.g., Cassata et al., 2008; Kissel et al., 2011). The related PSV index also reaches values over 0.5, but much less pronounced compared to the Laschamp excursion. On the other hand, the PSV index for the past 100 ka from global and regional stacks (Panovska et al., 2018) shows no anomalous/transitional activity at the time of the Mono Lake excursion. This is likely due to the stacking process, averaging globally distributed data, with most of them having not recorded the Mono Lake excursion, due to low sedimentation rates (Panovska et al., 2018). With a relative high resolution of 100 years in the studied Black Sea sediments for this time interval, the duration of the Mono Lake excursion can be estimated to be about 0.4 kyr, based on P_i values of ≥ 0.5.

Further intensity minima at 32.0 and 24.5 ka have similar field intensities like the Mono Lake excursion (around 20 µT). However, non-dipolar contributions are lower, resulting only in typical secular variation amplitudes in inclination and declination (Fig. 6.10e, f). A similar situation is the case at 18.5 ka, the postulated 'Hilina Pali excursion', with even a higher minimum intensity (B = 27 µT). Additionally, both their VGP positions and P_i Values (<0.3) exhibit no abnormal secular variations recorded in Black Sea sediments deposited after the Mono Lake excursion.

6.5 CONCLUSIONS

A comprehensive study on 16 (out of 18 investigated) sediment cores recovered from the SE Black Sea yielded a high-resolution and high-fidelity record of paleosecular variation (PSV) from 68.9 to 14.5 ka. Due to variable sedimentation rates and sedimentation gaps, stacking of the data, relative paleointensity as well as inclination and declination, had to be split into five time intervals with different temporal resolutions ranging from 40 to 100 years. The obtained record comprises three geomagnetic excursions, the 'Norwegian–Greenland Sea excursion',

the Laschamp excursion, and the Mono Lake excursion. They are characterized by abnormal secular variations at about 64.5 ka, 41.6 ka and 34.5 ka, respectively, quantified by the PSV index with values of $P_i > 0.5$. However, no excursional VGPs (< 45°N) were determined for the 'Norwegian–Greenland Sea excursion'. At about 18.5 ka, the postulated 'Hilina Pali excursion' exhibits fairly low paleointensities, but without excursional evidence, and P_i values < 0.3.

The Black Sea paleointensity stack demonstrates a general agreement with other global and regional paleointensity records, mainly on a millennial scale. Nevertheless, discrepancies between the GLOPIS-75 and the Black Sea paleointensity stack are evident on a centennial scale. Specifically, the deviations are anticorrelated to geomagnetic field intensity. That is, during times of a weak geomagnetic field, the non-dipolar field contributions are likely increased, resulting in distinct field intensity variations being specific only for the Black Sea area.

A separation of the Black Sea paleomagnetic data into components parallel and perpendicular to the direction expected from a geocentric axial dipole (GAD) points towards a dominance of dipolar field contributions during global intensity variations on millennial time scales, whereas non-GAD components seem to vary within a fairly constant amplitude range on centennial time scales for the whole time interval, as discussed in this study.

The Laschamp excursion (41 ka), characterized by a fully reversed geomagnetic field for 0.32 kyr, is indicated by a negative GAD parallel component, whereas the geomagnetic field during the Mono Lake excursion (34.5 ka) is mainly influenced by larger non-GAD contributions, relative to the low GAD component. Though the 'Norwegian–Greenland Sea excursion' (64.5 ka) exhibits the second deepest low in the GAD component of the study interval, the non-GAD components varied only little in amplitude. The postulated 'Hilina Pali excursion' shows a relatively low GAD component and insignificant non-GAD components.

The reversed field configuration during the Laschamp excursion is characterized by an interval of normal secular variations ($P_i < 0.5$), bracketed by two intervals of abnormal variations ($P_i > 0.5$). The reversed interval is, however, not coeval with the lowest field intensity recorded Black Sea sediments, but with values of estimates 12.5 µT. Instead, lowest field values of estimated 3 µT are coeval with the N-R reversal at the onset of the reversed field configuration of the Laschamp excursion. Based on the PSV index, the Laschamp excursion had a total duration of about 1.76 kyr, with a fairly stable reversed phase lasting for about 0.32 kyr. The

Mono Lake excursion, also indicated by PSV index ($P_i \geq 0.5$), was estimated to have lasted for about 0.4 kyr.

Thus, the Black Sea paleomagnetic data, covering field fluctuations from normal secular variations, over excursions, to a short but full reversal, point to a geomagnetic field characterized by a large dynamic in intensity and superposition of dipole and non-dipole contributions from the geodynamo. Nevertheless, presented data from a single site in this paper, is still not sufficient in order to completely disentangle the complex geodynamo processes inside the Earth's liquid outer core. Similar studies on sediments from other sites are therefore needed to further refine the conclusions obtained from Black Sea sediments.

Acknowledgements

We thank S. Plewe, M. Duwe, T. Moldenhawer, and F. Brendel for their technical and logistical help during processing and sub-sampling of the cores. We also thank the captains and crews of *RV Meteor*, cruise M72/5 and *RV Maria S. Merian*, cruise MSM33, for their efforts in providing optimal scientific working conditions. This work was partly funded by the German Research Foundation (Deutsche Forschungsgemeinschaft, DFG SPP 1266 “INTERDYNAMIC” grants AR 367/9-1 and AR 367/9-2), the Gary Comer Science and Education Foundation, U.S.A., and the Chinese Scholarship Council (CSC grant No. 201506180060).

7 Synthesis

7.1 Summary and conclusions

This doctoral thesis was aiming to establish high-resolution paleosecular variation (PSV) records from late Quaternary Black Sea sediments, and especially, to investigate the geomagnetic field behavior during excursions. To fulfill these aims, detailed rock magnetic and paleomagnetic analyses have been conducted on 16 sediment cores recovered from the southeastern Black Sea. The obtained data sets were used to create a stack covering the time window between 68.9 and 14.5 ka. This restriction is due to environmental and tectonic impacts, resulting in larger variations in sedimentation rates and even hiatuses. Therefore, the PSV record stacked from Black Sea sediments has been split up into five different time intervals with temporal resolutions ranging from 40 to 100 years. Nevertheless, it could be shown that reconstructed prominent lows in paleointensity at about 64.5 ka, 41.6 ka and 34.5 ka are coeval with the Norwegian–Greenland Sea excursion, the Laschamp excursion, and the Mono Lake excursion, respectively. The excursions are further evidenced by an abnormal PSV index, though only the Laschamp and the Mono Lake excursions exhibit excursional virtual geomagnetic pole (VGP) positions.

In the following, the main results and conclusions with respect to the aims of this doctoral thesis are indicated.

Diagenesis of magnetic minerals in Black Sea sediments

In the Black Sea, three hydrological phases, the lacustrine (40.5 - 17.5 ka), the transitional (17.5 - 8.3 ka), and the marine (8.3 – 0.0 ka) phases can be recognized for the past 41 ka. In order to identify the carriers of magnetization in sediments from the different hydrological phases, core MSM33-55-1 recovered from the southeastern Black Sea was subjected to detailed rock magnetic and electron microscopy investigations.

It was found that in sediments deposited before 17.5 ka, the magnetic minerals are dominated by a mixture of greigite and titanomagnetite in samples with SIRM/κ_{LF} >10 kAm^{-1}, or exclusively by titanomagnetite in samples with SIRM/κ_{LF} ≤10 kAm^{-1}. Greigite was generally found as crustal aggregates in locally reducing micro-environments. From 17.5 ka to 8.3 ka, the dominant magnetic mineral phase in this transition phase changed from greigite (17.5 – 10.0 ka) to probably silicate-hosted titanomagnetite (10.0 – 8.3 ka). After 8.3 ka, the meanwhile anoxic Black Sea was a favorable environment for the formation of pyrite framboids.

Nevertheless, some silicate-hosted titanomagnetite/magnetite particles, low in concentration, were evidenced in samples from the marine phase by electron microscopy.

Thus, the varying occurrences of different varieties of iron oxides and iron sulphides, revealed by this study, reflect the complexities of diagenetic processes by changing environments in the waterbody of the Black Sea basin. In addition, SIRM/κ_{LF} ratios ≤10 kAm^{-1} was evidenced to be reasonable criteria to exclude greigite bearing samples from paleomagnetic studies in the last glacial Black Sea sediments.

The Norwegian-Greenland Sea excursion

Between and 68.9 and 58.0 ka (~MIS4) the Black Sea paleosecular variation record was reconstructed from nine sediment cores with sedimentation rates of 20 to 40 cm ka^{-1}, thus yielding a temporal resolution of 100 years. At 64.5 ka, the second deepest minimum in relative paleointensity during the past 69 ka occurred, with the Laschamp geomagnetic excursion at 41 ka being associated with the lowest field intensities. The geomagnetic field minimum during MIS 4 is associated with large declination swings beginning about 3 ka before the minimum. While a swing to 50°E is associated with steep inclinations (50 - 60°) according to the coring site at 42°N, the subsequent declination swing to 30°W is associated with shallow inclinations of down to 40°. The pronounced intensity minimum at 64.5 ka and described directional variations are coeval with the so-called 'Norwegian-Greenland Sea excursion' reported from northern high-latitudes (e.g., Løvlie, 1989; Bleil and Gard, 1989; Channell et al., 1997; Nowaczyk et al., 2003).

According to the derived age model the directional variations during MIS4 are associated with VGP positions quickly changing positions between opposite sides of the globe, almost reaching excursional latitudes. These fast directional changes were accompanied by a quickly decaying field, finally reaching the second lowest intensity values of the past 69 ka. This is also seen in global compilations of paleointensity data as well as in reconstructions of the geomagnetic dipole moment from ^{10}Be flux data (Simon et al., 2016). Contemporaneous data from the Norwegian–Greenland Sea, thus from much higher northern latitudes, indicate much larger deviations from dipolar directions.

Therefore, the geomagnetic field during the middle of MIS 4 might have been characterized by a non-dipole field configuration, accompanied with fairly low field intensities. However, the current data base is far too sparse to quantify the global field geometry in terms of a (low-order) spherical harmonics model.

The Laschamp excursion

At around 41, the Black Sea paleomagnetic record indicates a short-term full reversal of the geomagnetic field in the Black Sea area. This is the most pronounced geomagnetic excursion of the past 100 ka, first found in lavas of the Massif Central, France (Bonhommet, 1967; Gillot et al., 1979; Guillou et al., 2004). According to PSV index analysis the central reversed phase of the excursion, with an intensity of about 25 % of today's field, can be characterized as a stable dipolar field configuration (PSV index <0.5), whereas the transitional phases are associated with very low field intensities and high PSV index (>0.5).

The Mono Lake excursion

For the time interval between 40.0 and 20.0 the full-vector PSV record from Black Sea sediments is only based on seven cores. Because of a hiatus at several sites and lower sedimentation rates (15 to 20 cm ka^{-1}) in the remaining sediments, the therefore reduced data density in the obtained PSV records of individual sediment cores were stacked by using 100-year bins. At about 34.5 cal. ka BP, the Mono Lake excursion (Denham and Cox, 1971; Liddicoat and Coe, 1979; Lund et al., 1988) is evidenced in the stacked Black Sea PSV record by both a minimum in relative paleointensity and larger directional variations.

During the Mono Lake excursion as recorded in the investigated Black Sea sediments, associated VGPs migrated from Alaska, via central Asia and the Tibetan Plateau, to Greenland, performing a clockwise loop. This pattern of the Mono Lake excursion VGP path is in good agreement with the ones recorded in the Wilson Creek Formation (Lund et al., 1988), the Iceland Sea sediments (core PS2644-5, Laj et al., 2000), and Tenerife lavas (Kissel et al., 2011). These paleomagnetic data sets suggest a global coherence of field behavior during the Mono Lake excursion. On the other hand, distinct excursional VGPs recorded from some further sites are in conflict with this interpretation and thus indicate a non-dipolar geomagnetic field geometry with regionally diverging vectorial behavior.

No evidences for the postulated 'Hilina Pali' excursion

For the time interval between 20.0 and 14.5 ka, the sixteen investigated Black Sea sediment cores provide a high-resolution paleosecular variation record with sedimentation rates of up to 50 cm ka^{-1}. Therefore, the obtained magnetostratigraphic records enabled a stacking using 50-year bins. A directional anomaly at 18.5 ka, associated with pronounced swings in inclination and declination, as well as a low in relative paleointensity (rPI), is probably contemporaneous with the Hilina Pali excursion, originally reported from Hawaiian lava flows (Coe et al., 1978).

However, virtual geomagnetic poles (VGPs) calculated from the Black Sea PSV record are not located at latitudes lower than 60° N, which denotes normal, though pronounced secular

variations. Specifically, during the postulated 'Hilina Pali' excursion, the VGPs calculated from Black Sea data migrated clockwise only along the coasts of the Arctic Ocean from NE Canada (20.0 ka), via Alaska (18.6 ka) and NE Siberia (18.0 ka) to Svalbard (17.0 ka), then looping clockwise through the Eastern Arctic Ocean.

Therefore, the Black Sea VGP path, together with VGPs obtained from lava flows and sediments from global sites shown in Fig. 5.8, do not support the presence of a geomagnetic excursion between 20 and 16 ka. Only one, probably questionable sedimentary record from Lake Baikal (Peck et al., 1996) and a single data set from volcanic rocks in Tianchi volcano (Singer et al., 2014; Zhu et al., 2000) give indications for an anomalous field behavior in this time interval.

The behavior of the geomagnetic field between 68.9 and 14.5 ka

This comprehensive study based on 16 sediment cores recovered from the SE Black Sea yielded a high-resolution and high-fidelity paleo-secular variation stack from 68.9 to 14.5 ka. The obtained record also comprises three geomagnetic excursions, the 'Norwegian–Greenland Sea excursion' (64.5 ka), the Laschamp excursion (41.0 ka), and the Mono Lake excursion (34.5 ka). They are characterized by abnormal secular variations quantified by the PSV index (P_i) with values of $P_i > 0.5$. However, no excursional VGPs (< 45°N) were determined for the 'Norwegian–Greenland Sea excursion'. For the postulated 'Hilina Pali excursion' at about 18.5 ka, though being characterized by fairly low paleointensities, no excursional evidence could be found since P_i values are < 0.3.

On a millennial scale, the Black Sea paleointensity stack is in general agreement with other global, e.g., the global paleointensity stack (GLOPIS-75, Laj et al., 2004) and regional paleointensity compilations (Fig. 6.11). Nevertheless, divergencies are evident on a centennial scale. Specifically, during times of a weak geomagnetic field, the deviations between the Black Sea stack and other records are partly even anticorrelated. This indicates that in these time intervals, the non-dipolar contributions to the geomagnetic field were likely increased, resulting in distinct field intensity variations being specific only for the Black Sea area.

In Order to get a first idea of dipole versus non-dipole contributions, the stacked Black Sea paleomagnetic record, directions and intensities, was converted into one component parallel to the direction expected from a geocentric axial dipole (GAD) and two components perpendicular to it, representing only non-GAD components of the geomagnetic field. The Laschamp excursion (41.0 ka), is then characterized by a fully reversed geomagnetic field for 0.32 kyr, as indicated by a negative GAD parallel component, whereas the geomagnetic field

during the Mono Lake excursion (34.5 ka) is mainly influenced by larger non-GAD contributions, relative to the low GAD component. Though the 'Norwegian–Greenland Sea excursion' (64.5 ka) exhibits the second deepest low in the GAD component of the study interval, the non-GAD components varied only little in amplitude. The postulated 'Hilina Pali excursion' shows a relatively low GAD component and insignificant non-GAD components.

In summary, the Black Sea paleomagnetic data record from 68.9 to 14.5 ka comprises field fluctuations from normal secular variations, over excursions, to a short but full reversal, accompanied by a large dynamic range in intensity. This points to a geomagnetic field characterized by a highly variable superposition of dipole and non-dipole contributions from the geodynamo throughout the studied time interval. Nevertheless, presented data from a single site such as presented in this study, is by far not sufficient in order to completely disentangle the complex geodynamo processes inside the Earth's liquid outer core maintaining the geomagnetic field with all its various features in time and space. Similar comprehensive studies on sediments from all over the globe are therefore needed to further refine the conclusions obtained from Black Sea sediments.

7.2 Future perspectives

The paleomagnetic studies on sixteen Black Sea sediment cores have yielded high-resolution paleosecular variation records for the time window between 68.9 and 14.5 ka ka. In addition to this time interval, lower sections in all studied cores, except cores M72/5-24GC3, M72/5-25GC1, and MSM33-53-1, contain also sediments from early marine isotope stage (MIS) 5 back to middle/early MIS 6. Due to earthquakes, and related slumping down of deposited material, the sediments spanning most of MIS 5 are missing in all studied cores. Nevertheless, the sediments from early MIS 5 back to MIS 6 are promising for future paleomagnetic interpretations. The preliminary results from these older sediments recovered from the Black Sea indicate reliable paleomagnetic data. However, the age models for sediments from MIS 5 and 6 are still under investigation. First age model tie points are provided by three tephra layers (132 ka, 161 ka, 167 ka) and the correlation of XRF-log data to other global climate records. Recently, also stable oxygen isotope determinations for MIS 5/6 sediments from several Black Sea cores, performed by co-workers, further refined the age models. Once the age models for the lower sections are sufficiently developed, a high-resolution paleosecular variation stack can be made available also for MIS 6, likely with a resolution of 100 years.

Due to the very detailed record of the Laschamp excursion it was decided to subject Black Sea sediments covering this prominent geomagnetic feature to high-resolution analyses for the cosmogenic radionuclide Beryllium-10 (^{10}Be), performed by co-workers at the Leibnitz-Institute of Baltic Sea Research, Rostok-Warnemünde. The Production rate of ^{10}Be is linked by a non-linear inverse relationship to the variability in intensity of both the Earth's and the Sun's magnetic fields. Therefore, the future Black Sea ^{10}Be record is expected to serve as a further proxy of geomagnetic field intensity and long-term solar variability. Since ^{10}Be measurements require less material (tens of milligram), ^{10}Be samples can be taken at higher resolution compared to paleomagnetic samples (~12 to 15 gram). Thus, the ^{10}Be results likely will reveal more detailed information about geomagnetic field behavior during the short lived Laschamp excursion.

Black Sea sediments are also used for re-sedimentation experiments under controlled field conditions using intensities between 2 and 130 μT. Field minima reconstructed from Black Sea sediments appear to be much too low when compared to reconstructions from globally distributed records, either derived from relative paleointensity data from sediment cores from other sites or from estimates based on ^{10}Be flux data. The results from the re-sedimentation experiments shall be used to evaluate the fidelity of the large dynamic range in the paleointensity record obtained from the Black Sea sediments. For re-sedimentation sample

preparation, over the days of a week, small amounts of a diluted slurry are being successively injected into standard paleomagnetic plastic boxes. The boxes are left open in order to achieve compaction by partial drying. For analyses, acquired magnetizations are stepwise demagnetized and imparted anhysteretic and isothermal remanent magnetizations are used for normalizing. The time consuming re-sedimentation experiments (one data point per week) are still going on and are particularly focusing on remanence acquisition at low field intensities. The preliminary results already indicate a clear linear relationship between the field intensity set during deposition and the normalized magnetizations obtained by the samples in the field range from 2 to 130 μT. Thus, these experiments seem to verify the very low field intensities during the geomagnetic excursions investigated by this doctoral thesis.

Bibliography

Allen, R.E., 2002. Role of diffusion-precipitation reactions in authigenic pyritization. Chem. Geol. 182, 461–472. doi:10.1016/S0009-2541(01)00334-5

Andersen, K.K., Svensson, A., Rasmussen, S.O., Steffensen, J.P., Johnsen, S.J., Bigler, M., Röthlisberger, R., Ruth, U., Siggaard-Andersen, M.-L., Dahl-Jensen, D., Vinther, B.M., Clausen, H.B., 2006. The Greenland Ice Core Chronology 2005, 15–42 ka. Part 1: constructing the time scale. Quat. Sci. Rev. 25, 3246-3257.

Badertscher, S., Fleitmann, D., Cheng, H., Edwards, R.L., Gokturk, O.M., Zumbuhl, a., Leuenberger, M., Tuysuz, O., 2011. Pleistocene water intrusions from the Mediterranean and Caspian Seas into the Black Sea. Nat. Geosci. 4, 236–239. doi:10.1038/ngeo1106

Bahr, A., Arz, H.W., Lamy, F., Wefer, G., 2006. Late glacial to Holocene paleoenvironmental evolution of the Black Sea, reconstructed with stable oxygen isotope records obtained on ostracod shells. Earth Planet. Sci. Lett. 241, 863–875. doi:10.1016/j.epsl.2005.10.036

Bahr, A., Lamy, F., Arz, H., Kuhlmann, H., Wefer, G., 2005. Late glacial to Holocene climate and sedimentation history in the NW Black Sea. Mar. Geol. 214, 309–322. doi:10.1016/j.margeo.2004.11.013

Bahr, A., Lamy, F., Arz, H.W., Major, C., Kwiecien, O., Wefer, G., 2008. Abrupt changes of temperature and water chemistry in the late Pleistocene and early Holocene Black Sea. Geochemistry, Geophys. Geosystems 9. doi:10.1029/2007GC001683

Barton, C.E., McElhinny, M.W., Edwards, D.J., 1980. Laboratory studies of depositional DRM. Geophys. J. R. Astron. Soc. 61, 355-377.

Beer, J., Muscheler, R., Wagner, G., Laj, C., Kissel, C., Kubik, P.W., Synal, H.-A., 2002. Cosmogenic nuclides during Isotope Stages 2 and 3. Quat. Sci. Rev. 21, 1129-1139.

Ben-yosef, E., Millman, M., Shaar, R., Tauxe, L., Lipschits, O., 2017. Six centuries of geomagnetic intensity variations recorded by royal Judean stamped jar handles 114, 2160–2165. doi:10.1073/pnas.1615797114

Benson, L., Liddicoat, J., Smoot, J., Sarna-Wojcicki, A., Negrini, R., Lund, S., 2003. Age of the Mono Lake excursion and associated tephra. Quat. Sci. Rev. 22, 135–140. doi:10.1016/S0277-3791(02)00249-4

Bleil, U., Gard, G., 1989. Chronology and correlation of Quaternary magnetostratigraphy and nannofossil biostratigraphy in Norwegian-Greenland Sea sediments. Geol. Rundschau 78, 1173-1187.

Blockley, S.P.E., Bourne, A.J., Brauer, A., Davies, S.M., Hardiman, M., Harding, P.R., Lane, C.S., MacLeod, A., Matthews, I.P., Pyne-O'Donnell, S.D.F., Rasmussen, S.O., Wulf, S., Zanchetta, G., 2014. Tephrochronology and the extended intimate (integration of ice-core, marine and terrestrial records) event stratigraphy 8-128 ka b2k. Quat. Sci. Rev. 106, 88-100.

Bonhommet, N., Babkine, J., 1967. Sur la présence d'aimantation inversée dans la Chaîne des Puys. C.R. Acad. Sc. Paris 264, 92-94.

Bourne, M., Mac Niocaill, C., Thomas, A.L., Knudsen, M.F., Henderson, G.M., 2012. Rapid directional changes associated with a 6.5kyr-long Blake geomagnetic excursion at the Blake-Bahama Outer Ridge. Earth Planet. Sci. Lett. 333–334, 21–34. doi:10.1016/j.epsl.2012.04.017

Bowles, J., Gee, J., Hildebrand, J., Tauxe, L., 2002. Archaeomagnetic intensity results from California and Ecuador: Evaluation of regional data. Earth Planet. Sci. Lett. 203, 967–981. doi:10.1016/S0012-821X(02)00927-5

Brandt, U., Nowaczyk, N.R., Ramrath, A., Brauer, A., Mingram, J., Wulf, S., Negendank, J.F.W., 1999. Palaeomagnetism of Holocene and late pleistocene sediments from Lago di Mezzano and Lago Grande di Monticchio (Italy): Initial results. Quat. Sci. Rev. 18, 961–976. doi:10.1016/S0277-3791(99)00008-6

Brown, M.C., Donadini, F., Korte, M., Nilsson, A., Korhonen, K., Lodge, A., Lengyel, S.N., Constable, C.G., 2015. GEOMAGIA50.v3: 1. general structure and modifications to the archeological and volcanic database. Earth, Planets Sp. 67, 83. doi:10.1186/s40623-015-0232-0

Cai, S., Tauxe, L., Deng, C., Qin, H., Pan, Y., Jin, G., Chen, X., Chen, W., Xie, F., Zhu, R., 2016. New archaeomagnetic direction results from China and their constraints on palaeosecular variation of the geomagnetic field in Eastern Asia. Geophys. J. Int. doi:10.1093/gji/ggw351

Cassata, W.S., Singer, B.S., Cassidy, J., 2008. Laschamp and Mono Lake geomagnetic excursions recorded in New Zealand. Earth Planet. Sci. Lett. 268, 76–88. doi:10.1016/j.epsl.2008.01.009

Chang, L., Heslop, D., Roberts, A.P., Rey, D., Mohamed, K.J., 2016a. Discrimination of biogenic and detrital magnetite through a double Verwey transition temperature. J. Geophys. Res. B Solid Earth 121, 3–14. doi:10.1002/2015JB012485

Chang, L., Roberts, A.P., Heslop, D., Hayashida, A., Li, J., Zhao, X., Tian, W., Huang, Q., 2016b. Widespread occurrence of silicate-hosted magnetic mineral inclusions in marine sediments and their contribution to paleomagnetic recording. J. Geophys. Res. Solid Earth 121, 8415–8431. doi:10.1002/2016JB013109

Channell, J.E.T., 2006. Late Brunhes polarity excursions (Mono Lake, Laschamp, Iceland Basin and Pringle Falls) recorded at ODP Site 919 (Irminger Basin). Earth Planet. Sci. Lett. 244, 378–393. doi:10.1016/j.epsl.2006.01.021

Channell, J.E.T., 2014. The Iceland Basin excursion: Age, duration, and excursion field geometry. Geochemistry, Geophys. Geosystems 15, 4920–4935. doi:10.1002/2014GC005564

Channell, J.E.T., Harrison, R.J., Lascu, I., McCave, I.N., Hibbert, F.D., Austin, W.E.N., 2016. Magnetic record of deglaciation using FORC-PCA, sortable-silt grain size, and magnetic excursion at 26 ka, from the Rockall Trough (NE Atlantic). Geochemistry, Geophys. Geosystems 17, 1823–1841. doi:10.1002/2016GC006300

Channell, J.E.T., Hodell, D. a., Lehman, B., 1997. Relative geomagnetic paleointensity and δ18O at ODP Site 983 (Gardar Drift, North Atlantic) since 350 ka. Earth Planet. Sci. Lett. 153, 103–118. doi:10.1016/S0012-821X(97)00164-7

Channell, J.E.T., Hodell, D.A., Crowhurst, S.J., Skinner, L.C., Muscheler, R., 2018. Relative paleointensity (RPI) in the latest Pleistocene (10 e 45 ka) and implications for deglacial atmospheric radiocarbon. Quat. Sci. Rev. 191, 57–72. doi:10.1016/j.quascirev.2018.05.007

Channell, J.E.T., Hodell, D.A., Curtis, J.H., 2012. ODP Site 1063 (Bermuda Rise) revisited: Oxygen isotopes, excursions and paleointensity in the Brunhes Chron. Geochemistry, Geophys. Geosystems 13, 1–27. doi:10.1029/2011GC003897

Channell, J.E.T., Hodell, D.A., Lehman, B., 1997. Relative geomagnetic paleointensity and d18O at ODP Site 983 (Gardar Drift, North Atlantic) since 350 ka. Earth Planet. Sci. Lett. 153, 103-118.

Channell, J.E.T., Vázquez Riveiros, N., Gottschalk, J., Waelbroeck, C., Skinner, L.C., 2017. Age and duration of Laschamp and Iceland Basin geomagnetic excursions in the South Atlantic Ocean. Quat. Sci. Rev. 167, 1–13. doi:10.1016/j.quascirev.2017.04.020

Channell, J.E.T., Xuan, C., Hodell, D.A., 2009. Stacking paleointensity and oxygen isotope data for the last 1.5 Myr (PISO-1500). Earth Planet. Sci. Lett. 283, 14–23. doi:10.1016/j.epsl.2009.03.012

Chmeleff, J., von Blanckenburg, F., Kossert, K., Jakob, D., 2010. Determination of the 10Be half-life by multicollector ICP-MS and liquid scintillation counting. Nucl. Instr. Meth. Phys. Res. B 263, 192-199, doi: 10.1016/j.nimb.2009.09.012.

Clark, H.C., Kennett, J.P., 1973. Paleomagnetic excursion recorded in latest Pleistocene deep-sea sediments, Gulf of Mexico. Earth Planet. Sci. Lett. 19, 267–274. doi:10.1016/0012-821X(73)90127-1

Coe, R.S., Grommé, S., Mankinen, E.A., 1978. Geomagnetic paleointensities from radiocarbon-dated lava flows on Hawaii and the question of the Pacific nondipole low. J. Geophys. Res. 83, 1740–1756. doi:10.1029/JB083iB04p01740

Constantinescu, A.M., Toucanne, S., Dennielou, B., Jorry, S.J., Mulder, T., Lericolais, G., 2015. Evolution of the danube deep-sea fan since the last glacial maximum: New insights into Black Sea water-level fluctuations. Mar. Geol. 367, 50–68. doi:10.1016/j.margeo.2015.05.007

Croudace, I.W., Rindby, A., Rothwell, R.G., 2006. ITRAX: description and evaluation of a new multi-function X-ray core scanner. Geol. Soc. London, Spec. Publ. 267, 51–63. doi:10.1144/GSL.SP.2006.267.01.04

Cullen, V.L., Smith, V.C., Arz, H.W., 2014. The detailed tephrostratigraphy of a core from the south-east Black Sea spanning the last ~60 ka. J. Quat. Sci. 29, 675–690. doi:10.1002/jqs.2739

Dansgaard, W., Johnsen, S.J., Clausen, H.B., Dahl-Jensen, D., Gundestrup, N.S., Hammer, C.U., Hvidberg, C.S., Steffensen, J.P., Sveinbjörnsdottir, A.E., Jouzel, J., Bond, G., 1993. Evidence for general instability of past climate from a 250-kyr ice-core record. Nature 364, 218–220. doi:10.1038/364218a0

De Vivo, B., Rolandi, G., Gans, P.B., Calvert, A., Bohrson, W.A., Spera, F.J., Belkin, H.E., 2001. New constraints on the pyroclastic eruptive history of the Campanian volcanic Plain (Italy). Mineral. Petrol. 73, 47–65. doi:10.1007/s007100170010

Demory, F., Nowaczyk, N.R., Witt, A., Oberhänsli, H., 2005a. High-resolution magnetostratigraphy of late quaternary sediments from Lake Baikal, Siberia: timing of intracontinental paleoclimatic responses. Glob. Planet. Change 46, 167–186. doi:10.1016/j.gloplacha.2004.09.016

Demory, F., Oberhänsli, H., Nowaczyk, N.R., Gottschalk, M., Wirth, R., Naumann, R., 2005b. Detrital input and early diagenesis in sediments from Lake Baikal revealed by rock magnetism. Glob. Planet. Change 46, 145–166. doi:10.1016/j.gloplacha.2004.11.010

Denham, C.R., Cox, A., 1971. Evidence that the Laschamp polarity event did not occur 13 300–30 400 years ago. Earth Planet. Sci. Lett. 13, 181–190. doi:10.1016/0012-821X(71)90122-1

Dunlop, D.J., Ozdemir, O., 2000. Effect of grain size and domain state on thermal demagnetization tails. Geophys. Res. Lett. 27, 1311–1314. doi:10.1029/1999GL008461

Dunlop, D.J., Waddington, E.D., 1975. The field dependence of thermoremanent magnetization in igneous rocks. Earth Planet. Sci. Lett. 25, 11–25. doi:10.1016/0012-821X(75)90205-8

Eckert, S., Brumsack, H.J., Severmann, S., Schnetger, B., März, C., Fröllje, H., 2013. Establishment of euxinic conditions in the Holocene Black Sea. Geology 41, 431–434. doi:10.1130/G33826.1

Fabbro, G.N., Druitt, T.H., Scaillet, S., 2013. Evolution of the crustal magma plumbing system during the build-up to the 22-ka caldera-forming eruption of Santorini (Greece). Bull. Volcanol. 75, 767. doi:10.1007/s00445-013-0767-5

Fisher, R., 1953. Dispersion on a Sphere. Proc. R. Soc. A Math. Phys. Eng. Sci. 217, 295–305. doi:10.1098/rspa.1953.0064

Gillot, P.Y., Labeyrie, J., Laj, C., Valladas, G., Guérin, G., Poupeau, G., Delibrias, G., 1979. Age of the Laschamp paleomagnetic excursion revisited. Earth Planet. Sci. Lett. 42, 444–450. doi:10.1016/0012-821X(79)90053-0

Gonzalez, S., Sherwood, G., Bohnel, H., Schnepp, E., 1997. Palaeosecular variation in Central Mexico over the last 30 000 years : the record from lavas. Geophys. J. Int. 130, 201–219. doi:10.1111/j.1365-246X.1997.tb00999.x

Gubbins, D. & Bloxham, J. 1987. Morphology of the geomagnetic field and implications for the geodynamo. Nature 325, 509-511.

Gubbins, D., 2008. Geomagnetic reversals. Nature 452, 165-167.

Guillou, H., Singer, B.S., Laj, C., Kissel, C., Scaillet, S., Jicha, B.R., 2004. On the age of the Laschamp geomagnetic excursion. Earth Planet. Sci. Lett. 227, 331–343. doi:10.1016/j.epsl.2004.09.018

Guyodo, Y., Valet, J.-P., 1996. Relative variations in geomagnetic intensity from sedimentary records: the past 200,000 years. Earth Planet. Sci. Lett. 143, 23–36. doi:10.1016/0012-821X(96)00121-5

Hagstrum, J.T., Champion, D.E., 2002. A Holocene paleosecular variation record from 14 C-dated volcanic rocks in western North America. J. Geophys. Res. Solid Earth 107, EPM 8-1-EPM 8-14. doi:10.1029/2001JB000524

Herrero-Bervera, E., Fucugauchi, J.U., Del Pozzo, A.L.M., Böhnel, H., Guerrero, J., 1986. Normal amplitude brunhes paleosecular variation at low-latitudes: A paleomagnetic record from the Trans-Mexican Volcanic Belt. Geophys. Res. Lett. 13, 1442–1445. doi:10.1029/GL013i013p01442

Hoffman, K.A., Singer, B.S., 2004. Regionally Recurrent Paleomagnetic Transitional Fields and Mantle Processes, in: Geophysical Monograph Series. pp. 233–243. doi:10.1029/145GM17

Höflmayer, F., 2012. The Date of the Minoan Santorini Eruption: Quantifying the “Offset.” Radiocarbon 54, 435–448. doi:10.1017/S0033822200047196

Johnson, C.L., McFadden, P., 2015. The Time-Averaged Field and Paleosecular Variation, in: Treatise on Geophysics: Second Edition. doi:10.1016/B978-0-444-53802-4.00105-6

Johnson, E.A., Murphy, T., Torreson, O.W., 1948. Pre-history of the Earth's magnetic field. Terrestrial Magnetism and Atmospheric Electricity, 53(4), 349-372.

Kent, D. V., Hemming, S.R., Turrin, B.D., 2002. Laschamp Excursion at Mono Lake? Earth Planet. Sci. Lett. 197, 151–164. doi:10.1016/S0012-821X(02)00474-0

Kirschvink, J.L., 1980. The least-squares line and plane and the analysis of palaeomagnetic data. Geophys. J. Int. 62, 699–718. doi:10.1111/j.1365-246X.1980.tb02601.x

Kissel, C., Guillou, H., Laj, C., Carracedo, J.C.C., Nomade, S., Perez-Torrado, F., Wandres, C., 2011. The Mono Lake excursion recorded in phonolitic lavas from Tenerife (Canary Islands): Paleomagnetic analyses and coupled K/Ar and Ar/Ar dating. Phys. Earth Planet. Inter. 187, 232–244. doi:10.1016/j.pepi.2011.04.014

Knudsen, M.F., Mac Niocaill, C., Henderson, G.M., 2006. High-resolution data of the Iceland Basin geomagnetic excursion from ODP sites 1063 and 983: Existence of intense flux patches during the excursion? Earth Planet. Sci. Lett. 251, 18–32. doi:10.1016/j.epsl.2006.08.016

Kono, M., 2007. Geomagnetism in Perspective, in: Treatise on Geophysics. doi:10.1016/B978-044452748-6.00086-9

Korschinek, G., Bergmaier, A., Faestermann, T., Gerstmann, U.C., Knie, K., Rugel, G., Wallner, A., Dillmann, I., Dollinger, G., Lierse von Gostomski, Ch., Kossert, K., Maiti, M., Poutivtsev, M., Remmert, A., 2010. A new value for the half-life of 10Be by heavy-ion elastic recoil detection and lquid scintillation counting. Nucl. Instr. Meth. Phys. Res. B 268, 187-191, doi: 10.1016/j.nimb.2009.09.020.

Krs, M., Krsová, M., Pruner, P., Zeman, A., Novák, F., Jansa, J., 1990. A petromagnetic study of Miocene rocks bearing micro-organic material and the magnetic mineral greigite (Sokolov and Cheb basins, Czechoslovakia). Phys. Earth Planet. Inter. doi:10.1016/0031-9201(90)90064-5

Kwiecien, O., Arz, H.W., Lamy, F., Wulf, S., Bahr, A., Röhl, U., Haug, G.H., 2008. Estimated reservoir ages of the black sea since the last glacial. Radiocarbon 50, 99–118. doi:10.1017/S0033822200043393

Laj, C., Channell, J.E.T., 2015. Geomagnetic Excursions, in: Treatise on Geophysics: Second Edition. doi:10.1016/B978-0-444-53802-4.00104-4

Laj, C., Guillou, H., Kissel, C., 2014. Dynamics of the earth magnetic field in the 10 – 75 kyr period comprising the Laschamp and Mono Lake excursions : New results from the French Chaîne des Puys in a global perspective. Earth Planet. Sci. Lett. 387, 184–197. doi:10.1016/j.epsl.2013.11.031

Laj, C., Kissel, C., Beer, J., 2004. High resolution global paleointensity stack since 75 kyr (GLOPIS-75) calibrated to absolute values. Geophys. Monogr. Ser. 145, 255–265. doi:10.1029/145GM19

Laj, C., Kissel, C., Mazaud, A., Channell, J.E.T., Beer, J., 2000. North Atlantic palaeointensity stack since 75ka (NAPIS-75) and the duration of the Laschamp event. Philos. Trans. R. Soc. A Math. Phys. Eng. Sci. 358, 1009–1025. doi:10.1098/rsta.2000.0571

Laj, C., Kissel, C., Roberts, A.P., 2006. Geomagnetic field behavior during the Iceland Basin and Laschamp geomagnetic excursions: A simple transitional field geometry? Geochemistry, Geophys. Geosystems 7, 1–17. doi:10.1029/2005GC001122

Laj, C., Kissel, C., Scao, V., Beer, J., Thomas, D.M., Guillou, H., Muscheler, R., Wagner, G., 2002. Geomagnetic intensity and inclination variations at Hawaii for the past 98 kyr from core SOH-4 (Big Island): A new study and a comparison with existing contemporary data, Physics of the Earth and Planetary Interiors. doi:10.1016/S0031-9201(01)00291-6

Lal. D. (1988) Theoretically expected variations in the terrestrial cosmic-ray production rates of isotopes. In: In: Castagnoli, G.C. (Ed.), Solar-terrestrial relationships and the earth environment in the last millenia. pp. 215-233.

Lamy, F., Arz, H.W., Bond, G.C., Bahr, A., Pätzold, J., 2006. Multicentennial-scale hydrological changes in the Black Sea and northern Red Sea during the Holocene and the Arctic/North Atlantic Oscillation. Paleoceanography 21, n/a-n/a. doi:10.1029/2005PA001184

Lanza, R., Zanella, E., 2003. Paleomagnetic secular variation at Vulcano (Aeolian Islands) during the last 135 kyr. Earth Planet. Sci. Lett. 213, 321–336. doi:10.1016/S0012-821X(03)00326-1

Leonard, G.S., Calvert, A.T., Hopkins, J.L., Wilson, C.J.N., Smid, E.R., Lindsay, J.M., Champion, D.E., 2017. High-precision 40Ar/39Ar dating of Quaternary basalts from Auckland Volcanic Field, New Zealand, with implications for eruption rates and paleomagnetic correlations. J. Volcanol. Geotherm. Res. 343, 60–74. doi:10.1016/j.jvolgeores.2017.05.033

Leveson D J. Orbicular rocks: a review[J]. Geological Society of America Bulletin, 1966, 77(4): 409-426.

Liddicoat, J.C., Coe, R.S., 1979. Mono Lake geomagnetic excursion. J. Geophys. Res. Solid Earth 84, 261–271. doi:10.1029/JB084iB01p00261

Lisé-Pronovost, A., St-Onge, G., Gogorza, C., Haberzettl, T., Preda, M., Kliem, P., Francus, P., Zolitschka, B., 2013. High-resolution paleomagnetic secular variations and relative paleointensity since the Late Pleistocene in southern South America. Quat. Sci. Rev. 71, 91–108. doi:10.1016/j.quascirev.2012.05.012

Liu, J., Nowaczyk, N.R., Frank, U., Arz, H.W., 2018. A 20–15 ka high-resolution paleomagnetic secular variation record from Black Sea sediments – no evidence for the 'Hilina Pali excursion'? Earth Planet. Sci. Lett. 492. doi:10.1016/j.epsl.2018.04.014

Liu, J., Nowaczyk, N., Frank, U., Arz, H., 2019. Geomagnetic paleosecular variation record spanning from 40 to 20 ka – implications for the Mono Lake excursion from Black Sea sediments. Earth Planet. Sci. Lett. 509, 114–124. doi:10.1016/j.epsl.2018.12.029

Liu, J. (sumb), Nowaczyk, N.R., Frank, U., Arz, H.W., 2018. Full-vector paleosecular variation from 14.5 ka back to 68.9 ka as reconstructed from Black Sea sediments. Quaternary Science Reviews. (under review)

Liu, Q., Roberts, A.P., Larrasoaña, J.C., Banerjee, S.K., Guyodo, Y., Tauxe, L., Oldfield, F., 2012. Environmental magnetism: Principles and applications. Rev. Geophys. 50, RG4002. doi:10.1029/2012RG000393

Løvlie, R., 1989. Palaeomagnetic excursions during the last interglacial/ glacial cycle: A synthesis. Quat. Int. 3–4, 5–11. doi:10.1016/1040-6182(89)90068-2

Lund, S., Benson, L., Negrini, R., Liddicoat, J., Mensing, S., 2017. A full-vector paleomagnetic secular variation record (PSV) from Pyramid Lake (Nevada) from 47–17 ka: Evidence for the successive Mono Lake and Laschamp Excursions. Earth Planet. Sci. Lett. 458, 120–129. doi:10.1016/j.epsl.2016.09.036

Lund, S., Stoner, J.S., Channell, J.E.T., Acton, G., 2006. A summary of Brunhes paleomagnetic field variability recorded in Ocean Drilling Program cores. Phys. Earth Planet. Inter. 156, 194–204. doi:10.1016/j.pepi.2005.10.009

Lund, S.P., 1996. A comparison of Holocene paleomagnetic secular variation records from North America. J. Geophys. Res. 101, 8007-8024.

Lund, S.P., Liddicoat, J.C., Lajoie, K.R., Henyey, T.L., Robinson, S.W., 1988. Paleomagnetic evidence for long-term (10 4 year) Memory and periodic behavior in the Earth's core dynamo process. Geophys. Res. Lett. 15, 1101–1104. doi:10.1029/GL015i010p01101

Lund, S.P., Stoner, J., Channell, J., Lamy, F., 2007. Detailed paleomagnetic and rock magnetic variability within three high-resolution study intervals from Site 1233. Proc. Ocean Drill. Program, 202 Sci. Results 202. doi:10.2973/odp.proc.sr.202.212.2007

Lund, S.P., Stoner, J., Lamy, F., 2006. Late Quaternary paleomagnetic secular variation and chronostratigraphy from ODP Sites 1233 and 1234 202. doi:10.2973/odp.proc.sr.202.208.2006

Major, C.O., Goldstein, S.L., Ryan, W.B.F., Lericolais, G., Piotrowski, A.M., Hajdas, I., 2006. The co-evolution of Black Sea level and composition through the last deglaciation and its paleoclimatic significance. Quat. Sci. Rev. 25, 2031–2047. doi:10.1016/j.quascirev.2006.01.032

Masarik, J., Beer, J., 1999. Simulation of particle fluxes and cosmogenic nuclide production in the Earth ' s atmosphere. J. Geophys. Res. 104, 12099–12111. doi:10.1029/2008JD010557

Maus, S., Silva, L., Hulot, G., 2008. Can core-surface flow models be used to improve the forecast of the Earth's main magnetic field? J. Geophys. Res., 113, B08102, doi:10.1029/2007JB005199.

Ménabréaz, L., Bourls, D.L., Thouveny, N., 2012. Amplitude and timing of the Laschamp geomagnetic dipole low from the global atmospheric 10Be overproduction: Contribution of authigenic 10Be/9Be ratios in west equatorial Pacific sediments. J. Geophys. Res. Solid Earth 117, 1–13. doi:10.1029/2012JB009256

Merrill, R.T., McFadden, P.L., 1999. Geomagnetic polarity transitions. Rev. Geophys. 37, 201–226. doi:10.1029/1998RG900004

Muscheler, R., Beer, J., Kubik, P.W., Synal, H.A., 2005. Geomagnetic field intensity during the last 60,000 years based on10Be and36Cl from the Summit ice cores and14C. Quat. Sci. Rev. 24, 1849–1860. doi:10.1016/j.quascirev.2005.01.012

Muscheler, R., Beer, J., Wagner, G., Laj, C., Kissel, C., Raisbeck, G.M., Yiou, F., Kubik, P.W., 2004. Changes in the carbon cycle during the last deglaciation as indicated by the comparison of10Be and14C records. Earth Planet. Sci. Lett. 219, 325–340. doi:10.1016/S0012-821X(03)00722-2

Negrini, R.M., McCuan, D.T., Horton, R.A., Lopez, J.D., Cassata, W.S., Channell, J.E.T., Verosub, K.L., Knott, J.R., Coe, R.S., Liddicoat, J.C., Lund, S.P., Benson, L. V, Sarna-Wojcicki, A.M., 2014. Nongeocentric axial dipole field behavior during the Mono Lake excursion. J. Geophys. Res. Solid Earth 119, 2567–2581. doi:10.1002/2013JB010846

Neretin, L.N., Bottcher, M.E., Jorgensen, B.B., Volkov, I.I., Luschen, H., Hilgenfeldt, K., 2004. Pyritization processes and greigite formaion in the advancing sulphidisation front in the Upper Pleistocene sediments of the Black Sea. Geochim. Cosmochim. Acta 68, 2081–2093. doi:10.1016/S0016-7037(00)00450-2

NGRIP, 2004. High-resolution record of Northern Hemisphere climate extending into the last interglacial period. Nature 431, 147–151. doi:10.1038/nature02805

Nowaczyk, N.R., 2001. Logging of Magnetic Susceptibility, in: Last, W.M., Smol, J.P. (Eds.), Tracking Environmental Change Using Lake Sediments. Kluwer Academic Publishers, Dordrecht, pp. 155–170. doi:10.1007/0-306-47669-X_8

Nowaczyk, N.R., 2011. Dissolution of titanomagnetite and sulphidization in sediments from Lake Kinneret, Israel. Geophys. J. Int. 187, 34–44. doi:10.1111/j.1365-246X.2011.05120.x

Nowaczyk, N.R., Antonow, M., Knies, J., Spielhagen, R.F., 2003. Further rock magnetic and chronostratigraphic results on reversal excursions during the last 50 ka as derived from northern high latitudes and discrepancies in precise AMS 14 C dating. Geophys. J. Int. 155, 1065–1080. doi:10.1111/j.1365-246X.2003.02115.x

Nowaczyk, N.R., Arz, H.W., Frank, U., Kind, J., Plessen, B., 2012. Dynamics of the Laschamp geomagnetic excursion from Black Sea sediments. Earth Planet. Sci. Lett. 351–352, 54–69. doi:10.1016/j.epsl.2012.06.050

Nowaczyk, N.R., Baumann, M. 1992. Combined high-resolution magnetostratigraphy and nanofossil biostratigraphy for Late Quaternary Arctic Ocean sediments, Deep-Sea Res., 39, 567–601.

Nowaczyk, N.R., Frank, U., Kind, J., Arz, H.W., 2013. A high-resolution paleointensity stack of the past 14 to 68 ka from black sea sediments. Earth Planet. Sci. Lett. 384, 1–16. doi:10.1016/j.epsl.2013.09.028

Nowaczyk, N.R., Frederichs, T.W., 1999. Geomagnetic events and relative paleointensity variations during the last 300 ka as recorded in Kolbeinsey Ridge Sediments, Iceland Sea—indication for a strongly variable geomagnetic field, Int. J. Earth Sci. 88, 116–131.

Nowaczyk, N.R., Frederichs, T.W., Eisenhauer, A., Gard, G., 1994. Magnetostratigraphic Data From Late Quaternary Sediments From the Yermak Plateau, Arctic Ocean: Evidence For Four Geomagnetic Polarity Events Within the Last 170 Ka of the Brunhes Chron. Geophys. J. Int. 117, 453–471. doi:10.1111/j.1365-246X.1994.tb03944.x

Nowaczyk, N.R., Jiabo, L., Frank, U., Arz, H.W., 2018. A high-resolution paleosecular variation record from Black Sea sediments indicating fast directional changes associated with low field intensities during marine isotope stage (MIS) 4. Earth Planet. Sci. Lett. 484, 15–29. doi:10.1016/j.epsl.2017.12.009

Nowaczyk, N.R., Knies, J., 2000. Magnetostratigraphic results from the eastern Arctic Ocean: AMS 14C ages and relative palaeointensity data of the Mono Lake and Laschamp geomagnetic reversal excursions. Geophys. J. Int. 140, 185–197. doi:10.1046/j.1365-246X.2000.00001.x

Panovska, S., Constable, C.G., 2017. An activity index for geomagnetic paleosecular variation, excursions, and reversals. Geochemistry, Geophys. Geosystems 18, 1366–1375. doi:10.1002/2016GC006668

Panovska, S., Constable, C.G., Brown, M.C., 2018. Global and Regional Assessments of Paleosecular Variation Activity Over the Past 100 ka. Geochemistry, Geophys. Geosystems 19, 1559–1580. doi:10.1029/2017GC007271

Peck, J.A., King, J.W., Colman, S.M., Kravchinsky, V.A., 1996. An 84-kyr paleomagnetic record from the sediments of Lake Baikal, Siberia. J. Geophys. Res. Solid Earth 101, 11365–11385. doi:10.1029/96JB00328

Peters, C., Dekkers, M.J., 2003. Selected room temperature magnetic parameters as a function of mineralogy, concentration and grain size. Phys. Chem. Earth, Parts A/B/C 28, 659–667. doi:10.1016/S1474-7065(03)00120-7

Plenier, G., Valet, J.-P., Guérin, G., Lefèvre, J.-C., LeGoff, M., Carter-Stiglitz, B., 2007. Origin and age of the directions recorded during the Laschamp event in the Chaîne des Puys (France). Earth Planet. Sci. Lett. 259, 414–431. doi:10.1016/j.epsl.2007.04.039

Pressling, N., Laj, C., Kissel, C., Champion, D., Gubbins, D., 2006. Palaeomagnetic intensities from14C-dated lava flows on the Big Island, Hawaii: 0-21 kyr. Earth Planet. Sci. Lett. 247, 26–40. doi:10.1016/j.epsl.2006.04.026

Reitner, J., Peckmann, J., Blumenberg, M., Michaelis, W., Reimer, A., Thiel, V., 2005. Concretionary methane-seep carbonates and associated microbial communities in Black Sea sediments. Palaeogeogr. Palaeoclimatol. Palaeoecol. 227, 18–30. doi:10.1016/j.palaeo.2005.04.033

Roberts, A.P., 2008. Geomagnetic excursions: Knowns and unknowns. Geophys. Res. Lett. 35, L17307. doi:10.1029/2008GL034719

Roberts, A.P., 2015. Magnetic mineral diagenesis. Earth-Science Rev. 151, 1–47. doi:10.1016/j.earscirev.2015.09.010

Roberts, A.P., Chang, L., Rowan, C.J., Horng, C.-S., Florindo, F., 2011. Magnetic properties of sedimentary greigite (Fe3S4): An update. Rev. Geophys. 49, RG1002, doi:10.1029/2010RG000336

Roberts, A.P., Heslop, D., Zhao, X., Pike, C.R., 2014. Understanding fine magnetic particle systems through use of first-order reversal curve diagrams. Rev. Geophys. 52, 557–602, doi:10.1002/2014RG000462.

Roberts, A.P., Tauxe, L., Heslop, D., 2013. Magnetic paleointensity stratigraphy and high-resolution Quaternary geochronology: Successes and future challenges. Quat. Sci. Rev. 61, 1–16. doi:10.1016/j.quascirev.2012.10.036

Roberts, A.P., Turner, G.M., 1993. Minerals in Rapidly Deposited Marine Sediments ,. Earth Planet. Sci. Lett. 115, 257–273.

Roberts, A.P., Weaver, R., 2005. Multiple mechanisms of remagnetization involving sedimentary greigite (Fe3S4). Earth Planet. Sci. Lett. 231, 263–277. doi:10.1016/j.epsl.2004.11.024

Röhl, U., Abrams, L.J., 2000. High-resolution, downhole, and nondestructive core measurements from site 999 and 1001 in the Caribbean sea: application to the Late Paleocene thermal maximum. Procedings Ocean Drill. Program, Sci. Results 165, 191–203. doi:10.2973/odp.proc.sr.165.009.2000

Ron, H., Nowaczyk, N.R., Frank, U., Schwab, M.J., Naumann, R., Striewski, B., Agnon, A., 2007. Greigite detected as dominating remanence carrier in Late Pleistocene sediments, Lisan formation, from Lake Kinneret (Sea of Galilee), Israel. Geophys. J. Int. 170, 117–131. doi:10.1111/j.1365-246X.2007.03425.x

Roperch, P., Bonhommet, N., Levi, S., 1988. Paleointensity of the earth's magnetic field during the Laschamp excursion and its geomagnetic implications. Earth Planet. Sci. Lett. 88, 209–219. doi:10.1016/0012-821X(88)90058-1

Rowan, C.J., Roberts, A.P., Broadbent, T., 2009. Reductive diagenesis, magnetite dissolution, greigite growth and paleomagnetic smoothing in marine sediments: A new view. Earth Planet. Sci. Lett. 277, 223–235. doi:10.1016/j.epsl.2008.10.016

Shaar, R., Tauxe, L., Ron, H., Ebert, Y., Zuckerman, S., Finkelstein, I., Agnon, A., 2016. Large geomagnetic field anomalies revealed in Bronze to Iron Age archeomagnetic data from Tel Megiddo and Tel Hazor, Israel. Earth Planet. Sci. Lett. 442, 173–185. doi:10.1016/j.epsl.2016.02.038

Shao, J.-C., Fuller, M., Tanimoto, T., Dunn, J.R., Stone, D.B., 1999. Spherical harmonic analyses of paleomagnetic data: The time-averaged geomagnetic field for the past 5 Myr and the Brunhes-Matuyama reversal. J. Geophys. Res. 104, 5015-5030.

Shibuya, H., Cassidy, J., Smith, I.E.M., Itaya, T., 1992. A geomagnetic excursion in the Brunhes epoch recorded in New Zealand basalts. Earth Planet. Sci. Lett. 111, 41–48. doi:10.1016/0012-821X(92)90167-T

Shumilovskikh, L.S., Marret, F., Fleitmann, D., Arz, H.W., Nowaczyk, N., Behling, H., 2013. Eemian and Holocene sea-surface conditions in the southern Black Sea: Organic-walled dinoflagellate cyst record from core 22-GC3. Mar. Micropaleontol. 101, 146–160. doi:10.1016/j.marmicro.2013.02.001

Shumilovskikh, L.S., Tarasov, P., Arz, H.W., Fleitmann, D., Marret, F., Nowaczyk, N., Plessen, B., Schlütz, F., Behling, H., 2012. Vegetation and environmental dynamics in the southern Black Sea region since 18kyr BP derived from the marine core 22-GC3. Palaeogeogr. Palaeoclimatol. Palaeoecol. 337–338, 177–193. doi:10.1016/j.palaeo.2012.04.015

Simon, Q., St-Onge, G., Hillaire-Marcel, C., 2012. Late Quaternary chronostratigraphic framework of deep Baffin Bay glaciomarine sediments from high-resolution paleomagnetic data. Geochemistry, Geophys. Geosystems 13, 1–24. doi:10.1029/2012GC004272

Simon, Q., Thouveny, N., Bourlès, D.L., Valet, J.-P., Bassinot, F., Ménabreaz, L., Guillou, V., Choy, S., Beaufort, L., 2016. Authigenic 10Be/9Be ratio signatures of the cosmogenic nuclide production linked to geomagnetic dipole moment variation since the Brunhes/Matuyama boundary. J. Geophys. Res. Solid Earth, 121, 7716-7741, doi:10.1002/2016JB013335.

Singer, B.S., Jicha, B.R., He, H., Zhu, R., 2014. Geomagnetic field excursion recorded 17 ka at Tianchi Volcano, China: New 40 Ar/ 39 Ar age and significance. Geophys. Res. Lett. 41, 2794–2802. doi:10.1002/2014GL059439

Skinner, B.J., Erd, R.C., Grimaldi, F.S., 1964. Greigite, the thiospinel of iron: a new mineral. Am. Mineral. 49, 543-555.

Snowball, I., Zillen, L., Ojala, A., Saarinen, T., Sandgren, P., 2007. FENNOSTACK and FENNORPIS: Varve dated Holocene palaeomagnetic secular variation and relative palaeointensity stacks for Fennoscandia. Earth Planet. Sci. Lett. 255, 106-116.

Snowball, I.F., 1991. Magnetic hysteresis properties of greigite (Fe3S4) and a new occurrence in Holocene sediments from Swedish Lappland. Phys. Earth Planet. Inter. 68, 32–40. doi:10.1016/0031-9201(91)90004-2

Snowball, I.F., 1993. Geochemical control of magnetite dissolution in subarctic lake sediments and the implications for environmental magnetism. J. Quat. Sci. 8, 339–346. doi:10.1002/jqs.3390080405

Snowball, I.F., 1997. Gyroremanent magnetization and the magnetic properties of greigite-bearing clays in southern Sweden. Geophys. J. Int. 129, 624–636. doi:10.1111/j.1365-246X.1997.tb04498.x

Soulet, G., Delaygue, G., Vallet-Coulomb, C., Böttcher, M.E., Sonzogni, C., Lericolais, G., Bard, E., 2010. Glacial hydrologic conditions in the Black Sea reconstructed using geochemical pore water profiles. Earth Planet. Sci. Lett. 296, 57–66. doi:10.1016/j.epsl.2010.04.045

Soulet, G., Ménot, G., Bayon, G., Rostek, F., Ponzevera, E., Toucanne, S., Lericolais, G., Bard, E., 2013. Abrupt drainage cycles of the Fennoscandian Ice Sheet. Proc. Natl. Acad. Sci. 110, 6682–6687. doi:10.1073/pnas.1214676110

Spassov, S., Valet, J.-P., 2012. Detrital magnetizations from redeposition experiments of different natural sediments. Earth. Planet. Sci. Lett. 351-352, 147-352.

Stoner, J.., Laj, C., Channell, J.E.., Kissel, C., 2002. South Atlantic and North Atlantic geomagnetic paleointensity stacks (0–80ka): implications for inter-hemispheric correlation. Quat. Sci. Rev. 21, 1141–1151. doi:10.1016/S0277-3791(01)00136-6

Stoner, J.S., Channell, J.E.T., Hodell, D.A., Charles, C.D., 2003. A ∼580 kyr paleomagnetic record from the sub-Antarctic South Atlantic (Ocean Drilling Program Site 1089). J. Geophys. Res. Solid Earth 108, 1–19. doi:10.1029/2001JB001390

Svensson, A., Andersen, K.K., Bigler, M., Clausen, H.B., Dahl-Jensen, D., Davies, S.M., Johnsen, S.J., Muscheler, R., Parrenin, F., Rasmussen, S.O., Röthlisberger, R., Seierstad, I., Steffensen, J.P., Vinther, B.M., 2008. A 60 000 year Greenland stratigraphic ice core chronology. Clim. Past, Eur. Geosci. Union 4, 47–57. doi:10.5194/cp-4-47-2008

Svensson, A., Andersen, K.K., Bigler, M., Clausen, H.B., Dahl-Jensen, D., Davies, S.M., Johnsen, S.J., Muscheler, R., Rasmussen, S.O., Röthlisberger, R., Peder Steffensen, J., Vinther, B.M., 2006. The Greenland Ice Core Chronology 2005, 15-42 ka. Part 2: comparison to other records. Quat. Sci. Rev. 25, 3258–3267. doi:10.1016/j.quascirev.2006.08.003

Taha, A.A., Hanbury, A., 2015. An Efficient Algorithm for Calculating the Exact Hausdorff Distance. IEEE Trans. Pattern Anal. Mach. Intell. doi:10.1109/TPAMI.2015.2408351

Tanaka, H., Komuro, N., Turner, G.M., 2009. Palaeosecular variation for 0.1-21 Ka from the Okataina Volcanic Centre, New Zealand. Earth Planets Sp. 61, 213–225. doi:10.1186/BF03352901

Tanaka, H., Otsuka, A., Tachibana, T., Kono, M., 1994. Paleointensities for 10-22 ka from volcanic-rocks in Japan and new- zealand. Earth Planet. Sci. Lett. 122, 29–42.

Tauxe, L., 1993. Sedimentary records of relative paleointensity of the geomagnetic field: Theory and practice. Rev. Geophys. 31, 319. doi:10.1029/93RG01771

Tauxe, L., Steindorf, J.L., Harris, A., 2006. Depositional remanent magnetization: Toward an improved theoretical and experimental foundation. Earth Planet. Sci. Lett. 244, 515–529. doi:10.1016/j.epsl.2006.02.003

Tauxe, L., Yamazaki, T., 2007. Paleointensities, in: Treatise on Geophysics. doi:10.1016/B978-044452748-6.00098-5

Teanby, N., Laj, C., Gubbins, D., Pringle, M., 2002. A detailed palaeointensity and inclination record from drill core SOH1 on Hawaii. Phys. Earth Planet. Inter. 131, 101–140. doi:10.1016/S0031-9201(02)00032-8

Valet, J.P., Meynadier, L., Guyodo, Y., 2005. Geomagnetic dipole strength and reversal rate over the past two million years. Nature 435, 802–805. doi:10.1038/nature03674

Valet, J.P., Plenier, G., Herrero-Bervera, E., 2008. Geomagnetic excursions reflect an aborted polarity state. Earth Planet. Sci. Lett. 274, 472–478. doi:10.1016/j.epsl.2008.07.056

Valet, J.P., Tric, E., Herrero-Bervera, E., Meynadier, L., Lockwood, J.P., 1998. Absolute paleointensity from Hawaiian lavas younger than 35 ka. Earth Planet. Sci. Lett. 161, 19–32. doi:10.1016/S0012-821X(98)00133-2

Wagner, G., Laj, C., Beer, J., Kissel, C., Muscheler, R., Masarik, J., Synal, H.A., 2001. Reconstruction of the paleoaccumulation rate of central Greenland during the last 75 kyr using the cosmogenic radionuclides36Cl and10Be and geomagnetic field intensity data. Earth Planet. Sci. Lett. 193, 515–521. doi:10.1016/S0012-821X(01)00504-0

Weeks, R.J., Laj, C., Endignoux, L., Mazaud, A., Labeyrie, L., Roberts, A.P., Kissel, C., Blanchard, E., 1995. Normalised natural remanent magnetisation intensity during the last 240 000 years in piston cores from the central North Atlantic Ocean: geomagnetic field intensity or environmental signal? Phys. Earth Planet. Inter. 87, 213–229. doi:10.1016/0031-9201(94)02966-F

Wegwerth, A., Dellwig, O., Kaiser, J., Ménot, G., Bard, E., Shumilovskikh, L., Schnetger, B., Kleinhanns, I.C., Wille, M., Arz, H.W., 2014. Meltwater events and the Mediterranean reconnection at the Saalian-Eemian transition in the Black Sea. Earth Planet. Sci. Lett. 404, 124–135. doi:10.1016/j.epsl.2014.07.030

Wegwerth, A., Ganopolski, A., Ménot, G., Kaiser, J., Dellwig, O., Bard, E., Lamy, F., Arz, H.W., 2015. Black Sea temperature response to glacial millennial-scale climate variability. Geophys. Res. Lett. 42, 8147–8154. doi:10.1002/2015GL065499

Wegwerth, A., Kaiser, J., Dellwig, O., Shumilovskikh, L.S., Nowaczyk, N.R., Arz, H.W., 2016. Northern hemisphere climate control on the environmental dynamics in the glacial Black Sea "Lake." Quat. Sci. Rev. 135, 41–53. doi:10.1016/j.quascirev.2016.01.016

Wilkin, R.T., Arthur, M., Dean, W., 1997. History of water-column anoxia in the Black Sea indicated by pyrite framboid size distributions. Earth Planet. Sci. Lett. 148, 517–525. doi:10.1016/S0012-821X(97)00053-8

Wilkin, R.T., Arthur, M.A., 2001. Variations in pyrite texture, sulfur isotope composition, and iron systematics in the black sea: Evidence for late pleistocene to holocene excursions of the O2-H2S redox transition. Geochim. Cosmochim. Acta 65, 1399–1416. doi:10.1016/S0016-7037(01)00552-X

Wilkin, R.T., Barnes, H.L., Brantley, S.L., 1996. The size distribution of framboidal pyrite in modern sediments: An indicator of redox conditions. Geochim. Cosmochim. Acta 60, 3897–3912. doi:10.1016/0016-7037(96)00209-8

Wirth, R., 2004. Focused Ion Beam (FIB): A novel technology for advanced application of micro- and nanoanalysis in geosciences and applied mineralogy. Eur. J. Mineral. 16, 863–876. doi:10.1127/0935-1221/2004/0016-0863

Wirth, R., 2009. Focused Ion Beam (FIB) combined with SEM and TEM: Advanced analytical tools for studies of chemical composition, microstructure and crystal structure in geomaterials on a nanometre scale. Chem. Geol. 261, 217–229. doi:10.1016/j.chemgeo.2008.05.019

Xuan, C., Channell, J.E.T., Polyak, L., Darby, D.A., 2012. Paleomagnetism of Quaternary sediments from Lomonosov Ridge and Yermak Plateau: Implications for age models in the Arctic Ocean. Quat. Sci. Rev. 32, 48–63. doi:10.1016/j.quascirev.2011.11.015

Yamazaki, T., 2008. Magnetostatic interactions in deep-sea sediments inferred from first-order reversal curve diagrams: Implications for relative paleointensity normalization. Geochemistry, Geophys. Geosystems 9. doi:10.1029/2007GC001797

Yamazaki, T., 2009. Environmental magnetism of Pleistocene sediments in the North Pacific and Ontong-Java Plateau: Temporal variations of detrital and biogenic components. Geochemistry, Geophys. Geosystems. doi:10.1029/2009GC002413

Yamazaki, T., 2012. Paleoposition of the Intertropical Convergence Zone in the eastern pacific inferred from glacial-interglacial changes in terrigenous and biogenic magnetic mineral fractions. Geology. doi:10.1130/G32646.1

Yamazaki, T., Ikehara, M., 2012. Origin of magnetic mineral concentration variation in the Southern Ocean. Paleoceanography 27, 1–13. doi:10.1029/2011PA002271

Zhao, X., Heslop, D., Roberts, A.P., 2015. A protocol for variable-resolution first-order reversal curve measurements. Geochemistry, Geophys. Geosystems 1364–1377. doi:10.1002/2014GC005680

Zhao, X., Roberts, A.P., Heslop, D., Paterson, G.A., Li, Y., Li, J., 2017. Magnetic domain state diagnosis using hysteresis reversal curves. J. Geophys. Res. Solid Earth 122, 4767–4789. doi:10.1002/2016JB013683

Zheng, Y., Zheng, H., Deng, C., Liu, Q., 2014. Holocene paleomagnetic secular variation from East China Sea and a PSV stack of East Asia. Phys. Earth Planet. Inter. 236, 69-78.

Zhu, R., Pan, Y., Coe, R.S., 2000. Paleointensity studies of a lava succession from Jilin Province, northeastern China: Evidence for the Blake event. J. Geophys. Res. Solid Earth 105, 8305–8317. doi:10.1029/1999JB900448

Zimmerman, S.H., Hemming, S.R., Kent, D. V, Searle, S.Y., 2006. Revised chronology for late Pleistocene Mono Lake sediments based on paleointensity correlation to the global reference curve 252, 94–106. doi:10.1016/j.epsl.2006.09.030

Appendix

A1: List of the acronyms used is the thesis

A2: Table Content of data CD

A1: list of the acronyms used is the thesis

κ_{LF}	low-field magnetic susceptibility, volume specific
ARM	anhysteretic remanent magnetization
κ_{ARM}	ARM normalized by the magnitude of the DC field used during ARM acquisition
NRM	natural remanent magnetization
ChRM	characteristic remanent magnetization
rPI	relative paleointensity
PSV	paleosecular variation
VGP	virtual geomagnetic poles
GAD	geocentric axial dipole
VDM	dipole moment
VADM	virtual axial dipole moments
IRM	isothermal remanent magnetization
SIRM	saturation isothermal remanent magnetization
S-ratio	0.5×(1-(IRM(-0.2 T)/SIRM))
SD	single domain
MD	multidomain
FORC	first order reversal curve
XRF	X-ray fluorescence
EDS	Energy-dispersive X-ray spectroscopy
SEM	Scanning Electron Microscope
TEM	Transmission Electron Microscope
NGRIP	North Greenland Ice Core Project

A2: Table Content of data CD

thesis.pdf:	pdf-file of this doctoral
Black_Sea_PSV.pdf:	summarized paleomagnetic data related this doctorate
CV.pdf:	curriculum vitae
publication.pdf:	list of publications